frontiers | Research Topics

Molecular diagnostics of pediatric cancer, volume II

Edited by
Jing He, Yizhuo Zhang, Jochen Rössler, Hua Tan and Jinhong Zhu

Published in
Frontiers in Oncology
Frontiers in Pediatrics

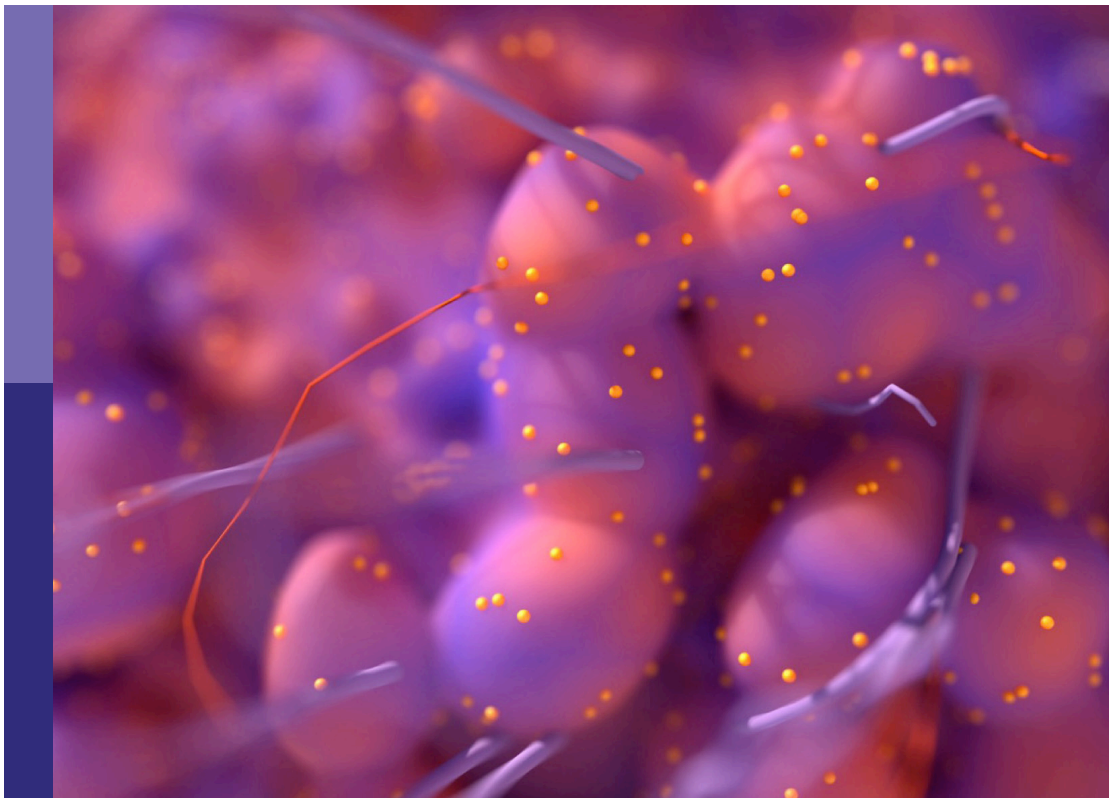

ISSN 1664-8714
ISBN 978-2-8325-5540-8
DOI 10.3389/978-2-8325-5540-8

About Frontiers

Frontiers is more than just an open access publisher of scholarly articles: it is a pioneering approach to the world of academia, radically improving the way scholarly research is managed. The grand vision of Frontiers is a world where all people have an equal opportunity to seek, share and generate knowledge. Frontiers provides immediate and permanent online open access to all its publications, but this alone is not enough to realize our grand goals.

Frontiers journal series

The Frontiers journal series is a multi-tier and interdisciplinary set of open-access, online journals, promising a paradigm shift from the current review, selection and dissemination processes in academic publishing. All Frontiers journals are driven by researchers for researchers; therefore, they constitute a service to the scholarly community. At the same time, the *Frontiers journal series* operates on a revolutionary invention, the tiered publishing system, initially addressing specific communities of scholars, and gradually climbing up to broader public understanding, thus serving the interests of the lay society, too.

Dedication to quality

Each Frontiers article is a landmark of the highest quality, thanks to genuinely collaborative interactions between authors and review editors, who include some of the world's best academicians. Research must be certified by peers before entering a stream of knowledge that may eventually reach the public - and shape society; therefore, Frontiers only applies the most rigorous and unbiased reviews. Frontiers revolutionizes research publishing by freely delivering the most outstanding research, evaluated with no bias from both the academic and social point of view. By applying the most advanced information technologies, Frontiers is catapulting scholarly publishing into a new generation.

What are Frontiers Research Topics?

Frontiers Research Topics are very popular trademarks of the *Frontiers journals series*: they are collections of at least ten articles, all centered on a particular subject. With their unique mix of varied contributions from Original Research to Review Articles, Frontiers Research Topics unify the most influential researchers, the latest key findings and historical advances in a hot research area.

Find out more on how to host your own Frontiers Research Topic or contribute to one as an author by contacting the Frontiers editorial office: frontiersin.org/about/contact

Molecular diagnostics of pediatric cancer, volume II

Topic editors

Jing He — Guangzhou Medical University, China
Yizhuo Zhang — Sun Yat-sen University Cancer Center (SYSUCC), China
Jochen Rössler — Insel Gruppe AG, Switzerland
Hua Tan — National Human Genome Research Institute (NIH), United States
Jinhong Zhu — Harbin Medical University Cancer Hospital, China

Citation

He, J., Zhang, Y., Rössler, J., Tan, H., Zhu, J., eds. (2024). *Molecular diagnostics of pediatric cancer, volume II*. Lausanne: Frontiers Media SA.
doi: 10.3389/978-2-8325-5540-8

Table of contents

frontiers | Frontiers in Oncology

TYPE Editorial
PUBLISHED 27 September 2024
DOI 10.3389/fonc.2024.1493791

OPEN ACCESS

EDITED AND REVIEWED BY
Jaume Mora,
Sant Joan de Déu Hospital, Spain

*CORRESPONDENCE
Jinhong Zhu
zhujinhong@hrbmu.edu.cn
Jing He
hejing198374@gmail.com

RECEIVED 09 September 2024
ACCEPTED 17 September 2024
PUBLISHED 27 September 2024

CITATION
He J, Zhang Y, Tan H, Rössler J and Zhu J (2024) Editorial: Molecular diagnostics of pediatric cancer, volume II.
Front. Oncol. 14:1493791.
doi: 10.3389/fonc.2024.1493791

Editorial: Molecular diagnostics of pediatric cancer, volume II

Jing He[1]*, Yizhuo Zhang[2], Hua Tan[3], Jochen Rössler[4] and Jinhong Zhu[5]*

[1]Department of Pediatric Surgery, Guangzhou Institute of Pediatrics, Guangdong Provincial Key Laboratory of Research in Structural Birth Defect Disease, Guangzhou Women and Children's Medical Center, Guangzhou Medical University, Guangzhou, Guangdong, China, [2]Department of Pediatric Oncology, State Key Laboratory of Oncology in South China, Collaborative Innovation Center for Cancer Medicine, Sun Yat-Sen University Cancer Center, Guangzhou, Guangdong, China, [3]School of Biomedical Informatics, The University of Texas Health Science Center at Houston, Houston, TX, United States, [4]Division of Pediatric Hematology and Oncology, Department of Pediatrics, Inselspital, Bern University Hospital, University of Bern, Bern, Switzerland, [5]Department of Clinical Laboratory, Biobank, Harbin Medical University Cancer Hospital, Harbin, Heilongjiang, China

KEYWORDS

pediatric cancer, prognostic, biomarker, molecular target, therapeutics

Editorial on the Research Topic
Molecular diagnostics of pediatric cancer, volume II

Pediatric tumors refer to various types of malignant tumors occurring in children and adolescents. Common pediatric tumors include brain and central nervous system tumors, lymphomas, neuroblastoma, Wilms tumor, osteosarcoma, rhabdomyosarcoma, and leukemia. Unlike adult cancers, pediatric tumors often exhibit unique genetic profiles and biological behaviors, necessitating age-specific diagnostic and therapeutic approaches (1). Molecular diagnostics have revolutionized pediatric cancer care, shifting diagnosis and treatment from traditional histological and clinical methods to a deeper understanding of the genetic basis of these malignancies. Innovations such as next-generation sequencing (NGS) and liquid biopsy techniques consequently expanded our ability to detect genetic mutations, chromosomal abnormalities, and tumor-specific biomarkers with unprecedented accuracy and sensitivity. However, molecular diagnostics in pediatric cancer still face significant challenges. First, the rarity of certain pediatric cancers limits the availability of large, statistically powerful cohorts needed for comprehensive molecular studies. Second, the diversity and complexity of pediatric tumors further complicate the diagnostic landscape. This complexity is particularly evident in neuroblastoma, where diverse genetic alterations and varying disease stages demand a more meticulous understanding of molecular underpinnings to improve diagnostic accuracy and treatment outcomes (2). This Research Topic brings together nine insightful studies that collectively expand our understanding of molecular diagnostics in pediatric cancer. The Research Topic cover a broad spectrum of pediatric malignancies and molecular mechanisms, spotlighting the intricate interplay between genetic and molecular factors in tumorigenesis and disease progression.

By retrospectively analyzing 21 retinoblastoma (RB) specimens, Al-Ghazzawi et al. demonstrated the pivotal role of growth factors in driving tumor development in high-risk RB, including platelet-derived growth factor (PDGF), nerve growth factor (NGF), and epidermal growth factor (EGF). Kaposiform Hemangioendothelioma (KHE), a rare, life-

threatening, regional vascular tumor, primarily affects infants and young children. The present case report identified a *PIK3CA* mosaic pathogenic variants (c.685delA and p.Thr229fs) in KHE and offered a successful example of using sirolimus (also known as rapamycin) for KHE with *PIK3CA* mutations (Wang et al.). These findings align with the conception that KHE may belong to the PIK3CA-related overgrowth spectrum (PROS), a heterogeneous group of disorders resulting from activating variants of the PIK3CA gene (3, 4).

Neuroblastoma, a recurrent theme in this Research Topic, is explored through several perspectives: the potential of circular RNAs (circRNAs) as diagnostic biomarkers, PET/CT imaging in relation to *MYCN* gene status, mitochondrial gene expression, differentially expressed genes (DEGs) between neuroblastoma in different stages, and the predictive value of an autophagy-related lncRNA signature for progression-free survival (PFS). Circular RNAs are a unique class of non-coding RNAs characterized by their covalently closed-loop structure. Circular RNAs regulate gene expression through several mechanisms, such as miRNA sponges, protein scaffolding, transcriptional regulation, and translation into proteins. Wu et al. provided a brief review of some recently discovered carcinogenic and tumor-suppressive circRNAs in neuroblastoma and their working mechanisms with a focus on miRNA sponges. ^{18}F-FDG PET/CT metabolic parameters and the presence of *MYCN* oncogene amplification or specific segmental chromosomal aberrations (e.g., 11q deletion, 1p deletion, and 17q gain) can contribute to prognosis assessment in neuroblastoma. Ren et al. attempted to investigate the relationship between these factors, as well as clinicopathological factors and laboratory test parameters. Interestingly, it was shown that lactate dehydrogenase (LDH), the maximal length of the lesion in the axial image (LEGmax), tumor volume (MTV), and total lesion glycolysis (TLG) may serve as effective predictors for *MYCN* oncogene and chromosome 1p36 status in pediatric neuroblastoma and ganglioneuroblastoma. The rapid evolution of gene sequencing and bioinformatics, along with the emergence of relevant tumor databases, opens up new possibilities for deciphering the molecular mechanisms of pediatric cancer and for developing precise drug therapies. Mitochondria are a key target in cancer therapy due to their role in altered energy production in malignant cells. Chai et al. used the machine learning method to identify potential therapeutic targets and prognostic biomarkers from mitochondria-associated proteins (MAPs) in pediatric neuroblastoma, by utilizing cell line-based bulk RNA-seq data, primary neuroblastoma tissue-based bulk RNA-seq data, single-cell RNA-seq (scRNA-seq) dataset of neuroblastoma tissues, *MAP* gene dependency of cell viability dataset, and genome-wide CRISPR screens in primary human T cells. This research broadens the role of *MAP* genes in enhancing neuroblastoma tumor stratification, prognosis prediction, and the development of targeted drugs. Stage "MS" (metastatic special) neuroblastoma 4S, also known as "stage 4 special (4S)", is characterized by localized primary tumors with limited metastasis. Unlike standard stage 4 neuroblastoma, which is more widespread and aggressive, stage MS may regress spontaneously and have a favorable prognosis. Through bioinformatics analysis, Wu and Zhang compared DEGs between stage M and stage MS neuroblastoma regarding regulatory cell death (RCD), such as apoptosis, autophagy, and ferroptosis. Five genes, *BIRC5*, *SLCO4A1*, *POPDC3*, *HK2*, and *TF*, showed great promise in predicting the prognosis of neuroblastoma. Consistently, Wang et al. also provided evidence of association between RCD and neuroblastoma prognosis. Based on machine learning and relevant tumor databases, they developed risk classifiers consisting of four autophagy-related lncRNAs, which could facilitate the prediction of progression-free survival (PFS) in neuroblastoma.

Additionally, studies on pediatric pilomyxoid and pilocytic astrocytomas, as well as genetic variants in m5C modification core genes in acute lymphoblastic leukemia (ALL), add to the growing body of literature aiming to refine molecular classification and risk stratification in pediatric oncology. The most common pediatric brain tumor, pilocytic astrocytoma (PA), generally grows slowly with favorable outcomes, but its subtype, pilomyxoid astrocytoma (PMA), has a more aggressive course and distinct histology. A genome-wide copy number screening was conducted in one of the largest Saudi cohorts of pediatric patients with PMA and PA (AlShail et al.). Overall, 41 copy number aberrations (CNAs) (34 gains, 7 losses) were detected across all patients, as well as the presence of the KIAA1549-BRAF fusion gene in over 88% of cases (89% in PMA, 80% in PA). Moreover, other genomic CNAs were identified in 12 patients. Pathway analysis showed alterations in retinoic acid-mediated apoptosis, MAPK signaling, and key genes linked to tumor growth, including *BRAF*, *TP53*, and *SOX4*. Genomic sequencing analyses suggest that pediatric cancers typically present with fewer somatic mutations and a higher occurrence of germline alterations in cancer susceptibility genes (5). Genetic predisposition plays a significant role in this patient population, contributing to approximately 10% of cases (6–8). A study on genetic variants in m5C modification core genes in ALL revealed that *NOL1* rs3764909 and *NSUN4* rs10252 polymorphisms were significantly associated with increased susceptibility to pediatric ALL (Wang et al.).

In conclusion, the articles on this Research Topic demonstrate the impacts of molecular diagnostics on early detection, personalized treatment, and improved patient outcomes with the most recent evidence, and they contribute valuable knowledge to this field. Emerging technologies such as multi-omics approaches, AI-driven diagnostics, and targeted genetic testing are leading to more precise and individualized interventions.

Author contributions

JH: Conceptualization, Investigation, Writing – original draft, Writing – review & editing. YZ: Investigation, Writing – review & editing. HT: Investigation, Writing – review & editing. JR: Investigation, Writing – review & editing. JZ: Investigation, Writing – original draft, Writing – review & editing.

Funding

The author(s) declare that financial support was received for the research, authorship, and/or publication of this article. This study was supported by a grant from the National Natural Science Foundation of China (No. 82173593).

Conflict of interest

The authors declare that the research was conducted in the absence of any commercial or financial relationships that could be construed as a potential conflict of interest.

The author(s) declared that they were an editorial board member of Frontiers, at the time of submission. This had no impact on the peer review process and the final decision.

Publisher's note

References

1. Kattner P, Strobel H, Khoshnevis N, Grunert M, Bartholomae S, Pruss M, et al. Compare and contrast: pediatric cancer versus adult Malignancies. *Cancer Metastasis Rev*. (2019) 38:673–82. doi: 10.1007/s10555-019-09836-y

2. Irwin MS, Goldsmith KC. Current and emerging biomarkers: impact on risk stratification for neuroblastoma. *J Natl Compr Canc Netw*. (2024) 22:e247051. doi: 10.6004/jnccn.2024.7051

3. Carli D, Kalantari S, Manicone R, Coppo P, Francia di Celle P, La Selva R, et al. Kaposiform hemangioendothelioma further broadens the phenotype of PIK3CA-related overgrowth spectrum. *Clin Genet*. (2021) 100:624–7. doi: 10.1111/cge.v100.5

4. Douzgou S, Rawson M, Baselga E, Danielpour M, Faivre L, Kashanian A, et al. A standard of care for individuals with PIK3CA-related disorders: An international expert consensus statement. *Clin Genet*. (2022) 101:32–47. doi: 10.1111/cge.v101.1

5. Sweet-Cordero EA, Biegel JA. The genomic landscape of pediatric cancers: Implications for diagnosis and treatment. *Science*. (2019) 363:1170–5. doi: 10.1126/science.aaw3535

6. Brodeur GM, Nichols KE, Plon SE, Schiffman JD, Malkin D. Pediatric cancer predisposition and surveillance: an overview, and a tribute to Alfred G. Knudson Jr. *Clin Cancer Res*. (2017) 23:e1–5. doi: 10.1158/1078-0432.CCR-17-0702

7. Grobner SN, Worst BC, Weischenfeldt J, Buchhalter I, Kleinheinz K, Rudneva VA, et al. The landscape of genomic alterations across childhood cancers. *Nature*. (2018) 555:321–7. doi: 10.1038/nature25480

8. Zhang J, Walsh MF, Wu G, Edmonson MN, Gruber TA, Easton J, et al. Germline mutations in predisposition genes in pediatric cancer. *N Engl J Med*. (2015) 373:2336–46. doi: 10.1056/NEJMoa1508054

frontiers | Frontiers in Oncology

TYPE Original Research
PUBLISHED 01 December 2022
DOI 10.3389/fonc.2022.1014845

OPEN ACCESS

EDITED BY
Jinhong Zhu,
Harbin Medical University Cancer Hospital, China

REVIEWED BY
Zeyan Li,
Shandong University, China
Hamed Shoorei,
Birjand University of Medical Sciences, Iran
Praveen Bhoopathi,
Virginia Commonwealth University, United States

*CORRESPONDENCE
Jiexiong Feng
jiexiongfeng@126.com

†These authors have contributed equally to this work and share first authorship

SPECIALTY SECTION
This article was submitted to Pediatric Oncology, a section of the journal Frontiers in Oncology

RECEIVED 22 August 2022
ACCEPTED 14 November 2022
PUBLISHED 01 December 2022

CITATION
Wang J, Meng X, Chen K and Feng J (2022) An autophagy-related four-lncRNA signature helps to predict progression-free survival of neuroblastoma patients.
Front. Oncol. 12:1014845.
doi: 10.3389/fonc.2022.1014845

An autophagy-related four-lncRNA signature helps to predict progression-free survival of neuroblastoma patients

Jing Wang†, Xinyao Meng†, Ke Chen and Jiexiong Feng*

Department of Pediatric Surgery, Tongji Hospital, Tongji Medical College, Huazhong University of Science and Technology, Wuhan, China

Background: This study aimed to identify autophagy-related long non-coding RNAs (lncRNAs) associated with progression of neuroblastoma (NB), and to build an autophagy-related lncRNA signature that helps to predict progression-free survival (PFS) of NB.

Methods: Three independent gene expression datasets were utilized in this study. Autophagy-related genes (ARG) associated with PFS of NB patients were firstly identified by univariate Cox survival analysis. lncRNAs correlated with those PFS-related ARGs were then identified. The least absolute shrinkage and selection operator (LASSO) regression and multivariate Cox regression analyses were performed to select out those lncRNAs with the best prognostic value for PFS. The Receiver Operating Characteristic (ROC) and Area Under Curve (AUC) analyses were performed to assess the prediction accuracy.

Results: Four autophagy-related lncRNAs (AL356599.1, AC022075.1, AC020928.1 and LINC02076) were found to be with the best prognostic value and integrated into a four-lncRNA risk signature for predicting PFS of NB patients. The four-lncRNA signature significantly stratify NB patients into two risk groups, with high-risk group has significantly poorer PFS than the low-risk group. The prognostic role of the lncRNA signature was independent with other clinical risk factors. The ROC curves revealed that the lncRNA signature has a good performance in predicting PFS (AUC > 0.70). A nomogram based on COG (Children's Oncology Group) risk and the lncRNA risk score was constructed, showing good prediction accuracy (C-index = 0.700). The prognostic ability of the nomogram was better than that of COG risk alone (AUC = 0.790 versus AUC = 0.748). GSEA analyses revealed that multiple autophagy-related gene sets are significantly enriched in the low-risk group.

Conclusions: We identified an autophagy-related four-lncRNA signature that could help to predict the PFS of NB patients. Autophagy-related gene sets are significantly enriched in low-risk group, suggesting tumor suppressive roles of autophagy in NB.

KEYWORDS

autophagy, neuroblastoma, progression-free survival, prognosis, long non-coding RNA

Introduction

Neuroblastoma (NB) is the most common extracranial solid tumor of childhood, originating from the adrenal medulla or paraspinal regions where sympathetic nervous tissue is present. It affects about 1 in 7000 live births, and about 650 cases per year are diagnosed in the United States (1, 2). Nowadays, most patients diagnosed with NB in North America are treated according to the Children's Oncology Group (COG) risk stratification system, and the COG is also in the process of revising the COG risk stratification schema. Based on age at diagnosis, MYCN amplification status, International Neuroblastoma Staging System (INSS) stage, histopathology and tumor cell ploidy, NB patients are stratified into low-, intermediate-, and high-risk groups according to the 2007 COG risk system (2, 3). The latest available data reveals that the 5-year overall survival (OS) rate was about 97% for the low-risk group (4); the 3-year OS rate was about 96% for the intermediate-risk group (5); while the overall survival rate for patients with high-risk NB is only about 50% despite multimodal aggressive therapy (3). Recurrence of the original NB tumor remains a major contributor of mortality, accounting for about 67% of total deaths (6). Patients with high-risk NB who were aggressively treated may even develop late recurrences more than 5 years after completion of therapy (6, 7). Thus, further improvement of the risk stratification system for predicting progression-free survival (PFS) may help to the management of NB patients.

The importance of autophagy in the development of malignancies has gained increasing attention since the Nobel Prize for Physiology or Medicine was awarded to Yoshinori Ohsumi for his work on the mechanism of autophagy in 2016 (8–10). Autophagy plays context-dependent roles in cancers, either can be tumor-suppressive or can be tumor-protective (10). Recently, strategies that stimulate or inhibit autophagy have also been suggested as cancer therapies (10–12). Studies have also been focusing on developing novel biomarkers that can be used to monitor autophagy and thus help to guide autophagy-related therapeutic strategies for cancer patients (10). The implications of autophagy in NB have also been reported in recent years (13–18), however, the association between autophagy and the progression of NB is still largely unknown.

In this study, we performed integrated analyses of transcriptome profiles of NB tissues by combing one RNA-seq datasets (TARGET NBL, n= 153) and two microarray datasets (GSE49710 and E-MTAB-8248, n = 498 and n =223 respectively) in order to get a comprehensive understanding of the relationship between autophagy and progression of NB. We focus on identifying autophagy-related lncRNAs that could help to predict PFS of NB patients in this study.

Finally, four autophagy-related lncRNAs were found to be with the best prognostic values and were integrated into a four-lncRNA risk signature for predicting PFS of NB patients. The four-lncRNA signature performs well in predicting PFS of NB patients and also improves the PFS prediction ability of COG risk classification. Gene Set Enrichment Analysis (GSEA) revealed that multiple autophagy-related gene sets were significantly enriched in the low-risk group, while no autophagy gene set was enriched in the high-risk group, indicating that autophagy tend to play tumor-suppressive roles in NB.

Materials and methods

Neuroblastoma datasets processing

The RNA-sequence transcriptome expression profiles of NB tissues (TARGET NBL, n = 153) were obtained from the National Cancer Institute GDC Data Portal. One of the transcriptome expression microarray profiles (GSE49710, n = 498) was obtained from Gene Expression Omnibus (GEO) database, the other one (E-MTAB-8248, n = 223) was obtained from ArrayExpress database. The clinical characteristics of the three cohorts are shown in Additional file 1 (Table S1). The RNA-sequence dataset (TARGET NBL) was used for initial exploration and termed as cohort 1. The microarray datasets (GSE49710 and E-MTAB-8248) were used for validation and termed as cohort 2 and cohort 3 respectively. Both of GSE49710 and E-MTAB-8248 are Aiglent microarrays performed on platform GPL16876 (Agilent-020382 Human Custom Microarray 44k). The Agilent microarray probes IDs were firstly annotated using the platform GPL16876; Then, the probes IDs were re-annotated according to their corresponding Genebank Accession number in order to renew the annotation. Finally, the Ensemble ID in the three datasets (TARGET NBL, GSE49710 and E-MTAB-8248) were transformed into gene symbols according to GRCh38.p12 in order to keep consistent with each other. The background of the three datasets were intersected adjusted. When multiple probes mapped to a same gene, the mean of the signal intensities will be used.

Abbreviations: LncRNA, long non-coding RNA; NB, neuroblastoma; PFS, progression-free survival; ARG, autophagy-related gene; LASSO, least absolute shrinkage and selection operator; ROC, receiver operating characteristic; AUC, area under curve; GSEA, Gene Set Enrichment Analysis; COG, Children's Oncology Group; INSS, International Neuroblastoma Staging System; OS, overall survival; GEO, Gene Expression Omnibus; HADb, Human Autophagy Database; FDR, false discovery rate; COX-2, cyclooxygenase-2; MPTP, 1-methyl-4-244 phenyl 1,2,3,6 tetrahydropyridine; CAMK2, Calcium/calmodulin-dependent protein kinase II; Id-1/2, inhibitor of differentiation 1/2; ULK1, unc-51-like autophagy kinase 1.

Construction of the autophagy-related lncRNA prognostic signature

Autophagy-related genes (ARGs) were obtained from Human Autophagy Database (HADb) (https://www.autophagy.lu/), with a total of 232 ARGs. Univariate Cox regression analyses were utilized to identify those ARGs associated with PFS of NB patients in cohort 1. A p-value of ≤ 0.5 was considered statistically significant. Any events (including death, relapse, metastasis, or progression) occurred during follow-up was considered as progression. The LncRNA of which the expression level is significantly correlated with the expression level of those ARGs with Pearson's correlation coefficient (r) ≥ 0.5 will be extracted as autophagy-related lncRNAs. Only those lncRNAs matched to GENCODE annotation of long non-coding RNA (release 31, GRCh38.p12) were selected. Those PFS-related lncRNAs were put into the least absolute shrinkage and selection operator (LASSO) penalty Cox regression model and multivariate Cox regression model survival analysis to eliminate false positives due to over-fitting (19). Finally, the autophagy-related lncRNA prognostic signature was constructed by weighting the Cox regression coefficients to calculate a risk score for each patient. The median value of the risk score was chosen as the cut-off value and the patients were group into low-risk and high-risk group accordingly. The same formula and the same cut-off value were applied to the validation cohorts.

Cell culture

Human neuroblastoma cell lines (BE2C, IMR-32, SH-SY5Y and SK-N-AS) and human embryonic kidney 293 (HEK293) cells were used for further researches. Cell lines BE2C and IMR-32 were cultured in MEM contained with 10% fetal bovine serum, and HEK293 and SK-N-AS in DMEM with 10% fetal bovine serum, and cell line SH-SY5Y in DMEM/F-12 contained with 10% fetal bovine serum. The cells were cultured at 37°C in an incubator with 5% CO_2 and passaged by 0.1% trypsin digestion every 3–4 days during the logarithmic growth period. All cells were grown addictively. To detect the association of lncRNAs and autophagy, cells were applied with 100 nM Rapamycin for 48h for further investigation.

Quantitative real-time polymerase chain reaction and western blot

Total RNA was obtained from tissues using TRIzol reagent as described by the manufacturer (Invitrogen Life Technologies Co, USA). Quantification of extracted RNA was performed using NanoDrop. For the mRNA detection, Real-time PCR was performed by using an SYBR Premix Ex Taq kit (TOYOBO Biotechnology, Japan) on a StepOnePlus Real-time PCR System (Applied Biosystems, Foster City, CA, USA), along with the Glyceraldehyde 3-phosphate dehydrogenase (GAPDH) as the endogenous control. The Ct value was calculated based on the ΔΔCt method. Fold change of gene expression was expressed as $2^{-\Delta\Delta Ct}$. The primers used in this study were as follows: AL356599.1, sense strand 5′- GGGTCAGTCAACAAGGTCA GTCAAG-3′, antisense strand 5′- AACACCGCTCA TCCTGGCAATTAG-3′, AC022075.1, sense strand 5′-CCTTGCTCGACCTTTGGTGA-3′, antisense strand 5′-GGAGGTAAAACCCGACAGGG-3′, AC020928.1, sense strand 5′-CAAGGCCTCCACCTGATGAA-3′, antisense strand 5′-CGTCTACGCCATTGTAGGGG-3′, and LINC02076, sense strand 5′- GGAGGGTGGAAAAGAAGACGATGAG-3′, antisense strand 5′- CAGCATGTTGGTCAGGCAGGTC-3′ Total protein was extracted using RIPA lysis buffer with PMSF and Cocktail added. Protein concentrations were determined by the BCA method. Protein bands were quantified by densitometry with Quantity One Software.

Statistical analysis and plots construction

The univariate and multivariate Cox proportional hazards regression analyses were performed by the R package "survival". The LASSO Cox survival analyses were performed by the R package "glmnet". The Pearson correlation matrix was generated by the R package "corrplot". The violin plots were constructed by the R package "ggpubr", and the differences between groups were compared by t-test. The Kaplan–Meier survival plots were constructed by R software (package "survival" and "survminer") or GraphPad Prism 5, and the statistical significance was assessed using the two-sided log-rank test. The receiver operating characteristic (ROC) curves and area under curve (AUC) analyses were performed by the R package "timeROC" and "survivalROC". The alluvial diagrams were generated by the R package "ggalluvial". The nomogram was constructed by R package "rms". Gene Set Enrichment Analysis (GSEA) was performed by GSEA software (version 4.0.03), and a nominal p-value < 0.05 as well as false discovery rate (FDR) q-value < 0.25 were considered statistically significant. The combined multiple GSEA plot was constructed by R package "plyr", "ggplot2", "grid" and "gridExtra". The R software version 4.0.0 was utilized in this study. All statistical tests were two-sided and p-value < 0.05 was considered statistically significant. Data were analyzed using the GraphPad Prism software package (version 5; GraphPad Software Inc., La Jolla, CA, USA) and are presented as the mean ± standard error of the mean. Differences between two groups were analyzed using an unpaired t-test with Welch's correction. Analysis of variance (ANOVA) was used to compare data of more than two groups.

Results

Identification of autophagy-related lncRNAs associated with progression-free survival

The flow diagram recapitulating this study is showing in Figure 1A. Firstly, univariate Cox survival analyses were performed for the 232 ARGs in cohort 1 (TARGERT NBL, n = 153). A total of 23 ARGs were identified to be significantly correlated with PFS of NB patients (Figure 1B). Pearson correlation analyses were then performed to identify those lncRNAs significantly correlated with each of those 23 PFS-related ARGs. A total of 752 autophagy-related lncRNA were identified, however, only 11 of them were significantly associated with PFS (Figure 1C). Then the 11 PFS-related lncRNAs were put into LASSO regression (Figures 1D, E) and nine of them were selected out. Finally, the multivariate Cox regression model were utilized and four autophagy-related lncRNAs (AL356599.1, AC022075.1, AC020928.1 and LINC02076) were screened out as being with the best prognostic value for PFS of NB patients. Two of them (AL356599.1 and AC022075.1) are protective factors for PFS of NB patients, while the other two (AC020928.1 and LINC02076) are risk factors (Figure 1F). The differential analysis of these four lncRNAs in Pan-cancer (Additional File 2, Figure S2). The expression of AL356599.1, AC022075.1, AC020928.1 and LINC02076 exhibited significant difference between normal and tumor tissue in most types of cancer.

The Pearson correlation among these PFS-related ARGs and lncRNAs were shown in the correlation matrix (Figure 2A) and the alluvial diagram (Figure 2B). Both of AL356599.1 and AC022075.1 are significantly positively corelated (with $r \geq 0.5$) with autophagy-related genes DAPK1 and ULK2, respectively. AC020928.1 is significantly positively correlated (with $r \geq 0.5$) with autophagy-related genes GNAI3 and EIF2S1, respectively. LINC02076 is significantly positively correlated (with $r \geq 0.5$) with autophagy-related gene MAP2K7.

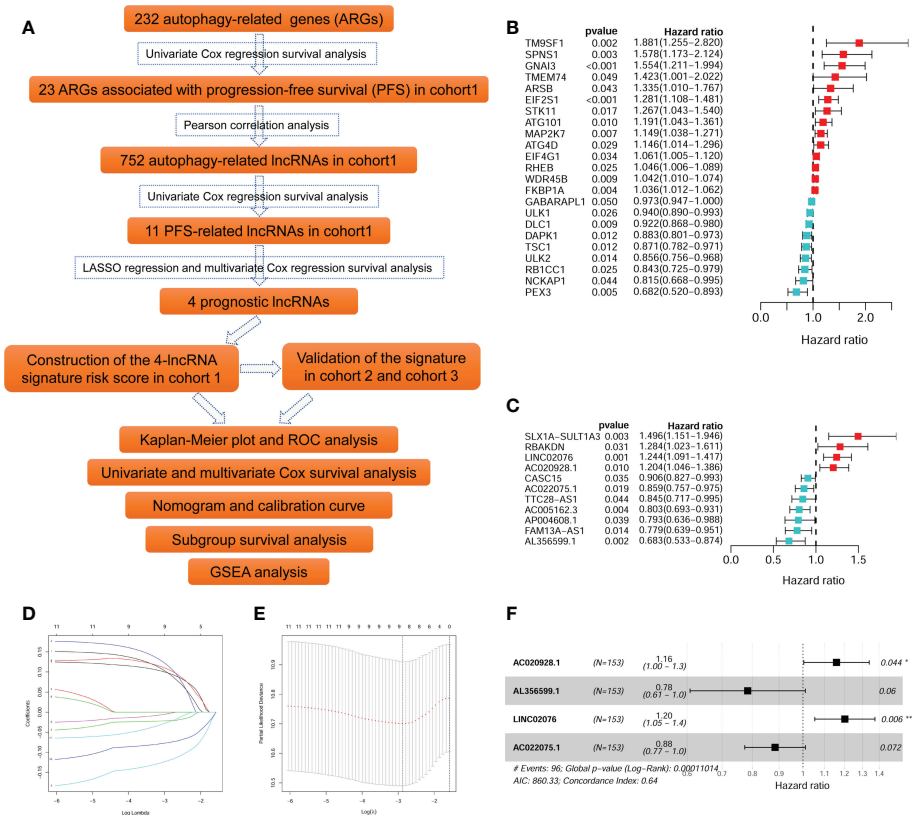

FIGURE 1
Identification of autophagy-related lncRNAs associated with PFS. **(A)** The flowchart of this study. **(B)** The univariate survival analysis of the 23 ARGs associated with PFS of NB patients in cohort 1. **(C)** The univariate survival analysis of the 11 autophagy-related lncRNAs associated with PFS of NB patients in cohort 1. **(D, E)** The LASSO regression analysis. **(F)** The multivariate survival analysis of the four lncRNAs with the best prognostic value for PFS. ARG, autophagy-related gene; PFS, progression-free survival; lncRNA, long noncoding RNA; NB, neuroblastoma; LASSO, least absolute shrinkage and selection operator. *$p < 0.05$ and **$p < 0.01$.

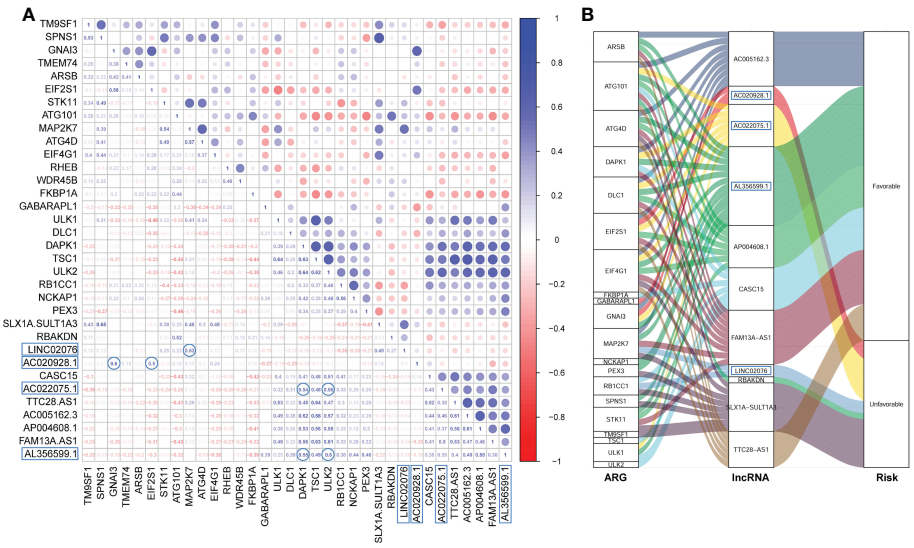

FIGURE 2
The Pearson correlation among the ARGs and lncRNAs. **(A)** The Pearson correlation matrix. **(B)** The alluvial plot represents the correlation between the ARGs and the lncRNAs (Pearson correlation threshold ≥ 0.5). ARG, autophagy-related gene; lncRNA, long noncoding RNA.

Clinical relevance of the four prognostic autophagy-related lncRNAs

The Kaplan-Meier plots showed that each of the four lncRNA could significantly stratify NB patients in cohort 1 into two risk groups, respectively, with the median expression values as the cut-of values (Figure 3). High expression of AL356599.1 and AC022075.1 are associated with relative good PFS (Figures 3A, B), while high expression of AC020928.1 and LINC02076 are associated with relative bad PFS (Figures 3A, B).

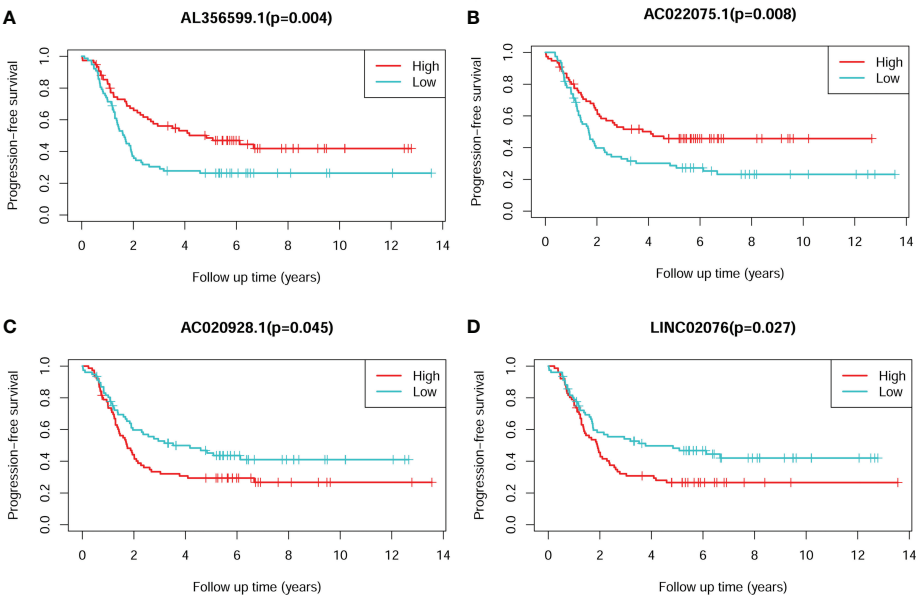

FIGURE 3
The Kaplan-Meier survival plots of the four lncRNAs for PFS of NB patients. **(A)** AL356599.1. **(B)** AC022075.1. **(C)** AC020928.1. **(D)** LINC02076. The Log-rank tests p-values were shown. PFS, progression-free survival; lncRNA, long noncoding RNA; NB, neuroblastoma.

The average expression values of the four lncRNA between different clinical subgroups are showed in Figure 4. The comparisons were performed between subgroups based on COG risk group (high versus low, Figure 4A), MYCN amplification status (amplified versus not-amplified, Figure 4B), age (< 18months versus > 18mouths, Figure 4C), survival status (death versus alive, Figure 4D), progress (yes versus no, Figure 4E), and INSS stage (2/3/4S versus 4, Figure 4F). As we can see in Figure 4, the average expression levels of each of the four lncRNA were significantly different between low COG risk group and high COG risk group (Figure 4A), death group and alive group (Figure 4D), and progress group and non-progression group (Figure 4E). However, the expression levels of three lncRNAs (AC022075.1, AC020928.1 and LINC02076) between MYCN amplified and MYCN not-amplified groups are not significantly different, suggesting that the prognostic role of these three lncRNAs are independent with MYCN amplification status.

Construction and validation of the four-lncRNA prognostic signature

The four-lncRNA signature risk score were constructed based on the multivariate coefficients and expression values of each of the lncRNA for each patient as the following formula: risk score = 0.1849*LINC02076 + 0.1480*AC020928.1- 0.1230*AC022075.1 - 0.2437*AL356599.1. Then the entire cohort 1 was classified into two risk groups according to the median value of the risk score. The risk score of each patient, PFS status of each patient, and heatmap of the expression pattern of each lncRNA are shown in Figure 5A. Kaplan-Meier plots show that patients with high risk score have a significantly poorer PFS than those with low risk score (Figure 5B). The 3-years, 5-years and 10-years PFS rates for patients with high risk score were 25.00%, 22.29% and 19.51%, respectively; whereas, the 3-years, 5-years and 10-years PFS rates for patients with low risk score were 61.88%, 52.94% and 48.68%, respectively. Time-dependent ROC curves reveal that the AUC of

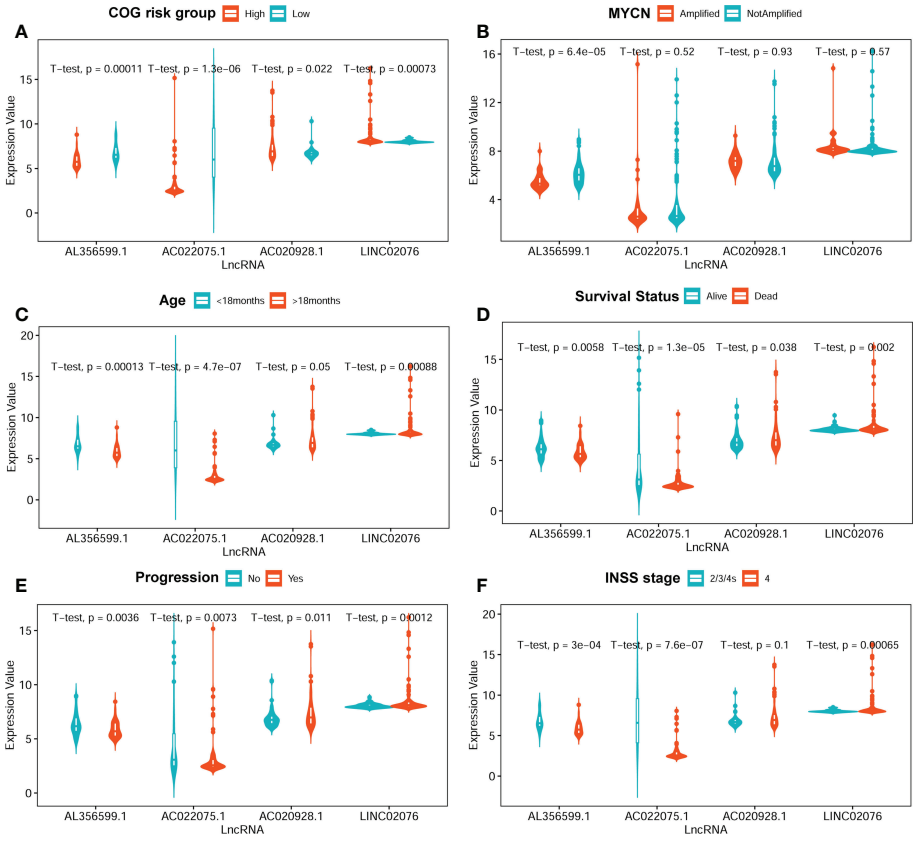

FIGURE 4
The average expression levels of the four lncRNA between different subgroups. **(A)** COG risk group (high vs low). **(B)** MYCN amplification (amplified vs not-amplified. **(C)** Age (< 18 months vs > 18 months). **(D)** Survival status (alive vs dead). **(E)** Progression (no vs yes). **(F)** INSS stage (2/3/4S vs 4). The two-sided t-tests p-values were shown. COG, Children's Oncology Group; lncRNA, long noncoding RNA.

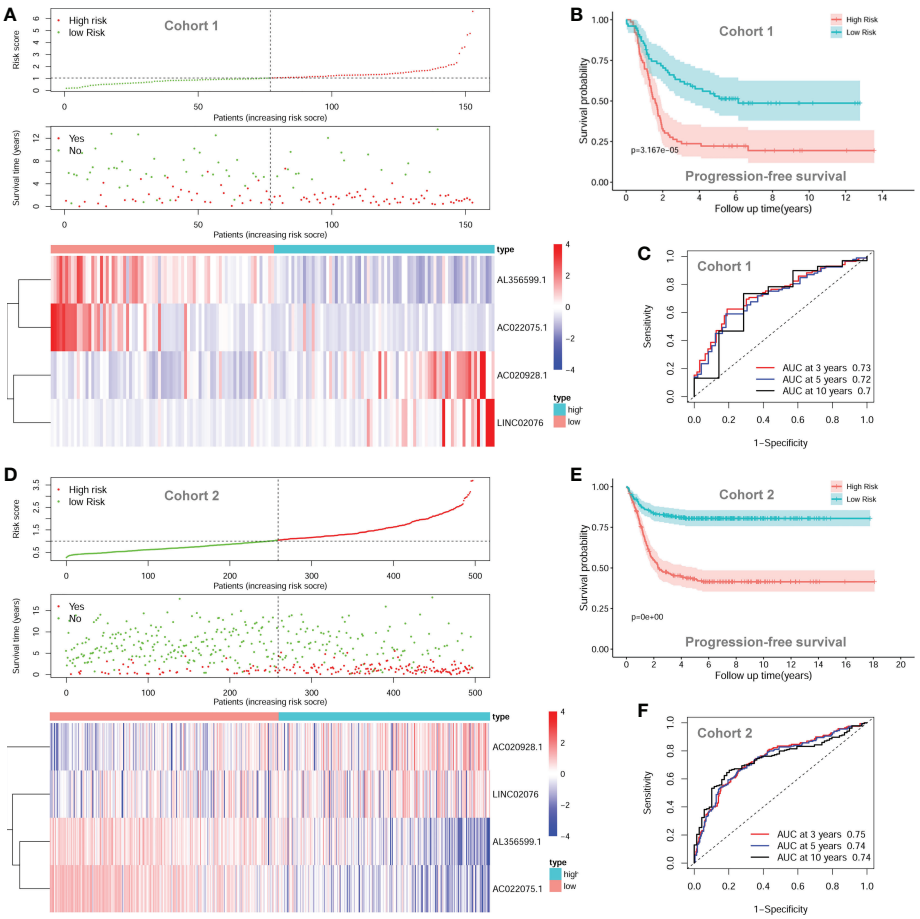

FIGURE 5
The autophagy-related four-lncRNA signature risk score. **(A)** The distribution of risk scores, survival status of each patient, and heatmap of lncRNAs expression pattern in cohort 1. **(B)** Kaplan-Meier survival curve for PFS of patients in the low-risk group and high-risk group for cohort 1. **(C)** Time-dependent ROC curves of the lncRNA signature in cohort 1. **(D)** The distribution of risk scores, survival status of each patient, and heatmap of lncRNAs expression pattern in cohort 2. **(E)** Kaplan-Meier survival curve for PFS of patients in the low-risk group and high-risk group for cohort 2. **(F)** Time-dependent ROC curves of the lncRNA signature in cohort 2. lncRNA, long noncoding RNA; PFS, progression-free survival; ROC, Receiver Operating Characteristic; AUC, Area Under Curve.

the lncRNA signature in predicting PFS of NB patients in cohort 1 at 3-years, 5-years and 10-years were 0.73, 0.72 and 0.70, respectively (Figure 5C), indicating good prediction performance.

The prognostic significance of the lncRNA signature was then tested in cohort 2 (n = 498) and cohort 3 (n = 223) according to the same formula respectively. The risk score of each patient, PFS status of each patient, and heatmap of the expression pattern of each lncRNA are shown in Figure 5D. Kaplan-Meier plots show that patients with high risk score have a significantly poorer PFS than those with low risk score in cohort 2 (Figure 5E). The 3-years, 5-years and 10-years PFS rates for the patients with high risk score were 47.03%, 43.20% and 41.48%, respectively; whereas, the 3-years, 5-years and 10-years PFS rates for patients with low risk score were 82.31%, 80.45% and 80.45%, respectively. Time-dependent ROC curves reveal that the AUC of the lncRNA signature in predicting PFS of NB patients in cohort 2 at 3-years, 5-years and 10-years were 0.75, 0.74 and 0.74, respectively (Figure 5F), indicating good prediction performance. The validation of the lncRNA signature in cohort 3 shows similar results (Additional File 2, Figure S1).

Survival analysis for the lncRNA signature in entire combined cohort

Since the expression backgrounds were intersected adjusted among the three datasets, and the same formula and the same cut-off value were utilized, we decided to combine the three datasets together as one entire cohort for further analyses in order to obtain more reliable results.

The univariate Cox regression survival analyses for the lncRNA signature risk score and other clinical risk factors in

the entire combined cohort are shown in Figure 6A. The multivariate Cox regression survival analyses including the lncRNA signature risk sore and other clinical risk factors as covariates in the combined cohort are shown in Figure 6B. The risk factors are classified as follows: age (< 18 months vs ≥ 18 months), MYCN amplification (non-amplified vs amplified), INSS stage (INSS 1/2/3/4S vs INSS 4), COG risk (low vs high), and lncRNA risk score (low vs high). Since there are only several cases classified as COG intermediate-risk and the survival rate between COG intermediate-risk group and COG low-risk group are similar, we combined COG intermediate-risk group and COG low-risk group together as one COG low-risk group during the analysis. In the multivariate model, only the COG risk (HR = 2.845; 95%CI: 1.631-4.961; $p < 0.001$) and lncRNA signature risk score (HR = 1.855; 95%CI: 1.388-2.480, $p < 0.001$) were independently associated with PFS (Figure 5B).

As we can see in the alluvial plot of Figure 6C, a portion of patients in COG low-risk group are classified as lncRNA signature high-risk, while a portion of patients in COG high-risk group are classified as lncRNA signature low-risk. In the subgroup survival analysis for the entire cohort (Figure 6D), we can see the lncRNA signature could successfully stratify patients in the COG high-risk group or COG low-risk group into two risk groups for PFS. These results suggested that the four-lncRNA signature could help COG risk group to predict PFS of NB patients. The four-lncRNA signature also successfully stratified patients in different age groups into two risk groups for PFS (Figure 6D). Except for INSS 4S subgroup, the four-lncRNA signature successfully stratified each of the other INSS subgroups (1, 2, 3 and 4) into two risk group. However, while the four-lncRNA signature successfully stratified patients in MYCN not-amplified group into two risk groups, it fails to stratify patients in MYCN amplified group into two risk groups.

Nomogram for prediction of progression-free survival

Since the COG risk group classification already considered age, MYCN amplification and INSS stage into its risk classification system, we built a nomogram incorporating only the COG risk classification and the four-lncRNA signature risk score for prediction of PFS based on the entire combined cohort (Figure 7A). The C-index for the nomogram was 0.70. The 1-

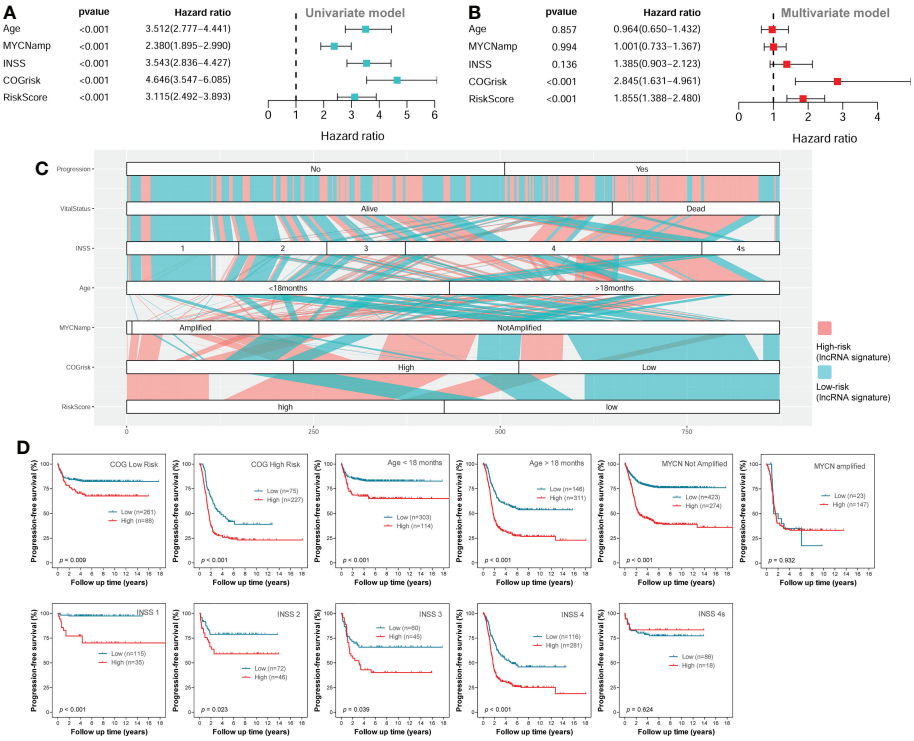

FIGURE 6
Survival analyses in the entire combined cohort. **(A)** The univariate survival analysis of the lncRNA signature and other clinical risk factors. **(B)** The multivariate survival analysis of the lncRNA signature and other clinical risk factors. **(C)** The alluvial diagram shows the relationship of lncRNA signature risk classification and other clinical risk factors. **(D)** The Kaplan-Meier plots show the PFS of different lncRNA signature risk classification (high-risk vs low-risk) in different subgroups of the entire combined cohort; the two-sided log-rank tests p-values were shown. lncRNA, long noncoding RNA; PFS, progression-free survival.

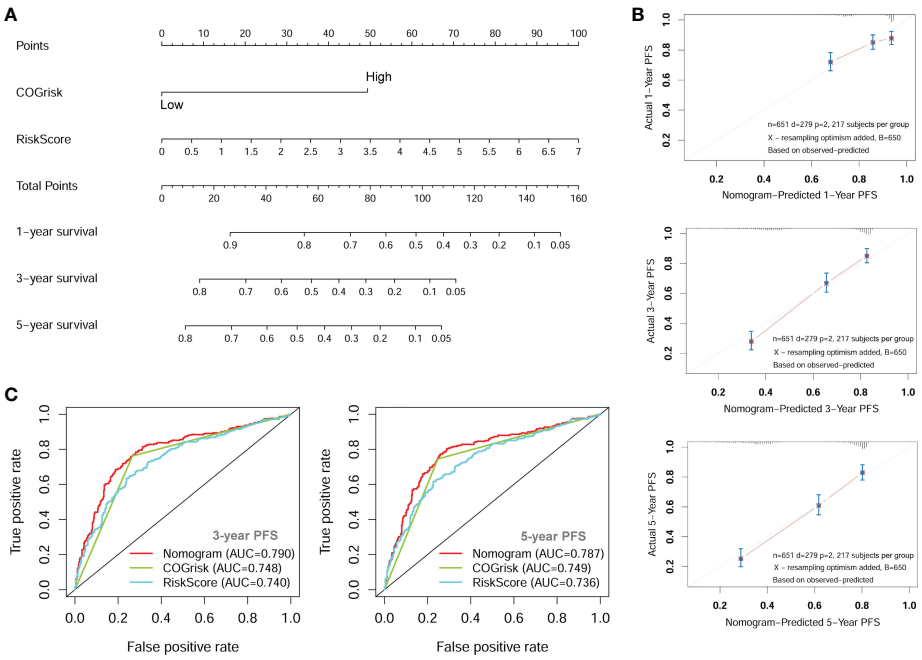

FIGURE 7
The nomogram for predicting of PFS of NB patients. **(A)** The nomogram incorporating COG risk classification and four-lncRNA risk score. **(B)** The calibration curves of the nomogram showing good consistency between predicted-PFS and actual-PFS. **(C)** The ROC curves showing the AUC of the COG risk classification and the AUC of the nomogram. lncRNA, long noncoding RNA; PFS, progression-free survival; COG, Children's Oncology Group; ROC, Receiver Operating Characteristic; AUC, Area Under Curve.

year, 3-year, and 5-year calibrate curves for nomogram all reveled that the predicted PFS was very close to the actual PFS (Figure 7B). The ROC curves analyses were also performed to compared the prognostic ability of the COG risk classification, the lncRNA signature risk and the nomogram (Figure 7C). We can see that the prediction ability of the nomogram was better than the COG risk alone (3-year AUC= 0.790 versus 3-year AUC=0.748). These results suggested that the four-lncRNA signature could improve the PFS prediction ability of COG risk classification system.

GSEA analyses for different risk groups of the lncRNA signature

GSEA analyses were conducted to see the different gene sets enrichment between low-risk group and high-risk group generated by the lncRNA signature in cohort 1. The results revealed that no autophagy related gene set was enriched in the high-risk group, while multiple autophagy-related gene sets were significantly enriched in the low-risk group (Figure 8). Those gene-sets significantly enriched in the low-risk group includes GO selective autophagy, GO positive regulation of autophagy, GO positive regulation of macroautophagy, GO autophagosome organization, GO negative regulation of autophagy, GO regulation of autophagy, GO positive regulation of autophagy of mitochondrion, and KEGG regulation of autophagy. These results suggested that autophagy biological processes tend to play tumor suppressive roles in NB.

Validation *in vitro*

Candidate lncRNAs were verified in normal cell line HEK293 and human neuroblastoma cell lines BE2C, IMR-32,

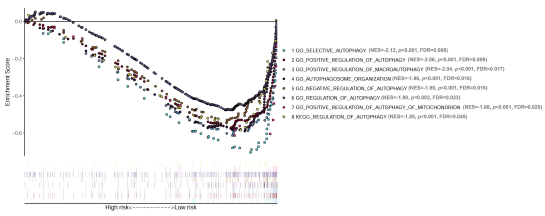

FIGURE 8
GSEA analyses showing the autophagy-related gene sets significantly enriched in the low-risk group of the lncRNA signature. No autophagy-related gene set is significantly enriched in the high-risk group. GSEA, Gene Set Enrichment Analysis; lncRNA, long noncoding RNA.

SH-SY5Yand SK-N-AS. As shown in Figure 9, the expression of the four lncRNAs selected was detected using qRT-PCR. AL356599.1, AC022075.1, AC020928.1 and LINC02076 were higher expressed in cell lines BE2C, IMR-32 and SH-SY5Y compared to HEK293, whereas in SK-N-AS were lower except LINC02076. To further explore the expression of these lncRNA in NB cell lines, we download the mRNA expression matrix of sixteen types of NB cell lines from the CCLE dataset (https://portals.broadinstitute.org/ccle). The expression of these lncRNAs in 16 types of NB cell lines were showed in Additional file 2, Figure S3, and the results showed that there is expression heterogeneity among these NB cell lines. Basically, the expression of these lncRNA in most of NB cell lines was higher than SK-N-AS. Furthermore, to detect the relation of these lncRNAs with autophagy, we stimulated the cells with Rapamycin to activate the autophagy and inspected autophagy-related proteins using western blot. As shown in the results, according to the expression of autophagy-related proteins in different wild type cell lines (Figure 10A), we selected IMR-32 and SK-N-AS cell lines stimulated by Rapamycin, and significant upregulation of LC3B and Beclin1 protein expression was observed in HEK293, IMR-32 and SK-N-AS, which suggested that autophagy was activated (Figures 10B, C). In addition, compared with normal cultured cells, the expression of AL356599.1, AC022075.1, AC020928.1 and LINC02076 was significantly increased in both IMR-32 and SK-N-AS cells after the addition of mTOR inhibitor (Figure 11), which suggested that these four lncRNAs were related to autophagy.

Discussion

Autophagy is an intracellular homeostatic mechanism that delivers intracellular material into degradation and recycling, providing energy and molecular precursors for the cell itself (8–10). Autophagy has context-dependent roles in cancers (10). While some cancers depend on autophagy for survival, in some other model autophagy could suppress cancer development (9). The implication of autophagy in NB has also been reported by studies recently, and the results are also somewhat contradictory. Some studies reported tumor-suppressive role of autophagy for NB. For example, one study reported that inhibition of cyclooxygenase-2 (COX-2) promotes 1-methyl-4-phenyl 1,2,3,6 tetrahydropyridine (MPTP)-induced autophagic cell death in human NB cell line SH-SY5Y (17); another study revealed that Calcium/calmodulin-dependent protein kinase II (CAMK2) potentiates autophagic degradation of inhibitor of differentiation 1/2 (Id-1/2) and then induce cell differentiation of NB cells (14). However, there are also studies found tumor-protective role of autophagy for NB. For example, one study reported that activation of autophagy in human NB cell lines alleviates amyloid-β-induced apoptosis and neurotoxicity (15); another study reported that inhibition of unc-51 like autophagy kinase 1 (ULK1) significantly reduces cell growth and promotes cell apoptosis in NB cell lines (16); one study also reported that autophagy was also associated with chemoresistance of NB (13). It seems that autophagy also plays context-dependent roles in NB itself, maybe depending on activation of different autophagic pathways.

LncRNAs are known as RNA transcripts longer than 200 nucleotides with no or tiny protein-coding capacity, and are believed to play crucial roles in the development of various cancers including NB (20–25). The association between lncRNA and autophagy in NB is largely unknown. In this study, we focus on identifying autophagy-related lncRNAs that are associated with PFS of NB patients. The transcriptome profiles of one RNA-seq dataset and two microarray datasets with large number of NB tissue samples were utilized in this study to obtain a high confidence level. Out of 232 ARGs in the HADb, a total of 23 ARGs were found to be associated with PFS of NB patients, with

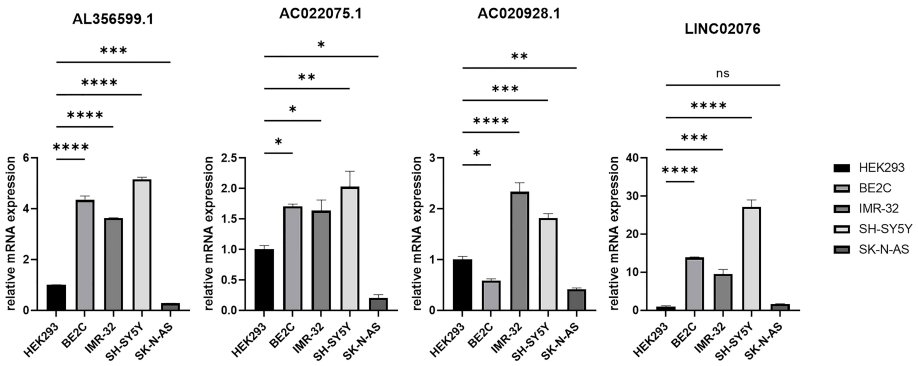

FIGURE 9
The expression of autophagy-related four-lncRNA in wild type cell lines. Results are representative of three independent experiments, ^{ns} $p > 0.05$; * $p < 0.05$; ** $p < 0.01$; *** $p < 0.001$; **** $p < 0.0001$.

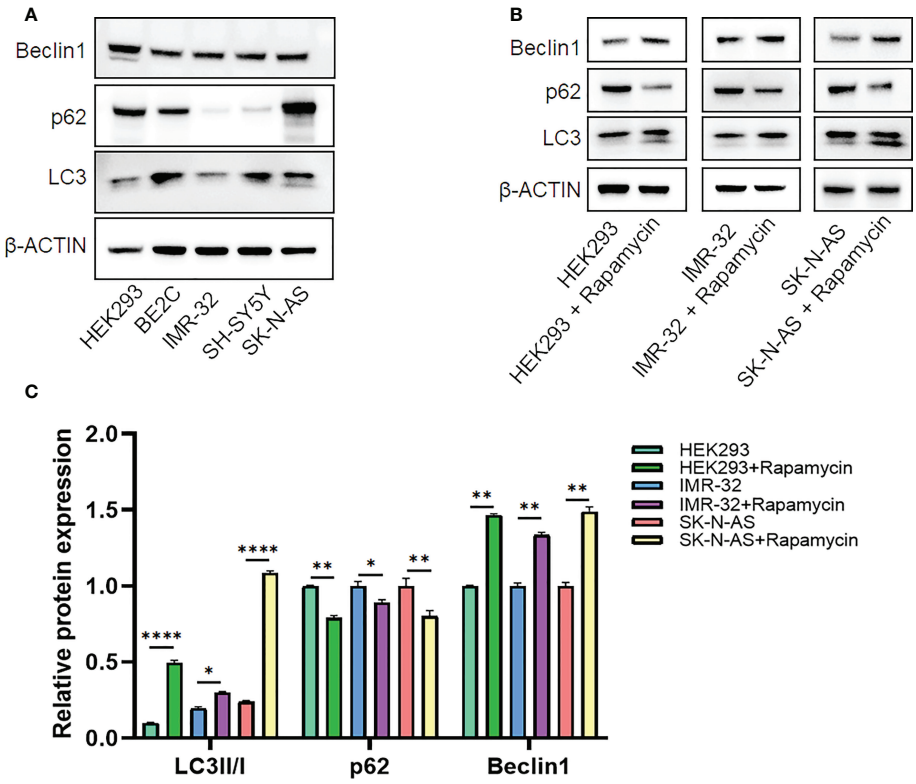

FIGURE 10
The expression of autophagy-related proteins. **(A)** Wild type cell lines. **(B, C)** Autophagy-activated cell lines. Results are representative of three independent experiments, * $p < 0.05$; ** $p < 0.01$; **** $p < 0.0001$.

14 of them are risk factors and 9 are protective factors. The expression of a total of 752 lncRNAs were found to be correlated with the expression of the 23 PFS-related ARGs. However, only 11 of them were significantly associated with PFS of NB patients. After LASSO regression and multivariate Cox regression survival analyses, only four lncRNAs (AL356599.1, AC022075.1, AC020928.1 and LINC02076) were left as having the best prognostic value for PFS of NB patients, with two of them are risk factors (AC020928.1 and LINC02076) and another two (AL356599.1 and AC022075.1) are protective factors. The four lncRNAs were then incorporated into a lncRNA signature risk model for prediction of PFS of NB patients.

The four-lncRNA signature risk score successfully divided each of the three cohorts into two different risk groups, with patients in the low-risk group have relatively good survival outcome than patients in the high-risk group. We then combined the three cohorts together as one entire large cohort to perform further analyses in order to get more reliable results. Multivariate survival analyses performed in the combined cohort revealed that the prognostic role of this lncRNA signature for PFS is independent with other clinical risk factors (including age, MYCN amplification, INSS stage, and COG risk). The lncRNA signature also has good performance in the subgroup survival analyses stratified by different clinical risk factors. It significantly stratified both of COG low-risk patients and COG high-risk patients into two risk groups respectively, indicating that it could be used as a risk stratification factor along with the COG risk stratification system. Furthermore, we constructed a nomogram for predicting PFS of NB patients by incorporating the lncRNA signature risk score and the COG risk classification together. This nomogram revealed good consistency between predicted-PFS and actual-PFS. Moreover, the AUC of the nomogram was higher than the AUC of the COG risk alone, indicating that the lncRNA signature could help the COG risk classification system to predict PFS of NB patients with higher accuracy. These results suggest the use of this lncRNA signature as a risk stratification factor for NB.

The expression of these four lncRNAs are significantly corelated with the expression of autophagy-related genes DAPK1, ULK2, GNAI3, EIF2S1and MAP2K7 (with $r \geq 0.5$). Data from this study revealed that high expression of DAPK1 and ULK2 are associated with good PFS of NB patients, while high expression of GNAI3, EIF2S1 and MAP2K7 are associated with bad PFS of NB patients (Figure 1B). For the two good

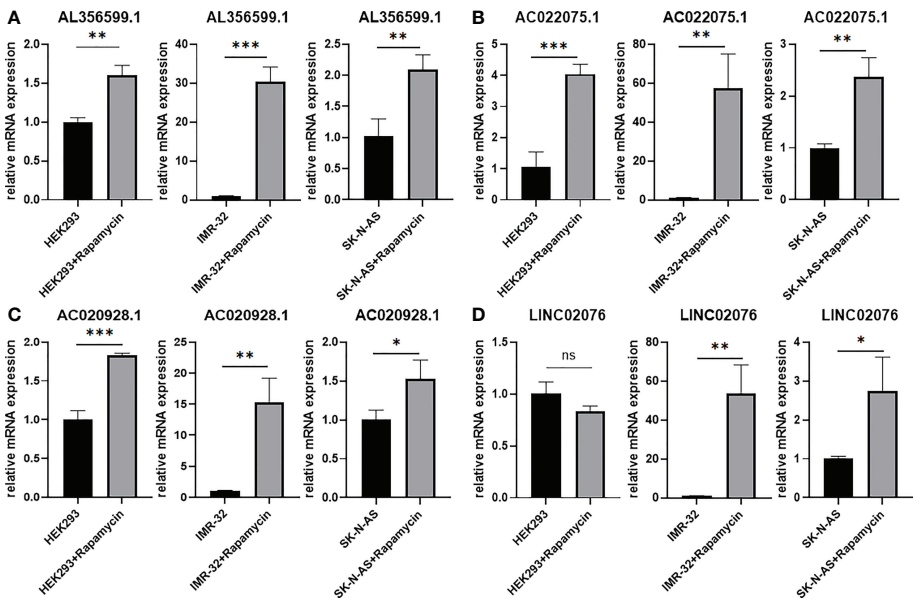

FIGURE 11
The expression of autophagy-related four-lncRNA **(A)** AL356599.1 **(B)** AC022075.1 **(C)** AC020928.1 **(D)** LINC02076 in autophagy-activated cell lines. Results are representative of three independent experiments, ^{ns} $p > 0.05$; * $p < 0.05$; ** $p < 0.01$; *** $p < 0.001$.

ARGs, DAPK1, as a regulator of autophagy and apoptosis, is reported to function as a tumor-suppressor in various cancers (26), and has been reported to contribute to neuronal apoptosis due to ischemia reperfusion injury in mouse NB cell line N2a cells (27, 28); ULK2 has not been reported in NB, however, it has been reported to be required for proper projection of axons in the forebrain (29), indicating a tumor-suppressive role for NB. The function of DAPK1 and ULK2 reported previously are consistent with the results of our study, which suggest tumor-suppressive roles in NB. For the three bad ARGs, GNAI3 and EIF2S1 have not been reported to be implicated in NB previously, however, EIF2S1 has been reported to be involved with pathogenesis of neurodegenerative diseases as a target gene of transcript factor nuclear respiratory factor 1 (NRF1) (30); Downregulation of MAP2K7 (also known as MKK7) has been reported to be associated with decreased proliferation of NB cells (31). Of course, the function mechanisms of these ARGs in NB as well as their relationship with the lncRNAs need to be further investigated.

The exact functions of the four autophagy-related lncRNAs in cancers including NB are unknown. However, one of our previous study revealed that AL356599.1 (updated as FBXO30-DT, and previously known as LOC1005075557) and AC022075.1(updated as KLRK1-AS1, and previously known as LOC101928100) might be implicated in the process of spontaneous regression of NB, as both of them are differentially expressed between stage 4 and stage 4S NB samples and are correlated with the expression of NTRK1 (a well-known factor involved in spontaneous regression of NB) (32–34). This result indicates that autophagy might be also participated in the spontaneous regression of NB, since these two lncRNAs are related to autophagic genes. As for AC020928.1 (updated as LOC728485) and LINC02076, no literature has reported their specific roles in cancers including NB. The exact roles of these four lncRNAs in the development of NB and the underling mechanisms as well as their relationship with autophagy need to be clarified by further studies.

It is also very interesting that the GESA analyses revealed no autophagy-related gene set enriched in the high-risk group, while multiple autophagy-related gene sets (GO selective autophagy, GO positive regulation of autophagy, GO positive regulation of macroautophagy, GO autophagosome organization, GO negative regulation of autophagy, GO regulation of autophagy, GO positive regulation of autophagy of mitochondrion, and KEGG regulation of autophagy) were significantly enriched in the low-risk group. These results suggest that autophagy tend to play tumor-suppressive roles in NB, which is consistent with previous studies revealing tumor-suppressive role of autophagy in NB (14, 17). However, this result is somewhat contrary to some of the previous studies revealing tumor-protective roles of autophagy in NB (15, 16). We presume that autophagy plays context-dependent roles in NB itself, and different autophagic genes or pathways might play different roles. Undoubtedly, further investigations are needed to clarify how different autophagic pathways affect the progression of NB, thus providing guidance for autophagy-related therapeutic strategies in NB patients.

Conclusion

In conclusion, we find that, in the tumor tissue level, autophagy is associated with the progression of NB. An autophagy-related four-lncRNA prognostic signature was built and performed well in predicting PFS of NB patients. The four-lncRNA signature is independent with other clinical risk factors and also helps the COG risk classification to better predict the PFS of NB patients with more accuracy. Our study provides potentially promising ways to obtain a prognosis for NB patients and show that autophagy associated therapies may be a potential treatment for NB.

Data availability statement

The original contributions presented in the study are included in the article/Supplementary Material. Further inquiries can be directed to the corresponding author.

Author contributions

JF designed the study. JW, KC, and XM performed the data analysis. JW and XM wrote the original manuscript. JF revised the manuscript and provided funding acquisition. All authors contributed to the article and approved the submitted version.

Funding

This research was supported by the National Natural Science Foundation of China (grant number 81873541).

Conflict of interest

The authors declare that the research was conducted in the absence of any commercial or financial relationships that could be construed as a potential conflict of interest.

Publisher's note

Supplementary material

The Supplementary Material for this article can be found online at: https://www.frontiersin.org/articles/10.3389/fonc.2022.1014845/full#supplementary-material

References

1. Gurney JG, Ross JA, Wall DA, Bleyer WA, Severson RK, Robison LL. Infant cancer in the U.S.: Histology-specific incidence and trend 1973 to 1992. *J Pediatr Hematol Oncol* (1997) 19(5):428–32. doi: 10.1097/00043426-199709000-00004

2. London WB, Castleberry RP, Matthay KK, Look AT, Seeger RC, Shimada H, et al. Evidence for an age cutoff greater than 365 days for neuroblastoma risk group stratification in the children's oncology group. *J Clin Oncol* (2005) 23(27):6459–65. doi: 10.1200/jco.2005.05.571

3. Maris JM. Recent advances in neuroblastoma. *N Engl J Med* (2010) 362 (23):2202–11. doi: 10.1056/NEJMra0804577

4. Strother DR, London WB, Schmidt ML, Brodeur GM, Shimada H, Thorner P, et al. Outcome after surgery alone or with restricted use of chemotherapy for patients with low-risk neuroblastoma: Results of children's oncology group study P9641. *J Clin Oncol* (2012) 30(15):1842–8. doi: 10.1200/JCO.2011.37.9990

5. Baker DL, Schmidt ML, Cohn SL, Maris JM, London WB, Buxton A, et al. Outcome after reduced chemotherapy for intermediate-risk neuroblastoma. *New Engl J Med* (2010) 363(14):1313–23. doi: 10.1056/NEJMoa1001527

6. Mertens AC, Yasui Y, Neglia JP, Potter JD, Nesbit ME, Ruccione K, et al. Late mortality experience in five-year survivors of childhood and adolescent cancer: the childhood cancer survivor study. *J Clin Oncol* (2001) 19(13):3163–72. doi: 10.1200/JCO.2001.19.13.3163

7. Cotterill SJ, Pearson AD, Pritchard J, Kohler JA, Foot AB. Late relapse and prognosis for neuroblastoma patients surviving 5 years or more: A report from the European neuroblastoma study group "Survey". *Med Pediatr Oncol* (2001) 36(1):235–8. doi: 10.1002/1096-911X(20010101)36:1<235::AID-MPO1057>3.0.CO;2-N

8. Chen P, Cescon M, Bonaldo P. Autophagy-mediated regulation of macrophages and its applications for cancer. *Autophagy* (2014) 10(2):192–200. doi: 10.4161/auto.26927

9. White E, Mehnert JM, Chan CS. Autophagy, metabolism, and cancer. *Clin Cancer Res* (2015) 21(22):5037–46. doi: 10.1158/1078-0432.Ccr-15-0490

10. Levy JMM, Towers CG, Thorburn A. Targeting autophagy in cancer. nature reviews. *Cancer* (2017) 17(9):528–42. doi: 10.1038/nrc.2017.53

11. Levy JMM, Thorburn A. Targeting autophagy during cancer therapy to improve clinical outcomes. *Pharmacol Ther* (2011) 131(1):130–41. doi: 10.1016/j.pharmthera.2011.03.009

12. Towers CG, Thorburn A. Therapeutic targeting of autophagy. *EBioMedicine* (2016) 14:15–23. doi: 10.1016/j.ebiom.2016.10.034

13. Belounis A, Nyalendo C, Le Gall R, Imbriglio TV, Mahma M, Teira P, et al. Autophagy is associated with chemoresistance in neuroblastoma. *BMC Cancer* (2016) 16(1):891. doi: 10.1186/s12885-016-2906-9

14. Li X, Wu XQ, Deng R, Li DD, Tang J, Chen WD, et al. CaMKII-mediated beclin 1 phosphorylation regulates autophagy that promotes degradation of id and neuroblastoma cell differentiation. *Nat Commun* (2017) 8(1):1159. doi: 10.1038/s41467-017-01272-2

15. Singh AK, Bissoyi A, Kashyap MP, Patra PK, Rizvi SI. Autophagy activation alleviates amyloid-β-Induced oxidative stress, apoptosis and neurotoxicity in human neuroblastoma SH-SY5Y cells. *Neurotoxicity Res* (2017) 32(3):351–61. doi: 10.1007/s12640-017-9746-5

16. Dower CM, Bhat N, Gebru MT, Chen L, Wills CA, Miller BA, et al. Targeted inhibition of ULK1 promotes apoptosis and suppresses tumor growth and metastasis in neuroblastoma. *Mol Cancer Ther* (2018) 17(11):2365–76. doi: 10.1158/1535-7163.Mct-18-0176

17. Niranjan R, Mishra KP, Thakur AK. Inhibition of cyclooxygenase-2 (COX-2) initiates autophagy and potentiates MPTP-induced autophagic cell death of human neuroblastoma cells, SH-SY5Y: An inside in the pathology of parkinson's disease. *Mol Neurobiol* (2018) 55(10):8038–50. doi: 10.1007/s12035-018-0950-y

18. Sha Z, Schnell HM, Ruoff K, Goldberg A. Rapid induction of p62 and GABARAPL1 upon proteasome inhibition promotes survival before autophagy activation. *J Cell Biol* (2018) 217(5):1757–76. doi: 10.1083/jcb.201708168

19. Tibshirani R. The lasso method for variable selection in the cox model. *Stat Med* (1997) 16(4):385–95. doi: 10.1002/(sici)1097-0258(19970228)16:4<385

20. Ma L, Bajic VB, Zhang Z. On the classification of long non-coding RNAs. *RNA Biol* (2013) 10(6):925–33. doi: 10.4161/rna.24604

21. Russell MR, Penikis A, Oldridge DA, Alvarez-Dominguez JR, McDaniel L, Diamond M, et al. CASC15-s is a tumor suppressor lncRNA at the 6p22 neuroblastoma susceptibility locus. *Cancer Res* (2015) 75(15):3155–66. doi: 10.1158/0008-5472.Can-14-3613

22. Bhan A, Soleimani M, Mandal SS. Long noncoding RNA and cancer: A new paradigm. *Cancer Res* (2017) 77(15):3965–81. doi: 10.1158/0008-5472.Can-16-2634

23. Tang Y, Cheung BB, Atmadibrata B, Marshall GM, Dinger ME, Liu PY, et al. The regulatory role of long noncoding RNAs in cancer. *Cancer Lett* (2017) 391:12–9. doi: 10.1016/j.canlet.2017.01.010

24. Li D, Wang X, Mei H, Fang E, Ye L, Song H, et al. Long noncoding RNA pancEts-1 promotes neuroblastoma progression through hnRNPK-mediated beta-catenin stabilization. *Cancer Res* (2018) 78(5):1169–83. doi: 10.1158/0008-5472.Can-17-2295

25. Liu PY, Tee AE, Milazzo G, Hannan KM, Maag J, Mondal S, et al. The long noncoding RNA lncNB1 promotes tumorigenesis by interacting with ribosomal protein RPL35. *Nat Commun* (2019) 10(1):5026. doi: 10.1038/s41467-019-12971-3

26. Singh P, Ravanan P, Talwar P. Death associated protein kinase 1 (DAPK1): A regulator of apoptosis and autophagy. *Front Mol Neurosci* (2016) 9:46. doi: 10.3389/fnmol.2016.00046

27. Xiong W, Wu Y, Xian W, Song L, Hu L, Pan S, et al. DAPK1-ERK signal mediates oxygen glucose deprivation reperfusion induced apoptosis in mouse N2a cells. *J Neurol Sci* (2018) 387:210–9. doi: 10.1016/j.jns.2018.01.003

28. Wei R, Zhang L, Hu W, Wu J, Zhang W. Long non-coding RNA AK038897 aggravates cerebral ischemia/reperfusion injury *via* acting as a ceRNA for miR-26a-5p to target DAPK1. *Exp Neurol* (2019) 314:100–10. doi: 10.1016/j.expneurol.2019.01.009

29. Wang B, Iyengar R, Li-Harms X, Joo JH, Wright C, Lavado A, et al. The autophagy-inducing kinases, ULK1 and ULK2, regulate axon guidance in the developing mouse forebrain *via* a noncanonical pathway. *Autophagy* (2018) 14 (5):796–811. doi: 10.1080/15548627.2017.1386820

30. Satoh J-I, Kawana N, Yamamoto Y. Pathway analysis of ChIP-Seq-Based NRF1 target genes suggests a logical hypothesis of their involvement in the pathogenesis of neurodegenerative diseases. *Gene Regul Syst Biol* (2013) 7:139–52. doi: 10.4137/GRSB.S13204

31. He W, Wu Y, Tang X, Xia Y, He G, Min Z, et al. HDAC inhibitors suppress c-Jun/Fra-1-mediated proliferation through transcriptionally downregulating MKK7 and Raf1 in neuroblastoma cells. *Oncotarget* (2016) 7(6):6727–47. doi: 10.18632/oncotarget.6797

32. Brodeur GM, Minturn JE, Ho R, Simpson AM, Iyer R, Varela CR, et al. Trk receptor expression and inhibition in neuroblastomas. *Clin Cancer Res* (2009) 15 (10):3244–50. doi: 10.1158/1078-0432.CCR-08-1815

33. Thiele CJ, Li Z, McKee AE. On trk–the TrkB signal transduction pathway is an increasingly important target in cancer biology. *Clin Cancer Res* (2009) 15 (19):5962–7. doi: 10.1158/1078-0432.CCR-08-0651

34. Meng X, Fang E, Zhao X, Feng J. Identification of prognostic long noncoding RNAs associated with spontaneous regression of neuroblastoma. *Cancer Med* (2020) 9(11):3800–15. doi: 10.1002/cam4.3022

frontiers | Frontiers in Oncology

TYPE Original Research
PUBLISHED 09 January 2023
DOI 10.3389/fonc.2022.1082525

OPEN ACCESS

EDITED BY
Jinhong Zhu,
Harbin Medical University Cancer Hospital, China

REVIEWED BY
Adolfo Martinez,
General Hospital of Mexico, Mexico
Juan Carlos Núñez-Enríquez,
Mexican Social Security Institute, Mexico

*CORRESPONDENCE
Xiaoping Liu
liu_xiaoping@gwcmc.org

SPECIALTY SECTION
This article was submitted to Pediatric Oncology, a section of the journal Frontiers in Oncology

RECEIVED 28 October 2022
ACCEPTED 12 December 2022
PUBLISHED 09 January 2023

CITATION
Wang X, Deng D, Yan Y, Cai M, Liu X, Luo A, Liu S, Zhang X, Jiang H and Liu X (2023) Genetic variants in m5C modification core genes are associated with the risk of Chinese pediatric acute lymphoblastic leukemia: A five-center case–control study. *Front. Oncol.* 12:1082525. doi: 10.3389/fonc.2022.1082525

Genetic variants in m5C modification core genes are associated with the risk of Chinese pediatric acute lymphoblastic leukemia: A five-center case–control study

Xueliang Wang[1], Decheng Deng[1], Yaping Yan[1], Mansi Cai[1], Xiaodan Liu[2], Ailing Luo[1], Shanshan Liu[1], Xiaohong Zhang[1], Hua Jiang[1] and Xiaoping Liu[1*]

[1]Department of Hematology/Oncology, Guangzhou Institute of Pediatrics, Guangzhou Women and Children's Medical Center, Guangzhou Medical University, Guangdong Province Clinical Research Center for Child Health, Guangzhou, Guangdong, China, [2]Division of Birth Cohort Study, Guangzhou Women and Children's Medical Center, Guangzhou Medical University, Guangdong Province Clinical Research Center for Child Health, Guangzhou, Guangdong, China

Objective: To explore the functions of the polymorphisms in 5-methylcytosine (m5C) modification-related coding genes on the susceptibility of pediatric acute lymphoblastic leukemia (ALL).

Methods: Case–control study and multinomial logistic regression analysis were performed to construct models to evaluate the susceptibility of pediatric ALL. The relationship between five functional SNPs in m5C modification-coding genes and pediatric ALL risk was analyzed. Genotyping of 808 cases and 1,340 healthy samples from South China was identified using a TaqMan assay; odds ratios (ORs) and 95% confidence intervals (CIs) were calculated to estimate the relationship between the five selected SNPs and pediatric ALL susceptibility.

Results: Among the five analyzed SNPs, *NOL1* rs3764909 and *NSUN4* rs10252 variants significantly increased the susceptibility of pediatric ALL, while *NSUN3* rs7653521, *NSUN5* rs1880948, and *NSUN6* rs3740102 variants were not associated with the risk of ALL. Stratification analyses demonstrated that *NOL1* rs3764909 C>A exhibited a significant association with increased pediatric ALL risk in subgroups of common B ALL, pre-B ALL, T-cell ALL, low and middle risk, other gene fusion types, non-gene fusion, hypodiploid, normal diploid, primitive lymphocytes in marrow < 5% on week 12, and minimal residual disease (MRD) <0.01% on week 12 after induced therapy; *NSUN4* rs10252 G>A was related to increased risk of ALL children in subgroups of age ≥ 120 months, normal white blood cell (WBC) number, middle risk, non-gene fusion, MRD ≥ 0.01 on days 15–19, and primitive lymphocytes in marrow < 5% on day 33 after induced therapy. Compared with the reference haplotype

CAGTA, children who harbored haplotypes CCGTG and ACATA were remarkably related to increased ALL susceptibility. rs3764909 and rs10252 varieties of alleles were not associated with MRD levels after the selected chemotherapeutics.

Conclusions: In conclusion, *NOL1* rs3764909 and *NSUN4* rs10252 variants were enhanced by pediatric ALL risk and were suggested to be potential biomarkers for pediatric ALL.

KEYWORDS

ALL, pediatric, 5-methylcytosine, susceptibility, polymorphism

Introduction

Acute lymphoblastic leukemia (ALL) is the most common malignant tumor in children and adolescents (1–3). Despite the heterogeneity, the clinical cure rate of childhood ALL is over 85%. Combination chemotherapy and allogeneic hematopoietic cell transplantation is the main treatment of ALL. In order to obtain the best treatment effect, different chemotherapy regimens are formulated according to the risk of recurrence. Even though these efforts were made, there are still a significant proportion of children with ALL having a high risk of relapse (4). Several genetic factors are verified to enhance the risk of pediatric ALL, but a certain percentage of children were not recognized to inherit risk genetic factors (5). Plenty of studies have discovered polymorphic variants in genes that are connected with an elevated risk of ALL (6–8).

In recent years, abundant studies have revealed that epigenetic regulation participates in the initiation and procession of tumors. The role and regulatory mechanism of RNA methylation in tumors have attracted the close attention of researchers. RNA methylation refers to the chemical modification of RNA methyladenine by the selective addition of methyl groups under the catalysis of methyltransferase. Common RNA methylations include several sites (9). A number of m6A-methylated genes take part in the carcinogenesis of leukemia. m6A methyltransferase *METTL14* was demonstrated to promote leukemogenesis *via* mRNA m6A modification (10). m6A demethylase FTO attenuates aerobic glycolysis and accelerates leukemia. Our previous studies identified that genetic variants in m6A methyltransferase *METTL3* and *METTL14* were associated with the increased risk of pediatric ALL (11, 12).

As we know, N^6-methyladenosine is the most common modification of RNA methylation, and 5-methylcytosine (m5C) is another common and conserved modification in RNA, including mRNAs and non-coding RNAs. m5C regulates RNA stability assembly and translation as well as m6A (13). The enzymes modulating m5C of RNAs can be functionally classified into writers, erasers, and readers. Methyltransferases (writers) can install m5C on RNA. The reported m5C writers include NSUN1–7 and DNMT2 (14). Ten-eleven translocation family proteins (TETs) can oxidize 5-methylcytosine to cytosine-5-hydroxymethylation (hm5C), so these are regarded as "erasers" for m5C (15). As for "reader", only YBX1 and ALYREF have been identified as recognition proteins for m5C modification sites at present (16). NOL1/NOP2/SUN family is also documented as m5C methyltransferase to regulate RNA stability and functions (14). These RNA modifiers can regulate the expression of various oncogenes and promote tumorigenesis and development. In addition, methyltransferases are abnormally expressed in a variety of tumors and have been used to predict the prognosis of patients. There is only one available study on the epidemiological assessment of single-nucleotide polymorphisms (SNPs) in the m5C modification core gene. Chen and Cao et al. performed a case–control study and verified that m5C modification genes were related to survival and chemotherapy efficacy of colorectal cancer. Two SNPs of *YBX1* gene, rs10890208 and rs3862218, may predict a reduction by using the Cox regression model to analyze the association between 13 candidate SNPs of m5C modifier gene and overall survival (OS) of colorectal cancer (CRC) after chemotherapy (17). However, the role of SNPs in the m5C methyltransferase gene in ALL risk has not been reported. Because of the evidence that cells regulated by the m5C methyltransferase gene promote tumorigenesis, we conducted a case–control study to explore the association of genetic variations in m5C modification-coding genes with the risk to pediatric ALL in China.

Materials and methods

Study subjects

A total of 808 pediatric ALL cases and 1,340 age-matched, gender-matched, and ethnicity-matched control samples from

South China were enrolled from January 2017 to May 2019 in this study, as summarized in our previous studies (11, 12). All children were diagnosed with ALL by at least two hematologists. The control samples were free from hematological diseases, malignancy, or any type of autoimmune disorder.

SNP selection

The potentially functional SNPs in five m5C methyltransferases were selected as previously described, and the protocol was as follows; the National Center for Biotechnology Information (NCBI) dbSNP database and SNP info (https://snpinfo.niehs.nih.gov/) were used. The selected SNPs should fulfill the following criteria: (1) the minor allele frequency (MAF) was >5% of Chinese Han subjects in HapMap and (2) located in the exon, 5′ untranslated regions (5′ UTR), and 3′ UTR of genes, which were predicted to be potential functional; (3) each SNP should be in low linkage disequilibrium ($R^2 < 0.8$). Five SNPs were selected (*NOL1* rs3764909, *NSUN3* rs7653521, *NSUN4* rs10252, *NSUN5* rs1880948, and *NSUN6* rs3740102). rs3764909 is located in the exonic region of *NOL1* and might be a transcriptional factor binding site. rs7653521 is located in the exonic region of *NSUN3* and was predicted to have the potential to bind transcriptional factors. rs10252 is located in the exon of *NSUN4* and was predicted as a miRNA binding site. rs1880948 is located upstream of *NSUN5* transcriptional start site and may be a transcriptional factor binding site. rs3740102 is located in an exon of *NSUN6* and was predicted to be a transcriptional factor binding site.

SNP genotyping

Peripheral blood genomic DNA was extracted using the QIAamp DNA blood mini kit (QIAGEN, Valencia, CA, USA). For genotyping, assay probes were purchased from Thermo Fisher (Waltham, MA, USA; TaqMan SNP Assays, 4351379). The detailed information on these assays is presented in Table S1. The genotype was identified by TaqMan PCR on an ABI 7900 (Applied Biosystems, Foster City, CA, USA). The conditions of reactions were described previously (11). To ensure the accuracy of these genotyping results, 10% of the samples were randomly selected to be genotyped by a DNA sequencing method. A concordance rate of 100% for the quality control samples was obtained (11).

Statistical analysis

The compliance of genotypes with the Hardy–Weinberg equilibrium (HWE) in the control group and differences in clinical characteristics between ALL children and healthy children were evaluated using the χ^2 test. The age- and gender-adjusted odds ratios (ORs) and 95% confidence intervals (CIs) for the association between the SNPs and ALL susceptibility were calculated by multivariate logistic regression analysis. All these analyses were performed using the software SAS v10.0 (SAS Institute, Cary, NC, USA).

Results

The association of m5C modification core genes and pediatric ALL risk

Five m5C modification core gene SNPs (*NOL1* rs3764909 C>A, *NSUN3* rs7653521 T>C, *NSUN4* rs10252 G>A, *NSUN5* rs1880948 G>A, and *NSUN6* rs3740102 C>A) were genotyped in 808 pediatric ALL samples and 1,340 age- and gender-matched healthy controls. The five SNPs comply with the HWE in control populations. Single-locus analysis was used to analyze the relationship between the five SNPs and pediatric ALL risk. The *NOL1* rs3764909 (AC/CC versus AA: adjusted OR = 1.684, 95% CI = 1.408–2.014, p < 0.001) and *NSUN4* rs10252 (adjusted OR = 1.140, 95% CI = 1.001–1.298, p = 0.049) variant alleles were associated with an increased risk of ALL. However, there was no association between the remaining polymorphisms, *NSUN3* rs7653521 (OR = 1.067, 95% CI = 0.946–1.203, p = 0.291), *NSUN5* rs1880948 (OR = 0.980, 95% CI = 0.862–1.114, p = 0.759), *NSUN6* rs3740102 (OR = 0.959, 95% CI = 0.825–1.114, p = 0.581), and pediatric ALL risk (Table 1).

Stratification analysis of rs3764909 and rs10252 with ALL susceptibility

SNPs rs3764909 C>A and rs10252 T>C with statistically significant differences were stratified according to age, gender, white blood cell (WBC), immunophenotype, gene infusion, karyotype, primitive lymphocytes in the marrow, minimal residual disease (MRD), and relapse (Table 2). *NOL1* rs3764909 AC/CC increased ALL risk in children aged <120 months (adjusted OR = 1.592, 95% CI = 1.319–1.923, p < 0.001), children aged ≥120 months (adjusted OR = 2.759, 95% CI = 1.568–4.855, p < 0.001), female (adjusted OR = 1.785, 95% CI = 1.408–2.265, p < 0.001), male (adjusted OR = 1.860, 95% CI = 1.381–2.505, p < 0.001), number of WBC > 10×10^7 (adjusted OR = 1.811, 95% CI = 1.417–2.315, p < 0.001), normal WBC number (adjusted OR = 1.668, 95% CI = 1.322–2.106, p < 0.001), common B ALL (adjusted OR = 3.323, 95% CI = 2.495–4.426, p < 0.001), pre-B ALL (adjusted OR = 1.566, 95% CI = 1.125–2.181, p = 0.008), T-ALL (adjusted OR = 1.890 95% CI = 1.132–3.155, p = 0.015), low-risk ALL (adjusted OR = 1.705, 95% CI = 1.278–2.276, p < 0.001), middle-risk ALL (adjusted OR = 2.074, 95% CI = 1.630–2.640, p < 0.001), other gene fusion types

TABLE 1 Logistic regression analysis of associations between m5C modification key gene polymorphisms and ALL susceptibility.

Genotype	Cases (N = 808)	Controls (N = 1,340)	p[a]	Crude OR (95% CI)	p	Adjusted OR (95% CI)[b]	p[b]
rs3740102 (HWE = 0.0978)							
CC	462 (57.39)	757 (56.66)		1		1	
CA	309 (38.39)	512 (38.32)		0.988 (0.823–1.185)	0.894	0.988 (0.824–1.186)	0.900
AA	34 (4.22)	67 (5.01)		0.830 (0.541–1.275)	0.396	0.836 (0.546–1.287)	0.420
Additive			0.700	0.957 (0.824–1.111)	0.562	0.959 (0.825–1.114)	0.581
Dominant	343 (42.61)	579 (43.34)	0.741	0.971 (0.813–1.158)	0.741	1.146 (0.815–1.160)	0.755
Recessive	771 (95.78)	1,269 (94.99)	0.403	0.835 (0.548–1.274)	0.403	0.842 (0.552–1.286)	0.427
rs3764909 (HWE = 0.2333)							
AA	297 (36.80)	661 (49.55)		1		1	
AC	414 (51.30)	543 (40.70)		1.706 (1.415–2.058)	<0.001	1.701 (1.411–2.052)	<0.001
CC	96 (11.90)	130 (9.75)		1.653 (1.228–2.224)	0.001	1.660 (1.233–2.234)	0.001
Additive			<0.001	0.405 (1.231–1.604)	<0.001	1.406 (1.231–1.805)	<0.001
Dominant	510 (63.20)	673 (50.45)	<0.001	1.687 (1.419–2.017)	<0.001	1.684 (1.408–2.014)	<0.001
Recessive	711 (88.10)	1,204 (90.25)	0.117	1.251 (0.946–1.654)	0.117	1.258 (0.951–1.664)	0.108
rs3776448 (HWE < 0.001)							
TT	501 (62.08)	688 (51.42)		1		1	
TC	23 (2.85)	60 (4.46)		0.527 (0.321–0.864)	0.011	0.523 (0.319–0.858)	0.010
CC	283 (35.07)	590 (44.10)		0.659 (0.549–0.791)	<0.001	0.658 (0.519–790)	<0.001
Additive			<0.001	0.809 (0.738–0.886)	<0.001	0.808 (0.738–0.886)	<0.001
Dominant	524 (35.07)	748 (55.10)	<0.001	1.460 (1.219–1.749)	<0.001	1.462 (1.220–1.751)	<0.001
Recessive	306 (37.92)	650 (48.58)	<0.001	1.547 (1.294–1.848)	<0.001	1.550 (1.297–1.852)	<0.001
rs1880948 (HWE = 0.9796)							
GG	335 (41.61)	540 (40.33)		1		1	
GA	361 (44.84)	621 (46.38)		0.960 (0.771–1.123)	0.752	0.931 (0.772–1.124)	0.458
AA	109 (13.54)	178 (13.29)		0.980 (0.745–1.289)	0.885	0.985 (0.749–1.296)	0.915
Additive			0.557	0.978 (0.860–1.112)	0.733	0.980 (0.862–1.114)	0.759
Dominant	470 (58.39)	799 (59.67)	0.100	0.948 (0.794–1.132)	0.557	0.950 (0.795–1.135)	0.573
Recessive	696 (86.46)	1,161 (86.71)	0.871	1.022 (0.791–1.320)	0.871	1.026 (0.794–1.326)	0.283
rs7653521 (HWE = 0.1783)							
TT	237 (31.91)	392 (29.41)		1		1	
TC	361 (44.68)	639 (47.94)		0.951 (0.774–1.169)	0.634	0.950 (0.773–1.167)	0.625
CC	210 (25.99)	302 (22.66)		1.171 (0.922–1.486)	0.195	1.172 (0.923–1.488)	0.193
Additive			0.175	1.066 (0.946–1.202)	0.294	1.067 (0.946–1.203)	0.291
Dominant	571 (70.67)	941 (70.59)	0.970	1.004 (0.828–1.216)	0.970	1.003 (0.828–1.215)	0.976
Recessive	598 (74.01)	1,031 (77.34)	0.080	1.199 (0.979–1.469)	0.080	1.201 (0.980–1.471)	0.077

(Continued)

TABLE 1 Continued

Genotype	Cases (N = 808)	Controls (N = 1,340)	p[a]	Crude OR (95% CI)	p	Adjusted OR (95% CI)[b]	p[b]
rs10252 (HWE = 0.3448)							
AA	342 (42.64)	628 (46.90)		1		1	
AG	361 (45.01)	567 (42.35)		1.151 (0.956–1.386)	0.139	1.151 (0.956–1.387)	0.137
GG	99 (12.34)	144 (10.75)		1.243 (0.932–1.656)	0.139	1.247 (0.936–1.663)	0.132
Additive			0.139	1.138 (0.999–1.295)	0.051	1.140 (1.001–1.298)	0.049
Dominant	460 (57.36)	711 (53.10)	0.055	1.188 (0.996–1.417)	0.056	1.190 (0.997–1.420)	0.054
Recessive	703 (87.66)	1,195 (89.25)	0.262	1.169 (0.890–1.534)	0.262	1.173 (0.893–1.541)	0.251

ALL, acute lymphoblastic leukemia; HWE, Hardy–Weinberg equilibrium.
[a]χ^2 test for genotype distributions between leukemia cases and cancer-free controls.
[b]Adjusted for age and gender.

(adjusted OR = 4.806, 95% CI = 1.623–14.242, p = 0.005), non-gene fusion (adjusted OR = 4.524, 95% CI = 2.896–7.065, p < 0.001), hypodiploid (adjusted OR = 3.330, 95% CI = 1.327–8.539, p = 0.010), normal diploid (OR = 3.403, 95% CI = 2.364–4.898, p < 0.001), primitive/naïve lymphocytes in marrow ≥ 5% on days 15–19 (adjusted OR = 1.718, 95% CI = 1.395–2.116, p < 0.001) and day 33 (adjusted OR = 1.466, 95% CI = 1.185–1.813, p < 0.001), and <5% (adjusted OR = 1.623, 95% CI = 1.247–

TABLE 2 Stratification analysis of m5C-related gene polymorphisms with ALL susceptibility.

Variables	rs3764909 (cases/controls)		Adjusted OR[a]	p[a]	rs10252 (cases/controls)		Adjusted OR[a]	p[a]
	AA	AC/CC	(95% CI)		AA	AG/GG	(95% CI)	
Age, month								
<120	270/661	446/673	1.592 (1.319–1.923)	<0.001	311/628	400/711	1.113 (0.924–1.341)	0.259
≥120	27/661	64/673	2.759 (1.568–4.855)	0.000	31/628	60/711	2.056 (1.184–3.570)	0.010
Gender								
Female	156/661	291/673	1.785 (1.408–2.265)	<0.001	183/628	260/711	1.205 (0.954–1.521)	0.118
Male	108/661	200/673	1.860 (1.381–2.505)	<0.001	135/628	172/711	1.252 (0.936–1.674)	0.129
WBC								
>10	122/661	225/673	1.811 (1.417–2.315)	<0.001	156/628	188/711	1.065 (0.839–1.352)	0.603
≤10	143/661	244/673	1.668 (1.322–2.106)	<0.001	158/628	228/711	1.286 (1.022–1.619)	0.032
Immunophenotyping								
Pro B	119/661	108/673	0.885 (0.668–1.175)	0.399	107/628	119/711	0.983 (0.740–1.305)	0.905
Common B	71/661	238/673	3.323 (2.495–4.426)	<0.001	134/628	173/711	1.137 (0.885–1.460)	0.316
Pre-B	64/661	102/673	1.566 (1.125–2.181)	0.008	67/628	98/711	1.304 (0.938–1.813)	0.114
T ALL	24/661	45/673	1.890 (1.132–3.155)	0.015	26/628	42/711	1.424 (0.858–2.364)	0.172
Mix	3/661	2/673	0.676 (0.112–4.082)	0.670	2/628	3/711	1.369 (0.226–8.300)	0.733
Risk								
Low	85/661	150/673	1.705 (1.278–2.276)	<0.001	98/628	136/711	1.241 (0.915–1.612)	0.174

(Continued)

TABLE 2 Continued

Variables	rs3764909 (cases/controls)		Adjusted OR[a] (95% CI)	p[a]	rs10252 (cases/controls)		Adjusted OR[a] (95% CI)	p[a]
	AA	AC/CC			AA	AG/GG		
Normalized	18/661	13/673	0.689 (0.334–1.419)	0.312	15/628	15/711	0.878 (0.425–1.814)	0.726
Middle	123/661	258/673	2.074 (1.630–2.640)	<0.001	156/628	224/711	1.285 (1.019–1.621)	0.034
High	35/661	54/673	1.525 (0.983–2.368)	0.060	44/628	43/711	0.861 (0.557–1.331)	0.501
Gene fusion type								
BCR-ABL	10/661	18/673	1.798 (0.820–3.942)	0.143	14/628	14/711	0.854 (0.401–1.815)	0.681
E2A-PBX	11/661	13/673	1.139 (0.506–2.565)	0.753	9/628	15/711	1.486 (0.645–1.424)	0.353
MLL	5/661	11/673	2.187 (0.754–0.339)	0.150	6/628	10/711	1.427 (0.514–3.962)	0.495
SIL-TAL	1/661	7/673	7.003 (0.857–57.188)	0.069	1/628	7/711	0.964 (0.729–46.782)	0.096
TCF3-PBX1	0/661	9/673	>999.999 (<0.001, >999.999)	0.938	3/628	6/711	1.964 (0.485–7.957)	0.344
TEL/ETV6	0/661	7/673	>999.999 (<0.001, >999.999)	0.952	3/628	4/711	1.153 (0.257–5.176)	0.853
TEL-AML	41/661	47/673	1.119 (0.726–1.725)	0.610	36/628	53/711	1.122 (0.851–2.055)	0.214
Others	4/661	19/673	4.806 (1.623–14.242)	0.005	11/628	12/711	0.989 (0.432–2.264)	0.978
Non	24/661	115/673	4.524 (2.896–7.065)	<0.001	48/628	92/711	1.684 (1.169–2.428)	0.005
Karyotype								
Hypo-diploid	6/661	20/673	3.330 (1.327–8.539)	0.010	11/628	15/711	1.236 (0.562–2.721)	0.598
Normal diploid	41/661	142/673	3.403 (2.364–4.898)	<0.001	81/628	102/711	1.129 (0.827–1.542)	0.445
Abnormal diploid	100/661	134/673	1.314 (0.993–1.740)	0.056	101/628	133/711	1.168 (0.882–1.546)	0.278
Low hyperdiploid	10/661	19/673	1.896 (0.874–4.116)	0.106	9/628	20/711	2.031 (0.916–4.503)	0.081
High hyperdiploid	31/661	34/673	0.905 (0.561–1.460)	0.683	27/628	43/711	1.429 (0.872–2.343)	0.157
Primitive/naïve lymphocytes in marrow (%, 15–19 days)								
<5	107/661	176/673	1.623 (1.247–2.112)	<0.001	115/628	166/711	1.273 (0.980–1.653)	0.971
≥5	190/661	334/673	1.718 (1.395–2.116)	<0.001	227/628	294/711	1.152 (0.939–1.413)	0.174
MRD in marrow (%, 15–19 days)								
<0.01	170/661	257/673	1.486 (1.190–1.854)	<0.001	186/628	239/711	1.133 (0.909–1.411)	0.267
≥0.01	127/661	253/673	1.952 (1.537–2.479)	<0.001	156/628	221/711	1.264 (1.002–1.594)	0.048
Primitive/naïve lymphocytes in marrow (%, 33 days)								
<5	106/661	224/673	2.082 (1.603–2.688)	<0.001	134/628	194/711	1.281 (1.002–1.837)	0.048
≥5	191/661	286/673	1.466 (1.185–1.813)	0.000	208/628	266/711	1.136 (0.920–1.403)	0.237
MRD in marrow (%, 33 days)								
<0.01	259/661	443/673	1.677 (1.1.391–2.023)	<0.001	288/628	409/711	1.256 (1.044–1.512)	0.016
≥0.01	38/661	67/673	1.729 (1.144–2.613)	0.009	54/628	51/711	0.841 (0.565–1.253)	0.395
Primitive/naïve lymphocytes in marrow (%, 12 weeks)								
<5	130/661	356/673	2.704 (2.153–3.397)	<0.001	205/628	279/711	1.200 (0.972–1.381)	0.089
≥5	167/661	154/673	0.900 (0.705–1.150)	0.400	137/628	181/711	1.173 (0.916–1.501)	0.206

(Continued)

TABLE 2 Continued

Variables	rs3764909 (cases/controls)		Adjusted OR[a] (95% CI)	p[a]	rs10252 (cases/controls)		Adjusted OR[a] (95% CI)	p[a]
	AA	AC/CC			AA	AG/GG		
MRD in marrow (%, 12 weeks)								
<0.01	289/661	504/673	1.710 (1.428–2.048)	<0.001	406/628	381/711	1.190 (0.996–1.421)	0.055
≥0.01	8/661	6/673	0.761 (0.262–2.213)	0.616	6/628	8/711	1.239 (0.426–3.606)	0.695
Relapse								
–	243/661	314/673	1.262 (1.034–1.541)	0.022	236/628	317/711	1.204 (0.985–1.472)	0.069
+	9/661	21/673	2.332 (1.058–5.138)	0.036	18/628	12/711	0.571 (0.273–1.198)	0.139

ALL, acute lymphoblastic leukemia; WBC, white blood cell; MRD, minimal residual disease.
[a]Adjusted for age and gender.
-: no ALL relapse.
+: ALL relapse.

2.112, p < 0.001) on days 15–19, day 33 (adjusted OR = 2.082, 95% CI = 1.603–2.688, p < 0.001), and week 12 (adjusted OR = 2.704, 95% CI = 2.153–3.397, p < 0.001) after induced therapy with MRD ≥ 0.01% on days 15–19 (adjusted OR = 1.952, 95% CI = 1.537–2.479, p < 0.001) and day 33 (adjusted OR = 1.729, 95% CI = 1.144–2.613, p = 0.009), with MRD < 0.01% on days 15–19 (adjusted OR = 1.486, 95% CI = 1.190–1.854, p < 0.001), day 33 (adjusted OR = 1.677, 95% CI = 1.391–2.023, p < 0.001), and week 12 (adjusted OR = 1.710, 95% CI = 1.428–3.397, p < 0.001) after induced chemotherapy, with relapse (adjusted OR = 2.332, 95% CI = 1.058–5.138, p = 0.036) and no relapse (adjusted OR = 1.262, 95% CI = 1.034–1.541, p = 0.022).

NSUN4 rs10252 AG/GG also increased ALL risk in children of age ≥ 120 months (adjusted OR = 2.056, 95% CI = 1.184–3.570, p = 0.010), normal WBC number (adjusted OR = 1.286, 95% CI = 1.022–1.619, p = 0.032), middle risk (adjusted OR = 1.285, 95% CI = 1.019–1.621, p = 0.034), non-gene fusion (adjusted OR = 1.684, 95% CI = 1.169–2.428, p = 0.005), primitive/naïve lymphocyte <5% on days 15–19 (adjusted OR = 1.281, 95% CI = 1.002–1.837, p = 0.048), MRD ≥ 0.01% on days 15–19 (adjusted OR = 1.264 95% CI = 1.002–1.594 p = 0.048), and MRD < 0.01% (adjusted OR = 1.256, 95% CI = 1.044–1.512, p = 0.016) after induced chemotherapy.

Haplotype analysis of SNPs in m5C methyltransferase coding gene correlated with pediatric ALL susceptibility

Furtherly, whether the haplotypes of *NOL1* rs3764909, *NSUN3* rs7653521, *NSUN4* rs10252, *NSUN5* rs1880948, and *NSUN6* rs3740102 are linked to pediatric ALL susceptibility were evaluated. The wild-type allele CAGTA was considered as the reference group The results showed that children with haplotypes CCGTG (adjusted OR = 2.035, 95% CI = 1.095–3.782, p = 0.025) and ACATA (adjusted OR = 3.169, 95% CI = 1.455–6.899, p = 0.004) would have enhanced ALL susceptibility (Table 3).

The influence of SNPs on the effect of different treatment strategies based on MRD levels

The MRD in the marrow of pediatric ALL samples with different *NOL1* rs3764909 and *NSUN4* rs10252 alleles after treatment with Chinese Children Cancer Group chemotherapeutics (CCCGs) or South China Children Leukemia Group chemotherapeutics (SCCLGs) was detected. The differences between varieties of alleles were estimated. Unfortunately, we did not identify the association between rs3764909 or rs10252 varieties of alleles and the sensitivity to CCCG treatment or SCCLG treatment in ALL children (Table 4).

Discussion

In this case–control study, the possible relationship of m5C methyltransferase coding gene polymorphisms with pediatric ALL risk from a population in southern China was explored. The results discovered that two of the five selected SNPs, *NOL1* rs3764909 G>A and *NSUN4* rs10252 G>A, were associated with increased pediatric ALL, and the other m5C methyltransferase coding genes SNPs were not related to pediatric ALL risk. This is the first study on the association between m5C methyltransferase coding gene polymorphisms and pediatric ALL susceptibility.

TABLE 3 Association between inferred haplotypes of the m5C-related genes and pediatric ALL risk.

Haplotypes	Cases (n = 1,594)	Controls (n = 2,644)	Crude OR (95% CI)	p	Adjusted OR (95% CI)	p
	No.%	No.%				
CAGTA	386 (24.22)	708 (26.78)	1.000		1.000	
ACGTG	14 (0.88)	18 (0.68)	0.984 (0.662–1.463)	0.936	0.988 (0.664–1.469)	0.951
CAGTG	53 (3.95)	106 (4.01)	1.031 (0.650–1.732)	0.812	1.065 (0.653–1.738)	0.801
CAATG	20 (1.25)	42 (1.59)	0.850 (0.443–1.634)	0.627	0.861 (0.448–1.655)	0.653
AAGTG	10 (0.63)	28 (1.06)	0.638 (0.282–1.441)	0.280	0.641 (0.284–1.447)	0.284
AAATG	15 (0.94)	32 (1.21)	0.837 (0.407–1.720)	0.628	0.844 (0.411–1.735)	0.644
ACATG	13 (0.82)	26 (0.98)	0.893 (0.415–1.920)	0.772	0.897 (0.417–1.929)	0.781
CCATG	29 (1.82)	34 (1.29)	1.523 (0.817–2.840)	0.186	1.531 (0.821–2.855)	0.180
CCGTA	68 (4.27)	91 (3.44)	1.334 (0.816–2.181)	0.250	1.342 (0.821–2.194)	0.241
ACGTA	10 (0.63)	25 (0.95)	0.714 (0.313–1.630)	0.424	0.715 (0.313–1.631)	0.425
CCGTG	34 (2.13)	30 (1.13)	2.024 (1.089–3.760)	0.026	2.035 (1.095–3.782)	0.025
CAATA	75 (4.71)	135 (5.11)	0.992 (0.619–1.590)	0.974	0.999 (0.623–1.601)	0.997
AAGTA	19 (1.19)	50 (1.89)	0.679 (0.355–1.299)	0.242	0.683 (0.357–1.308)	0.260
AAATA	18 (1.13)	25 (0.95)	1.286 (0.630–2.626)	0.490	1.282 (0.628–2.618)	0.495
ACATA	23 (1.44)	13 (0.49)	3.158 (1.451–6.876)	0.004	3.169 (1.455–6.899)	0.004
CCATA	23 (1.44)	47 (1.78)	0.874 (0.467–1.634)	0.673	0.874 (0.468–1.634)	0.674
CCGCG	53 (3.32)	60 (2.27)	1.577 (0.930–2.676)	0.091	0.594 (0.940–2.706)	0.084
ACGCG	35 (2.20)	47 (1.78)	1.330 (0.746–2.370)	0.334	1.333 (0.748–2.377)	0.330
CAGCG	45 (2.82)	60 (2.27)	1.339 (0.780–2.299)	0.289	1.350 (0.786–2.319)	0.276
CAACG	44 (2.76)	87 (3.29)	0.903 (0.536–1.525)	0.703	0.912 (0.540–1.540)	0.731
AAGCG	23 (1.44)	47 (1.78)	0.874 (0.467–1.634)	0.673	0.878 (0.469–1.641)	0.682
AAACG	30 (1.88)	58 (2.19)	0.924 (0.517–1.650)	0.789	0.930 (0.520–1.662)	0.807
ACACG	56 (3.51)	69 (2.61)	1.449 (0.864–2.430)	0.159	1.461 (0.872–2.451)	0.150
CCACG	70 (4.39)	96 (3.63)	1.302 (0.800–2.120)	0.289	1.302 (0.800–2.120)	0.289
CCGCA	60 (3.76)	80 (3.03)	1.339 (0.809–2.219)	0.257	1.343 (0.811–2.225)	0.252
ACGCA	32 (2.01)	33 (1.25)	1.732 (0.936–3.205)	0.081	1.735 (0.937–3.211)	0.080
CAGCA	151 (9.47)	244 (9.23)	1.105 (0.720–1.697)	0.648	1.111 (0.723–1.706)	0.631
CAACA	54 (3.39)	112 (4.24)	0.861 (0.523–1.417)	0.556	0.864 (0.525–1.421)	0.564
AAGCA	18 (1.13)	54 (2.04)	0.596 (0.310–1.145)	0.120	0.600 (0.312–1.154)	0.126
AAACA	24 (1.51)	60 (2.27)	0.714 (0.390–1.309)	0.276	0.720 (0.393–1.320)	0.289
ACACA	37 (2.32)	52 (1.97)	1.271 (0.721–2.238)	0.407	1.278 (0.726–2.251)	0.396
CCACA	42 (2.63)	75 (2.84)	0.928 (0.639–1.360)	0.701	0.922 (0.629–1.353)	0.679

In recent years, it has been reported that epigenetic changes, including DNA methylation, RNA methylation, histone modification, and non-coding RNAs, can promote the progression of ALL (18). Several lines of data have introduced m5C modification as an important regulator in post-transcription. In the study of carcinogenesis, m5C-modified genes have been reported to be associated with a variety of cancers, including bladder cancer (19), hepatocellular carcinoma

TABLE 4 The influence of m5C-related gene polymorphisms on sensitivity to different treatment strategies based on MRD levels.

SNP	Variables	Genotype	MRD in marrow (%, 19 days)				MRD in marrow (%, 33 days)				MRD in marrow (%, 12 weeks)			
			Case (%)		p[a]	Adjusted OR [a]	Case (%)		p[a]	Adjusted OR [a]	Case (%)		p[a]	Adjusted OR [a]
			<0.01	≥0.01		(95% CI)	<0.01	≥0.01		(95% CI)	<0.01	≥0.01		(95% CI)
rs3764909	CCCG-	AA	10 (13.70)	109 (34.71)			15 (11.36)	30 (37.04)			7 (58.33)	3 (25.00)		
	ALL-2015	AC/CC	63 (86.30)	205 (65.29)	0.233	0.682 (0.364–1.279)	117 (88.64)	51 (62.96)	0.078	1.514 (0.954–2.403)	5 (41.67)	9 (75.00)	0.737	1.083 (0.679–1.728)
	SCCLG-	AA	3 (60.00)	7 (21.21)			1 (20.00)	3 (23.08)			0 (0.00)	1 (50.00)		
	ALL-2016	AC/CC	2 (40.00)	26 (78.79)	0.869	1.046 (0.615–1.779)	4 (80.00)	10 (76.92)	0.412	1.215 (0.763–1.934)	2 (100.00)	1 (50.00)	0.156	1.370 (0.887–2.116)
rs10252	CCCG-	AA	27 (36.99)	131 (41.99)			45 (34.09)	42 (51.82)			4 (33.33)	6 (50.00)		
	ALL-2015	AG/GG	46 (63.01)	181 (58.01)	0.813	0.927 (0.494–1.739)	87 (65.91)	39 (48.15	0.333	0.802 (0.513–1.254)	8 (66.67)	6 (50.00)	0.823	1.054 (0.565–1.669)
	SCCLG-	AA	2 (40.00)	13 (40.63)			3 (60.00)	6 (46.15)			2 (100.00)	0		
	ALL-2016	AG/GG	3 (60.00)	19 (59.38)	0.939	0.980 (0.574–1.670)	2 (40.00)	7 (53.85)	0.575	1.143 (0.716–1.825)	0	2 (100.00)	0.954	>999.999 (<0.001, >999.999)

CCCG, Chinese Children Cancer Group; SCCLG, South China Children Leukemia Group; MRD, minimal residual disease; SNP, single-nucleotide polymorphism.
[a]Adjusted for age and gender.

10.3389/fonc.2022.1082525

(20), glioblastoma multiforme (21), and leukemia (22). However, limited pieces of evidence have focused on the function of polymorphisms of m5C genes on disease susceptibility. There is only one available study on the epidemiological assessment of SNPs in the m5C modification core gene and cancer. In July of this year, a case–control study was performed and revealed that two SNPs of YBX1 gene, rs10890208 and rs3862218, may predict a reduction by using the Cox regression model to analyze the association between 13 candidate SNPs of the m5C modifier gene and OS of CRC after chemotherapy (17).

Our study identified that *NOL1* rs3764909 and *NSUN4* rs10252 variants could contribute to the increased pediatric ALL risk. *NOL1* and *NSUN4* are important methyltransferases involved in m5C RNA modification (14). Similar to m6A methylation modification, m5C RNA modification can participate in other biological processes including cell growth, proliferation, apoptosis, and differentiation by affecting RNA translation, nuclear export, and stability (23). *NOL1*, one of the m5C methyltransferases, can generate m5C at C72 of tRNA (24, 25). Hong et al. demonstrated that *NOL1* could bind to the T-cell factor binding element of the cyclin D1 gene promoter and enhance transcriptional expression (26). Interestingly, telomerase can also interact with *NOL1* to affect the transcription of the cyclin D1 gene. *NOL1* can promote tumor proliferation by activating cyclins (26). *NOL1*-E2A fusion was regarded as the pathogenesis of acute leukemia in a case report (27). *NOL1* was also reported to promote hepatocellular carcinoma cell proliferation by TGF-β1/hPVT1/NOP2 pathway (28). *NSUN4* is located at chr1 1p33, as the "writer" of m5C, involved in rRNA methylation. It can mediate mitochondrial protein synthesis by regulating the assembly processing and maturation of mt-ribosome (24, 29). It has been shown to be involved in tumor effects. *NSUN4* promotes the malignant progression of hepatocellular carcinoma (30). *NOL1* and *NSUN4* polymorphisms may be involved in tumor risk-related biological functions by affecting m5C modification of coding and non-coding RNAs (24, 31).

In this study, we found that *NOL1* rs3764909 C>A and *NSUN4* rs10252 G>A were associated with increased ALL susceptibility. *NOL1* has been found to be associated with the pathogenesis of leukemia (27), so *NOL1* SNP variants may contribute to the development of ALL. *NSUN4* can affect tumorigenesis by affecting mitochondrial protein synthesis (24). *NSUN4* rs10252 variants may regulate mitochondrial protein synthesis in ALL cells and increase the risk of ALL.

However, there are some limitations to this study. On the one hand, we did not perform independent experimental studies to verify the relationship between selected SNPs and specific risk factors in children with leukemia. On the other hand, for rs3764909 and rs10252, deeply functional verifications are needed to explain the mechanisms of *NOL1* and *NSUN4* in ALL.

In conclusion, *NOL1* rs3764909 and *NSUN4* rs10252 variants are associated with increased ALL tumor susceptibility. The specific mechanisms by which *NOL1* and *NSUN4* polymorphisms are involved in pediatric ALL susceptibility require further study. Genetic variants in m5C modification coding genes were associated with enhanced pediatric ALL susceptibility and suggested that *NOL1* and *NSUN4* gene polymorphisms might be a potential liquid biopsy biomarker for pediatric ALL.

Data availability statement

The original contributions presented in the study are included in the article/Supplementary material. Further inquiries can be directed to the corresponding author.

Ethics statement

The studies involving human participants were reviewed and approved by Guangzhou Women and Children's Medical Center. Written informed consent to participate in this study was provided by the participants' legal guardian/next of kin.

Author contributions

XPL and HJ contributed to the conception and design of the study. XW and DD wrote the first draft of the manuscript. DD and MC extracted genomic DNA. XW, YY and SL conducted Taqman PCR. AL and XDL collected samples. XZ performed the statistical analysis. XPL revised the manuscript. All authors contributed to the manuscript revision and read and approved the submitted version.

Funding

Guangzhou Municipal Science and Technology Project (202201020603 and 202102010262) and Guangzhou Municipal Clinical Featured Technology Project (2019TS56).

Acknowledgments

We thank the Clinical Biological Resource Bank of Guangzhou Women and Children's Medical Center for providing part of the clinical samples.

Conflict of interest

The authors declare that the research was conducted in the absence of any commercial or financial relationships that could be construed as a potential conflict of interest.

Publisher's note

All claims expressed in this article are solely those of the authors and do not necessarily represent those of their affiliated organizations, or those of the publisher, the editors and the reviewers. Any product that may be evaluated in this article, or claim that may be made by its manufacturer, is not guaranteed or endorsed by the publisher.

Supplementary material

The Supplementary Material for this article can be found online at: https://www.frontiersin.org/articles/10.3389/fonc.2022.1082525/full#supplementary-material

References

1. Hunger SP, Mullighan CG. Redefining ALL classification: toward detecting high-risk ALL and implementing precision medicine. *Blood* (2015) 125:3977–87. doi: 10.1182/blood-2015-02-580043

2. Iacobucci I, Mullighan CG. Genetic basis of acute lymphoblastic leukemia. *J Clin Oncol Off J Am Soc Clin Oncol* (2017) 35:975–83. doi: 10.1200/JCO.2016.70.7836

3. Pui C, Yang JJ, Hunger SP, Pieters R, Schrappe M, Biondi A, et al. Childhood acute lymphoblastic leukemia: Progress through collaboration. *J Clin Oncol Off J Am Soc Clin Oncol* (2015) 33:2938–48. doi: 10.1200/JCO.2014.59.1636

4. Vrooman LM, Silverman LB. Treatment of childhood acute lymphoblastic leukemia: Prognostic factors and clinical advances. *Curr Hematol Malig Rep* (2016) 11:385–94. doi: 10.1007/s11899-016-0337-y

5. Hunger SP, Mullighan CG. Acute lymphoblastic leukemia in children. *N Engl J Med* (2015) 373:1541–52. doi: 10.1056/NEJMra1400972

6. Papaemmanuil E, Hosking FJ, Vijayakrishnan J, Price A, Olver B, Sheridan E, et al. Loci on 7p12.2, 10q21.2 and 14q11.2 are associated with risk of childhood acute lymphoblastic leukemia. *Nat Genet* (2009) 41:1006–10. doi: 10.1038/ng.430

7. Perez-Andreu V, Roberts KG, Harvey RC, Yang W, Cheng C, Pei D, et al. Inherited GATA3 variants are associated with ph-like childhood acute lymphoblastic leukemia and risk of relapse. *Nat Genet* (2013) 45:1494–98. doi: 10.1038/ng.2803

8. Treviño LR, Yang W, French D, Hunger SP, Carroll WL, Devidas M, et al. Germline genomic variants associated with childhood acute lymphoblastic leukemia. *Nat Genet* (2009) 41:1001–05. doi: 10.1038/ng.432

9. You C, Dai X, Wang Y. Position-dependent effects of regioisomeric methylated adenine and guanine ribonucleosides on translation. *Nucleic Acids Res* (2017) 45:9059–67. doi: 10.1093/nar/gkx515

10. Weng H, Huang H, Wu H, Qin X, Zhao BS, Dong L, et al. METTL14 inhibits hematopoietic Stem/Progenitor differentiation and promotes leukemogenesis *via* mRNA m(6)A modification. *Cell Stem Cell* (2018) 22:191–205. doi: 10.1016/j.stem.2017.11.016

11. Luo A, Yang L, Li M, Cai M, Huang A, Liu X, et al. Genetic variants in METTL14 are associated with the risk of acute lymphoblastic leukemia in southern Chinese children: A five-center case-control study. *Cancer Manag Res* (2021) 13:9189–200. doi: 10.2147/CMAR.S335925

12. Liu X, Huang L, Huang K, Yang L, Yang X, Luo A, et al. Novel associations between METTL3 gene polymorphisms and pediatric acute lymphoblastic leukemia: A five-center case-control study. *Front Oncol* (2021) 11:635251. doi: 10.3389/fonc.2021.635251

13. Gao Y, Fang J. RNA 5-methylcytosine modification and its emerging role as an epitranscriptomic mark. *RNA Biol* (2021) 18:117–27. doi: 10.1080/15476286.2021.1950993

14. Li M, Tao Z, Zhao Y, Li L, Zheng J, Li Z, et al. 5-methylcytosine RNA methyltransferases and their potential roles in cancer. *J Transl Med* (2022) 20:214. doi: 10.1186/s12967-022-03427-2

15. Fu L, Guerrero CR, Zhong N, Amato NJ, Liu Y, Liu S, et al. Tet-mediated formation of 5-hydroxymethylcytosine in RNA. *J Am Chem Soc* (2014) 136:11582–85. doi: 10.1021/ja505305z

16. Yang X, Yang Y, Sun B, Chen Y, Xu J, Lai W, et al. 5-methylcytosine promotes mRNA export - NSUN2 as the methyltransferase and ALYREF as an m(5)C reader. *Cell Res* (2017) 27:606–25. doi: 10.1038/cr.2017.55

17. Chen S, Cao X, Ben S, Zhu L, Gu D, Wu Y, et al. Genetic variants in RNA m(5) c modification genes associated with survival and chemotherapy efficacy of colorectal cancer. *Cancer Med* (2022). doi: 10.1002/cam4.5018

18. Cruz-Rodriguez N, Combita AL, Zabaleta J. Epigenetics in hematological malignancies. *Methods Mol Biol (Clifton NJ)* (2018) 1856:87–101. doi: 10.1007/978-1-4939-8751-1_5

19. Chen X, Li A, Sun B, Yang Y, Han Y, Yuan X, et al. 5-methylcytosine promotes pathogenesis of bladder cancer through stabilizing mRNAs. *Nat Cell Biol* (2019) 21:978–90. doi: 10.1038/s41556-019-0361-y

20. Yang X, Yang F, Lan L, Wen N, Li H, Sun X. Diagnostic and prognostic value of m5C regulatory genes in hepatocellular carcinoma. *Front Genet* (2022) 13:972043. doi: 10.3389/fgene.2022.972043

21. Zhou H, Meng M, Wang Z, Zhang H, Yang L, Li C, et al. The role of m5C-related lncRNAs in predicting overall prognosis and regulating the lower grade glioma microenvironment. *Front Oncol* (2022) 12:814742. doi: 10.3389/fonc.2022.814742

22. Xue C, Zhao Y, Li L. Advances in RNA cytosine-5 methylation: detection, regulatory mechanisms, biological functions and links to cancer. *Biomark Res* (2020) 8:43. doi: 10.1186/s40364-020-00225-0

23. Dominissini D, Rechavi G. 5-methylcytosine mediates nuclear export of mRNA. *Cell Res* (2017) 27:717–19. doi: 10.1038/cr.2017.73

24. Lenarčič T, Jaskolowski M, Leibundgut M, Scaiola A, Schönhut T, Saurer M, et al. Stepwise maturation of the peptidyl transferase region of human mitoribosomes. *Nat Commun* (2021) 12:3671. doi: 10.1038/s41467-021-23811-8

25. Li J, Li H, Long T, Dong H, Wang E, Liu R. Archaeal NSUN6 catalyzes m5C72 modification on a wide-range of specific tRNAs. *Nucleic Acids Res* (2019) 47:2041–55. doi: 10.1093/nar/gky1236

26. Hong J, Lee JH, Chung IK. Telomerase activates transcription of cyclin D1 gene through an interaction with *NOL1*. *J Cell Sci* (2016) 129:1566–79. doi: 10.1242/jcs.181040

27. Zhong C, Prima V, Liang X, Frye C, McGavran L, Meltesen L, et al. E2A-ZNF384 and *NOL1*-E2A fusion created by a cryptic t(12;19)(p13.3; p13.3) in acute leukemia. *Leukemia* (2008) 22:723–29. doi: 10.1038/sj.leu.2405084

28. Wang F, Yuan J, Wang S, Yang F, Yuan S, Ye C, et al. Oncofetal long noncoding RNA PVT1 promotes proliferation and stem cell-like property of hepatocellular carcinoma cells by stabilizing NOP2. *Hepatol (Baltimore Md)* (2014) 60:1278–90. doi: 10.1002/hep.27239

29. Cámara Y, Asin-Cayuela J, Park CB, Metodiev MD, Shi Y, Ruzzenente B, et al. MTERF4 regulates translation by targeting the methyltransferase *NSUN4* to the mammalian mitochondrial ribosome. *Cell Metab* (2011) 13:527–39. doi: 10.1016/j.cmet.2011.04.002

30. Cui M, Qu F, Wang L, Liu X, Yu J, Tang Z, et al. m5C RNA methyltransferase-related gene *NSUN4* stimulates malignant progression of hepatocellular carcinoma and can be a prognostic marker. *Cancer Biomark A Dis Markers* (2022) 33:389–400. doi: 10.3233/CBM-210154

31. Kong W, Biswas A, Zhou D, Fiches G, Fujinaga K, Santoso N, et al. Nucleolar protein NOP2/NSUN1 suppresses HIV-1 transcription and promotes viral latency by competing with tat for TAR binding and methylation. *PloS Pathog* (2020) 16:e1008430. doi: 10.1371/journal.ppat.1008430

frontiers | Frontiers in Oncology

TYPE Original Research
PUBLISHED 13 January 2023
DOI 10.3389/fonc.2022.1083570

OPEN ACCESS

EDITED BY
Jing He,
Guangzhou Medical University, China

REVIEWED BY
Zhen Dong,
Southwest University, China
Yan-fang Tao,
Children's Hospital of Soochow University, China

*CORRESPONDENCE
Jun Zhang
surgjun@gmail.com

SPECIALTY SECTION
This article was submitted to Pediatric Oncology, a section of the journal Frontiers in Oncology

RECEIVED 29 October 2022
ACCEPTED 22 December 2022
PUBLISHED 13 January 2023

CITATION
Wu Y and Zhang J (2023) Study on differentially expressed genes between stage M and stage MS neuroblastoma. *Front. Oncol.* 12:1083570. doi: 10.3389/fonc.2022.1083570

Study on differentially expressed genes between stage M and stage MS neuroblastoma

Yuying Wu and Jun Zhang*

Department of Surgical Oncology Children's Hospital of Chongqing Medical University, National Clinical Research Center for Child Health and Disorders, Ministry of Education Key Laboratory of Child Development and Disorders, Chongqing Key Laboratory of Pediatrics, Chongqing, China

Objective: To search for the DEGs between stage MS NB and stage M NB and speculate the possible mechanism of spontaneous regression of stage MS NB.

Materials and methods: The NB datasets GSE49710 and GSE45547 in the GEO database were selected to screen the DEGs between children with NB stage MS vs. stage M, < 18 months. GO enrichment and KEGG pathway analysis of DEGs was performed using DAVID. The intersecting genes among DEGs and RCD-related genes were selected, and their survival roles and functions were assessed. We then used the collected clinical samples to validate the expression of these genes at the protein level using IHC methods and further analysis to explore their role.

Results: BIRC5, SLCO4A1, POPDC3, and HK2 were found to be downregulated in stage MS NB and related to apoptosis. BIRC5 and HK2 also participate in autophagy. The TF gene is upregulated in stage MS NB and related to ferroptosis. The above five genes are closely related to the survival of children with NB. And the expression levels of all five genes at the protein level were verified by IHC to be consistent with the results of the preliminary screening described above.

Conclusion: BIRC5, SLCO4A1, POPDC3, HK2 and TF are expected to become new important indicators to predict the prognosis of NB and can be used as the basis for further explored the benign prognosis and spontaneous regression mechanism of stage MS NB.

KEYWORDS

neuroblastoma, stage MS, DEGs, immunohistochemistry, apoptosis, ferroptosis

Abbreviations: NB, neuroblastoma; RCD, regulated cell death; MSigDB, the Molecular Signatures Database; HADb, Human Autophagy Database; DEG, differentially expressed genes; GEO, the Gene Expression Omnibus; DAVID, The Database for Annotation, Visualization and Integrated Discovery; GO, Gene Ontology; KEGG, Kyoto Encyclopedia of Genes and Genome; BP, biological process; CC, cellular component; MF, molecular function; K-M, Kaplan–Meier; IHC, Immunohistochemistry; IOD, Integrated Optical Density.

Introduction

Neuroblastoma (NB) is the most common extracranial solid tumor in children. It most often occurs in the adrenal gland, accounting for approximately 15% of all pediatric cancer-related deaths (1, 2). Although active multimodal treatment is adopted, the prognosis of children in different stages of disease still varies greatly (3). At present, it is generally believed that children with distant metastasis often have a poor prognosis. Nevertheless, there is a special stage–stage MS–that exhibits a phenomenon of spontaneous regression and a good prognosis (4).

To date, it is believed that the spontaneous regression of stage MS NB may involve the following mechanisms: (1) neurotrophin deficiency, (2) telomerase inactivation, (3) humoral or cellular immunity and (4) changes in epigenetic regulation(4). However, these mechanisms are still in the preliminary research stage, and the spontaneous regression of stage MS NB has not been fully explained.

The modes of cell death include accidental cell death and regulatory cell death (RCD). At present, many evidences show that RCD is the main factor of cell death, which is a spontaneous mode of cell death, including apoptosis, autophagy, ferroptosis and other modes, and is closely related to tumor progression (5, 6). Here, we speculate that the spontaneous regression of stage MS NB may be related to RCD.

Materials and methods

Search for RCD-related genes

The keywords “apoptosis”, “autophagy”, “ferroptosis”, “pyroptosis”, and “necroptosis” were entered into the Molecular Signatures Database (MSigDB) to search for RCD-related genes. We searched for additional autophagy-related genes in a dedicated Human Autophagy Database (HADb) and found additional ferroptosis-related genes on the FerrDb website (http://www.zhounan.org/ferrdb/), which is a database with information on regulators and markers of ferroptosis and ferroptosis-disease associations (7).

Identification of shared differentially expressed genes (DEGs)

Two NB datasets GSE49710 and GSE45547 were selected from the Gene Expression Omnibus (GEO) database. There were 498 NB samples in the GSE49710 dataset, which was submitted by Wang C et al. (8). There were 649 NB samples in GSE45547, which was submitted by Kocak H et al. (9). The two datasets are based on the platform GPL16876 Agilent-020382 Human Custom Microarray 44k (Feature Number version). We only included children with stage MS and stage M (<18 months) for DEG analysis to exclude age interference. The detailed dataset information of the two NB datasets is shown in Table 1.

Using the limma package in R software (version 4.1.2), DEGs between stage MS and stage M (<18 months) were screened in two datasets, and the parameters for judging the difference were set as adj. $P < 0.05$ and $|\log2FC| > 1$. The difference between upregulation and downregulation refers to stage MS relative to stage M. The network analysis tool Venny (https://bioinfogp.cnb.csic.es/tools/venny/index.html) was chosen, and the intersecting DEGs were obtained *via* a Venn diagram.

Functional analysis of common DEGs

The Database for Annotation, Visualization and Integrated Discovery (DAVID) online tool was used to conduct Gene Ontology (GO) enrichment analysis and Kyoto Encyclopedia of Genes and Genome (KEGG) pathway analysis on the screened common DEGs. The GO analysis included biological process (BP), cellular component (CC), and molecular function (MF) categories. Then, the enrichment results are visualized.

Survival analysis

The R2 (https://hgserver1.amc.nl/cgi-bin/r2/main.cgi) online website was used to analyze the effects of age variables and intersecting DEGs on the survival rate of children, determine the DEGs that are closely related to survival, and draw Kaplan–Meier (K-M) survival curves.

TABLE 1 Details for datasets from GEO.

GEO	Platform	Sample	Stage M (<18months)	Stage MS	Submission	Update	Author
GSE49710	GPL16876	NB	52	53	Aug9,2013	Oct15,2015	Zhang H
GSE45547	GPL16876	NB	66	78	Mar27,2013	Apr16,2013	Kocak H

Clinical materials and immunohistochemistry (IHC)

To determine DEGs expression in NB, we performed IHC staining of DEGs in the NB tissues of 21 children with M stage and 9 children with MS stage. The study, authorized by the ethics committee of Children's Hospital of Chongqing Medical University. NB tumor tissues were embedded in paraffin and severed into slices (4 mm). After dewaxing, hydration and antigen repair, each sample was titrated with five primary antibodies: Anti-BIRC5 (No.380719, ZENBIO, China), Anti-SLCO4A1 (No. YT3221, Immunoway), Anti-POPDC3 (No. 11800-1-AP, Proteintech), Anti-HK2 (No. R24552, ZENBIO, China) and Anti-TF (No. R25969, ZENBIO, China), respectively. Then incubated overnight at 4° C. Then the steps of incubation with the secondary antibody Goat anti-Rabbit IgG (No. PV-9001, ZSGB-BIO, China), DAB (No. ZLI-9018, ZSGB-BIO, China) staining and blocking were performed, and the staining effect was observed under the microscope. The mean Integrated Optical Density (IOD) value of each slice was determined using Image-Pro Plus 6.0 software. Three to five fields of view were taken for each slice and the average IOD value was taken as the final IOD value for that slice. Subsequently, the IOD values between the M and MS groups for each protein were tested for differences using Student's t test.

Results

The genes involved in RCD were selected

A total of 430 apoptosis gene sets which contained 790 apoptosis-related genes were retrieved from the MSigDB website, and one of them, M12113 (10), was selected. For autophagy-related genes, we selected the genes in all 20 gene sets retrieved from MSigDB, retrieved an additional 232 genes in the HADB database, deleted the duplicate genes, and finally identified 727 autophagy-related genes. A gene set which contains 40 ferroptosis-related genes (M39768) was retrieved from MSigDB. In addition, ferroptosis-related genes in the FerrDb website were downloaded, duplicate genes were deleted, and 275 ferroptosis-related genes were finally screened. MSigDB has only one pyroptosis gene set, M41804, which contains 27 pyroptosis genes. Finally, we retrieved the only necroptosis gene set, M24779, which contains 8 necroptosis genes.

Identification of the common DEGs

The NB expression microarray datasets GSE49710 and GSE45547 were background corrected and normalized, and the DEGs between stage MS and stage M (<18 months) samples in the two datasets were screened by using the limma package in R software. There were 563 DEGs, including 322 upregulated and 241 downregulated DEGs, in GSE49710. In GSE45547, there were 308 DEGs, of which 192 were upregulated and 116 were downregulated (Table 2). A volcano plot was made for these DEGs of the two datasets (Figures 1A, B). Then, the Venny website was used to intersect the upregulated DEGs and downregulated DEGs separately, and 172 common upregulated DEGs and 110 common downregulated DEGs between the two datasets were obtained (Figures 1C, D).

GO enrichment and KEGG pathway analysis of DEGs

To further understand the functions and pathways of the intersecting DEGs, we conducted GO enrichment and KEGG pathway analyses and visualized the results. In terms of BPs, DEGs were significantly enriched in the response to drug, pancreatic A cell differentiation, the response to xenobiotic stimulus and other processes (Figure 2A). In the CC category, DEGs were mainly involved in extracellular region, extracellular space, blood microparticle, endoplasmic reticulum lumen, etc. (Figure 2B). The analysis of MF showed that DEGs were mainly enriched in extracellular matrix structural constituents, extracellular matrix structural constituents conferring tensile strength, serine-type endopeptidase inhibitor activity, platelet-derived growth factor binding, etc. (Figure 2C). In addition, KEGG pathway analysis showed that DEGs were mainly involved in amebiasis, protein digestion and absorption, ECM-receptor interaction, the relaxin signaling pathway, and the AGE-RAGE signaling pathway in diabetes complications (Figure 2D).

Survival analysis based on the intersecting genes

We first compared the survival differences between children with stage MS NB and stage M (<18 months) NB in the two datasets. The results confirmed that there were definite survival differences between the two groups, which provided a basis for the selection and analysis of DEGs (Figures 3A, B). Then, we took the intersection of all DEGs and RCD genes (Table 3 for the results) to analyze the effects of these intersecting genes on survival. The results showed that the expression levels (grouped by median) of five genes (BIRC5, SLCO4A1, POPDC3, HK2, and TF) were closely

TABLE 2 DEGs screened from two datasets.

	Up-regulated	Down-regulated	Sum
GSE49710	322	241	563
GSE45547	192	116	308
Common genes	172	110	282

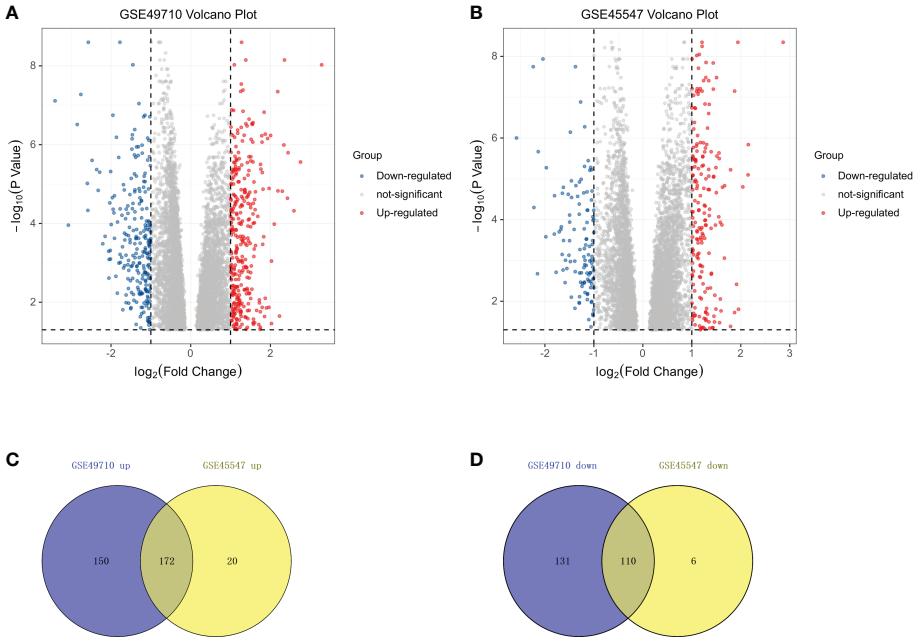

FIGURE 1
DEGs in two datasets from the GEO. **(A)** Volcano plots showing the DEGs in GSE49710. **(B)** Volcano plots showing the DEGs in GSE45547.The red dots represent upregulated genes, blue dots represent downregulated genes, and gray dots indicate genes with no significant differences. **(C)** Venn diagram showing the intersection of upregulated genes. **(D)** Venn diagram showing the intersection of downregulated genes. All DEGs are screened based on an Adjust P value < 0.05 and |Fold Change| > 1.

related to the survival of children in both datasets (the K-M survival curves are shown in Figures 4A–J). The heatmap of these five genes is shown in Figures 5A, B. Low expression levels of BIRC5, SLCO4A1, POPDC3 and HK2 are favorable factors in terms of the prognosis of children, while high expression of TF is a favorable factor. In addition, GO enrichment and KEGG pathway analysis of the above five genes showed that both TF and HK2 participate in the HIF-1 signaling pathway.

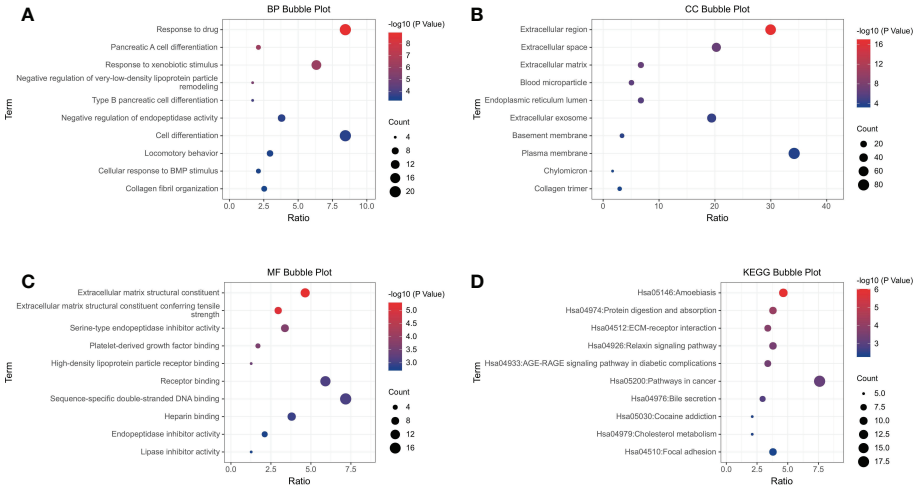

FIGURE 2
GO function and KEGG pathway analysis of 282 common DEGs. Analysis of **(A)** Biological Process, **(B)** Cellular Component, and **(C)** Molecular Function. **(D)** KEGG analysis showed the enriched pathways. Each functional section shows 10 terms.

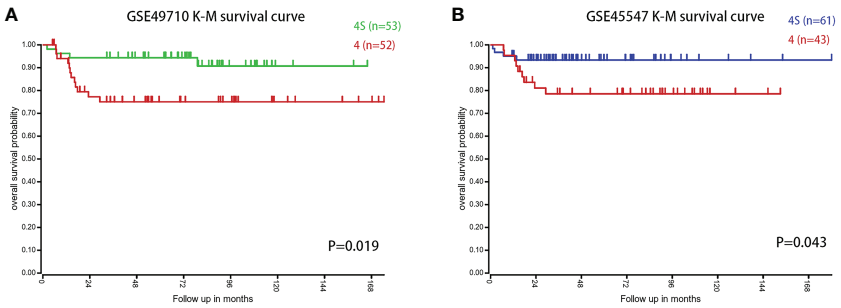

FIGURE 3
The survival difference between children with stage MS and stage M NB (<18 months) in the two datasets. **(A)** K-M survival curves of children with stage MS and stage M (<18 months) NB in GSE49710. **(B)** K-M survival curves of children with stage MS and stage M (<18 months) NB in GSE45547.

Detection of antibodies using IHC

In total, we collected a sample of 30 eligible children with NB, including 21 with stage M and 9 with stage MS. All children were ≤18 months of age and had intact preserved paraffin tissue sections. Slicing thickness of 4μm. Quantitative analysis of IHC showed that the expression of five genes, BIRC5, SLCO4A1, POPDC3, HK2 and TF, were significantly different in M- and MS-stage NB samples(P<0.05, Figure 6). Among them, BIRC5, SLCO4A1, POPDC3 and HK2 were significantly higher in the M-stage samples than in the MS-stage, while TF was significantly higher in the MS-stage samples, which is consistent with the results of the preliminary screening described above.

Discussion

Apoptosis is the most deeply studied RCD mode at present. The process of apoptosis eventually activates caspase protein, resulting in cell death (11). The weakening of apoptosis often leads to tumorigenesis, and the overexpression of antiapoptotic oncogenes such as BCL-2/BCL-XL, MCL1 or the IAP proteins is conducive to the survival of tumor cells (12). The results of our study showed that BIRC5, SLCO4A1, POPDC3, and HK2 were involved in the process of apoptosis.

BIRC5, also known as survivin, is the strongest inhibitor of apoptosis found thus far (13), and its main role is related to the inhibition of caspase activity (14). The expression of BIRC5 is downregulated during normal tissue development and cannot be detected in most final differentiated adult tissues (15). In a variety of tumors, such as ovarian cancer, breast cancer, colorectal cancer (16) and renal cell carcinoma (17), the expression is increased and is positively correlated with metastasis and a low survival rate. SLCO4A1 is proved to be highly expressed in colorectal cancer and affect prognosis (18), but its role in NB has not been studied. POPDC3 belongs to the Popeye domain containing (POPDC) family, and is a recently discovered cyclic 3′,5′-adenosine monophosphate (cAMP) effector protein (19). Recent studies have shown that the expression level of POPDC3 is closely related to the cell proliferation, metastasis and prognosis of a variety of cancers, especially gastric cancer, and can be used as a potential cancer treatment target (20–22). In addition, research on POPDC3 covers topics including muscular dystrophy, cardiac function and other aspects (23, 24); research on POPDC3 in NB is lacking, but this is a topic worthy of in-depth exploration. HK2, hexokinase 2, is an important glycolytic enzyme that catalyzes the conversion of glucose to glucose 6-phosphate. Studies have shown that the expression level and activity of HK2 in metastatic NB tumor tissues are higher than those in local NB tumor tissues, suggesting that HK2 plays an important

TABLE 3 Intersection genes of DEGs and RCD genes.

RCD	Count	Intersection with up-regulated DEG	Intersection with down-regulated DEG
apoptosis	790	AKAP7,MYLK,KANK1,MGST1	BIRC5,CDCA5,HK2,POPDC3,SLC18A3,SLCO4A1
autophagy	727	EXOC4,EPAS1,COL3A1,FN1,COL1A1	BIRC5,HK2,DYNC1I1
ferroptosis	275	TF,EPAS1,MAP3K5	/
pyroptosis	27	/	/
necroptosis	8	/	/

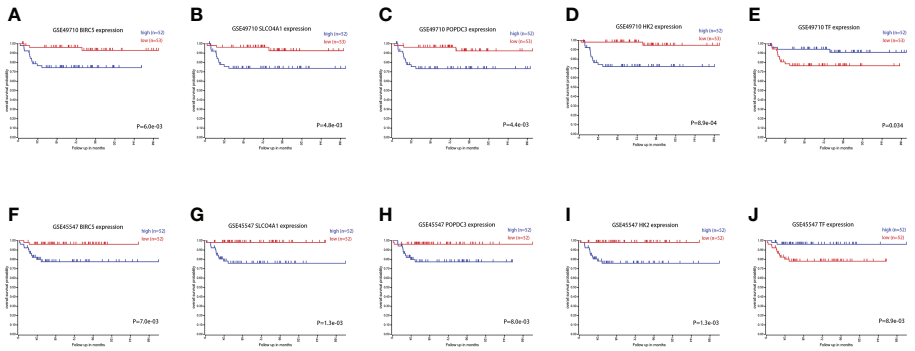

FIGURE 4
Survival curves of patients grouped by BIRC5, SLCO4A1, POPDC3, HK2 and TF expression in the two datasets. **(A–E)** The prognostic value of BIRC5, SLCO4A1, POPDC3, HK2 and TF in the GSE49710 dataset. **(F–J)** The prognostic value of BIRC5, SLCO4A1, POPDC3, HK2 and TF in the GSE45547 dataset. Gene expression levels are grouped by median.

role in the formation of the malignant phenotype of NB and affects the progression of the disease (25).

This study showed that BIRC5, SLCO4A1, POPDC3, and HK2 were significantly downregulated in stage MS NB and affected the survival rate of children, indicating that the low expression of these four genes is a factor conducive to tumor regression. All these factors are involved in the process of apoptosis. We propose that the spontaneous regression of stage MS NB is closely related to the process of apoptosis, and the above four genes play an important role in this process of apoptosis.

In addition, our results show that BIRC5 and HK2 are also involved in autophagy. Autophagy is a cellular pathway involved in the degradation of proteins and organelles, and it is the mechanism of cell survival under stress stimulation. Currently, autophagy is considered to play a dual role in cancer. It inhibits the growth of benign tumors but promotes the growth of advanced tumors. Many research groups have established autophagy as a potential therapeutic target for cancer (26). A study showed that some autophagy-related genes were differentially expressed between stage MS and stage M (<18 months) NB. The results showed that autophagy inhibited the progression and promoted the spontaneous regression of NB (27).

It is generally believed that apoptosis and autophagy are not completely isolated processes (28). BIRC5 is an important molecule connecting the two processes (29). BIRC5 is positively regulated by the AKT/mTOR pathway to inhibit autophagy and apoptosis and

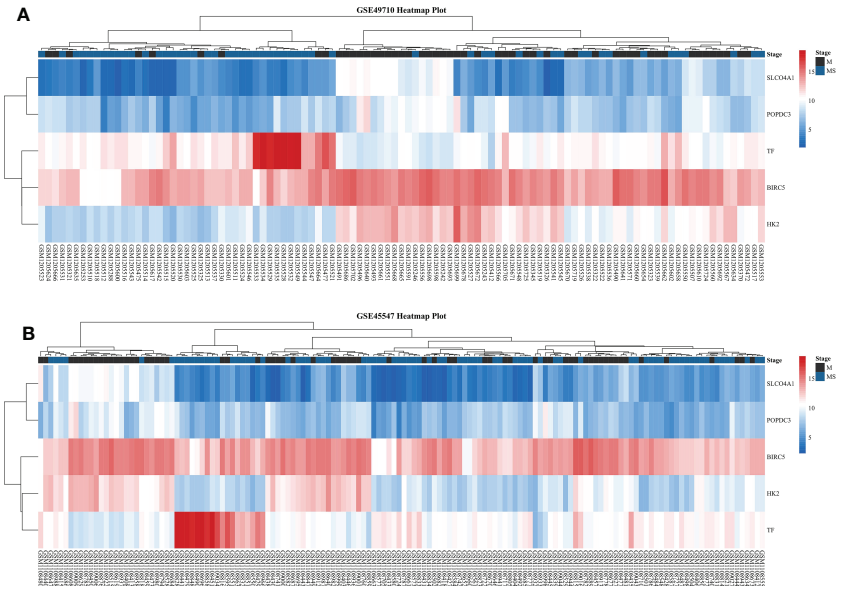

FIGURE 5
Heatmaps of five DEGs in two datasets. **(A)** Heatmap of five DEGs in GSE49710. **(B)** Heatmap of five DEGs in GSE45547. From red to blue, the expression level of the DEGs in the sample gradually decreases.

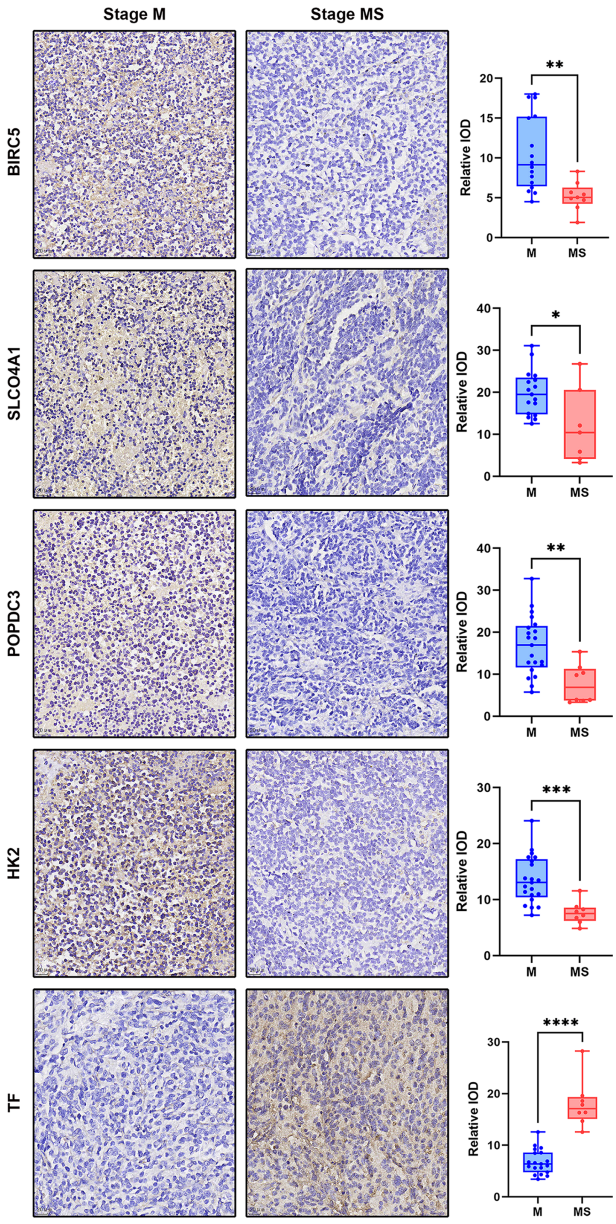

FIGURE 6
Display of IHC dyeing effect of DEGs and the dot plot of relative IOD values of each group. The magnification of the IHC images was 40×, scale bar=20μm. The dot plot shows the difference of IOD values between samples of each protein in M and MS stage. *p < 0.05, **p < 0.01, ***p < 0.001, ****p < 0.0001.

promote tumor cell survival (14). The degradation of BIRC5 releases bound beclin-1, enhances autophagy and induces cell death, which also shows that the increase in BIRC5 levels is closely related to the inhibition of autophagy (30). In addition, some studies have pointed out that HK2 plays the same role as BIRC5 and participates in the process of autophagy and apoptosis through the AKT/mTOR pathway. Targeting HK2 to treat cancer is also a promising strategy (31–33). This is consistent with our results (BIRC5 and HK2 are downregulated genes), so we speculate that the spontaneous regression of stage MS NB is likely to be related to the autophagy and apoptosis processes related to BIRC5 and HK2 because when the expression levels of BIRC5 and HK2 are low, the inhibition of apoptosis and autophagy by other factors will be relieved.

TF, transferrin, was the only gene upregulated in stage MS NB in our results. It is a key molecule involved in ferroptosis. Its function is to transport iron from the site where heme is absorbed and degraded to the site where heme is stored and utilized. TF and its receptor TFR can regulate the process of ferroptosis directly or indirectly (34).

Ferroptosis is a newly defined RCD mode that was first proposed by Scott J. Dixon and others in 2012 (35). Ferroptosis is associated with a variety of pathological conditions, such as acute tissue injury, infection, inflammation, cancer and neurodegeneration (36, 37). The molecules involved in ferroptosis include Nrf2, p53, heme oxygenase-1, FANCD2, and BECN1, and the role of ferroptosis in breast cancer, hepatocellular carcinoma, renal cancer and other diseases has been studied (38). Our study shows that the TF gene is differentially expressed between stage MS and stage M (<18 months) NB and affects the survival of children. We propose that the spontaneous regression of stage MS NB involves ferroptosis regulation and that TF plays an important role in this process.

GO enrichment and KEGG pathway analysis revealed that the DEGs were mainly involved in response to drug, response to xenobiotic stimulus and other processes, as well as in amebiasis, protein digestion and absorption, ECM-receptor interaction and other pathways. Among the above five DEGs that affect survival, both TF and HK2 are involved in the HIF-1 signaling pathway; TF is involved in the process of cell ferroptosis; and HK2 is involved in the processes of autophagy and apoptosis.

HIF-1 is a member of the hypoxia inducible factor protein family, which can help cells adapt to the hypoxic environment. HIF-1 is a signaling center, and its role in cancer has been fully described. Inhibiting HIF-1 is a promising treatment strategy for cancer and cancer-related inflammation (39, 40). The function of HIF-1 in NB has also been widely studied. The increased expression and activity of HIF-1 promotes the proliferation, invasion and migration of NB cells, which is positively correlated with the malignant degree of NB (41). Some studies have shown that HIF-1/HK2 can synergistically promote the development of breast cancer (42). However, this synergistic effect has not been studied in NB. In addition, in studies of different kinds of cells, it has been shown that an increase in HIF-1 levels can inhibit ferroptosis, and inactivation of this pathway can induce ferroptosis (43, 44). In osteoclasts, elevated HIF-1 expression can inhibit not only ferroptosis but also autophagy (45). Therefore, we think that the spontaneous regression of stage MS NB involves autophagy and ferroptosis regulated by TF, HK2 and the HIF-1 signaling pathway.

Summary

Our study showed that there were significant differences in the expression levels of BIRC5, SLCO4A1, POPDC3, HK2 and TF between stage MS and stage M (<18 months) NB. Survival analysis showed that they were closely related to the prognosis of children with NB. GO enrichment and KEGG pathway analyses of DEGs further revealed their functions and pathways. These genes may become potential markers for improving NB diagnosis, optimizing treatment and predicting prognosis. Since these genes are important genes involved in the RCD mode, they also provide a breakthrough point for further exploration of the spontaneous regression of stage MS NB. Moreover, there are few studies on the role of these genes in NB. It is necessary for us to further verify and explore the potential functions and pathways of these genes.

Data availability statement

The datasets presented in this study can be found in online repositories. The names of the repository/repositories and accession number(s) can be found in the article/supplementary material.

Ethics statement

The studies involving human participants were reviewed and approved by Children's Hospital of Chongqing Medical University. Written informed consent to participate in this study was provided by the participants' legal guardian/next of kin. Written informed consent was obtained from the minor(s)' legal guardian/next of kin for the publication of any potentially identifiable images or data included in this article.

Author contributions

All authors listed have made a substantial, direct, and intellectual contribution to the work, and approved it for publication.

Funding

All phases of this study were supported by a Nature Science Foundation of Chongqing Municipality grant (cstc2017jcyjAX0139).

Conflict of interest

The authors declare that the research was conducted in the absence of any commercial or financial relationships that could be construed as a potential conflict of interest.

Publisher's note

Abbreviations key

References

1. Swift CC, Eklund MJ, Kraveka JM, Alazraki AL. Updates in diagnosis, management, and treatment of neuroblastoma. *Radiographics* (2018) 38(2):566–80. doi: 10.1148/rg.2018170132

2. Zafar A, Wang W, Liu G, Wang X, Xian W, McKeon F, et al. Molecular targeting therapies for neuroblastoma: Progress and challenges. *Med Res Rev* (2021) 41(2):961–1021. doi: 10.1002/med.21750

3. Whittle SB, Smith V, Doherty E, Zhao S, McCarty S, Zage PE. Overview and recent advances in the treatment of neuroblastoma. *Expert Rev Anticancer Ther* (2017) 17(4):369–86. doi: 10.1080/14737140.2017.1285230

4. Brodeur GM. Spontaneous regression of neuroblastoma. *Cell Tissue Res* (2018) 372(2):277–86. doi: 10.1007/s00441-017-2761-2

5. Tang D, Kang R, Berghe TV, Vandenabeele P, Kroemer G. The molecular machinery of regulated cell death. *Cell Res* (2019) 29(5):347–64. doi: 10.1038/s41422-019-0164-5

6. Strasser A, Vaux DL. Cell death in the origin and treatment of cancer. *Mol Cell* (2020) 78(6):1045–54. doi: 10.1016/j.molcel.2020.05.014

7. Zhou N, Bao J. Ferrdb: A manually curated resource for regulators and markers of ferroptosis and ferroptosis-disease associations. *Database (Oxford)* (2020) 2020:baaa021. doi: 10.1093/database/baaa021

8. Wang C, Gong B, Bushel PR, Thierry-Mieg J, Thierry-Mieg D, Xu J, et al. The concordance between rna-seq and microarray data depends on chemical treatment and transcript abundance. *Nat Biotechnol* (2014) 32(9):926–32. doi: 10.1038/nbt.3001

9. Kocak H, Ackermann S, Hero B, Kahlert Y, Oberthuer A, Juraeva D, et al. Hox-C9 activates the intrinsic pathway of apoptosis and is associated with spontaneous regression in neuroblastoma. *Cell Death Dis* (2013) 4:e586. doi: 10.1038/cddis.2013.84

10. Wei JS, Song YK, Durinck S, Chen QR, Cheuk AT, Tsang P, et al. The mycn oncogene is a direct target of mir-34a. *Oncogene* (2008) 27(39):5204–13. doi: 10.1038/onc.2008.154

11. Tompkins. KD, Thorburn. A. Regulation of apoptosis by autophagy to enhance cancer therapy. *Yale J OF Biol AND Med* (2019) 92(4):707–18.

12. Carneiro BA, El-Deiry WS. Targeting apoptosis in cancer therapy. *Nat Rev Clin Oncol* (2020) 17(7):395–417. doi: 10.1038/s41571-020-0341-y

13. Hu F, Deng C, Zhou Y, Liu Y, Zhang T, Zhang P, et al. Multistage targeting and dual inhibiting strategies based on bioengineered tumor matrix microenvironment-mediated protein nanocages for enhancing cancer biotherapy. *Bioengineering Trans Med* (2022) 7(2):e10290. doi: 10.1002/btm2.10290

14. Cheung CHA, Chang YC, Lin TY, Cheng SM, Leung E. Anti-apoptotic proteins in the autophagic world: An update on functions of xiap, survivin, and Bruce. *J BioMed Sci* (2020) 27(1):31. doi: 10.1186/s12929-020-0627-5

15. Ju L, Zhang X, Deng Y, Han J, Yang J, Chen S, et al. Enhanced expression of survivin has distinct roles in adipocyte homeostasis. *Cell Death Dis* (2017) 8(1):e2533. doi: 10.1038/cddis.2016.439

16. Rödel F, Sprenger T, Kaina B, Liersch T, Rödel C, Fulda S, et al. Survivin as a Prognostic/Predictive marker and molecular target in cancer therapy. *Curr Medicinal Chem* (2012) 19(22):3679–88. doi: 10.2174/092986712801661040.

17. Carew JS, Espitia CM, Zhao W, Mita MM, Mita AC, Nawrocki ST. Targeting survivin inhibits renal cell carcinoma progression and enhances the activity of temsirolimus. *Mol Cancer Ther* (2015) 14(6):1404–13. doi: 10.1158/1535-7163.MCT-14-1036

18. Ban MJ, Ji SH, Lee CK, Bae SB, Kim HJ, Ahn TS, et al. Solute carrier organic anion transporter family member 4a1 (Slco4a1) as a prognosis marker of colorectal cancer. *J Cancer Res Clin Oncol* (2017) 143(8):1437–47. doi: 10.1007/s00432-017-2393-7

19. Brand T, Schindler R. New kids on the block: The popeye domain containing (Popdc) protein family acting as a novel class of camp effector proteins in striated muscle. *Cell Signal* (2017) 40:156–65. doi: 10.1016/j.cellsig.2017.09.015

20. Gingold-Belfer R, Kessler-Icekson G, Morgenstern S, Rath-Wolfson L, Zemel R, Boltin D, et al. The transition from gastric intestinal metaplasia to gastric cancer involves Popdc1 and Popdc3 downregulation. *Int J Mol Sci* (2021) 22 (10):5359. doi: 10.3390/ijms22105359

21. Luo. D, Lu. M-L, Zhao. G-F, Huang. H, Zheng. M-Y, Chang. J, et al. Reduced Popdc3 expression correlates with high risk and poor survival in patients with gastric cancer. *World J Gastroenterol* (2012) 18(19):2423–9. doi: 10.3748/wjg.v18.i19.2423

22. Amunjela JN, Tucker SJ. Popdc proteins as potential novel therapeutic targets in cancer. *Drug Discov Today* (2016) 21(12):1920–7. doi: 10.1016/j.drudis.2016.07.011

23. Vissing J, Johnson K, Topf A, Nafissi S, Diaz-Manera J, French VM, et al. Popdc3 gene variants associate with a new form of limb girdle muscular dystrophy. *Ann Neurol* (2019) 86(6):832–43. doi: 10.1002/ana.25620

24. Gingold-Belfer R, Bergman M, Alcalay Y, Schlesinger H, Aravot D, Berman M, et al. Popeye domain-containing 1 is down-regulated in failing human hearts. *Int J Mol Med* (2011) 27(1):25–31. doi: 10.3892/ijmm.2010.558

25. Botzer LE, Maman S, Sagi-Assif O, Meshel T, Nevo I, Yron I, et al. Hexokinase 2 is a determinant of neuroblastoma metastasis. *Br J Cancer* (2016) 114(7):759–66. doi: 10.1038/bjc.2016.26

26. Onorati AV, Dyczynski M, Ojha R, Amaravadi RK. Targeting autophagy in cancer. *Cancer* (2018) 124(16):3307–18. doi: 10.1002/cncr.31335

27. Meng X, Li H, Fang E, Feng J, Zhao X. Comparison of stage 4 and stage 4s neuroblastoma identifies autophagy-related gene and lncrna signatures associated with prognosis. *Front Oncol* (2020) 10:1411. doi: 10.3389/fonc.2020.01411

28. Maiuri MC, Zalckvar E, Kimchi A, Kroemer G. Self-eating and self-killing: Crosstalk between autophagy and apoptosis. *Nat Rev Mol Cell Biol* (2007) 8 (9):741–52. doi: 10.1038/nrm2239

29. Lin TY, Chan HH, Chen SH, Sarvagalla S, Chen PS, Coumar MS, et al. Birc5/Survivin is a novel Atg12-Atg5 conjugate interactor and an autophagy-induced DNA damage suppressor in human cancer and mouse embryonic fibroblast cells. *Autophagy* (2020) 16(7):1296–313. doi: 10.1080/15548627.2019.1671643

30. Hagenbuchner J, Kiechl-Kohlendorfer U, Obexer P, Ausserlechner MJ. Birc5/Survivin as a target for glycolysis inhibition in high-stage neuroblastoma. *Oncogene* (2016) 35(16):2052–61. doi: 10.1038/onc.2015.264

31. Liu T, Ye P, Ye Y, Han B. Microrna-216b targets Hk2 to potentiate autophagy and apoptosis of breast cancer cells *Via* the mtor signaling pathway. *Int J Biol Sci* (2021) 17(11):2970–83. doi: 10.7150/ijbs.48933

32. Ciscato F, Ferrone L, Masgras I, Laquatra C, Rasola A. Hexokinase 2 in cancer: A prima Donna playing multiple characters. *Int J Mol Sci* (2021) 22 (9):4716. doi: 10.3390/ijms22094716

33. Roh JI, Kim Y, Oh J, Kim Y, Lee J, Lee J, et al. Hexokinase 2 is a molecular bridge linking telomerase and autophagy. *PloS One* (2018) 13(2):e0193182. doi: 10.1371/journal.pone.0193182

34. Zhang Y, Xia M, Zhou Z, Hu X, Wang J, Zhang M, et al. P53 promoted ferroptosis in ovarian cancer cells treated with human serum incubated-superparamagnetic iron oxides. *Int J Nanomedicine* (2021) 16:283–96. doi: 10.2147/IJN.S282489

35. Dixon SJ, Lemberg KM, Lamprecht MR, Skouta R, Zaitsev EM, Gleason CE, et al. Ferroptosis: An iron-dependent form of nonapoptotic cell death. *Cell* (2012) 149(5):1060–72. doi: 10.1016/j.cell.2012.03.042

36. Tang D, Kroemer G. Ferroptosis. *Curr Biol* (2020) 30(21):R1292–R7. doi: 10.1016/j.cub.2020.09.068

37. Sun Y, Chen P, Zhai B, Zhang M, Xiang Y, Fang J, et al. The emerging role of ferroptosis in inflammation. *BioMed Pharmacother* (2020) 127:110108. doi: 10.1016/j.biopha.2020.110108

38. Xu T, Ding W, Ji X, Ao X, Liu Y, Yu W, et al. Molecular mechanisms of ferroptosis and its role in cancer therapy. *J Cell Mol Med* (2019) 23(8):4900–12. doi: 10.1111/jcmm.14511

39. Balamurugan K. Hif-1 at the crossroads of hypoxia, inflammation, and cancer. *Int J Cancer* (2016) 138(5):1058–66. doi: 10.1002/ijc.29519

40. Masoud GN, Li W. Hif-1alpha pathway: Role, regulation and intervention for cancer therapy. *Acta Pharm Sin B* (2015) 5(5):378–89. doi: 10.1016/j.apsb.2015.05.007

41. Chen S, Zhang M, Xing L, Wang Y, Xiao Y, Wu Y. Hif-1alpha contributes to proliferation and invasiveness of neuroblastoma cells *Via* shh signaling. *PloS One* (2015) 10(3):e0121115. doi: 10.1371/journal.pone.0121115

42. Cao L, Wang M, Dong Y, Xu B, Chen J, Ding Y, et al. Circular rna Circrnf20 promotes breast cancer tumorigenesis and warburg effect through mir-487a/Hif-1alpha/Hk2. *Cell Death Dis* (2020) 11(2):145. doi: 10.1038/s41419-020-2336-0

43. Yuan S, Wei C, Liu G, Zhang L, Li J, Li L, et al. Sorafenib attenuates liver fibrosis by triggering hepatic stellate cell ferroptosis *Via* hif-1α/Slc7a11 pathway. *Cell Proliferation* (2022) 55(1):e13158. doi: 10.1111/cpr.13158

44. Wu Y, Wang J, Zhao T, Chen J, Kang L, Wei Y, et al. Di-(2-Ethylhexyl) phthalate exposure leads to ferroptosis *Via* the hif-1α/Ho-1 signaling pathway in mouse testes. *J Hazardous Materials* (2022) 426:127807. doi: 10.1016/j.jhazmat.2021.127807

45. Ni S, Yuan Y, Qian Z, Zhong Z, Lv T, Kuang Y, et al. Hypoxia inhibits rankl-induced ferritinophagy and protects osteoclasts from ferroptosis. *Free Radic Biol Med* (2021) 169:271–82. doi: 10.1016/j.freeradbiomed.2021.04.027

frontiers | Frontiers in Oncology

TYPE Original Research
PUBLISHED 13 February 2023
DOI 10.3389/fonc.2023.1034292

OPEN ACCESS

EDITED BY
Jing He,
Guangzhou Medical University, China

REVIEWED BY
Prerana Jha,
All India Institute of Medical Sciences, India
Andrew Michael Donson,
University of Colorado Denver,
United States
Markus Bookland,
Connecticut Children's Medical Center,
United States

*CORRESPONDENCE
Namik Kaya
nkaya@kfshrc.edu.sa
namikkaya@gmail.com
Dilek Colak
dkcolak@gmail.com

†These authors have contributed equally to this work

SPECIALTY SECTION
This article was submitted to Pediatric Oncology, a section of the journal Frontiers in Oncology

RECEIVED 01 September 2022
ACCEPTED 13 January 2023
PUBLISHED 13 February 2023

CITATION
AlShail E, Alahmari AN, Dababo AAM, Alsagob M, Al-Hindi H, Khalil H, Al Masseri Z, AlSalamah R, Almohseny E, Alduhaish A, Colak D and Kaya N (2023) A molecular study of pediatric pilomyxoid and pilocytic astrocytomas: Genome-wide copy number screening, retrospective analysis of clinicopathological features and long-term clinical outcome.
Front. Oncol. 13:1034292.
doi: 10.3389/fonc.2023.1034292

A molecular study of pediatric pilomyxoid and pilocytic astrocytomas: Genome-wide copy number screening, retrospective analysis of clinicopathological features and long-term clinical outcome

Essam AlShail[1†], Ahmed Nasser Alahmari[1†], Anas A. M. Dababo[2†], Maysoon Alsagob[3,4†], Hindi Al-Hindi[2], Hala Khalil[5], Zainab Al Masseri[6], Razan AlSalamah[3], Ethar Almohseny[3], Amjad Alduhaish[7], Dilek Colak[8*] and Namik Kaya[3*]

[1]Department of Neurosciences, King Faisal Specialist Hospital and Research Centre (KFSHRC), Riyadh, Saudi Arabia, [2]Department of Pathology and Laboratory Medicine, King Faisal Specialist Hospital and Research Centre (KFSHRC), Riyadh, Saudi Arabia, [3]Department of Translational Genomics, Center for Genomic Medicine, King Faisal Specialist Hospital and Research Centre (KFSHRC), Riyadh, Saudi Arabia, [4]Applied Genomics Technologies Institute, King Abdulaziz City for Science and Technology, Riyadh, Saudi Arabia, [5]Department of Biostatistics, Epidemiology and Scientific Computing, King Faisal Specialist Hospital and Research Centre (KFSHRC), Riyadh, Saudi Arabia, [6]Medical Genetics Department, King Faisal Specialist Hospital and Research Centre (KFSHRC), Riyadh, Saudi Arabia, [7]Neuroscience Department, King Abdullah Medical City, Mecca, Saudi Arabia, [8]Department of Molecular Oncology, King Faisal Specialist Hospital and Research Centre (KFSHRC), Riyadh, Saudi Arabia

Background: Pilocytic Astrocytoma (PA) is the most common pediatric brain tumors. PAs are slow-growing tumors with high survival rates. However, a distinct subgroup of tumors defined as pilomyxoid astrocytoma (PMA) presents unique histological characteristics and have more aggressive clinical course. The studies on genetics of PMA are scarce.

Methods: In this study, we report one of the largest cohort of pediatric patients with pilomyxoid (PMA) and pilocytic astrocytomas (PA) in Saudi population providing a comprehensive clinical picture, retrospective analysis with long-term follow-up, genome-wide copy number changes, and clinical outcome of these pediatric tumors. We examined and compared genome-wide copy number aberrations (CNAs) and the clinical outcome of the patients with PA and PMA.

Results: The median progression free survival for the whole cohort was 156 months and it was 111 months for the PMA, however, not statistically significantly different between the groups (log-rank test, P = 0.726). We have identified 41 CNAs (34 gains and 7 losses) in all tested patients. Our study yielded the previously reported KIAA1549-BRAF Fusion gene in over 88% of the tested patients (89% and 80% in PMA and PA, respectively). Besides the fusion gene, twelve patients had additional genomic CNAs. Furthermore, pathway and gene network analyses of genes in the fusion region revealed alterations in retinoic acid mediated apoptosis and MAPK signaling pathways and key hub genes that may

potentially be involved in tumor growth and progression, including *BRAF*, *LUC7L2*, *MKRN1*, *RICTOR*, *TP53*, *HIPK2*, *HNF4A*, *POU5F*, and *SOX4*.

Conclusion: Our study is the first report of a large cohort of patients with PMA and PA in the Saudi population that provides detailed clinical features, genomic copy number changes, and outcome of these pediatric tumors and may help better diagnosis and characterization of PMA.

KEYWORDS

pilomyxoid astrocytoma, *BRAF*, *KIAA1549*, copy number alteration, pilocytic astrocytoma, genomics, brain tumor, gene network

Introduction

Brain and other central nervous system related tumors are the largest group of childhood cancers and the leading cause of cancer-related death in children. Among these, pilocytic astrocytomas (PAs) are the most frequently encountered tumors with peak incidence in the first decade of life (1, 2). Auspiciously, PAs are not aggressive, typically slow growing brain tumors and have a much better prognosis compared to other more aggressive neoplasms. These tumors are considered being grade I tumors according to the WHO (World Health Organization), and progression to higher grades is quite unusual. Patients with PA have high survival rates and only a small percentage of the patients demonstrate a variable clinical course with decreased length of disease-free survival and higher mortality rates (3). However, a distinct subtype of tumors termed pilomyxoid astrocytomas (PMAs) displays more aggressive clinical course and higher recurrence rate (4). The PMAs prefer the optic-chiasmatic/hypothalamic region, however, there are several studies reporting PMAs in several other locations (5). In addition, some tumors present transitional morphological features with combined pilocytic and pilomyxoid features (mixed) (3). The PMAs were previously considered as WHO grade II tumor (4, 5).

Previous reports have shown that about two thirds of PAs display a recurrent gain at 7q34 (6, 7). This leads to gain of *BRAF*, with subsequent BRAF activation. Another study indicated that low-grade gliomas have distinct copy number gains at chr6q23 (8). Interestingly, genetic changes may vary among PA, PMA, and IPT (intermediate pilomyxoid tumors). For instance, among 15 patients only 3 had *KIAA1549-BRAF*-fusion and 2 had $BRAF^{V600E}$-mutation whereas six patients had wild type *BRAF* (9). Similarly, it was reported that there was significant difference in the gene expression patterns between PA vs PMA (10). Compared to the general knowledge on PAs, very little is known about the molecular characteristics of PMAs. The molecular mechanisms that may explain PMA's more aggressive behavior are still lacking. In this study, we examined and compared the clinical features and outcome in a large cohort of the PA and PMA patients, majority of which were PMAs. We also delineated genetic characteristics using genomic arrays and identified copy number changes associated with PMA and PA.

Abbreviations: PA, Pilocytic Astrocytoma; PMA, Pilomyxoid Astrocytoma; AG, Angiocentric Glioma; FG, Fusion gene referring to KIAA1549:BRAF; IAT, Intermediate with anaplastic transformation; CNA, Copy number aberration; CNG, Copy number gain; CNL, Copy number loss; DAVID, Database for Annotation, Visualization and Integrated Discovery; SR, Subtotal resection; D, Debulking; NTR, Near total resection; IPA, Ingenuity Pathways Analysis.

Materials and methods

Tumor samples

We performed a retrospective chart review study of selected patients (n=27) who were histologically determined to have pilomyxoid (PMA) and pilocytic astrocytomas (PA) who were diagnosed between November 1998 and March 2015 at King Faisal Specialist Hospital and Research Centre (KFSHRC). The patients' charts were reviewed until March 07, 2021. The study was performed under a locally approved IRB (King Faisal Specialist Hospital and Research Centre, Research Advisory Council, Basic Research as well as Ethics Committees, RAC# 2111055) and fulfilled the principles of the Helsinki Declaration, 2013. The histopathological assessment and determination of the tumors were done by neuropathologists at KFSHRC based on microscopic, morphological, and immunohistochemical characteristics of the tumors (5, 11, 12). Among the 27 patients, 17 of them were cytogenetically examined using OncoScan arrays.

DNA isolation

Samples were obtained from the FFPE blocks as several microtome shaves; each is around 5 to 6 µm thick. DNA was extracted using QIAamp DNA FFPE Tissue Kit (Qiagen, Hilden, Germany) or similar kits based on the Affymetrix's recommended protocols. DNA was quantified *via* two different systems Quant-iT (Thermo Fisher, Waltham, Massachusetts, US) and Bioanalyzer (Agilent Technologies, Santa Clara, US). The quality and quantity of the DNA samples were evaluated by assessing the results from both systems.

Genechip OncoScan arrays

OncoScan arrays and related assays were used for detection of chromosomal abnormalities. The array workflow is based on company's

protocols (Affymetrix, Santa Clara, CA, US). The FFPE DNA sample preparation, array hybridization, as well as subsequent reactions such as amplification and labeling were strictly followed according to the assay user guide (P/N 703175). The labeled samples were hybridized to the arrays, washed and scanned using Affymetrix scanner. The data was analyzed using Affymetrix's Chromosome Analysis Suite (ChAS) using the default settings (high resolution) of the chromosomal abnormality detection.

PCR

We utilized some of the remaining DNA from FFPE samples during DNA amplification. PCR was carried out using the Qiagen HotStar Tag (Life Technologies, USA) according to standard protocols. The products were visually inspected by agarose gel electrophoresis. Afterwards, PCR amplicons were sequenced using the BigDye Terminator reaction mix and run on the Sequencing equipment (Applied Biosystems' 3730 Sequence Analyzer, Thermo Fisher).

Sanger sequencing

To determine the absence or presence of several known mutations Sanger sequencing (SS) was utilized. Particular mutations, including hotspot mutations in *TP53*, *PIK3CA*, *KRAS*, *EGFR*, *PTEN*, *BRAF*, *IDH1*, and *NRAS*, were picked up (Supplementary Table 1) as these are already targeted by OncoScan arrays using molecular inversion probes (MIP). The Sanger sequencing (SS) was carried out as a confirmatory approach to interrogate these mutations. Gene/mutation specific primers (GSP) were used in the PCRs. These primers were modified for SS (M13 universal primer sites were added to the GSP and each primer was used in separate reactions for SS).

Functional pathway and network analysis

We performed gene network and functional analysis using Ingenuity Pathways Analysis (IPA) (QIAGEN Inc., https://www.qiagenbioinformatics.com/products/ingenuity-pathway-analysis). We also performed gene ontology (GO) enrichment analysis using Database for Annotation, Visualization and Integrated Discovery (DAVID) (13) and Protein ANalysis Through Evolutionary Relationships (PANTHER™) classification systems (14). The genes affected by copy number changes were mapped in the Ingenuity pathway knowledge base. A right-tailed Fisher's exact test was used to calculate a p-value determining the probability that the biological function (or pathway) assigned to that data set is explained by chance alone.

Statistical analysis

Comparison of the patients' characteristics by tumor type (PMA, PA, and others) was performed using non-parametric Kruskal- Wallis test for continuous variables and Fisher's exact test for categorical variables. Kaplan–Meier survival curves for each tumor type were generated to estimate the progression-free time over the observation period, followed by log-rank test to assess differences between the groups. Statistical analysis was performed using IBM SPSS Statistics Version 26.0. All statistical tests were two-sided and p-value < 0.05 was considered statistically significant.

Results

Clinical features of pilomyxoid and pilocytic astrocytoma patients

We first retrospectively reviewed the clinical and tumor characteristics of 27 pediatric patients who were diagnosed with PMA, PA, angiocentric glioma (AG), and others (intermediate tumor with anaplastic features (IAT). Some representative histopathological images of pilocytic astrocytoma (PA) and pilomyxoid astrocytoma (PMA) are shown in Figure 1A. The median follow-ups for PMA and PA were 60 months and 99 months, respectively. The most common location for PMA was suprasellar area (67%). The clinical and tumor characteristics of the patient cohort that we studied are summarized in Table 1.

All patients underwent surgeries, with earliest PMA surgery performed in 1998 and all other surgeries were performed from 1998 through 2015, that included unilateral subfrontal, bilateral subfrontal, transcortical transventricular, pterional, temporal or combined subfrontal and pterional approaches. Three-quarters of our patients underwent debulking or subtotal resection (Table 2). Twelve PMA patients (86%) received chemotherapy. Twenty-one patients (80%) received chemotherapy with low-grade glioma protocol consisting of vincristine and carboplatin. The Temozolamide was used in recurrent or resistant cases. Radiation treatment was used for 10 patients (38%). There was only one mortality in a patient with atypical glioma who died after two weeks due to rapid progression of the disease. Three patients had metastases (one to CSF), and all were PMAs.

Treatment related morbidities among the cohort included visual impairment leading to visual field defect or blindness in 50% (n=12), endocrine deficits in 56% (n=14), such as cortisol deficiency, hypothyroidism, growth hormone deficiency, diabetes insipidus, or panhypopituitarism as well as cognitive impairment in 36% (n=9), such as memory loss or learning difficulties (Table 2). The median progression free survival (PFS) for the whole cohort was 156 months and for PMA it was 111 months that was not statistically significantly different between the groups (log-rank test, P=0.726).

Genomewide copy number analysis of PA and PMAs

We next employed OncoScan® CNV assays in order to identify genome-wide chromosomal aberrations in our 27 tumor samples. The data was analyzed using Affymetrix's Chromosome Analysis Suite (ChAS) using the default settings. The OncoScan® assays use molecular inversion probes (MIP) for the identification of genomic copy number alterations, loss of heterozygosity (LOH), and somatic mutations. It targets genome-wide chromosomal aberrations with one of the highest resolutions provided by microarrays. The interrogating MIP probes are 40 base pairs and extensively wet-validated using archived FFPE samples of

10.3389/fonc.2023.1034292

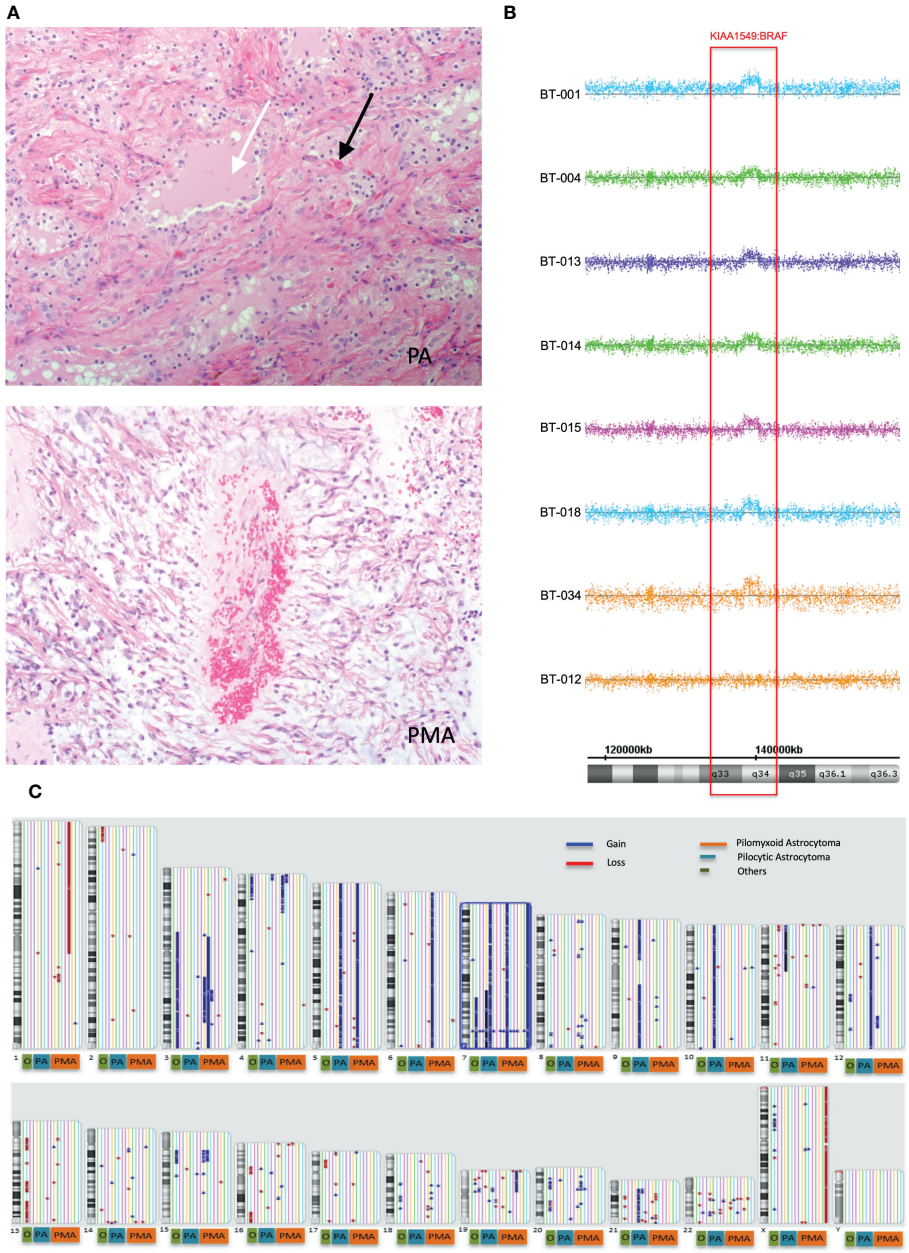

FIGURE 1
Global copy number analyses of pediatric pilomyxoid and pilocystic astrocytomas. **(A)** Representative histopathological images of pilocytic astrocytoma (PA) and pilomyxoid astrocytoma (PMA) (original magnification, 200×). The PA shows biphasic pattern with microcystic changes (white arrow) and Rosenthal fibers (black arrows) and the PMA shows perivascular arrangement with myxoid background (bluish color) and the mononmorphic piloid cells without Rosenthal fibers **(B)** Global copy number analyses of PMA samples, displaying the KIAA1549:BRAF fusion gene. Each sample is color coded. The baseline is represented as a straight line while the region consisting the fusion gene is pointed out by raised probes above the baseline (indicating the gain). The red block covers the region containing the fusion gene/gain. Below the figure, schematic chromosome bands and coordinates on chromosome 7 are illustrated. **(C)** Global copy number analyses results for all samples tested (PMA, PA and others). Each chromosome and related cytobands are represented in separate boxes. Next to each chromosome displays all samples with different colors. The samples are ordered as PMA, PA, and "others" from right to left next to the chromosome number; with orange, blue and red boxes, respectively, underneath the respective samples. The gains and losses are indicated as blue and red lines/arrow heads, respectively.

major solid tumor types. It also utilizes MIPs for hotspot mutations in nine genes implicated in cancer (*BRAF, KRAS, EGFR, IDH1, IDH2, PTEN, PIK3CA, NRAS* and *TP53*). In our cohort, none of the targeted mutations on the arrays was positively detected. We also performed Sanger sequencing (SS) using standard PCR primers targeting the same mutations (Supplementary Table 1), that also confirmed the OncoScan results.

Genome-wide copy number aberration (CNA) analyses revealed 41 CNAs (34 gains (CNGs) and 7 losses (CNLs)) in all tested patients (n=17) (Figures 1B, C; Table 3). All nine PMAs harbored 20 CNAs (17 gains and 3 losses) and five PAs have 11 CNAs (all gains). Our study yielded the previously reported gain on chromosome 7q34 in over 88% of our patient cohort (89% and 80% in PMA and PA, respectively). The duplication has been previously reported in PA and

10.3389/fonc.2023.1034292

TABLE 1 Characteristics of patients and tumors by tumor type.

	Total (n=27)	PMA (n=15)	PA (n=7)	Others* (n=5)	p-value
Age at diagnosis (years), median (min-max)	**2 (0.9-9)**	2 (0.9-9)	4 (0.9-7)	2 (0.9-4)	0.684
Follow-up duration (months), median (min-max)	**88 (11-367)**	60 (11-132)	98.5 (24-240)	102 (76-367)	0.069
Gender, n (%)					
Male	13 (48.0)	8 (53.3)	4 (57.1)	1 (20.0)	0.508
Female	14 (52.0)	7 (46.7)	3 (42.9)	4 (80.0)	
Tumor characteristics					
Tumor location, n (%)					
Suprasellar region	14 (51.9)	10 (66.7)	1 (14.3)	3 (60.0)	**0.040**
Brainstem	1 (3.7)	0	0	1 (20.0)	
Cerebellum	1 (3.7)	1 (6.7)	0	0	
Chiasm/hypothalmus	3 (11.1)	1 (6.7)	2 (28.6)	0	
Left temporal	1 (3.7)	1 (6.7)	0	0	
Left thalamus	1 (3.7)	0	0	1 (20.0)	
Optic nerve	2 (7.4)	0	2 (28.6)	0	
Pineal region	1 (3.7)	0	1 (14.3)	0	
Sella/suprasellar	1 (3.7)	0	1 (14.3)	0	
Spinal cord	1 (3.7)	1 (6.7)	0	0	
Suprasellar/hypothalamic	1 (3.7)	1 (6.7)	0	0	
Lesion type, n (%)					
Solid	9 (36.0)	5 (38.5)	3 (42.9)	1 (20.0)	0.926
Mixed	10 (40.0)	5 (38.5)	2 (28.6)	3 (60.0)	
Cystic	6 (24.0)	3 (23.1)	2 (28.6)	1 (20.0)	
Pattern of enhancement, n (%)					
Homogeneous	5 (20.0)	1 (7.7)	4 (57.1)	0	**0.016**
Heterogeneous	19 (76.0)	12 (92.3)	3 (42.9)	4 (80.0)	
Non-enhancing	1 (4.0)	0	0	1 (20.0)	
Metastasis, n (%)					
No	23 (85.5)	11 (78.6)	7 (100)	5 (100)	0.392
Yes	3 (11.5)	3 (21.4)	0	0	

*n=3 IAT, n=1 atypical glioma, n=1 AG. AG, Angiocentric Glioma; IAT, Intermediate with Anaplastic Transformation; PA, Pilocytic Astrocytoma; PMA, Pilomyxoid Astrocytoma. Bold indicates statistical significance.

known as "*KIAA1549:BRAF* fusion gene" (15, 16). Nearly all samples have similar proximal and distal end breakpoints starting from *KIAA1549* gene and reaching to *BRAF* (Figure 1B). The duplication outspreads nearly 1.87Mb region and comprises 9 pseudogenes, 9 uncharacterized genes, and 10 genes with OMIM ID including *KIAA1549* and *BRAF* at the breakpoints. Other genes that may also have importance in disease pathogenesis include *MKRN1, LUC7L2, UBN2, DENND2A, SLC37A3, PARP12, TBXAS1, HIPK2*, and *C7orf55* (Figure 2).

Besides the fusion gene, twelve patients have additional genomic CNAs (Table 3). Briefly, five patients have either partial (n=2) or full (n=3) trisomy of chromosome 7 (Figure S1). Interestingly, only two (BT-001 and BT-010) harbored tetrasomy of the fusion gene region (Figure S2). The partial trisomies in BT-10 and BT-28 are large and cover majority of the q arm. BT-013 (PMA) has a deletion on chromosome 1 (1p36.33q21.1) (Figure S3) and a duplication on chromosome 19 (19p13.3p11) (Figure S4). BT-021 has various large gains of chromosomes 5, 7, 9, 10, and 21 (Figure S5).

10.3389/fonc.2023.1034292

TABLE 2 Management and outcomes after treatment by tumor type.

	Total (n=27)	PMA (n=15)	PA (n=7)	Others* (n=5)	p-value
Management	n (%)	n (%)	n (%)	n (%)	
Surgery approach					
Bifrontal craniotomy	7 (26.9)	3 (21.4)	3 (42.9)	1 (20.0)	0.988
Cervical laminoplasty and biopsy	1 (3.8)	1 (7.1)	0	0	
Frontal craniotomy	8 (30.8)	4 (28.6)	2 (28.6)	0	
Pterional craniotomy	5 (19.2)	3 (21.4)	1 (14.3)	3 (60.0)	
Subfrontal craniotomy	2 (7.7)	2 (14.3)	0	0	
Suboccipital craniotomy	3 (11.5)	1 (7.1)	1 (14.3)	1 (20.0)	
Extent of resection					
Biopsy	2 (8.0)	2 (15.4)	0	0	0.262
D	11 (44.0)	7 (53.8)	3 (42.9)	1 (20.0)	
NTR	4 (16.0)	2 (15.4)	2 (28.6)	0	
SR	8 (32.0)	2 (15.4)	2 (28.6)	4 (80.0)	
Ventriculoperitoneal shunt (VPS)					
No	8 (32.0)	3 (21.4)	3 (50.0)	2 (40.0)	0.435
Yes	17 (68.0)	11 (78.6)	3 (50.0)	3 (60.0)	
Radiotherapy					
No	16 (61.5)	9 (64.3)	4 (57.1)	3 (60.0)	1.00
Yes	10 (38.5)	5 (35.7)	3 (42.9)	2 (40.0)	
Chemotherapy					
No	5 (19.2)	2 (14.3)	3 (42.9)	0	0.210
Yes	21 (80.8)	12 (85.7)	4 (57.1)	5 (100)	
Redo surgery					
No	22 (84.6)	12 (85.7)	6 (85.7)	4 (80.0)	1.00
Yes	4 (15.4)	2 (14.3)	1 (14.3)	1 (20.0)	
Outcomes after treatment					
Visual impairment					
Blindness	4 (16.7)	3 (21.4)	0	1 (20.0)	0.266
Decrease visual acuity	3 (12.5)	0	2 (28.6)	1 (20.0)	
Eye squint	1 (4.2)	0	0	1 (20.0)	
Left eye blindness	1 (4.2)	0	1 (14.3)	0	
Right eye blindness	3 (12.5)	2 (14.3)	1 (14.3)	0	
NO	12 (50.0)	7 (50.0)	3 (42.9)	2 (40.0)	
Endocrine outcome					
No	11 (44.0)	4 (28.6)	3 (50.0)	4 (80.0)	0.159
Yes	14 (56.0)	10 (71.4)	3 (50.0)	1 (20.0)	
Hypothalamic dysfunction					
No	18 (72.0)	8 (57.1)	6 (100)	4 (80.0)	0.138
Yes	7 (28.0)	6 (42.9)	0	1 (20.0)	

(Continued)

10.3389/fonc.2023.1034292

TABLE 2 Continued

	Total (n=27)	PMA (n=15)	PA (n=7)	Others* (n=5)	p-value
Management	n (%)	n (%)	n (%)	n (%)	
Cognitive					
Normal	16 (64.0)	8 (57.1)	4 (66.7)	4 (80.0)	0.853
Impaired	9 (36.0)	6 (42.9)	2 (33.3)	1 (20.0)	

*n=3 IAT, n=1 atypical glioma, n=1 AG. PA, Pilocytic Astrocytoma; PMA, Pilomyxoid Astrocytoma; AG, Angiocentric Glioma; IAT, Intermediate with Anaplastic Transformation; SR, subtotal resection; D, debulking; NTR, Near total resection.

TABLE 3 Genomic copy number alterations (CNAs) in PA and PMA. CNAs identified in PA/PMA (archived as FFPE) samples using OncoScan arrays.

Tumor Type	Sample ID	CN	TYPE	CHRS	CYTOBAND	START	END	SIZE (bp)	#MARKER	#GENES
PMA	BT-001*	4	Gain	7	q34	138549074	140491678	1942604	222	24
		3	Gain	7	p22.3-136.3	41,420	159,118,443	159077023	11975	948
		1.5	Loss	X	p22.33-q28	177,941	155,219,364	155041423	10838	874
PMA	BT-004*	3	Gain	7	q34	138,549,074	140,491,678	1942604	222	24
		3	Gain	1	q41	221,043,002	221,724,913	681911	59	2
PMA	BT-012	1.5	Loss	8	q24.3	144,994,887	145,050,051	55164	23	2
		3	Gain	10	q11.22	47,033,943	47,702,691	668748	37	12
PMA	BT-013*	2.5	Gain	7	q34	138,549,074	140,871,571	2322497	298	25
		3	Gain	19	p13.3p11	247,231	24,544,320	24297089	2120	655
		1	Loss	1	p36.33	754,191	145,382,341	144628150	9789	1241
PMA	BT-014*	3	Gain	7	q34	138,550,993	140,499,107	1948114	224	24
PMA	BT-015*	3	Gain	7	q34	138,615,645	140,485,335	186969	207	24
PMA	BT-018*	3	Gain	7	q34	138,550,993	140,854,420	2303427	295	24
PMA	BT-019*	2.33	Gain	3	p12.3q29	75,331,108	197,852,564	122521456	8958	710
		2.44	Gain	4	p16.3p13	1,248,918	41,827,875	40578957	2629	221
		2.4	Gain	5	p15.33q35.3	38,138	180,698,312	180660174	12360	1037
		2.41	Gain	6	p25.3q27	204,908	170,913,051	170708143	12578	1196
		2.44	Gain	7	p22.3q36.3	41,420	159,118,443	159077023	11887	1142
		2.44	Gain	15	q11.12q13.3	20,161	33,073	12912	626	173
PMA	BT-034*	3	Gain	7	q34	138541150	140490207	1949057	222	24
PA	BT-002	2.67	Gain	12	p13.33q24.33	189,399	133,818,115	133628716	10358	1190
PA	BT-006*	3	Gain	7	q34	138,645,000	140,276,997	1631997	170	16
		3	Gain	22	q11.23	24,346,427	24,390,318	43891	20	4
PA	BT-020*	3	Gain	7	q34	138,561,416	140,485,335	1923919	214	23
PA	BT-021*	2.5	Gain	5	p13.1	38,138	180,698	142560	11928	989
		2.5	Gain	7	p22.3q36.3	41,420	159,118,443	159077023	11588	1108
		2.5	Gain	9	p24.3q34.3	204	141,055	140851	8472	929
		2.5	Gain	10	p15.3q26.3	463	135,434	134971	9220	892
		2.5	Gain	21	p11.2q22.3	9,648	47,707	38059	2249	289

(Continued)

10.3389/fonc.2023.1034292

TABLE 3 Continued

Tumor Type	Sample ID	CN	TYPE	CHRS	CYTOBAND	START	END	SIZE (bp)	#MARKER	#GENES
PA	BT-028*	3.33	Gain	7	q21.3q36.3	95,430,276	159,118,443	63688167	5107	554
		3.17	Gain	11	p15.5p11.12	192,763	50,766,362	50573599	3637	510
IAT	BT-005*	4	Gain	7	q34	138,549,074	140,487,260	1938186	220	24
		1	Loss	19	p13.3	1,232,376	1,283,188	50812	29	6
IAT	BT-011*	3	Gain	7	q34	138,609,656	140,499,107	1889451	215	24
		3	Gain	8	p11.21	42,898,470	43,767,534	869064	58	4
AG	BT-010*	3.67	Gain	7	q34	138,561,416	140,499,107	1937691	221	24
		2.33	Gain	3	p13q29	70,319,707	197,852,564	127532857	9151	714
		2.84	Gain	7	q22.1q36.3	103,292,486	159,118,443	55825957	9008	403
		1.33	Loss	2	p25.3p24.2	21,493	16,743,453	16721960	1261	75
		1.33	Loss	16	p12.1p11.1	26,415,932	35,214,165	8798233	487	157
		1.33	Loss	17	p13.1p11.2	9,561,542	18,678,548	9117006	706	107

PA, Pilocytic Astrocytoma; PMA, Pilomyxoid Astrocytoma; AG, Angiocentric Glioma; IAT, Intermediate with anaplastic transformation; CN, copy number; CNA, copy number aberration; CHR, chromosome. Asterisk (*) indicates CNG in the KIAA1549:BRAF Fusion gene.

Functional, pathway, and gene network analyses

Functional, pathway, and gene network analyses of genes within the KIAA1549:BRAF fusion region were performed using several bioinformatics tools, including DAVID (13) and IPA (QIAGEN Inc.) that indicated enrichment in cancer, cell cycle, cellular development, and nervous system development and function, and significant alterations in retinoic acid mediated apoptosis signaling, MAPK and death receptor signaling pathways (all p values < 0.01) (Figures 2A, B). Furthermore, gene interaction network analysis revealed hub genes that may potentially be involved in PA/PMA, including *BRAF, LUC7L2, TP53, MKRN1, RICTOR, HIPK2, HNF4A, POU5F*, and *SOX4* (Figure 2C).

Discussion

Though PMA shares similar molecular features with PA, the commonest central nervous system (CNS) tumor, however, it presents more aggressive course and higher grade. Histologically, in contrast to PA, PMA does not exhibit calcification, Rosenthal fibers, and eosinophilic granule bodies (4). It mostly appears with angiocentric pattern with small and compact monomorphous piloid cells in myxoid matrix-like background. Although PMA is well characterized histologically, and similarities and differences with PA are recognized at the histological level, the studies on PMAs and differentiating both tumor types genetically are scarce. In this study, we gathered one of the largest cohorts of PA and PMA in Saudi

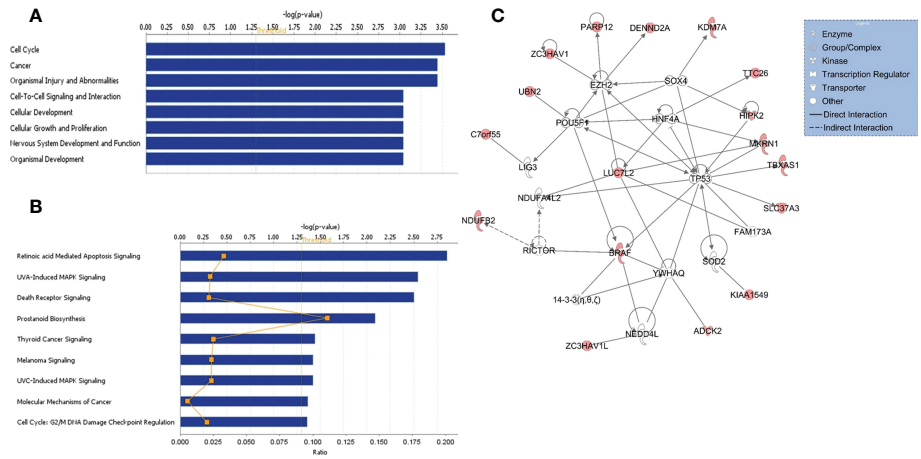

FIGURE 2
Functional/pathway and network analyses of genes in KIAA1549:BRAF fusion. Enriched biological functions **(A)** and canonical pathways **(B)** that are associated with the genes in the fusion region. The significance of function and pathway are shown in X-axis. The P value of 0.05 is indicated as the threshold line. **(C)** Gene interaction network analysis. Nodes represent genes, with their shape indicating the functional class of the gene product (see legend). The edges indicate biological relationship between the genes, with straight and dashed lines representing direct or indirect gene to gene interactions, respectively. The red color indicate genes in the fusion.

population and investigated genomic copy number changes and outcome of these pediatric tumors.

In one of the earliest studies, Forshew et al. identified the fusion in 23 out of 26 PA samples as well as in singleton PMA (17). Gains on chromosome 5 and 6 were also detected in a few samples. Interestingly, both fusions lack the auto-inhibitory domains of BRAF and RAF1 that were interchanged by in-frame start units of the KIAA1549 and SRGAP3. This replacement creates a constitutive kinase activity. We provided a summary of the previous studies of PAs/PMAs and the identified CNAs using different array platforms (Supplementary Table 2).

We used Affymetrix's OncoScan arrays that have MIPs targeting selected hot spot mutations in cancers as well as global copy number changes. Interestingly, these arrays did not identify any hot spot mutations in our patient cohort. However, we were able to identify 41 CNAs, including 34 CNGs and 7 CNLs in 17 patients tested (Table 3). Nine PMA samples harbor 20 CNAs (17 CNGs and 3 CNLs) and five PAs have 11 CNGs. Over 88% our patient cohort (89% in PMA and 80% in PA) have the well-defined BRAF fusion. Previous pioneering array studies, mostly done on PA tumors, indicated involvement of KIAA1549-BRAF fusion gene in low-grade brain tumors (15, 16). Alternative approaches such as RNAseq and utilization of droplet-PCR also indicated similar findings in PA (18). Such fusion is predicted to occur owing to tandem duplication events happening especially during homologous recombination of Alu elements (19–21). A large series of pilocytic astrocytoma tumors were screened for likely copy number changes using a custom designed arrays constructed with clones obtained from the Wellcome Trust Sanger Institute. The analysis indicated that 29 samples had duplication between clones RP11-355D18 and RP11-543P6 on chromosome 7. Further analysis confirmed the presence of a newly formed fusion gene between intron 16 of *KIAA1549* and intron 8 of *BRAF*. The fusion gene derives few different transcripts but essentially the fusions retain BRAF's kinase domain (15). Under normal circumstances, BRAF's kinase activity is regulated by NH2-terminal region that includes Ras-binding domain and is truncated in the new fusion. Once such truncation removes NH2-terminal of the *BRAF*, then regulation of fusion gene is not under autoregulation of wild type NH2-terminal but rather it is controlled by newly generated mutant NH2-terminal. Besides the fusion gene, twelve patients in our study had additional genomic CNAs (Table 3).

As over 88% of the samples (15 out of 17) had the gain in KIAA1549-BRAF fusion gene in our study, we investigated the gene interaction network analysis of genes in this region. The analysis indicated alterations in retinoic acid mediated apoptosis signaling, MAPK and death receptor signaling pathways and hub genes, including *BRAF, LUC7L2, MKRN1, TP53, HNF4A, RICTOR, POU5F*, *HIPK2*, and *SOX4* that may have potentially important role in tumorigenesis and cancer progression (2, 16, 22–25).

This study has potential limitations. We had a relatively small sample size of patients in each comparison group (PA, PMA, and other) and the analysis is based on a retrospective design; hence may have inherent bias. Moreover, though the KFSHRC is a referral hospital and our cohort included local as well as referred patients within Saudi Arabia, the results obtained in this study may not be generalizable to the whole population. Despite these limitations, this study is the first comprehensive study of pediatric patients with PMA and PA in Saudi population providing genome-wide copy number screening, retrospective analysis of clinicopathological features and long-term clinical outcome of these pediatric tumors. In conclusion, our study reports the first comprehensive molecular and clinicopathological analyses of one of the largest cohorts of PMA/PA samples to date in a previously unstudied population to understand the clinical features and genomic makeup of these solid types of tumors and hence may help better diagnosis and characterization of these tumors.

Data availability statement

The dataset generated and analyzed during the current study is available at this link (https://www.dropbox.com/s/fg2vo8ebiwbc8th/Affy-Oncoscan-All-PMA-Data.rar?dl=0).

Ethics statement

This study involved in using archived FFPE samples and was performed under IRB-approved protocols at King Faisal Specialist Hospital and Research Center (KFSHRC's Research Advisory Council Committees including Basic Research Committee and Research Ethics Committee, RAC# 2111055). All patients were de-identified to the research team and hence the study was exempted from collecting written informed consent for their participation accordance with the institutional requirements.

Author contributions

NK conceived and designed the experiments. NK, EAS, and DC drafted the manuscript. NK, DC, MA, and HK performed the data analyses. AA and MA involved in reviewing and editing manuscript. HA-H and AD review the pathology reports and performed pathology related tests. EAS, HA-H, AD, ANA, AA, EAM, and ZA reviewed the charts, collected clinical data, and prepared the tables related to clinical information. MA and RA performed the experiments. All authors contributed to the article and approved the submitted version.

Funding

This study was supported by King Faisal Specialist Hospital and Research Centre's seed grants (KFSHRC-RAC# 2120022) for NK and EAS and also for DC (RAC# 2110 006). This research was conducted through intramural funds provided by King Faisal Specialist Hospital and Research Center (KFSHRC, RAC Project # 2111055).

Acknowledgments

We extend our special thanks to KFSHRC Genotyping and Sequencing Core Facilities, and Purchasing Departments for facilitating and expediting our requests. We thank Ibrahim H. Kaya for preparing scientific figures. One of the authors of this study, Dr. Anwar Ul-Haq, passed away due to COVID-19, and we would like to dedicate this work to his memory.

Conflict of interest

The authors declare that the research was conducted in the absence of any commercial or financial relationships that could be construed as a potential conflict of interest.

Publisher's note

All claims expressed in this article are solely those of the authors and do not necessarily represent those of their affiliated organizations, or those of the publisher, the editors and the reviewers. Any product that may be evaluated in this article, or claim that may be made by its manufacturer, is not guaranteed or endorsed by the publisher.

Supplementary material

The Supplementary Material for this article can be found online at: https://www.frontiersin.org/articles/10.3389/fonc.2023.1034292/full#supplementary-material

References

1. Ohgaki H, Kleihues P. Population-based studies on incidence, survival rates, and genetic alterations in astrocytic and oligodendroglial gliomas. *J Neuropathol Exp Neurol* (2005) 64:479–89. doi: 10.1093/jnen/64.6.479

2. Roth JJ, Santi M, Rorke-Adams LB, Harding BN, Busse TM, Tooke LS, et al. Diagnostic application of high resolution single nucleotide polymorphism array analysis for children with brain tumors. *Cancer Genet* (2014) 207:111–23. doi: 10.1016/j.cancergen.2014.03.002

3. Kulac I, Tihan T. Pilomyxoid astrocytomas: a short review. *Brain tumor Pathol* (2019) 36:52–5. doi: 10.1007/s10014-019-00343-0

4. Ding C, Tihan T. Recent progress in the pathology and genetics of pilocytic and pilomyxoid astrocytomas. *Balkan Med J* (2019) 36:3–11. doi: 10.4274/balkanmedj.2018.1001

5. Louis DN, Ohgaki H, Wiestler OD, Cavenee WK, Burger PC, Jouvet A, et al. The 2007 WHO classification of tumours of the central nervous system. *Acta Neuropathol* (2007) 114:97–109. doi: 10.1007/s00401-007-0243-4

6. Bar EE, Lin A, Tihan T, Burger PC, Eberhart CG. Frequent gains at chromosome 7q34 involving BRAF in pilocytic astrocytoma. *J Neuropathol Exp Neurol* (2008) 67:878–87. doi: 10.1097/NEN.0b013e3181845622

7. Taha H, Yehia M, Mahmoud M, El-Beltagy M, Ghabriel M, El-Naggar S. Incidence of kiaa1549-braf fusion gene in Egyptian pediatric low grade glioma. *Clin Transl Med* (2015) 4:10. doi: 10.1186/s40169-015-0052-7

8. Tatevossian RG, Tang B, Dalton J, Forshew T, Lawson AR, Ma J, et al. MYB upregulation and genetic aberrations in a subset of pediatric low-grade gliomas. *Acta Neuropathol* (2010) 120:731–43. doi: 10.1007/s00401-010-0763-1

9. Fadel SA, Von Reppert M, Kazarian E, Omay EZE, Marks A, Linder N, et al. Spectrum of qualitative and quantitative imaging of pilomyxoid, intermediate pilomyxoid and pilocytic astrocytomas in relation to their genetic alterations. *Neuroradiology*. (2022). doi: 10.1007/s00234-022-03027-3

10. Kleinschmidt-Demasters BK, Donson AM, Vogel H, Foreman NK. Pilomyxoid astrocytoma (PMA) shows significant differences in gene expression vs. pilocytic astrocytoma (PA) and variable tendency toward maturation to PA. *Brain Pathol* (2015) 25:429–40. doi: 10.1111/bpa.12239

11. Komotar RJ, Mocco J, Carson BS, Sughrue ME, Zacharia BE, Sisti AC, et al. Pilomyxoid astrocytoma: a review. *MedGenMed* (2004) 6:42.

12. Komotar RJ, Mocco J, Jones JE, Zacharia BE, Tihan T, Feldstein NA, et al. Pilomyxoid astrocytoma: diagnosis, prognosis, and management. *Neurosurg Focus* (2005) 18:E7. doi: 10.3171/foc.2005.18.6.8

13. Sherman BT, Huang DW, Tan Q, Guo Y, Bour S, Liu D, et al. DAVID knowledgebase: a gene-centered database integrating heterogeneous gene annotation resources to facilitate high-throughput gene functional analysis. *BMC Bioinf* (2007) 8:426. doi: 10.1186/1471-2105-8-426

14. Thomas PD, Kejariwal A, Campbell MJ, Mi H, Diemer K, Guo N, et al. PANTHER: a browsable database of gene products organized by biological function, using curated protein family and subfamily classification. *Nucleic Acids Res* (2003) 31:334–41. doi: 10.1093/nar/gkg115

15. Jones DT, Kocialkowski S, Liu L, Pearson DM, Backlund LM, Ichimura K, et al. Tandem duplication producing a novel oncogenic BRAF fusion gene defines the majority of pilocytic astrocytomas. *Cancer Res* (2008) 68:8673–7. doi: 10.1158/0008-5472.CAN-08-2097

16. Jones DT, Kocialkowski S, Liu L, Pearson DM, Ichimura K, Collins VP. Oncogenic RAF1 rearrangement and a novel BRAF mutation as alternatives to KIAA1549:BRAF fusion in activating the MAPK pathway in pilocytic astrocytoma. *Oncogene* (2009) 28:2119–23. doi: 10.1038/onc.2009.73

17. Forshew T, Tatevossian RG, Lawson AR, Ma J, Neale G, Ogunkolade BW, et al. Activation of the ERK/MAPK pathway: a signature genetic defect in posterior fossa pilocytic astrocytomas. *J Pathol* (2009) 218:172–81. doi: 10.1002/path.2558

18. Appay R, Fina F, Macagno N, Padovani L, Colin C, Barets D, et al. Duplications of KIAA1549 and BRAF screening by droplet digital PCR from formalin-fixed paraffin-embedded DNA is an accurate alternative for KIAA1549-BRAF fusion detection in pilocytic astrocytomas. *Mod Pathol* (2018) 31:1490–501. doi: 10.1038/s41379-018-0050-6

19. Kolomietz E, Meyn MS, Pandita A, Squire JA. The role of alu repeat clusters as mediators of recurrent chromosomal aberrations in tumors. *Genes Chromosomes Cancer* (2002) 35:97–112. doi: 10.1002/gcc.10111

20. Olesen LH, Aggerholm A, Andersen BL, Nyvold CG, Guldberg P, Norgaard JM, et al. Molecular typing of adult acute myeloid leukaemia: significance of translocations, tandem duplications, methylation, and selective gene expression profiling. *Br J Haematol* (2005) 131:457–67. doi: 10.1111/j.1365-2141.2005.05791.x

21. O'neil J, Tchinda J, Gutierrez A, Moreau L, Maser RS, Wong KK, et al. Alu elements mediate MYB gene tandem duplication in human T-ALL. *J Exp Med* (2007) 204:3059–66. doi: 10.1084/jem.20071637

22. Gkountakos A, Pilotto S, Mafficini A, Vicentini C, Simbolo M, Milella M, et al. Unmasking the impact of rictor in cancer: novel insights of mTORC2 complex. *Carcinogenesis* (2018) 39:971–80. doi: 10.1093/carcin/bgy086

23. Chen P, Duan X, Li X, Li J, Ba Q, Wang H. HIPK2 suppresses tumor growth and progression of hepatocellular carcinoma through promoting the degradation of HIF-1alpha. *Oncogene* (2020) 39:2863–76. doi: 10.1038/s41388-020-1190-y

24. Basheer AS, Abas F, Othman I, Naidu R. Role of inflammatory mediators, macrophages, and neutrophils in glioma maintenance and progression: Mechanistic understanding and potential therapeutic applications. *Cancers (Basel)* (2021) 13. doi: 10.3390/cancers13164226

25. Bale TA, Rosenblum MK. The 2021 WHO classification of tumors of the central nervous system: An update on pediatric low-grade gliomas and glioneuronal tumors. *Brain Pathol* (2022) 32:e13060. doi: 10.1111/bpa.13060

frontiers | Frontiers in Pediatrics

TYPE Original Research
PUBLISHED 21 March 2023
DOI 10.3389/fped.2023.1094926

OPEN ACCESS

EDITED BY
Jinhong Zhu,
Harbin Medical University Cancer Hospital, China

REVIEWED BY
Kunzhe Dong,
Augusta University, United States
Xingyu Zhang,
University of Pittsburgh, United States

*CORRESPONDENCE
Chengwei Chai
✉ 2018760140@gzhmu.edu.cn
Qiang Wu
✉ wuqiangll@hotmail.com

†These authors share first authorship

SPECIALTY SECTION
This article was submitted to Pediatric Oncology, a section of the journal Frontiers in Pediatrics

RECEIVED 10 November 2022
ACCEPTED 01 March 2023
PUBLISHED 21 March 2023

CITATION
Chai C, Chen Y, Luo Y, Zhang H, Ye Z, He X, Zou Y, Xu Y, Li L, Tang J and Wu Q (2023) Mitochondria-associated gene expression perturbation predicts clinical outcomes and shows potential for targeted therapy in neuroblastoma.
Front. Pediatr. 11:1094926.
doi: 10.3389/fped.2023.1094926

Mitochondria-associated gene expression perturbation predicts clinical outcomes and shows potential for targeted therapy in neuroblastoma

Chengwei Chai[1*†], Yan Chen[1†], Yuanyuan Luo[2], Hong Zhang[1], Zhihua Ye[1], Xiaobing He[1], Yan Zou[1], Yingyi Xu[3], Le Li[1], Jue Tang[1,2] and Qiang Wu[1*]

[1]Department of Pediatric Surgery, Guangzhou Women and Children's Medical Center, Guangzhou Medical University, Guangzhou, China, [2]Guangdong Provincial Key Laboratory of Research in Structural Birth Defect Disease, Guangzhou Women and Children's Medical Center, Guangzhou Medical University, Guangzhou, China, [3]Department of Anesthesiology, Guangzhou Women and Children's Medical Center, Guangzhou Medical University, Guangzhou, China

Background: Mitochondria have long been considered a potential target in cancer therapy because malignant cells are known for their altered energy production. However, there is a lack of comprehensive research on the involvement of mitochondria-associated proteins (MAPs) in neuroblastoma (NB), and their potential as therapeutic targets is yet to be fully explored.
Methods: MAP genes were defined based on the protein-coding genes with mitochondrial localization. The mRNA expression patterns and dynamics of MAP genes associated with NB were investigated by integrating publicly available transcriptional profiles at the cellular and tissue levels. Multivariate Cox regression analysis was conducted to reveal the association of MAP genes with the overall survival (OS) and clinical subgroups of NB patients. The single-cell RNA-seq dataset and gene dependency screening datasets were analyzed to reveal the therapeutic potential of targeting MAP genes.
Results: We compiled a total of 1,712 MAP genes. We found the global and cell type-specific mRNA expression changes of the MAP genes associated with NB status and survival. Our analyses revealed a group of MAP gene signatures independent of *MYCN*-amplification status associated with NB outcome. We provided computational evidence with selected MAP genes showing good performance in predicting long-term prognosis. By analyzing gene dependency of the MAP genes in NB cell lines and *ex vivo* human primary T cells, we demonstrated the therapeutic potential of targeting several MAP genes in NB tumors.
Conclusions: Collectively, our study provides evidence for the MAP genes as extended candidates in NB tumor stratification and staging, prognostic prediction, and targeted drug development.

KEYWORDS

neuroblastoma, mitochondria associated protein, targeted therapy, clinical outcome, multi-omic

Background

Childhood neuroblastoma (NB), one of the most common extracranial solid tumors in children, accounts for approximately 6%~10% of all childhood cancers (1). Although NB has been revealed to arise from the precursor cells of the sympathetic nervous system and adrenal medulla (2, 3), the clinical course of NB is highly heterogeneous, which poses a challenge for NB therapy, particularly for high-risk patients whose long-term survival is below 50%. Advances in our understanding of the relevant clinical and biological features have made it possible to more accurately stratify tumor risk and improve NB treatment (4). A unified clinical consensus on NB treatment recommends combining multiple molecular markers (5).

The understanding of NB development, risk classification, and tumor staging have been improved through many tumor genetic analyses, which revealed the importance of segmental chromosomal alterations (SCAs) and specific genetic variants. Different SCAs have been found, including loss of 1p (6), 3p (7), 4p (6), 6q (8), and 11q (9), and gain of 1q (10), 2p (11), and 17q (12). The specific genetic variants associated with the outcome of NB patients include amplification of *MYCN* (13), *DDX1* (14), *NAG* (15), and *ALX* (16), and mutations in genes *CASC15, BARD1, CHEK2, LMO1, LIN28B, AXIN2, BRCA1, TP53, SMARCA4*, and *CDK1NB* (17). Despite such genetic findings, only a few have been applied in clinical practice. *MYCN* amplification is one of the most studied in predicting the prognosis of NB patients. High-throughput technologies advanced translational research in clinical oncology by allowing us to explore the NB at different molecular levels. Gene expression signatures derived from the transcriptomes associated with NB subgroups can better characterize tumors' molecular profile and heterogeneity. In addition, integrating different gene expression datasets can result in better NB patient stratification compared to using these datasets individually (18).

Cancer cells are partially characterized by reprogrammed energy generation; Therefore, studying mitochondrial-related gene expression and regulation is of particular significance for revealing NB prognosis and developing a potential target in cancer therapy. However, a comprehensive assessment of the role of mitochondria-associated proteins (MAPs) in NB has yet to be conducted. Here, by integrating publicly available high-throughput transcriptional profiles at the bulk tissue-level and single cell-level resolutions, we systematically analyzed the MAP gene expression dynamics in NB. We found the global and cell-type-specific mRNA expression changes of the MAP genes associated with NB status and OS. Our analyses revealed MAP gene signatures independent of *MYCN*-amplification status associated with the clinical outcome of NB patients. We provided computational evidence for selected MAP genes showing good performance in predicting long-term prognosis. By analyzing gene dependency or essentiality for cell proliferation and survival of these MAP genes in NB cell lines and human primary T cells, we demonstrated the therapeutic potential of targeting several MAP genes in NB tumors. Collectively, our study shows that MAP genes could be potential candidates for staging tumors, predicting the prognosis of NB, and developing targeted drugs for the disease.

Methods

Collection and processing of datasets

Dataset 1: cell line-based bulk RNA-seq data, obtained from the Gene Expression Omnibus (GEO) database (19) under accession number GSE89413 (20). This dataset is comprised of 39 commonly used NB cell lines and the other two control samples: the hTERT-immortalized retinal pigmented epithelial cell RPE-1, which is widely used as a non-neuroblastoma control, and the cells from the pooled fetal brain, which can serve as a non-neuroblastoma neural-cell derived control.

Fragments Per Kilobase of transcript per Million mapped reads (FPKM) values were downloaded and converted to TPM, short for transcripts-per-million, following the formula: $TPM_i = FPKM_i / Sum(FPKM_j)*10^6$, where i denotes the i-th gene and j denotes the j-th subject. We further excluded low-expressed genes with the averaged TPM ≤ 3 across all the samples. Log2-transformed (TPM + 1) values were used and further normalized with the *normalize.quantile* function in the "preprocessCore" (v1.50.0) package. Differential expression analysis based on the linear model by weighted least squares was conducted with the "limma" package (25), and genes with the adjusted P values < 0.05 were identified to be differentially expressed.

Dataset 2: primary NB tissue-based bulk RNA-seq data from the RNA Sequencing Quality Control (SEQC) cohort, downloaded from the GEO under accession number GSE49711 and GSE62564 (21). This dataset contained gene expression profiles of 498 NB patients and the corresponding clinical information, including *MYCN* status, clinical risk level (high or low), disease stage according to International Neuroblastoma Staging System (INSS) (1, 2, 3, 4, and 4S) (22), the occurrence of a tumor progression event (yes = 1; no = 0), and occurrence of death from the disease (yes = 1; no = 0).

In this project, gene expression was quantified using log base 2 of the number of bases aligned in the gene, divided by the number of terabases aligned in known genes and by the length of the gene (21). We directly downloaded this gene expression matrix. 1,259 MAP genes were included. Principle component analyses (PCA) of the MAP gene expression matrix subset were conducted and visualized with the functions from the "FactoMineR" (v2.4) and "factoextra" (v.1.0.7) packages. Differential expression analyses were conducted between subgroups for each clinical parameter with the "limma" package.

Dataset 3: single-cell RNA-seq (scRNA-seq) dataset of NB tissues, downloaded from the GEO under accession number GSE137804 (2). Raw counts of single cells were obtained. We first excluded low-quality cells with less than 500 genes detected and more than 10% of genes derived from the mitochondrial genome. The filtered gene expression matrix was then normalized with Seurat's *NormalizeData* function (23), in which feature counts for each cell were divided by the total counts for

that cell, multiplied by the scale factor (10,000), and then subjected to natural-log transformation using log1p. Highly variable genes were identified and used for the subsequent PCA, which was performed using graph-based clustering and visualized using *t*-Distributed Stochastic Neighbor Embedding (*t*-SNE) or Uniform Manifold Approximation and Projection (UMAP) with the *RunTSNE* and *RunUMAP* functions. We integrated the cells from each NB tumor with Seurat's *FindIntegrationAnchors* and *IntegrateData* functions.

Dataset 4: MAP gene dependency of cell viability dataset, downloaded from the Dependency Map (DepMap) portal (v21Q3, https://depmap.org/portal/) (24), one of the largest collections of CRISPR screening studies in 1,054 kinds of human cancer cells from 30 lineages. Genome-wide gene dependency scores were quantified using CERES method by adjusting copy number amplification effect, where the scores of 0 and −1 represent the median effects of nonessential genes and common core essential genes, respectively (25). In this study, we used a cutoff of −0.5 to define cellular dependency and essentiality of the MAP genes in 31 cell lines belonging to the NB lineage.

Dataset 5: Genome-wide CRISPR screens in primary human T cells for identifying gene targets that regulate T cell proliferation in response to T cell receptor stimulation. The sgRNAs targeting specific genes were defined to be regulators of T cell proliferation by calculating the abundance-based rank difference between the highly dividing cells and non-dividing cells (26).

MAP gene collection

The MAP genes were extracted and combined from the MitoCarta (v3.0; https://www.broadinstitute.org/mitocarta) (27) and the human protein atlas (HPA; https://www.proteinatlas.org/) databases (28). Specifically, the MitoCarta3.0 is an inventory of 1,136 human and 1,140 mouse genes encoding proteins with support of mitochondrial localization, now with sub-mitochondrial compartment and pathway annotations; the cell atlas of the HPA project contains 1,156 genes which have been shown to localize to mitochondria.

Mapping MAP genes to MitoPathways

According to the MitoCarta database, MAP genes were annotated to eight major Mitochondrial Pathways (MitoPathways), including mitochondrial central dogma, protein import and sorting, protein homeostasis, oxidative phosphorylation (OXPHOS), metabolism, small molecule transport, signaling, and mitochondrial dynamics and surveillance (29). For the MAP genes exclusively in the HPA database, we conducted Gene Ontology (GO)-based gene-level semantic similarity analysis with the GOSemSim package (v2.14.2) (30). Each of these genes was annotated to the MitoPathway with the highest similarity score with the *clusterSim* function by comparing the target genes to those annotated in each MitoPathway with parameters: *measure="Wang", combine="BMA"*. The genes annotated to >3 sub-pathways were excluded from our annotation pipeline. We obtained a total of 1,191 MAP genes annotated to the eight MitoPathways.

Collection of putative target genes of MYC transcription factor

This gene set was downloaded from the Gene Set Enrichment Analysis website (https://www.gsea-msigdb.org/) (31) with the standard gene set name of DANG_MYC_TARGETS_UP, which was defined by the genes upregulated by MYC and whose promoters are bound by MYC, according to MYC target Gene Database. This gene set contains 144 members mapped to 130 genes.

Pan-cancer analysis of MAP genes

The mRNA expression data sets generated by The Cancer Genome Atlas (TCGA) project (32) were downloaded using the UCSCXenaTools package (33). Sample barcode was annotated with the TCGAutils package (34). We used the Level-3 gene expression data sets from 21 cancer types, including the LUAD (Lung Adenocarcinoma), ACC (Adrenocortical Cancer), CHOL (Bile Duct Cancer), BLCA (Bladder Cancer), BRCA (Breast invasive carcinoma), CESC (Cervical Cancer), COAD (Colon adenocarcinoma), ESCA (Esophageal cancer), GBM (Glioblastoma), KIRC (Kidney Clear Cell Carcinoma), KIRP (Kidney Papillary Cell Carcinoma), LUSC (Lung Squamous Cell Carcinoma), SKCM (Melanoma), LIHC (Liver Cancer), LGG (Lower Grade Glioma), OV(Ovarian Cancer), UVM (Ocular melanomas), PAAD (Pancreatic Cancer), PRAD (Prostate Cancer), STAD (Stomach Cancer), and THCA (Thyroid Cancer). Because normal samples from the TCGA project are typically limited in the number for many cancer types, we used normal expression data from the GTEx project (https://www.gtexportal.org/). For GTEx datasets, we downloaded the "gene expression RNAseq—TOIL RSEM expected_count" matrix from the Xena project. GTEx samples were grouped according to the tissues corresponding to the TCGA cancers. Gene IDs and symbols were mapped and converted with the "org.Hs.eg.db" package (35). All the gene expression RNAseq datasets from Xena were generated with a same data processing pipeline to create a consistent meta-analysis of different datasets free of computational batch effects (36). Differential gene expression analyses were conducted with the "limma" package, and survival analyses were conducted with the GEPIA webserver (37).

Functional enrichment analyses

We employed different methods for functional enrichment analysis based on the different gene lists we were concerned with as indicated in our manuscript. Gene-set enrichment analysis

(GSEA) is a computational method that determines whether an *a priori*-defined set of genes shows statistically significant, concordant differences between two conditions. For dataset 1, we tested the enrichment of each MitoPathway gene set using the ranked MAP genes based on their mRNA fold changes values. Gene Ontology (GO) term analysis was performed by comparing the gene set of interest to a reference set of genes that have been annotated with GO terms. GSEA and GEO term analyses were performed with the *runGSA* and *runGSAhyper* functions, respectively, which were embedded in the piano package (38).

Cox regression-based survival analyses and important gene/feature selection

A univariate Cox regression analysis was performed to reveal the association between the genes and the OS of NB with the "survival" package (v3.1.12) in the R environment. The genes with log-rank $P < 0.05$ were considered to be the prognosis-related genes and further subjected to a feature selection procedure. The mRNA expression levels of the tested genes in Cox regression analysis were separated into "high" and "low" groups based on the ranking of the genes across all the patients. A Lasso regression within a framework of five-fold cross-validation was conducted to reduce the variable dimension and select essential genes related to prognosis. The rated genes were further subjected to a multivariate Cox regression analysis. Cox regression and Lasso regression analyses were conducted with the "glmnet" package (v4.1–2) (39). The model assessment was performed using the time-dependent ROC analysis with the "timeROC" package (v0.4)(40).

Results

MAP mRNAs express differently in NB cell lines from normal cell types

At the beginning of our study, we compiled a list of 1,712 MAP genes by integrating the HPA and the MitoCarta3.0 databases (see Methods). Using publicly available bulk RNA-Seq data containing 39 NB cell lines and two types of normal cells (Dataset 1, GSE89413; see Methods), clustering analyses based on the mRNA abundance of top variant genes and MAP genes showed a distinct separation between NB and normal cell types (**Figure 1A**), suggesting a different pattern of global gene expression in the NB cells and the ability of MAP genes to characterize NB cell identity. To further assess the gene expression alteration of these MAP genes in NB, we compared their mRNA levels between NB cells and normal ones and found 143 MAP genes (adjusted $P < 0.05$; **Supplementary Table S1**) showing significantly differential mRNA expression in NB cells (**Figure 1B**). Based on the MitoPathway annotation (see Methods), GSEA was performed to reveal the changes and preference of molecular pathways in NB cells. We found several gene sets that were significantly enriched (adjusted $P < 0.1$) by increased mRNA expression in NB cells, including the mitochondrial central dogma, mitochondrial RNA metabolism, translation, mitochondrial ribosome, mitochondrial DNA maintenance, and oxidative phosphorylation (OXPHOS). In contrary, the gene sets of vitamin A metabolism and ROS and glutathione metabolism were enriched by repressed mRNA expression in NB cells (**Figure 1C**). Of note, our differential expression analysis of MAP genes revealed some known mRNA expression biomarkers, such as *LDHB* (41), and *HSPD1* (42), whose upregulation was associated with NB tumor cell survival and prognosis. We also noted 38 genes annotated in the significantly changed pathways, including upregulation of mitochondrial DNA encoding genes (*MRPL50*, *MRPS23*, *MRPL42*, *MRPL32*, *MRPL47*, *MRPL3*, *MRPL21*, and *MRPS21*) and downregulation of *CEP89*, *AIFM2*, and *ZNFX1* in the NB cell lines (**Figure 1D**). These results indicated that mitochondria-related molecules undergo rewiring to create a supportive cellular environment for NB cells to survive, thus demonstrating the significance of monitoring the mRNA expression of MAP genes in NB cells.

Characterizing MAP gene expression in primary NB tumors in different clinical subgroups

Although immortalized cell lines represent the most widely used methods, they cannot reliably reflect the *in vivo* cellular environment of tumors because human tumor tissues contain a complex mixture of cell types and microenvironments (43). Therefore, we examined MAP gene expression dynamics in primary NB tumors using another publicly available bulk RNA-Seq data from 498 subjects (Dataset 2, GSE49711; see Methods). Interestingly, clustering analysis based on the MAP genes showed that NB tumors were grouped by *MYCN* status, progression events, high risk, or death from NB (**Figure 2A**), indicating that MAP gene expression were associated with amplified *MYCN*, tumor progression, higher clinical risk and higher risk of death of NB tumors. In contrast, we found a weak classification effect of the INSS stage information in NB tumors (**Figure 2A**), suggesting a weak correlation between global expression of MAP mRNAs and the four-level ordinal scale in the INSS stage, which was further excluded from our following analyses.

Differential gene expression analysis (DEA) was performed between subgroups for each of the remaining four parameters. A total of 1,149 MAP genes (**Supplementary Table S2**) were identified to be differentially expressed by combining the DEA results, where approximately 61% were shared by all four parameters, and 86% were shared by at least two parameters (**Figure 2B**), indicating that these clinical parameters have largely common molecular basis. This result was consistent with the clinical relevance between these parameters, as shown by overlapping the 239 NB tissues positive in high risk, progression occurrence, *MYCN* status, or death of the disease (**Figure 2C**). In order to thoroughly uncover these molecular changes, we employed hierarchical clustering analysis of NB tumors according

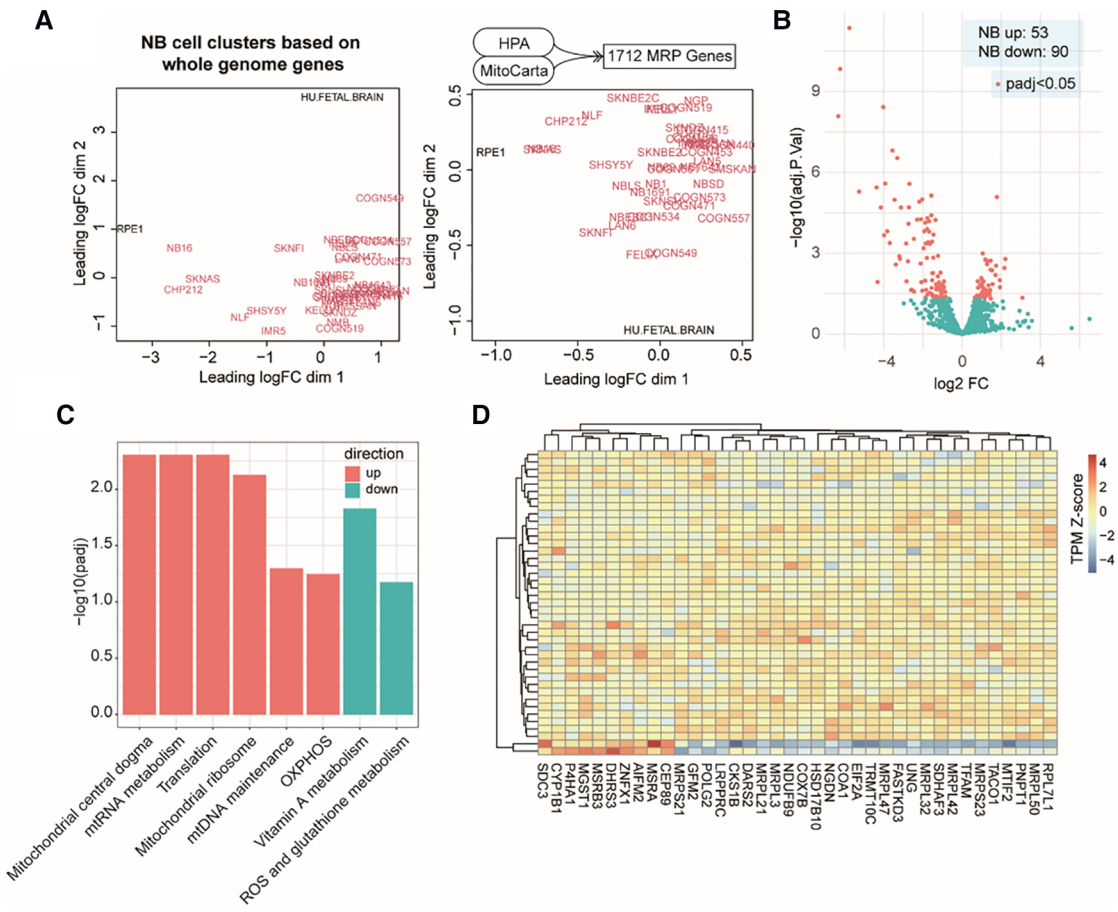

FIGURE 1
MAP mRNA expression changes in NB cell lines. (A). Multidimensional scaling plots of distances between gene expression profiles using the top 1,000 genes with the largest standard deviations between samples (left) or using all the MAP genes (right). Red colored labels indicate NB cell lines, black colored labels indicate the control samples. (B). Volcano plot of MAP gene expression changes in NB cell lines. (C). Bar plot of significant MitoPathways by GSEA analyses. Logarithmic adjusted *P* values are compared and plotted. Red bars indicate MitoPathways enriched by gene expression upregulation, and cyan bars indicate that enriched by gene expression downregulation. (D). Heatmap of normalized mRNA levels of highlighted MAP genes from significant pathways in NB cell lines and normal samples.

to these four parameters and MAP genes with high fold changes (>2-fold). The analysis revealed NB subgroups and subgroup-specific MAP mRNA change signatures. Notably, our analysis highlighted two groups of MAP genes: G1 group (62 genes), which showed increased expression in concordance with *MYCN* amplification; and G2 group (14 genes), which was uniquely associated with NB tumors without *MYCN* amplification but with high clinical risk (**Figure 2D**). Because *MYCN* encodes the Myc oncogenic transcription factor, we compared the G1 genes to those putative Myc target genes that can be up-regulated by Myc and whose promoters are bound by Myc (see Methods), we found only three genes (*CKS2*, *APEX1*, *HSPD1*) shared between these two gene sets, indicating that the genetic regulatory networks underlying the genesis of NB are much more complicated than those related to the Myc regulatory network.

We noted that our analysis based on the primary NB tissues reproduced some known markers for NB prognosis and high-risk, including *CKS2* that was considered a prognostic marker of various tumors (44), *PDK1* that could provide significant hints for high-risk NB patients (45), and *PIF1*, one Myc-target gene, that could significantly repress tumor upon knockdown (46). We also compared the differential gene sets obtained from the bulk RNA-seq data of cell lines and primary tissues and found only ten common genes in these two groups, including *DGKA*, *HSPD1*, *MTHFD2*, *LDHB*, *PAICS*, *SUV39H2*, *UNG*, *NT5DC5*, and *DHFR* (**Figure 2E**), which indicated the importance of using tissue data to validate cell line-based data. Collectively, these results demonstrated that MAP genes also altered their expression pattern in primary NB tissues and showed a clinical potential to stratify NB patients.

MAP genes exert cell type-specific mRNA expression in NB tumor microenvironment (TME)

Because tumor tissues are a complex mixture of cell types, we next asked whether the expression changes of these MAP genes are specific to certain cell types in NB TME or not. Therefore, we investigated 160,839 single-cell transcriptomes from 16 NB

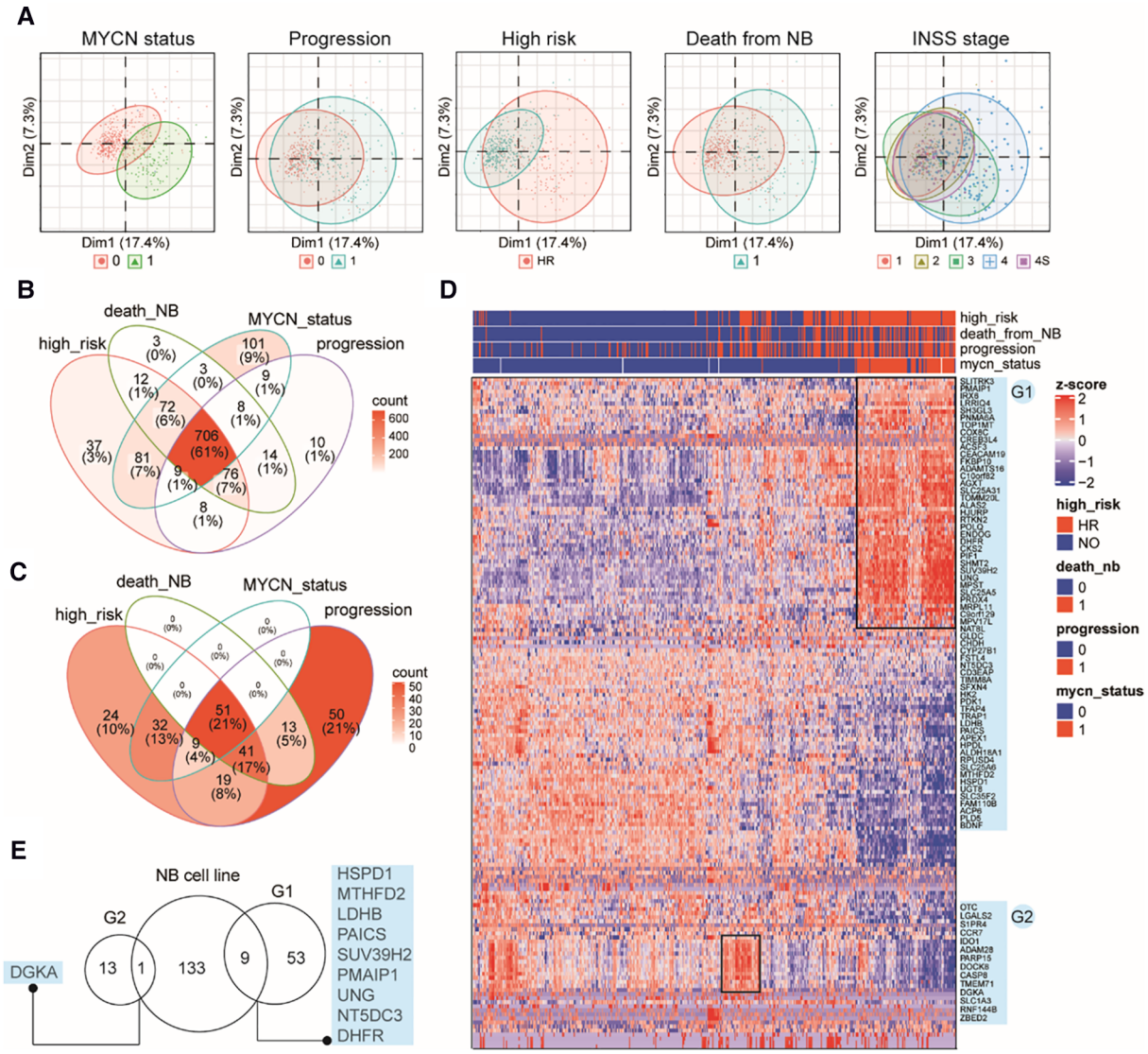

FIGURE 2
Characterizing MAP gene expression in primary NB tumors in different clinical subgroups. (A) Principal component analysis (PCA) plots of the top two PCs showing clustering relationship of 498 primary NB tumors by *MYCN* status, progression events, higher clinical risk, death from NB and INSS stages. (B) Venn diagram of differential MAP genes by comparing subgroups in four clinical parameters. (C) Venn diagram of NB tumors positive in four clinical parameters. (D) Heatmap of mRNA levels of top differential MAP genes (>2-fold) in NB tumors. Rows indicate MAP genes and columns indicate NB patients, both clustered by hierarchical clustering method. Clinical annotations for each patient are shown on the top of the heatmap. Two groups of MAP genes are highlighted and named as G1 and G2, shown on the right of the heatmap. (E) Venn diagram of MAP genes in G1, G2 and differential ones in the bulk cell line dataset.

tissues (Dataset 3, GSE137804; see Methods). Cell identity was defined according to the original study (2), including eight major cell types: neuroendocrine cells (tumor cell), T cells, myeloid cells, B cells, Schwann stromal cells, fibroblasts, plasmacytoid dendritic cells (pDCs), and endothelium cells (**Figure 3A**). Comparing mRNA expression profiles between different cell types revealed 106 MAP genes showing diverged mRNA levels (adjusted $P < 0.05$; **Supplementary Table S3**). We identified 27 genes, which showed increasing mRNA levels specifically in tumor cells (**Figures 3B,C**). Comparing the percentage of cells with identified expression of these genes revealed that 22 out of 27 genes were mainly enriched in tumor cells (**Figure 3C**). We noted several mtDNA encoding genes, including *MT-CO1, MT-CO2, MT-ND2,* and *MT-ND4*, and nuclear DNA encoding genes but showing important roles in mitochondrial biogenesis, including *DUT* and *SOX4*. Accordingly, we inferred that mitochondrial production of NB tumor cells is accelerated. As expected, we observed a high abundance of short read counts mapping to mitochondrial DNA genes in tumor cells even after the removal of low-quality cells (**Figure 3D**; see Methods).

To uncover the relevant molecular functions involved in the complex ecosystem, we conducted gene co-expression analysis between the MAP and non-MAP genes across all of the single cells. We found 248 non-MAP genes showing a significant high

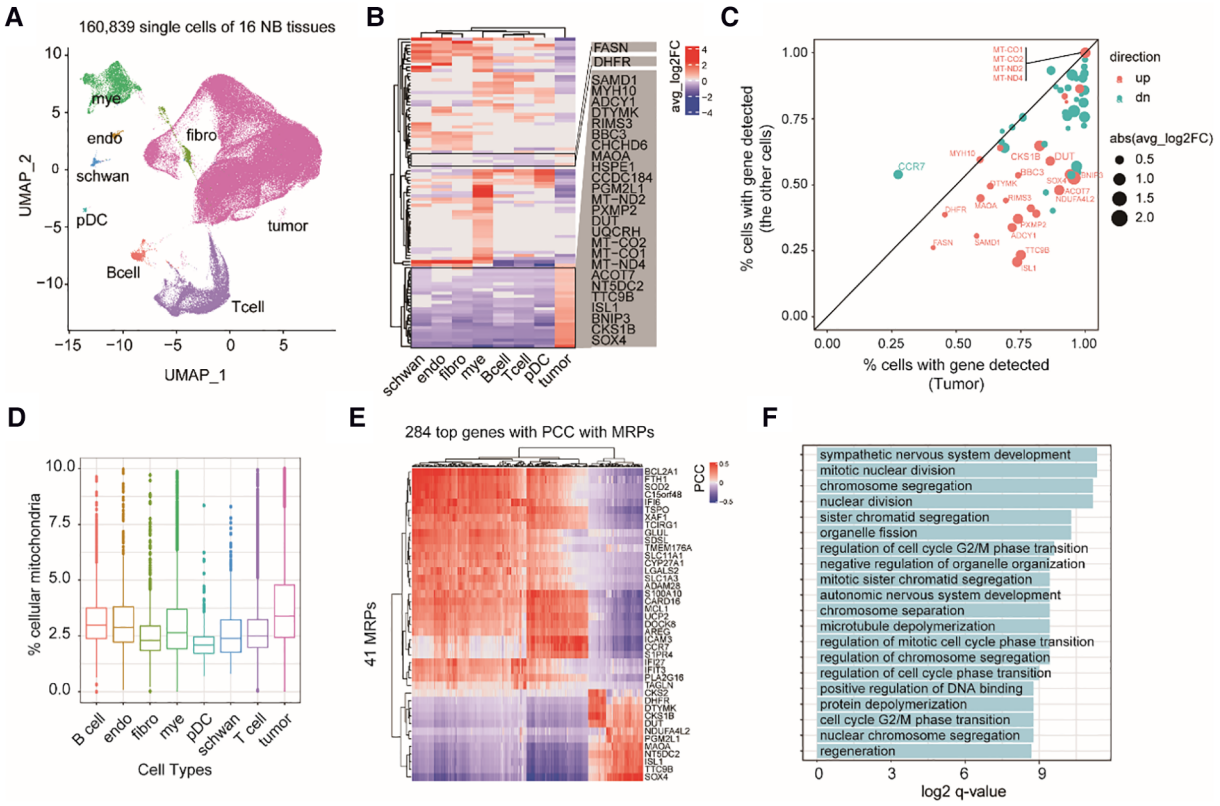

FIGURE 3
Exploring cell type-specific expression changes of MAP genes in NB TME. (**A**) UMAP projection of the single cell dataset colored according to cell type identity. Mye, myeloid cells; endo, endothelium cells; schwan, Schwann stromal cells; pDC, plasmacytoid dendritic cells; Bcell, B cells; Tcell, T cells; fibro, fibroblasts. (**B**) Heatmap of differential MAP genes in each cell type. (**C**) Scatter plot of the percentage of cells with detected expression of differential MAP genes in tumor and non-tumor cell types. Point size indicates the degree of gene expression foldchanges, point colors indicate up-regulation (red) and down-regulation (cyan) in the tumor cells. (**D**) boxplots of the percentage of shorted reads aligned to mtDNAs in each cell type. (**E**) Heatmap of 284 genes showing high correlation with MAP genes by pairwise gene expression correlation analysis across all the cells. (PCC > 0.4 or < −0.4). (**F**) Barplot of significant enriched GO terms by the top correlated genes with MAP genes.

correlation with MAP genes with Pearson correlation coefficient (PCC) > 0.4 or <−0.4 (Figure 3E). GO term analysis revealed that these correlated non-MAP genes were mainly from cell cycle-related cellular pathways (adjusted $P < 0.05$), such as mitotic nuclear division and chromosome segregation terms (Figure 3F). Taken together, our analyses suggested that MAP genes exert cell type-specific expression changes in NB tumors and possibly underlie the malignancy characteristics of tumor cells, such as an enhanced cell proliferation capacity than those non-tumor cells.

MAP genes can predict the clinical outcome of NB patients

Combining the DEA results from each dataset, we totally identified 1,301 differentially expressed MAP genes associated with NB tumors or clinical subtypes, accounting for approximately 76% of all MAP genes. Most of these differential MAP genes had a high mRNA expression abundance in primary NB tissues (Figure 4A). Univariant Cox proportional hazard regression modeling revealed 880 MAP genes showing significant association with the overall survival (OS) of NB patients ($P <$ 0.05). Out of these genes, 542 were identified to be risk factors with higher mRNA levels in NB tumors, with the estimated hazard ratio (HR) ranging from 1.48 to 17.03 (Figure 4A).

We next examined whether these OS-related MAP genes were redundant and to what extent these genes could predict the prognosis of NB. Pearson correlation analysis of the OS-related MAP genes showed that around 27% of all pairwise genes showed a significant correlation in the NB cohort with the absolute values of PCC > 0.3 (Figure 4B), which was a challenge to multivariate regression modeling because of the possible multicollinearity problem. Therefore, we conducted a multivariate regression analysis following an informative feature selection procedure. The feature selection was conducted from 147 differential MAP genes shared by at least two datasets and associated with NB OS. To minimize the adverse impacts raised by overfitting or selection bias, we rated the importance of these genes for clinical outcomes of the patients, dead or censored in our data, using Lasso regression within a framework of 5-fold cross-validation (see Methods). By doing so, we narrowed the long gene list down to 15 (Figure 4C). We constructed a 15-gene model to predict the death event in a time-dependent way with the accuracy ranging from 0.8765 to 0.9678, which was

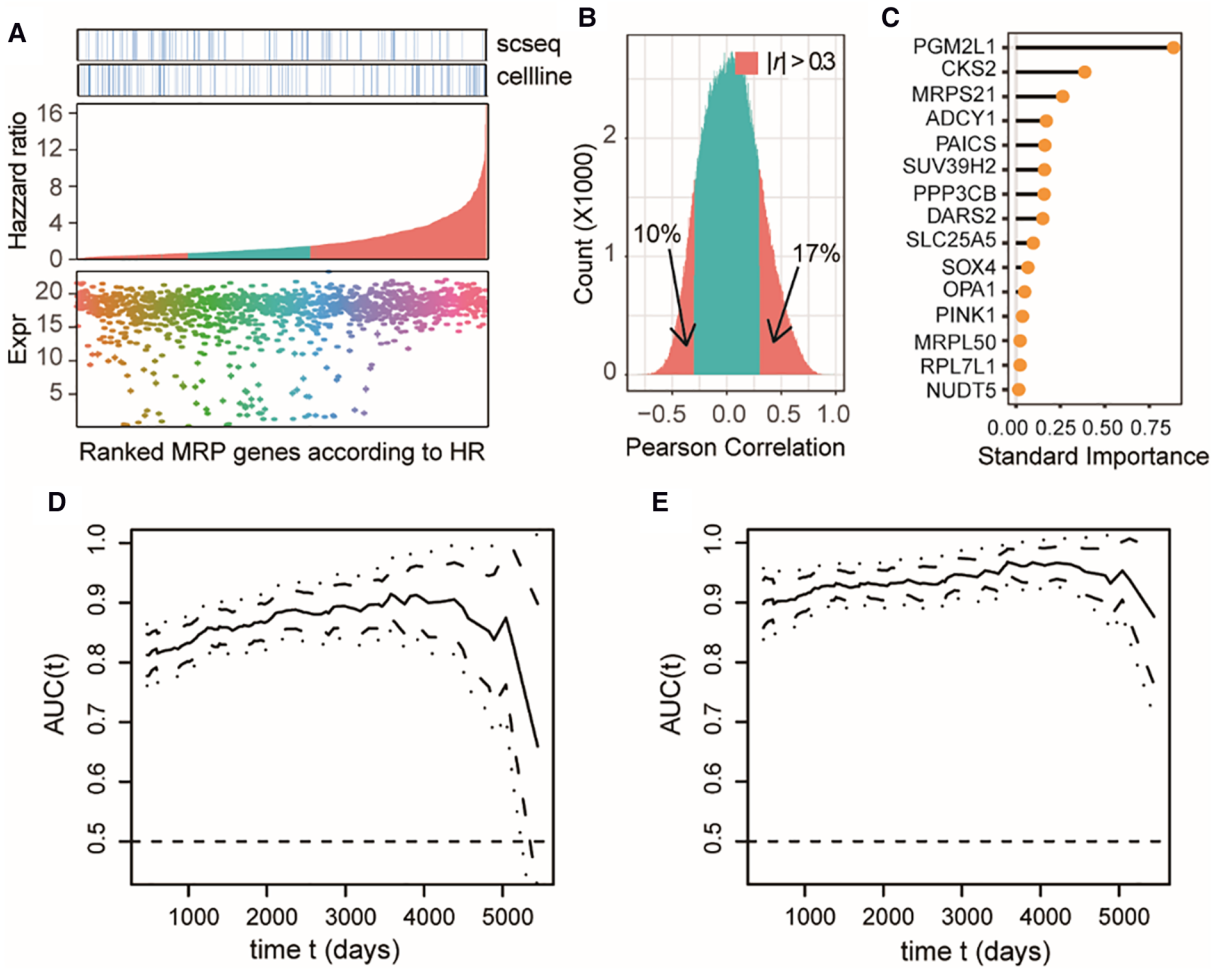

FIGURE 4
MAP genes can predict clinical outcome of NB patients and exert additive effects. (**A**) Dot plot of expression levels in the bulk tissue dataset of differential MAP genes combining all three datasets (bottom); barplot of the differential MAP genes by ranking the hazzard ratio values obtained by univariant Cox proportional hazard regression analyses (middle); annotation differential MAP genes in the single cell dataset and bulk cell line dataset (top). Red bars in the middle panel indicate significant association with overall survival ($P < 0.05$). (**B**) Histogram of Pearson correlation coefficient between all pairwise of MAP genes by comparing their mRNA level in all samples in the bulk tissue dataset. (**C**) Line plot of ranked standard importance of selected MAP genes by a Lasso regression analysis. (**D**,**E**) Line plots of the estimated AUC under the time-dependent ROC at each time point with the two-gene model (**D**) and the full-gene model (**E**).

significantly higher than that of the 2-gene model based on the top 2 important genes (*PGM2L1*, *CKS2*) (*t*-test, $P < 2.2e\text{-}16$; **Figures 4D,E**). Moreover, the accuracy of the 2-gene model decreased sharply over time in comparison with the 15-gene model, especially for survival predictions after 4,000 days. We also compared our 15-gene model to those proposed in previous studies: The first one is a three-gene model, including *CKB*, *DST*, and *DUT*; and the second one is a six-gene model, including *CYLD*, *JAK1*, *APC*, *ERH*, *CNBP*, and *BAX*. In our used NB cohort dataset, we didn't find the expression of *DST* and *APC*. Therefore, we compared our 15-gene model to the two-gene model (*CKB*, and *DUT*) and the five-gene model (*CYLD*, *JAK1*, *ERH*, *CNBP*, and *BAX*). Our 15-gene model perform better than these two models (**Supplementary Figures S1, S2**). These results together demonstrated that our 15-gene model can accurately predict NB prognosis.

MAP genes are essential for cancer cells but not for the proliferation of *ex vivo* human primary T cells

Because our study revealed that NB cells tend to aberrantly increase mitochondrial synthesis, we next evaluated the potential of targeting MAP genes in NB therapy by analyzing gene dependency assay based on genome-wide CRISPR screening (Dataset 4, see Methods), which is an informative and powerful tool for identifying the gene that are critical for the survival and proliferation of cancer cells. We found a total of 544 MAP genes that were essential for at least one NB cell line, out of which 278 showed higher degree of essentialities that repressed cell survival upon knockout in at least 10 cell lines (**Figures 5A,B**).

We next evaluated whether targeting these genes in clinical therapeutics, if possible, can disturb the tumor-associated

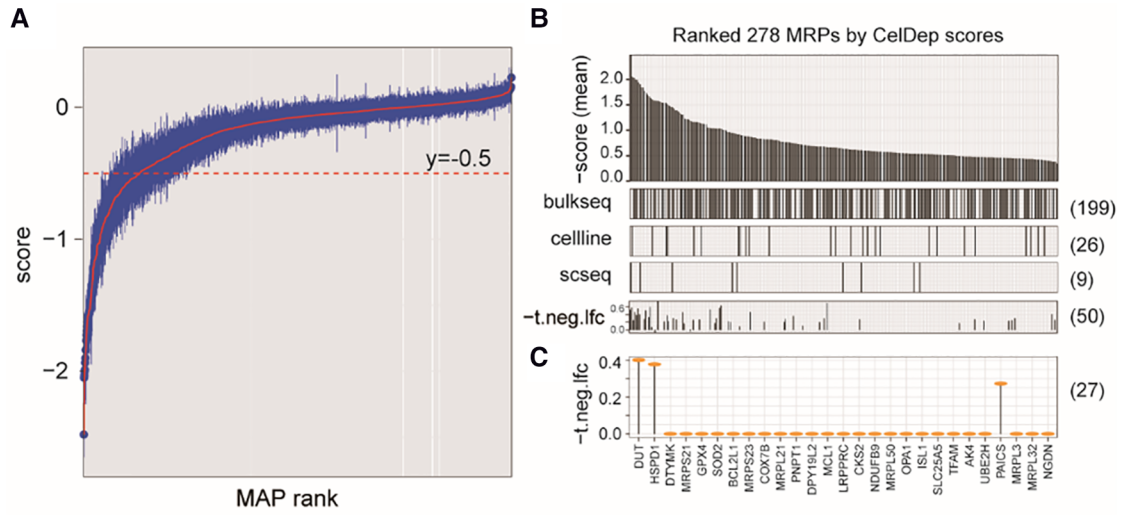

FIGURE 5
Characterizing MAP genes essential for cancer cells but not for *ex vivo* human primary T cells. (**A**) Simplified boxplots of all MAP genes ranked based on the estimation of gene essentiality in NB cell lines. (**B**) Barplot of ranked MAP genes based on the gene essentiality scores (up panel), indications of overlap with the DEGs identified in three datasets (middle panels), and indications of overlap with the MAPs identified in CRISP-Cas9 dataset derived from T cells (bottom panel). (**C**) Selected MAP gene candidates overlapped between at least two dataset and the T cell dataset.

immune microenvironment. We investigated the cellular effects of targeting these genes on the T cells, which play the most important roles in the anti-tumor immune response. Using a genome-wide CRISPR-Cas9 screening data from the primary human T cells (26) (Dataset 5; see Methods), we found that 50 of these MAP genes would not inhibit T cell differentiation *ex vivo* ($P > 0.05$), our of which 27 MAP genes were identified in at least two datasets of Dataset 1–3 used in our study. Of note, our study reproduced *DUT* to be a therapeutic candidate, which was consistent with a previous study showing that targeted inhibition of mitochondrial DNA transcription has shown an anti-tumor effect in mice containing human ovarian carcinoma and colorectal cancer cell xenografts (47). These collective results were suggestive of the potential of targeting MAP genes in NB therapeutics.

Pan-Cancer analysis of MAP genes

To explore whether some MAPs are always overexpressed or underexpressed in many tumors, we also tested the expression dynamics of these MAP genes in Pan-cancer datasets (see Methods). We performed DEA by comparing the TCGA mRNA expression dataset to the normal tissue expression data from the GTEx. We found that each type of TCGA tumors contained an average of 1,212 differential MAP genes (adjusted $P < 0.05$; **Supplementary Figure S3**). Of note, approximately 85% of these differential MAP genes were shared in more than 14 cancer types (**Supplementary Figure S4**). We further found 104 differential MAP genes with high-fold change (>2 fold) and high-frequency (>14 types) in human cancers (**Supplementary Figure S5**). Interestingly, these MAP genes mainly exhibit two patterns: 43 MAP genes are mainly upregulated in the majority of cancers, and the other genes are mainly downregulated in the majority of cancers. Overlapping these MAP genes with NB-associated differential MAP genes, we found some shared genes including *SOX4, CKS2, SUV39H2, DARS2, PYCR1*, and *PMAIP1*. These results collectively demonstrated the significance of studying MAP genes in human pan-cancers.

Discussion

A feasible targeted therapy in NB is still urgently needed, especially for patients with high-risk tumors. Because an expanded set of targets would offer additional therapeutic opportunities (26), in-depth and careful reanalysis of publicly available NB-related gene expression profiles at different dimensions will be helpful in identifying potential targets for new treatments. In this study, we conducted a comprehensive and integrated bioinformatics analysis on publicly accessible gene expression data from neuroblastoma (NB) cell lines and primary tissues at both the tissue and single cell level. Our results support the use of MAP genes as potential markers for categorizing and determining the stage of NB tumors, predicting outcomes, and guiding the development of targeted treatments.

With the advance in the development of research techniques in life science, genetic and molecular biomarkers have been frequently examined for risk stratification and prognosis prediction in NB. For instance, the outcome of NB patients has been revealed to be associated with varying molecular signatures, including genetic mutations of specific genes (48), the methylation status of *RB1* and *TDGF1* (49), detectable circulating tumor DNAs in blood biopsy (50), and altered mRNA expression levels of specific gene

lists (51–54). In this study, it was found that 542 mitochondria-related protein-encoding genes were associated with the elevated HR of NB patients, which reduced the OS with higher mRNA levels. In addition, this adverse effect on the OS can be addictive.

Targeting mitochondria with activation of the cell death machinery in cancer cells by inhibiting tumor-specific alterations of the mitochondrial metabolism or by stimulating mitochondrial membrane permeabilization has long been thought to be a promising therapeutic approach (55, 56). Targeting mitochondria of cancer cells requires precise delivery of the drugs to the subcellular localizations, which poses challenges for the choice of targets and the design of drug molecules. Our study presented candidates by employing integration of tumor-associated mRNA expression changes at the bulk tissue and single cell resolutions, which extends the choice of molecular targets for targeting mitochondria strategies.

Data availability statement

The datasets presented in this study can be found in online repositories. The names of the repository/repositories and accession number(s) can be found in the article/**Supplementary Material**.

Author contributions

Conceptualization, CC; Formal analysis, CC and YL; Investigation, HZ, ZY, XH, YZ, YX, LL and JT; Methodology, YL; Resources, HZ; Supervision, CC and QW; Validation, ZY; Writing—original draft, CC; Writing—review & editing, CC and QW. All authors contributed to the article and approved the submitted version.

Funding

This work was supported by the Municipal School (College) Joint Funding Project (202201020594 to CWC and 202201020591 to QW) of Guangzhou Women and Children's Medical Center, Guangzhou Medical University.

Conflict of interest

The authors declare that the research was conducted in the absence of any commercial or financial relationships that could be construed as a potential conflict of interest.

Publisher's note

All claims expressed in this article are solely those of the authors and do not necessarily represent those of their affiliated organizations, or those of the publisher, the editors and the reviewers. Any product that may be evaluated in this article, or claim that may be made by its manufacturer, is not guaranteed or endorsed by the publisher.

Supplementary material

The Supplementary Material for this article can be found online at: https://www.frontiersin.org/articles/10.3389/fped.2023.1094926/full#supplementary-material.

References

1. Nakagawara A, Li Y, Izumi H, Muramori K, Inada H, Nishi M. Neuroblastoma. *Jpn J Clin Oncol*. (2018) 48(3):214–41. doi: 10.1093/jjco/hyx176

2. Dong R, Yang R, Zhan Y, Lai HD, Ye CJ, Yao XY, et al. Single-Cell characterization of malignant phenotypes and developmental trajectories of adrenal neuroblastoma. *Cancer Cell*. (2020) 38(5):716–733 e6. doi: 10.1016/j.ccell.2020.08.014

3. Kameneva P, Artemov AV, Kastriti ME, Faure L, Olsen TK, Otte J, et al. Single-cell transcriptomics of human embryos identifies multiple sympathoblast lineages with potential implications for neuroblastoma origin. *Nat Genet*. (2021) 53(5):694–706. doi: 10.1038/s41588-021-00818-x

4. Tolbert VP, Matthay KK. Neuroblastoma: clinical and biological approach to risk stratification and treatment. *Cell Tissue Res*. (2018) 372(2):195–209. doi: 10.1007/s00441-018-2821-2

5. Ambros PF, Ambros IM, Brodeur GM, Haber M, Khan J, Nakagawara A, et al. International consensus for neuroblastoma molecular diagnostics: report from the international neuroblastoma risk group (INRG) biology committee. *Br J Cancer*. (2009) 100(9):1471–82. doi: 10.1038/sj.bjc.6605014

6. Caron H, van Sluis P, de Kraker J, Bokkerink J, Egeler M, Laureys G, et al. Allelic loss of chromosome 1p as a predictor of unfavorable outcome in patients with neuroblastoma. *N Engl J Med*. (1996) 334(4):225–30. doi: 10.1056/NEJM199601253340404

7. Spitz R, Hero B, Ernestus K, Berthold F. Deletions in chromosome arms 3p and 11q are new prognostic markers in localized and 4s neuroblastoma. *Clin Cancer Res*. (2003) 9(1):52–8.

8. Depuydt P, Boeva V, Hocking TD, Cannoodt R, Ambros IM, Ambros PF, et al. Genomic amplifications and distal 6q loss: novel markers for poor survival in high-risk neuroblastoma patients. *J Natl Cancer Inst*. (2018) 110(10):1084–93. doi: 10.1093/jnci/djy022

9. Caren H, Kryh H, Nethander M, Sjoberg RM, Trager C, Nilsson S, et al. High-risk neuroblastoma tumors with 11q-deletion display a poor prognostic, chromosome instability phenotype with later onset. *Proc Natl Acad Sci U S A*. (2010) 107(9):4323–8. doi: 10.1073/pnas.0910684107

10. Gilbert F, Feder M, Balaban G, Brangman D, Lurie DK, Podolsky R, et al. Human neuroblastomas and abnormalities of chromosomes 1 and 17. *Cancer Res*. (1984) 44(11):5444–9.

11. Szewczyk K, Wieczorek A, Mlynarski W, Janczar S, Woszczyk M, Gamrot Z, et al. Unfavorable outcome of neuroblastoma in patients with 2p gain. *Front Oncol*. (2019) 9:1018. doi: 10.3389/fonc.2019.01018

12. Bown N, Cotterill S, Lastowska M, O'Neill S, Pearson AD, Plantaz D, et al. Gain of chromosome arm 17q and adverse outcome in patients with neuroblastoma. *N Engl J Med*. (1999) 340(25):1954–61. doi: 10.1056/NEJM199906243402504

13. Brodeur GM, Seeger RC, Schwab M, Varmus HE, Bishop JM. Amplification of N-myc in untreated human neuroblastomas correlates with advanced disease stage. *Science*. (1984) 224(4653):1121–4. doi: 10.1126/science.6719137

14. Amler LC, Schurmann J, Schwab M. The DDX1 gene maps within 400 kbp 5' to MYCN and is frequently coamplified in human neuroblastoma. *Genes Chromosomes Cancer*. (1996) 15(2):134–7. doi: 10.1002/(SICI)1098-2264(199602)15:2<134::AID-GCC9>3.0.CO;2-4

15. Wimmer K, Zhu XX, Lamb BJ, Kuick R, Ambros PF, Kovar H, et al. Co-amplification of a novel gene, NAG, with the N-myc gene in neuroblastoma. *Oncogene*. (1999) 18(1):233–8. doi: 10.1038/sj.onc.1202287

16. Javanmardi N, Fransson S, Djos A, Umapathy G, Ostensson M, Milosevic J, et al. Analysis of ALK, MYCN, and the ALK ligand ALKAL2 (FAM150B/AUGalpha) in neuroblastoma patient samples with chromosome arm 2p rearrangements. *Genes Chromosomes Cancer*. (2019) 59(1):50–7. doi: 10.1002/gcc.22790

17. Lerone M, Ognibene M, Pezzolo A, Martucciello G, Zara F, Morini M, et al. Molecular genetics in neuroblastoma prognosis. *Children (Basel)*. (2021) 8(6):456. doi: 10.3390/children8060456

18. Baali I, Acar DAE, Aderinwale TW, HafezQorani S, Kazan H. Predicting clinical outcomes in neuroblastoma with genomic data integration. *Biol Direct*. (2018) 13 (1):20. doi: 10.1186/s13062-018-0223-8

19. Barrett T, Wilhite SE, Ledoux P, Evangelista C, Kim IF, Tomashevsky M, et al. NCBI GEO: archive for functional genomics data sets–update. *Nucleic Acids Res*. (2013) 41(Database issue):D991–5. doi: 10.1093/nar/gks1193

20. Harenza JL, Diamond MA, Adams RN, Song MM, Davidson HL, Hart LS, et al. Transcriptomic profiling of 39 commonly-used neuroblastoma cell lines. *Sci Data*. (2017) 4:170033. doi: 10.1038/sdata.2017.33

21. Wang C, Gong B, Bushel PR, Thierry-Mieg J, Thierry-Mieg D, Xu J, et al. The concordance between RNA-seq and microarray data depends on chemical treatment and transcript abundance. *Nat Biotechnol*. (2014) 32(9):926–32. doi: 10.1038/nbt.3001

22. Monclair T, Brodeur GM, Ambros PF, Brisse HJ, Cecchetto G, Holmes K, et al. The international neuroblastoma risk group (INRG) staging system: an INRG task force report. *J Clin Oncol*. (2009) 27(2):298–303. doi: 10.1200/JCO.2008.16.6876

23. Butler A, Hoffman P, Smibert P, Papalexi E, Satija R, et al. Integrating single-cell transcriptomic data across different conditions, technologies, and species. *Nat Biotechnol*. (2018) 36(5):411–20. doi: 10.1038/nbt.4096

24. Tsherniak A, Vazquez F, Montgomery PG, Weir BA, Kryukov G, Cowley GS, et al. Defining a cancer dependency map. *Cell*. (2017) 170(3):564–76. e16. doi: 10.1016/j.cell.2017.06.010

25. Meyers RM, Bryan JG, McFarland JM, Weir BA, Sizemore AE, Xu H, et al. Computational correction of copy number effect improves specificity of CRISPR-Cas9 essentiality screens in cancer cells. *Nat Genet*. (2017) 49(12):1779–84. doi: 10.1038/ng.3984

26. Shifrut E, Carnevale J, Tobin V, Roth TL, Woo JM, Bui CT, et al. Genome-wide CRISPR screens in primary human T cells reveal key regulators of immune function. *Cell*. (2018) 175(7):1958–71. e15. doi: 10.1016/j.cell.2018.10.024

27. Rath S, Sharma R, Gupta R, Ast T, Chan C, Durham TJ, et al. Mitocarta3.0: an updated mitochondrial proteome now with sub-organelle localization and pathway annotations. *Nucleic Acids Res*. (2021) 49(D1):D1541–7. doi: 10.1093/nar/gkaa1011

28. Uhlen M, Fagerberg L, Hallstrom BM, Lindskog C, Oksvold P, Mardinoglu A, et al. Tissue-based map of the human proteome. *Science*. (2015) 347(6220):1260419. doi: 10.1126/science.1260419

29. Pagliarini DJ, Calvo SE, Chang B, Sheth SA, Vafai SB, Ong SE, et al. A mitochondrial protein compendium elucidates complex I disease biology. *Cell*. (2008) 134(1):112–23. doi: 10.1016/j.cell.2008.06.016

30. Yu G, Li F, Qin Y, Bo X, Wu Y, Wang S. GOSemsim: an R package for measuring semantic similarity among GO terms and gene products. *Bioinformatics*. (2010) 26(7):976–8. doi: 10.1093/bioinformatics/btq064

31. Subramanian A, Tamayo P, Mootha VK, Mukherjee S, Ebert BL, Gillette MA, et al. Gene set enrichment analysis: a knowledge-based approach for interpreting genome-wide expression profiles. *Proc Natl Acad Sci U S A*. (2005) 102 (43):15545–50. doi: 10.1073/pnas.0506580102

32. Weinstein JN, Collisson EA, Mills GB, Shaw KR, Ozenberger BA, Ellrott K, et al. The cancer genome atlas pan-cancer analysis project. *Nat Genet*. (2013) 45 (10):1113–20. doi: 10.1038/ng.2764

33. Shixiang W, Xuesong L. The UCSCXenaTools R package: a toolkit for accessing genomics data from UCSC Xena platform, from cancer multi-omics to single-cell RNA-seq. *Journal of Open Source Software*. (2019) 4(40):1627. doi: 10.21105/joss.01627

34. Ramos M, Schiffer L, Davis S, Waldron L. *TCGAutils: TCGA utility functions for data management* (2022).

35. Carlson M. org. *Hs.eg.db: Genome wide annotatin for Human* (2019).

36. Vivian J, Rao AA, Nothaft FA, Ketchum C, Armstrong J, Novak A, et al. Toil enables reproducible, open source, big biomedical data analyses. *Nat Biotechnol*. (2017) 35(4):314–6. doi: 10.1038/nbt.3772

37. Tang Z, Li C, Kang B, Gao G, Zhang Z. GEPIA: a web server for cancer and normal gene expression profiling and interactive analyses. *Nucleic Acids Res*. (2017) 45(W1):W98–W102. doi: 10.1093/nar/gkx247

38. Varemo L, Nielsen J, Nookaew I. Enriching the gene set analysis of genome-wide data by incorporating directionality of gene expression and combining statistical hypotheses and methods. *Nucleic Acids Res*. (2013) 41(8):4378–91. doi: 10.1093/nar/gkt111

39. Friedman J, Hastie T, Tibshirani R. Regularization paths for generalized linear models via coordinate descent. *J Stat Softw*. (2010) 33(1):1–22. doi: 10.18637/jss.v033.i01

40. Blanche P, Dartigues JF, Jacqmin-Gadda H. Estimating and comparing time-dependent areas under receiver operating characteristic curves for censored event times with competing risks. *Stat Med*. (2013) 32(30):5381–97. doi: 10.1002/sim.5958

41. Dorneburg C, Fischer M, Barth TFE, Mueller-Klieser W, Hero B, Gecht J, et al. LDHA In neuroblastoma is associated with poor outcome and its depletion decreases neuroblastoma growth independent of aerobic glycolysis. *Clin Cancer Res*. (2018) 24 (22):5772–83. doi: 10.1158/1078-0432.CCR-17-2578

42. Kim W, Ryu J, Kim JE. CCAR2/DBC1 and Hsp60 positively regulate expression of survivin in neuroblastoma cells. *Int J Mol Sci*. (2019) 20(1):131. doi: 10.3390/ijms20010131

43. Gillet JP, Varma S, Gottesman MM. The clinical relevance of cancer cell lines. *J Natl Cancer Inst*. (2013) 105(7):452–8. doi: 10.1093/jnci/djt007

44. Yu K, Ji Y, Liu M, Shen F, Xiong X, Gu L, et al. High expression of CKS2 predicts adverse outcomes: a potential therapeutic target for glioma. *Front Immunol*. (2022) 13:881453. doi: 10.3389/fimmu.2022.881453

45. Ognibene M, Cangelosi D, Morini M, Segalerba D, Bosco MC, Sementa AR, et al. Immunohistochemical analysis of PDK1, PHD3 and HIF-1alpha expression defines the hypoxic status of neuroblastoma tumors. *PLoS One*. (2017) 12(11): e0187206. doi: 10.1371/journal.pone.0187206

46. Chen B, Hua Z, Gong B, Tan X, Zhang S, Li Q, et al. Downregulation of PIF1, a potential new target of MYCN, induces apoptosis and inhibits cell migration in neuroblastoma cells. *Life Sci*. (2020) 256:117820. doi: 10.1016/j.lfs.2020.117820

47. Bonekamp NA, Peter B, Hillen HS, Felser A, Bergbrede T, Choidas A, et al. Small-molecule inhibitors of human mitochondrial DNA transcription. *Nature*. (2020) 588(7839):712–6. doi: 10.1038/s41586-020-03048-z

48. Marachelian A, Villablanca JG, Liu CW, Liu B, Goodarzian F, Lai HA, et al. Expression of five neuroblastoma genes in bone marrow or blood of patients with relapsed/refractory neuroblastoma provides a new biomarker for disease and prognosis. *Clin Cancer Res*. (2017) 23(18):5374–83. doi: 10.1158/1078-0432.CCR-16-2647

49. Yanez Y, Grau E, Rodriguez-Cortez VC, Hervas D, Vidal E, Noguera R, et al. Two independent epigenetic biomarkers predict survival in neuroblastoma. *Clin Epigenetics*. (2015) 7:16. doi: 10.1186/s13148-015-0054-8

50. Trigg RM, Shaw JA, Turner SD. Opportunities and challenges of circulating biomarkers in neuroblastoma. *Open Biol*. (2019) 9(5):190056. doi: 10.1098/rsob.190056

51. Giwa A, Fatai A, Gamieldien J, Christoffels A, Bendou H. Identification of novel prognostic markers of survival time in high-risk neuroblastoma using gene expression profiles. *Oncotarget*. (2020) 11(46):4293–305. doi: 10.18632/oncotarget.27808

52. Utnes P, Lokke C, Flaegstad T, Einvik C. Clinically relevant biomarker discovery in high-risk recurrent neuroblastoma. *Cancer Inform*. (2019) 18:1176935119832910. doi: 10.1177/1176935119832910

53. Schramm A, Schulte JH, Klein-Hitpass L, Havers W, Sieverts H, Berwanger B, et al. Prediction of clinical outcome and biological characterization of neuroblastoma by expression profiling. *Oncogene*. (2005) 24(53):7902–12. doi: 10.1038/sj.onc.1208936

54. Zhong X, Tao Y, Chang J, Zhang Y, Zhang H, Wang L, et al. Prognostic signature of immune genes and immune-related LncRNAs in neuroblastoma: a study based on GEO and TARGET datasets. *Front Oncol*. (2021) 11:631546. doi: 10.3389/fonc.2021.631546

55. Weinberg SE, Chandel NS. Targeting mitochondria metabolism for cancer therapy. *Nat Chem Biol*. (2015) 11(1):9–15. doi: 10.1038/nchembio.1712

56. Guo X, Yang N, Ji W, Zhang H, Dong X, Zhou Z, et al. Mito-Bomb: targeting mitochondria for cancer therapy. *Adv Mater*. (2021) 33(43):e2007778. doi: 10.1002/adma.202007778

frontiers | Frontiers in Oncology

TYPE Original Research
PUBLISHED 24 March 2023
DOI 10.3389/fonc.2023.1099290

OPEN ACCESS

EDITED BY
Chi-kong Li,
The Chinese University of Hong Kong, China

REVIEWED BY
Salvatore Annunziata,
Fondazione Policlinico Universitario A. Gemelli IRCCS, Italy
Alessandro Inserra,
Bambino Gesù Children's Hospital (IRCCS), Italy

*CORRESPONDENCE
Yaqing Zhao
bettertomorrow18@163.com

SPECIALTY SECTION
This article was submitted to Pediatric Oncology, a section of the journal Frontiers in Oncology

RECEIVED 15 November 2022
ACCEPTED 07 March 2023
PUBLISHED 24 March 2023

CITATION
Ren J, Fu Z and Zhao Y (2023) Clinical value of ^{18}F-FDG PET/CT to predict MYCN gene, chromosome 1p36 and 11q status in pediatric neuroblastoma and ganglioneuroblastoma. *Front. Oncol.* 13:1099290. doi: 10.3389/fonc.2023.1099290

Clinical value of ^{18}F-FDG PET/CT to predict MYCN gene, chromosome 1p36 and 11q status in pediatric neuroblastoma and ganglioneuroblastoma

Jiazhong Ren[1], Zheng Fu[1] and Yaqing Zhao[2]*

[1]Department of Medical Imaging, PET-CT Center, Shandong Cancer Hospital and Institute, Shandong First Medical University and Shandong Academy of Medical Sciences, Jinan, Shandong, China, [2]Department of General Affairs Section, The Second Affiliated Hospital of Shandong University of Traditional Chinese Medicine, Jinan, Shandong, China

Objective: To explore the value of ^{18}F-2-fluoro-2-deoxyglucose (FDG) positron emission tomography (PET)/computed tomography(CT) in MYCN gene and chromosome 1p36 and 11 statuses in newly diagnosed pediatric NB (neuroblastoma) and GNB(ganglioneuroblastoma).

Methods: We retrospectively analyzed newly diagnosed patients with 48 NB and 12 with GNB in our hospital. The data obtained from the clinical medical records included age, sex, pathologic type, and laboratory parameters such as lactate dehydrogenase (LDH), neuron-specific enolase (NSE) and the status of MYCN gene and chromosome 1p36 and 11q. The bone conditions were also obtained in the examination of bone marrow biopsy. Primary tumors were manually segmented to measure the maximum standardized uptake value (SUVmax), mean standardized uptake value (SUVmean), tumor volume(MTV) and total lesion glycolysis(TLG) and the maximal length of the lesion in the axial image (LEGmax).

Results: The differences in bone marrow involvement and lymph node metastases in patients with chromosome 11q deletions were statistically significant (all $p < 0.05$). Chromosome 11q deletion was an independent factor affecting bone marrow involvement (OR=17.796, p=0.011). The levels of NSE, LDH, LEGmax and SUVmax, SUVmean, MTV, TLG all predicted MYCN gene amplification (all $p < 0.05$). The levels of LDH, LEGmax and MTV, TLG all predicted deletions in chromosomes 1p36 (all $p < 0.05$), while NSE, SUVmax and SUVmean did not (all $p > 005$).

Conclusion: The LDH levels, LEGmax, MTV and TLG can effectively predict the status of the MYCN oncogene and chromosome 1p36 in pediatric neuroblastoma and ganglioneuroblastoma. Those patients with chromosome 11q deletions are more likely to develop bone marrow involvement and lymph node metastases, showing a worse progression-free survival.

KEYWORDS

neuroblastoma, ganglioneuroblastoma, ^{18}F-FDG PET/CT, MYCN, 1p36, 11q

1 Introduction

Neuroblastoma is the most common pediatric solid tumor in the sympathetic nervous system and accounts for approximately 15% of childhood cancer-related mortality (1). Seventy percent of patients with NB have metastatic disease. The time of diagnosis, which commonly involves the cortical bone and the bone marrow, implies a poor prognosis (2, 3). Several clinicohistopathological factors, including age, stage (distant metastases in lymph nodes, cortical bone, bone marrow, and liver), laboratory test parameters (neuron-specific enolase (NSE), lactic dehydrogenase (LDH)) and molecular pathology (the status of MYCN gene, chromosome1p36 and 11q) (4, 5).

Some authors suggest that any gene and chromosomal segmental alteration is associated with an increased risk of relapse and poor outcomes in neuroblastoma[6]. Currently, the most clinically useful genetic marker is an amplification of the MYCN oncogene (6). In approximately 25% of primary untreated patients amplification of the MYCN oncogene is frequently associated with a poor outcome (6). However, specific segmental chromosomal aberrations, such as 11q deletion,1p deletion and 17q gain, are also biological factors associated with poor prognosis (5). The 2-year event-free survival rate for 11q deletion cases was 30%, compared to 34% for MYCN-amplified patients and 100% for cases without these abnormalities (6). Helena Carén et al. revealed that the MYCN-amplified and 11q-deletion groups are significantly associated with poor prognosis (7). Deletion of the short arm of chromosome 1p36 is one of the most characteristic changes in neuroblastomas (8), suggesting that a tumor suppressor gene resides in this region (9). A strong correlation between 1p36 deletion, MYCN amplification, and advanced-stage disease (10). Chromosome 17q gain is observed in approximately half of all tumors and is associated with a low survival rate (11).

Nowadays, iodine-123 metaiodobenzylguanidine (^{123}I-MIBG) scintigraphy is a mainstay method in pediatric NB (12). Nevertheless, ^{123}I-MIBG scintigraphy imaging has several disadvantages, such as no concentration of MIBG in 10% of tumors, limited spatial resolution, and limited sensitivity in small lesions. ^{18}F-fluorodeoxyglucose (^{18}F-FDG) positron emission tomography (PET)/computed tomography (CT) (^{18}F-FDG PET/CT) is commonly used to complete the staging and prognosis prediction of neuroblastoma. Compared with ^{123}I-MIBG scintigraphy imaging, superiorities of PET are high ^{18}F-FDG avidity of the bone marrow and better identification of FDG abnormalities in the bone marrow and bone (13, 14). Moreover, another critical advantage of PET/CT is that PET/CT can assess the whole body at once and find unintended distant lymph nodes, bone and skin metastases where traditional imaging or bone marrow biopsies are not usually performed (15). ^{18}F-FDG PET/CT has an excellent overall diagnostic accuracy with high sensitivity and specificity in detecting bone-bone marrow involvement and soft-tissue lesions in pediatric neuroblastoma (13, 16, 17). ^{18}F-FDG PET/CT scans may help assess the full extent of disease involvement, particularly at therapeutic decision points (18).

^{18}F-FDG PET/CT can be used for tumor characterization and prognostic assessment in patients with neuroblastoma (18). Tumor metabolic activity was higher in higher-stage MYCN-amplified patients (19). However, little research has studied the relationship between the status of the MYCN gene and 1p and 11q chromosomal and ^{18}F-FDG PET/CT metabolic parameters. This study aimed to explore the correlation between ^{18}F-FDG PET/CT metabolism parameters and the status of the MYCN gene, chromosomal 1p and 11q in newly diagnosed pediatric neuroblastoma by reviewing our clinical experience.

2 Materials and methods

2.1 Patients

This retrospective study was approved by the Institutional Review Board of the Affiliated Cancer Hospital of Shandong First Medical University and was exempted from obtaining informed consent. We retrospectively collected all the data of patients with neuroblastoma (age < 18 years) who had undergone ^{18}F-FDG PET/CT before treatment from June 1, 2019, to August 31, 2022. Sixty patients were included, including 48 patients with NB and 12 with GNB. They were diagnosed for the first time and underwent ^{18}F-FDG PET/CT scan. Some patients underwent bone marrow biopsy (BMB) within one week. Patients were undergoing any treatment procedures before ^{18}F-FDG PET/CT were excluded.

The data obtained from the clinical medical records included age, sex, pathologic type, and laboratory parameters, such as lactate dehydrogenase (LDH), neuron-specific enolase (NSE), and the status of MYCN gene and 1p and 11q chromosome. All methods are performed according to the relevant guidelines and regulations. Clinical data was reviewed to assess disease status after follow-up. Progression-free survival (PFS) was calculated as the time from the ^{18}F-FDG PET scan showing disease progression or if the patient died.

Pediatric neuroblastoma usually has three histological types: NB, GNB, and ganglioneuroma (GN). We excluded GN because it is a benign tumor (20) and not present with bone-bone marrow involvement. We used the international neuroblastoma risk group staging system (INRGSS) and the INRG risk classification system for neuroblastoma (21).

2.2 ^{18}F-FDG PET-CT imaging protocol

^{18}F-FDG is produced by a MiniTrace Cyclotron and automatic synthesis system by GE Healthcare, with a radiochemical purity of more than 95%. Patients fasted for at least six hours before the examination and had blood glucose lower than 10 mmol/L. The intravenous injection of FDG ranged from 4.44 MBq/kg to 5.55 MBq/kg. Thirty-eight patients were given oral sedation for PET scans. PET/CT scans were performed 60 minutes after injecting radiolabeled ^{18}F-FDG using a Siemens PET/CT system (Horizon). The examination included a head-to-toe CT scan (80 kV; 50-100 mAs) and a three-dimensional (3D) PET scan (2 mins per bed; 6-7 beds). The rotation time was 0.6. The slice thickness was 3.75 mm. The increment was 3.27. The pitch was 0.984. The images were displayed on the Syngo.via workstation.

2.3 ^{18}F-FDG PET/CT image analysis

Two experienced nuclear medicine physicians independently reviewed ^{18}F-FDG PET/CT findings. Depending on the axis and the coronal and sagittal projections, the physicians placed the region of interest (ROI) on the primary tumor. Metabolic parameters, such as maximum standardized uptake value (SUVmax), average standard uptake value (SUVmean), metabolic tumor volume (MTV), and total lesion glycolysis (TLG), were measured on PET/CT images. TLG was then calculated as TLG = SUVmean × MTV. Our study selected a SUVmax of 30% as the threshold for generating the ROI. Meanwhile, the maximal length of the lesion in the reconstructed axial image(LEGmax) was also measured and collected in the CT features of the ^{18}F-FDG PET/CT scan.

2.4 Identification of bone marrow disease by iliac crest biopsy

At our hospital, BMBs are obtained by pediatric oncologists from the common area of the posterior iliac epicondyle only and are not collected from other sites. Biopsy results are reported according to histopathology and immunophenotyping and are evaluated by the oncology and pathology departments.

2.5 The MYCN gene, the chromosome 1p36 and 11q analysis

MYCN gene status, chromosome 1p36 and 11q status were determined by FISH using standard methods. Tumors were considered amplified MYCN when copy number was increased > 5-fold.

2.6 Statistical analysis

Statistical analyzes were performed using SPSS software (version 28.0 for Windows; SPSS INC.). Continuous data were described as the mean ± standard deviation (mean ± SD) or median and interquartile, depending on whether they followed a normal distribution. The categorical variables are described as numbers. Differences between groups were compared using the Mann-Whitney U tests for the continuous variables, chi-squared tests, and Fisher's exact test for the categorical variables. Receiver operating characteristic (ROC) curves were used to determine the best cut-off values of the level of NSE, LDH, LEGmax of the lesion and PET/CT metabolic parameters to predict the MYCN amplification and the positive of 1p36 and 11q. Binary logistic regression was used to analyze whether MYCN oncogene status, chromosome 11q and 1p36 statuses were influential factors leading to bone marrow infiltration and lymph node metastasis. Correlation analysis between MYCN deletions and chromosome 1p36,11q was performed using Spearman's rank correlation analysis. Survival curves were created using the Kaplan-Meier method, and log-rank tests were used to determine whether the survival rates of the curves were statistically significant. All tests were two-sided, and a probability of less than 0.05 was considered statistically significant.

3 Results

3.1 Patients' characteristics

We retrospectively studied 60 patients with 48 NB and 12 GNB (age < 18 years). This study included 34 males and 26 females with an average age of 34.78 months. The general characteristics of patients are summarized in Table 1. The status of the MYCN gene and chromosomes 1p36 and 11q was collected from 47 of 60 patients, of whom 34% were positive for MYCN amplification and approximately 38.3% and 36.2% for chromosome 1p36 and 11q deletions, respectively.

3.2 Relationship between amplification of MYCN gene, deletion of chromosome 1p36 and 11q and clinicopathological features

The clinical biological characteristics and ^{18}F-FDG PET/CT metabolic parameters of patients with the MYCN gene and chromosome 1p36 and 11q status are shown in Table 2. The differences in bone marrow involvement and lymph node metastases in patients with chromosome 11q deletion were statistically significant. Binary logistic regression analysis showed that chromosome 11q deletion was an independent factor affecting bone marrow involvement. The incidence of bone marrow involvement was 17.796 times higher in patients with chromosome 11q deletion than in those without chromosome 11q deletions, as shown in Table 3.

3.3 Relationship of different states of MYCN gene, chromosome 1p36 and 11q with PFS

The PFS between chromosome 11q deletion and chromosome 11q non-deletion group PFS is significantly different(X^2 = 5.314, p=0.021), as shown in Figure 1. The chromosome 11q non-deletion group has a longer PFS than the chromosome 11q deletion group. MYCN gene amplification and chromosome 1p36 deletion are not associated with PFS.

3.4 Correlation between MYCN gene amplification, chromosomes 1p36 and 11q deletion

Using Spearman's rank correlation analysis, it can be concluded that MYCN gene amplification was positively correlated with chromosome 1P36 deletion (p=0.002, rs=0.450), while it was not correlated with chromosome 11q deletion (p=0.077, rs=-0.260) in Table 4. The deletion of chromosome 1P36 was not correlated with

TABLE 1 General characteristics of 60 patients.

Characteristics		No. of patients	%
Age (months)	Median (range)	34 (2-144)	
Gender	Male	34	56.7
	Female	26	43.3
Histology	NB	48	80.0
	GNB	12	20.0
Location	Neck	1	1.7
	Chest	5	8.3
	Abdomen	53	88.3
	Pelvis	1	1.7
MYCN[#]	Amplified	16	34.0
	Not amplified	31	66.0
1P36[#]	Positive	18	38.3
	Negative	29	61.7
11q[#]	Positive	17	36.2
	Negative	30	63.8
BMB[##]	Positive	37	61.7
	Negative	23	38.3
Lymph node metastasis	Metastasis	50	83.3
	No metastasis	10	16.7
INRGSS	L1	7	11.7
	L2	9	15.0
	M	40	66.7
	Ms	4	6.7
INRG risk stratification[##]	Very low	5	9.8
	Low	5	9.8
	Intermediate	4	7.8
	High	37	72.5

[#]47 patients obtained the status of MYCN gene and chromosome 1p36 and 11q. [##]51 patients obtained INRG risk stratification. BMB, bone marrow biopsy; INRGSS, International neuroblastoma risk group staging system; INRG, International neuroblastoma risk group.

the deletion of chromosome 11q (p=0.356, rs=-0.138). The clinical biological characteristics and ^{18}F-FDG PET/CT metabolic parameters of the different combinations with the different status of MYCN gene and chromosome 1p36 and 11q are shown in Table 5.

3.5 Performance of ROC curves to predict MYCN amplification and chromosome 1p36 and 11q deletion

NSE and LDH levels, LEGmax, SUVmax, SUVmean, MTV, and TLG all predicted MYCN gene amplification (all $p < 0.05$), with LDH being the best, as shown in Table 6 and Figure 2A. LDH levels, LEGmax and MTV, TLG all predicted the deletion of chromosome 1p36 (all $p < 0.05$), with the LDH being the best, while NSE, SUVmax and SUVmean did not (all $p > 0.05$), as shown in Table 6 and Figure 2B. NSE and LDH levels, LEGmax, SUVmax, SUVmean, MTV and TLG could not predict chromosome11q deletion (all $p>0.05$).

3.6 Relationship of LDH and NSE levels, age, gender, ^{18}F-FDG PET/CT metabolic parameters with PFS

In addition to gender (p=0.543), the age, the levels of LDH and NSE, the LEGmax, ^{18}F-FDG PET/CT metabolic parameters (all $p <$

TABLE 2 General characteristics of MYCN gene and chromosomes 1p36 and 11q status.

	The status of the MYCN gene and chromosomes 1p36 and 11q								
	MYCN gene		p	1P36 chromosome		p	11q chromosome		p
	Amplification	Not amplification		mutation	No-mutation		mutation	No-mutation	
Age (months)									
≤18	4	6	0.606	3	7	0.570	2	8	0.240
>18	12	25		15	22		15	22	
Gender									
Male	7	18	0.351	6	19	0.032#	10	15	0.560
Female	9	13		12	10		7	15	
Histology									
NB	17	21	0.017#	18	20	0.064	15	23	1.000
GNB	0	9		1	8		3	6	
Primary site									
Chest	0	5	0.169	2	3	0.728	4	1	0.034#
Abdomen	16	25		16	25		12	29	
Pelvis	0	1		0	1		1	0	
INRG stage									
L1	0	5	0.066	0	5	0.123	1	4	0.230
L2	1	7		2	6		1	7	
M	14	19		16	17		15	18	
Ms	1	0		0	1		0	1	
INRG risk stratification									
Very low	0	5	0.013#	0	5	0.116	1	4	0.101
Low	0	5		1	4		0	5	
Intermediate	0	4		1	3		3	1	
High	16	16		16	16		13	19	
Bone marrow involvement									
Positive	8	22	0.156	9	21	0.120	16	14	0.01#
Negative	8	9		9	8		1	16	
Lymph node metastasis									
metastasis	14	26	1.000	16	24	0.692	17	23	0.039#
No metastasis	2	5		2	5		0	7	
LDH (IU/L)	2637.000 ±1334.187	547.807±223.195	<0.001#	1956.611 ±1356.043	826.034 ±1014.193	0.002#	895.823±727.453	1464.833 ±1465.428	0.142
NSE	521.150±150.790	249.639±170.358	<0.001#	415.967±211.561	296.200±195.438	0.054	371.565±179.180	325.353±223.825	0.470
LEGmax	10.975 (8.685,13.083)	7.550 (4.630,10.180)	0.050#	10.830 (8.405,13.225)	7.320 (4.920,10.080)	2.18	7.670 (6.800,10.080)	9.575 (5.738,12.550)	0.204
SUVmax	9.558±4.642	6.532±3.500	0.016#	7.681±3.544	7.489±4.525	0.879	6.384±2.458	8.230±4.748	0.144
SUVmean	4.194±1.490	2.953±1.571	0.012#	3.546±1.873	3.270±1.501	0.279	3.270±1.406	3.435±1.778	0.743

(Continued)

TABLE 2 Continued

	The status of the MYCN gene and chromosomes 1p36 and 11q								
	MYCN gene		p	1P36 chromosome		p	11q chromosome		p
	Amplification	Not amplification		mutation	No-mutation		mutation	No-mutation	
MTV	353.904±194.387	262.900±379.524	0.374	451.140±455.761	196.270±160.655	0.008#	223.506±185.535	333.759±384.738	0.724
TLG	1549.191 ±1051.693	617.908±683.038	<0.001#	1396.290 ±1213.845	648.586±550.403	0.006#	617.068±453.706	1115.069 ±1078.824	0.039#

NB, Neuroblastoma; GNB, Ganglioneuroblastoma; INRG, International neuroblastoma risk group; SUVmax, maximum standardized uptake value; SUVmean, average standard uptake value; MTV, metabolic tumor volume; TLG, total lesion glycolysis; LEGmax, the maximal length of the lesion; LDH, lactate dehydrogenase; NSE, neuron-specific enolase. #p<0.05.

TABLE 3 MYCN oncogene status, chromosome 11q and 1p36 status as factors influencing bone marrow infiltration.

Modalities	B	Exp(B)	p	95% lower	95% upper
MYCN	-0.040	0.961	0.963	0.175	5.273
1P36	-0.901	0.406	0.289	0.077	2.146
11q	2.879	17.796	0.011#	1.945	162.812

#p<0.05.

0.01), including SUVmax, SUVmean, MTV and TLG, were all associated with PFS, as shown in Table 7.

4 Discussion

^{123}I-MIBG scintigraphy and ^{68}Ga-1,4,7,10-tetraazacyclododecane1,4,7,10-tetraacetic acid (DOTA) peptides are now the mainstay nuclear imaging agents for neuroblastoma (22). ^{123}I-MIBG imaging is primarily due to its structural similarity to norepinephrine, tissue that selectively concentrates ^{123}I-MIBG with abundant adrenergic innervation, and mostly neuroectodermal tissues, including neuroblastoma (23). High affinity binding of different ^{68}Ga-DOTA peptides to SSTR for PET/CT imaging (24, 25). Somatostatin receptors (SSTR) are expressed in 77%–89% of neuroblastoma cells. Most studies have confirmed the feasibility of ^{18}F-FDG PET for neuroblastoma imaging, which is seen as an important and widespread alternative to ^{123}I-MIBG scanning, especially for non-MIBG uptake (26). ^{18}F-FDG scan may be useful in assessing the full extent of disease involvement, particularly at therapeutic decision points (26). We report the ^{18}F-FDG PET/CT metabolic parameters in newly diagnosed

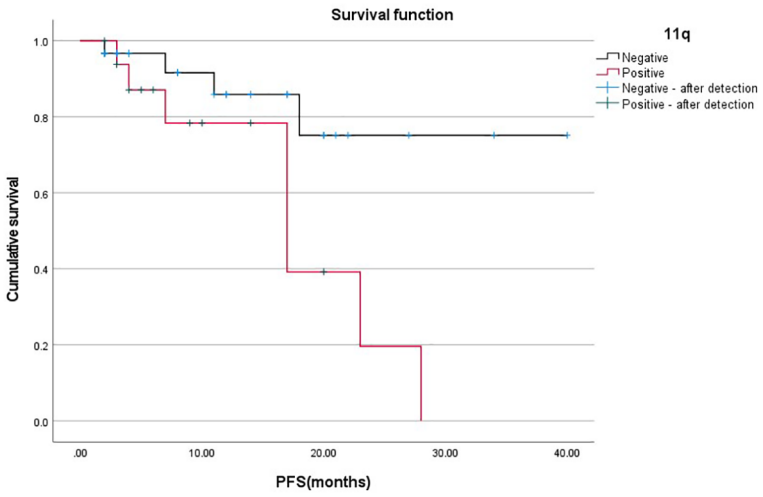

FIGURE 1
Relationship between 11q gene deletion and PFS.

TABLE 4 Correlation between MYCN gene, chromosome 1p36 and 11q.

		MYCN		p	Rs
		Amplification	Not amplification		
1p36	Deletion	11	7	0.002	0.450
	No-deletion	5	24		
11q	Deletion	3	14	0.077	-0.260
	No-deletion	13	17		

pediatric neuroblastoma and their association with the other indicators of disease clinical biological characteristics and survival status.

In our study, 47 of 60 patients had molecular pathology results, including the status of MYCN gene and chromosomal 1p36 and 11q. We found that the rates of MYCN gene amplification, the chromosome 1p36 and 11q deletion were 34%, 38.3% and 36.2%, respectively, which is in general agreement with other reports on pediatric neuroblastoma (6, 10, 19, 27). In our study, we also found a correlation between MYCN gene amplification and chromosome 1p36 deletions (27, 28). In contrast, there was no correlation between MYCN gene amplification and chromosome 11q deletion and between chromosome 1p36 and 11q deletions.

Much research has found that MYCN gene amplification, chromosome 1p36 and 11q deletions can predict stage and prognosis in patients with neuroblastoma. In our study, MYCN gene amplification

TABLE 5 The clinical biological characteristics and ^{18}F-FDG PET/CT metabolic parameters of the different combinations with the status of MYCN gene and t chromosomes 1p36 and 11q.

	MYCN gene amplification and chromosome 1P36 deletion	MYCN gene and chromosome 11q deletion	chromosome 1P36 and 11q deletion	MYCN gene amplification, chromosome 1P36 and 11q deletion
Total	10	2	4	1
Age (months)	1≤18 month; 9>18 month	108 month; 41 month	4 >18 month	54 month
Gender	4 male; 6 female	1 male; 1 female	1 male;2 female	female
Histology	10 neuroblastoma	2 neuroblastoma	3 neuroblastoma; 1 ganglioneuroblastoma	neuroblastoma
Primary site	10 Abdomen	2 Abdomen	2 Chest; 2 Abdomen	Abdomen
INRG stage	9 M; 1 L2	2 M	4 M	M
INRG risk stratification	10 High	2 High	4 High	High
Bone marrow involvement	2 Positive; 8 negative	2 Positive	4 Positive	Negative
Lymph node metastasis	8 Metastasis; 2 No metastasis	2 Metastasis	4 Metastasis	Metastasis
LDH	2686.5 (1680.0,3291.5)	1471; 1704	736.0 (551.75,1212.0)	1817
NSE	569.4 (462.0,600)	542; 600	200.5 (347.5,553.75)	53.60
LEGmax	11.635 (9.803,13.216)	7.32; 11.35	5.575 (4.035,10.758)	13.53
SUVmax	9.165 (6.798,10.743)	6.93; 9.13	5.575 (4.035,6.500)	13.47
SUVmean	4.400 (2.730,5.118)	4.17; 4.93	2.585 (1.540,3.645)	6.37
MTV	327.40 (228.455,616.450)	212.50; 349.79	252.055 (65.513,704.415)	492.74
TLG	1222.510 (910.298,3220.478)	898.75; 1647.60	260.625(115.578,1096.213)	3183.75
Follow-up status	7 No progression; 3 Progression (1 die)	2 No progression	2 No progression; 2 Progression	Progression (die)

LDH, lactate dehydrogenase; NSE, neuron-specific enolase; INRG, International neuroblastoma risk group; SUVmax, maximum standardized uptake value; SUVmean, average standard uptake value; MTV, metabolic tumor volume; TLG, total lesion glycolysis; LEGmax, the maximal length of the lesion.

TABLE 6 Performance of ROC curves predict the MYCN gene amplification and chromosome 1p36 deletion.

		MYCN gene							chromosome 1P36			
		NSE	LDH	LEGmax	SUVmax	SUVmean	MTV	TLG	LDH	LEGmax	MTV	TLG
p		0.001#	0.001#	0.003#	0.012#	0.007#	0.013#	0.001#	0.001#	0.002#	0.007#	0.034#
Optimal threshold		>472	>927	>8.75	>6.92	>4.14	>209.02	>562.41	>792	>7.99	>229.52	>982.43
AUC		0.875	0.990	0.764	0.726	0.742	0.724	0.813	0.814	0.767	0.736	0.686
Sensitivity		0.813	0.938	0.750	0.813	0.630	0.813	0.875	0.722	0.833	0.722	0.611
Specificity		0.903	0.968	0.710	0.613	0.871	0.677	0.645	0.828	0.655	0.724	0.793
95% CI	Upper limit	0.746	0.906	0.618	0.576	0.594	0.574	0.687	0.689	0.621	0.588	0.525
	Lower limit	0.953	1.000	0.876	0.846	0.858	0.844	0.938	0.939	0.914	0.883	0.847

NSE, neuron-specific enolase; LDH, lactate dehydrogenase; SUVmax, maximum standardized uptake value; SUVmean, average standard uptake value; MTV, metabolic tumor volume; TLG, total lesion glycolysis; LEGmax, the maximal length of the lesion. #p<0.05.

and chromosome 11q deletion predict high-risk stratification. What's more, chromosomal deletion in 11q is highly correlated with lymph node metastasis and bone marrow involvement, suggesting a causal relationship between this region and the disease stage. Based on the Kaplan Meier method and log-rank test, chromosome11q deletion can affect PFS, and patients with chromosome 11q deletions are more likely to progress or die. These results are consistent with other reports of chromosome 11q mutations in pediatric neuroblastoma (27, 28). In addition, we also found that MYCN oncogene amplification is only found in patients with NB, about 100%.

^{18}F-FDG PET/CT can be used for tumor characterization and prognostic assessment in patients with neuroblastoma (18). However, fewer reports have been reported on the ability of ^{18}F-FDG PET/CT metabolic parameters in predicting the case of MYCN oncogene amplification, chromosome 1p36 and 11q deletion. In our study, the levels of LDH, NSE and LEGmax, SUVmax, SUVmean, TLG were higher in the MYCN gene amplification group than in the non-amplified group, and the differences were statistically significant in both groups, except for MTV. Meanwhile, the levels of LDH, the lesion MTV and TLG were higher in the chromosome 1p36 deletion group than in the non-deletion group. The differences were statistically significant in both groups. The lesion MTV was higher in the chromosome 11q deletion group than in the non-deletion group, and the difference between them was statistically significant.

Based on receiver operating characteristic (ROC) curve analysis, we obtained optimal threshold values of SUVmax 6.92, SUVmean 4.14, MTV 209.02 cm^3, TLG 562.41, NSE 472.0 ng/ml, LDH 927.0 U/L and LEGmax 8.75cm, which can determine whether amplification of the MYCN gene occurred. Meanwhile, we also obtained optimal threshold values of MTV 229.52 cm^3, TLG 982.43, LDH 792 U/L and LEGmax 7.99cm, these can determine whether a deletion of chromosome 1p36 has occurred. Surprisingly, there are no ^{18}F-FDG PET/CT metabolic parameters and laboratory indicators that can effectively determine whether chromosome 11q is mutated.

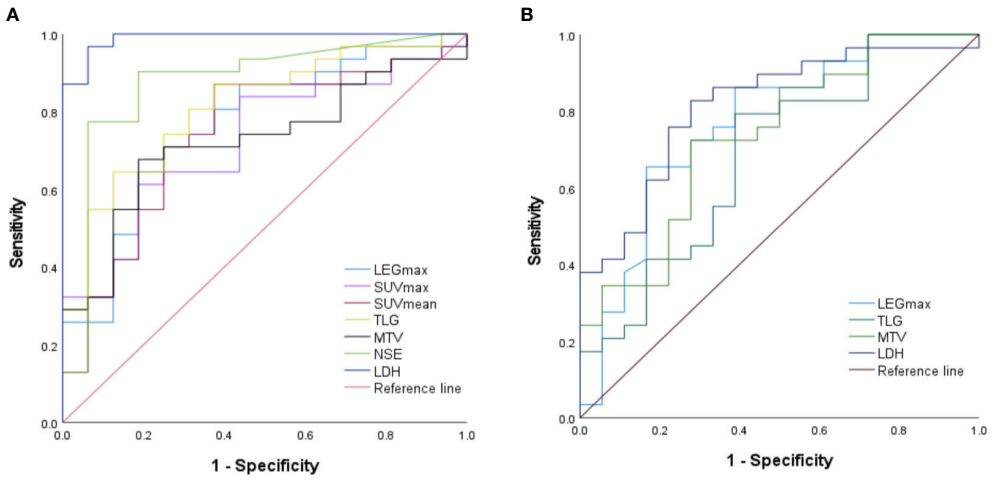

FIGURE 2
Performance of ROC curves predict the **(A)** MYCN gene amplification and **(B)** chromosome 1p36 deletion..

TABLE 7 Relationship of the age, gender and the levels of LDH, NSE and ^{18}F-FDG PET/CT metabolic parameters with PFS.

	Age	Gender	LDH	NSE	LEGmax	SUVmax	SUVmean	MTV	TLG
χ^2	113.907	0.369	154.810	100.147	154.802	154.832	152.396	154.832	154.832
p	<0.01#	0.543	<0.01#	<0.01#	<0.01#	<0.01#	<0.01#	<0.01#	<0.01#

LDH, lactate dehydrogenase; NSE, neuron-specific enolase; SUVmax, maximum standardized uptake value; SUVmean, average standard uptake value; MTV, metabolic tumor volume; TLG, total lesion glycolysis; LEGmax, the maximal length of the lesion. #p<0.05.

In addition to gender (p=0.543), the age, the levels of LDH and NSE, the LEGmax, ^{18}F-FDG PET/CT metabolic parameters (all p < 0.01), including SUVmax, SUVmean, MTV and TLG are all associated with PFS. In ^{18}F-FDG PET/CT metabolic parameters, higher SUVmax, SUVmean, MTV and TLG were associated with worse PFS.

There are several limitations to our study. First, our results are inherently subject to selection bias as a retrospective study. Second, it may be that the small number of patients collected does not allow for a valid assessment of the differences in metabolic parameters of ^{18}F-FDG PET/CT in multiple patients with simultaneous several molecular deletions. Third, we only performed correlation analyzes for PFS because of the short follow-up of patients (2-42 months; median time 9.5 months). It is also possible that the observation of the influence of the MYCN oncogene amplification and the chromosome 1p36 deletions on PFS was limited by the short follow-up period. Another shortcoming is that the status of chromosome 17q was not evaluated in our hospital.

5 Conclusion

The LDH levels, LEGmax, MTV and TLG can effectively predict the status of the MYCN oncogene and chromosome 1p36 in pediatric neuroblastoma and ganglioneuroblastoma. Those patients with chromosome 11q deletions are more likely to develop bone marrow involvement and lymph node metastases, showing a worse progression-free survival.

Data availability statement

The raw data supporting the conclusions of this article will be made available by the authors, without undue reservation.

Ethics statement

The studies involving human participants were reviewed and approved by Ethics Committee of Cancer Hospital Affiliated to Shandong First Medical University. Written informed consent to participate in this study was provided by the participants' legal guardian/next of kin. Written informed consent was obtained from the minor(s)' legal guardian/next of kin for the publication of any potentially identifiable images or data included in this article.

Author contributions

JR: acquisition of data, analysis of data, drafting of the manuscript. YZ: analysis of data and revision of the manuscript. ZF: revision of the manuscript, supervision. All authors contributed to the article and approved the submitted version.

Conflict of interest

The authors declare that the research was conducted in the absence of any commercial or financial relationships that could be construed as a potential conflict of interest.

Publisher's note

All claims expressed in this article are solely those of the authors and do not necessarily represent those of their affiliated organizations, or those of the publisher, the editors and the reviewers. Any product that may be evaluated in this article, or claim that may be made by its manufacturer, is not guaranteed or endorsed by the publisher.

References

1. Tsubota S, Kadomatsu K. Origin and initiation mechanisms of neuroblastoma. *Cell Tissue Res* (2018) 372:211–21. doi: 10.1007/s00441-018-2796-z

2. Cohn SL, Pearson AD, London WB, Monclair T, Ambros PF, Brodeur GM, et al. The international neuroblastoma risk group (INRG) classification system: An INRG task force report. *J Clin Oncol* (2009) 27:289–97. doi: 10.1200/JCO.2008.16.6785

3. Monclair T, Brodeur GM, Ambros PF, Brisse HJ, Cecchetto G, Holmes K, et al. The international neuroblastoma risk group (INRG) staging system: An INRG task force report. *J Clin Oncol* (2009) 27:298–303. doi: 10.1200/JCO.2008.16.6876

4. Maris JM. Recent advances in neuroblastoma. *N Engl J Med* (2010) 362(23):2202–11. doi: 10.1056/NEJMra0804577

5. Mlakar V, Jurkovic Mlakar S, Lopez G, Maris JM, Ansari M, Gumy-Pause F. 11q deletion in neuroblastoma: A review of biological and clinical implications. *Mol Cancer* (2017) 16:114. doi: 10.1186/s12943-017-0686-8

6. Luttikhuis ME, Powell JE, Rees SA, Genus T, Chughtai S, Ramani P, et al. Neuroblastomas with chromosome 11q loss and single copy MYCN comprise a biologically distinct group of tumours with adverse prognosis. *Br J Cancer* (2001) 85 (4):531–7. doi: 10.1054/bjoc.2001.1960

7. Caren H, Kryh H, Nethander M, Sjoberg RM, Trager C, Nilsson S, et al. High-risk neuroblastoma tumors with 11q-deletion display a poor prognostic, chromosome instability phenotype with later onset. *Proc Natl Acad Sci USA* (2010) 107:4323–8. doi: 10.1073/pnas.0910684107

8. Brodeur GM, Sekhon G, Goldstein MN. Chromosomal aberrations in human neuroblastomas. *Cancer* (1977) 40(5):2256–63. doi: 10.1002/10970142(197711)40:5<2256::aid-cncr2820400536>3.0.co;2-1

9. Okawa ER, Gotoh T, Manne J, Igarashi J, Fujita T, Silverman KA, et al. Expression and sequence analysis of candidates for the 1p36.31 tumor suppressor gene deleted in neuroblastomas. *Oncogene* (2008) 27:803–10. doi: 10.1038/sj.onc.1210675

10. White PS, Thompson PM, Gotoh T, Okawa ER, Igarashi J, Kok M, et al. Definition and characterization of a region of 1p36.3 consistently deleted in neuroblastoma. *Oncogene* (2005) 24:2684–94. doi: 10.1038/sj.onc.1208306

11. Bown N, Cotterill S, Lastowska M, O'Neill S, Pearson AD, Plantaz D, et al. Gain of chromosome arm 17q and adverse outcome in patients with neuroblastoma. *N Engl J Med* (1999) 340(25):1954–61. doi: 10.1056/NEJM199906243402504

12. Liu CJ, Lu MY, Liu YL, Ko CL, Ko KY, Tzen KY, et al. Risk stratification of pediatric patients with neuroblastoma using volumetric parameters of 18F-FDG and 18F-DOPA PET/CT. *Clin Nucl Med* (2017) 42:e142–e8. doi: 10.1097/RLU.0000000000001529

13. Kushner BH, Yeung HW, Larson SM, Kramer K, Cheung NK. Extending positron emission tomography scan utility to high-risk neuroblastoma: Fluorine-18 fluorodeoxyglucose positron emission tomography as sole imaging modality in follow-up of patients. *J Clin Oncol* (2001) 19(14):3397–405. doi: 10.1200/JCO.2001.19.14.3397

14. Wang Y, Xu Y, Kan Y, Wang W, Yang J. Diagnostic value of seven different imaging modalities for patients with neuroblastic tumors: A network meta-analysis. *Contrast Media Mol Imaging* (2021) 2021:5333366. doi: 10.1155/2021/5333366

15. Adams HJ, Kwee TC, de Keizer B, Fijnheer R, de Klerk JM, Littooij AS, et al. Systematic review and meta-analysis on the diagnostic performance of FDG-PET/CT in detecting bone marrow involvement in newly diagnosed Hodgkin lymphoma: is bone marrow biopsy still necessary? *Ann Oncol* (2014) 25:921–7. doi: 10.1093/annonc/mdt533

16. Ishiguchi H, Ito S, Kato K, Sakurai Y, Kawai H, Fujita N, et al. Diagnostic performance of (18)F-FDG PET/CT and whole-body diffusion-weighted imaging with background body suppression (DWIBS) in detection of lymph node and bone metastases from pediatric neuroblastoma. *Ann Nucl Med* (2018) 32:348–62. doi: 10.1007/s12149-018-1254-z

17. Sun L, Zhang B, Peng R. Diagnostic performance of (18)F-FDG PET(CT) in bone-bone marrow involvement in pediatric neuroblastoma: A systemic review and meta-analysis. *Contrast Media Mol Imaging* (2021) 2021:8125373. doi: 10.1155/2021/8125373

18. Bar-Sever Z, Biassoni L, Shulkin B, Kong G, Hofman MS, Lopci E, et al. Guidelines on nuclear medicine imaging in neuroblastoma. *Eur J Nucl Med Mol Imaging* (2018) 45:2009–24. doi: 10.1007/s00259-018-4070-8

19. Sung AJ, Weiss BD, Sharp SE, Zhang B, Trout AT. Prognostic significance of pretreatment (18)F-FDG positron emission tomography/computed tomography in pediatric neuroblastoma. *Pediatr Radiol* (2021) 51:1400–5. doi: 10.1007/s00247-021-05005-y

20. He W-G, Yan Y, Tang W, Cai R, Ren G. Clinical and biological features of neuroblastic tumors: A comparison of neuroblastoma and ganglioneuroblastoma. *Oncotarget* (2017) 8(23):37730–9. doi: 10.18632/oncotarget.17146

21. Brisse HJ, McCarville MB, Granata C, Krug KB, Wootton-Gorges SL, Kanegawa K, et al. Guidelines for imaging and staging of neuroblastic tumors: consensus report from the international neuroblastoma risk group project. *Radiology* (2011) 261(1):243–57. doi: 10.1148/radiol.11101352/-/DC1

22. Piccardo A, Lopci E, Conte M, Foppiani L, Garaventa A, Cabria M, et al. PET/CT imaging in neuroblastoma. *Q J Nucl Med Mol Imaging* (2013) 57(1):29–39.

23. Giammarile F, Chiti A, Lassmann M, Brans B, Flux G. EANM procedure guidelines for 131I-meta-iodobenzylguanidine (131I-mIBG) therapy. *Eur J Nucl Med Mol Imaging* (2008) 35(5):1039–47. doi: 10.1007/s00259-008-0715-3

24. Alexander N, Vali R, Ahmadzadehfar H, Shammas A, Baruchel S. Review: The role of radiolabeled DOTA-conjugated peptides for imaging and treatment of childhood neuroblastoma. *Curr Radiopharm* (2018) 11(1):14–21. doi: 10.2174/1874471011666171215093112

25. Matteo B, Domenico A, Salvatore A, Giulia S, Priscilla G, Viviana F, et al. Somatostatin receptor PET/CT imaging for the detection and staging of pancreatic NET: A systematic review and meta-analysis. *Diagnostics (Basel)* (2020) 10(8):598. doi: 10.3390/diagnostics10080598

26. Pfluger T, Piccardo A. Neuroblastoma: MIBG imaging and new tracers. *Semin Nucl Med* (2017) 47(2):143–57. doi: 10.1053/j.semnuclmed.2016.10.007

27. Sanmartin E, Munoz L, Piqueras M, Sirerol JA, Berlanga P, Canete A, et al. Deletion of 11q in neuroblastomas drives sensitivity to PARP inhibition. *Clin Cancer Res* (2017) 23:6875–87. doi: 10.1158/1078-0432.CCR-17-0593

28. Spitz R, Hero B, Simon T, Berthold F. Loss in chromosome 11q identifies tumors with increased risk for metastatic relapses in localized and 4S neuroblastoma. *Clin Cancer Res* (2006) 12:3368–73. doi: 10.1158/1078-0432.CCR-05-2495

frontiers | Frontiers in Oncology

TYPE Mini Review
PUBLISHED 06 April 2023
DOI 10.3389/fonc.2023.1180300

OPEN ACCESS

EDITED BY
Jing He,
Guangzhou Medical University, China

REVIEWED BY
Rui Dong,
Fudan University, China
Zhonghua Yang,
China Medical University, China

*CORRESPONDENCE
Chao Yang
400843@hospital.cqmu.edu.cn

SPECIALTY SECTION
This article was submitted to Pediatric Oncology, a section of the journal Frontiers in Oncology

RECEIVED 06 March 2023
ACCEPTED 27 March 2023
PUBLISHED 06 April 2023

CITATION
Wu K, Tan J and Yang C (2023) Recent advances and application value of circRNA in neuroblastoma. *Front. Oncol.* 13:1180300. doi: 10.3389/fonc.2023.1180300

Recent advances and application value of circRNA in neuroblastoma

Ke Wu[1], Juan Tan[2] and Chao Yang[2,3]*

[1]Department of Pharmacology, Chongqing Key Laboratory of Biochemistry and Molecular Pharmacology, Chongqing Medical University, Chongqing, China, [2]Child Healthcare Department, Children's Hospital of Chongqing Medical University, Chongqing, China, [3]Department of Pediatric Surgical Oncology, Ministry of Education Key Laboratory of Child Development and Disorders, National Clinical Research Center for Child Health and Disorders, China International Science and Technology Cooperation Base of Child Development and Critical Disorders, Chongqing Key Laboratory of Pediatrics, Children's Hospital of Chongqing Medical University, Chongqing, China

Neuroblastoma (NB) is children's most prevalent solid malignant tumor, accounting for 15% of childhood cancer mortality. Non-coding RNA is important in NB pathogenesis. As a newly identified non-coding RNA, abnormal regulation (abnormal up-regulation or down-regulation) of the circRNAs expression is implicated in the tumorigenesis of various tumors, including NB. CircRNAs primarily regulate the expression of microRNA (miRNA) target genes by microRNA (miRNA) sponge adsorption. Clinical evidence suggests that the expression of certain circRNAs is associated with the prognosis and clinical features of NB and hence may be exploited as a biomarker or therapeutic target. This review examines circRNAs that have been demonstrated to play a function in NB.

KEYWORDS

circRNA, neuroblastoma, pathogenesis, biomarkers, tumor targeted therapy

Introduction

Neuroblastoma (NB) is the most prevalent extracranial malignant solid tumor in children, accounting for 8–10% of all malignant tumors in children and 15% of all childhood cancer deaths (1). This tumor develops from primitive sympathetic crest cells and is characterized by various clinical manifestations. It can be a benign tumor or widely metastasized (2). The adrenal gland is the most common primary site, accounting for about half of all tumors. Other tumor sites include the retroperitoneum, posterior mediastinum, neck, and bone cavity (2). Most children are diagnosed in infancy, and the five-year survival rate of children diagnosed before one year is greater (3). Available treatment methods include chemotherapy, surgery, radiotherapy, autologous stem cell transplants, and immunotherapy. Despite adopting several therapeutic techniques, the five-year survival rate for children with neuroblastoma in the high-risk group is still approximately 50%. Studying the potential pathogenesis of neuroblastoma is of great significance for early diagnosis, scientific staging, and precise treatment. Several investigations have demonstrated that gene modifications in regulating the cell cycle, cell proliferation, and

programmed cell death contribute to the pathogenesis of the disease. There are numerous epigenetic factors involved in gene expression regulation, including DNA and RNA methylation, histone modification, non-coding RNAs (including long-chain non-coding RNAs (lncRNAs), microRNAs (miRNAs), and circular RNAs (circRNAs)). These epigenetic factors may directly affect tumor initiation and progression (4). Numerous research has examined the role of lncRNAs and miRNAs in the occurrence and progression of NB. The role of circRNAs in NB has garnered increasing attention in recent years.

Non-coding RNA is believed to regulate gene expression in eukaryotic cells. Recently, it was shown that circRNAs serve a critical function in regulating gene expression in eukaryotic cells. Despite being single-stranded, cyclic RNAs have two ends that combine to form cyclic polynucleotide chains. They have superior stability over miRNAs and lncRNAs because of their circular nature, which makes them resistant to exonucleases (5). Up to now, several types of circRNAs have been identified according to their distribution and biogenesis (Figure 1): exonic circRNAs (EcRNAs), intronic circRNAs (ciRNAs), and exon-intron circRNAs (EIciRNAs). Research has shown that circRNAs importantly regulate gene expression. It can alter transcriptional and translational modifications in several ways (Figure 1). circRNAs can boost the expansion of polymerase II in the nucleus, enhancing their parent gene's expression level. It can also recruit splicing bodies to promote reverse splicing, thus suppressing parent gene expression (6). The interaction between circRNAs and miRNAs is currently being studied intensively. By binding to specific sequences on miRNA targets, circRNAs inhibit miRNAs' functions, regulating the miRNA-targeted genes expression. The relationship between circRNAs and microRNAs is currently the subject of most research. circRNAs restrict the actions of miRNAs by binding to certain target sequences, hence regulating the miRNA-targeted genes expression. It has also been demonstrated that some circRNAs contain open reading frames, which are translated into short peptides and control the translation of the specific mRNAs. CircRNAs influence cell growth, proliferation, and differentiation (7, 8) and can initiate, promote, and expedite the spread of cancer (9, 10). Consequently, they may serve as diagnostic and prognostic biomarkers and therapeutic targets (11, 12). This article will review the recent research progress and clinical value of circRNAs in NB.

Carcinogenic circRNAs

CircCUX1(circ_0132813)

CircCUX1 (circ_0132813) is the most studied circRNA in NB at present. It comes from the CUX gene located on chromosome 7 (chr7:101870650-101870949). Li originally investigated the mechanism of action and therapeutic potential of circCUX1 in NB (13). In this study, they discovered that circCUX1 was involved in aerobic glycolysis and the progression of NB. According to clinical data, circCUX1 was an independent risk factor for adverse outcomes in NB patients. Patients who exhibited high levels of circCUX1 had a decreased survival probability. CircCUX1 interacted with EWS RNA binding protein 1 (EWSR1) to stimulate MYC-related zinc finger protein (MAZ) trans-activation, resulting in CUX1 transcription modification and other tumor progression-related genes being transcribed. By

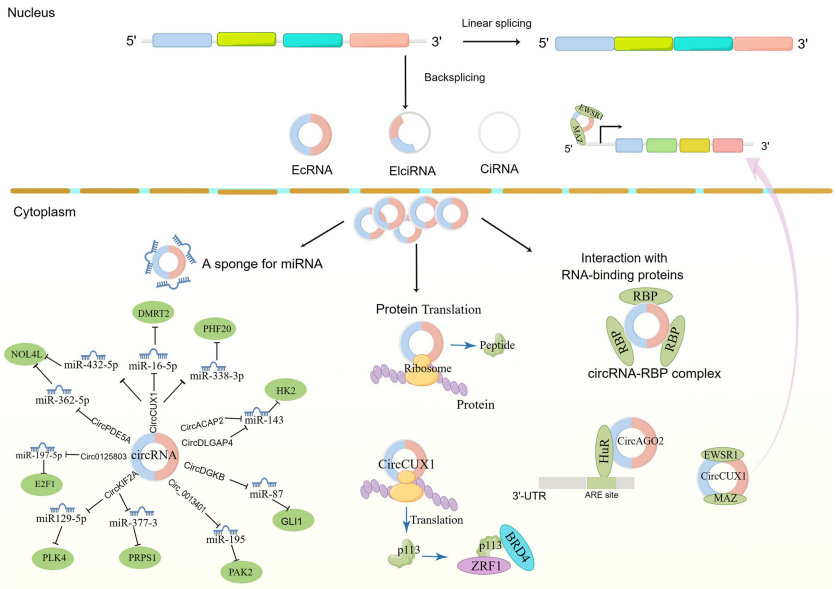

FIGURE 1
The biogenesis of circRNAs and mechanism in neuroblastoma cancer cell progression. EcRNAs, Exonic circRNAs; EIciRNAs, Exonic-intronic circRNAs; CiRNAs, intronic circRNA. EWSR1,EWS RNA binding protein 1; MAZ, MYC-related zinc finger protein; DMRT2, Doublesex and mab-3 related transcription factor 2; NOL4L, Nucleolar protein 4 like; PHF20, PHD Finger Protein 20; Zuotin-related factor 1; BRD4, bromodomain protein 4; PLK4, Polo-like kinase 4; PRPS1, Phosphoribosyl pyrophosphate synthetase 1; GLI1, Glioma-associated oncogene 1; AGO2, Argonaute 2; HK2, hexokinase 2; PAK2, P21-activated kinase 2; HuR, Human antigen R.

inhibiting the interaction between Circux1 and EWSR1, the NB cell growth and invasion can be inhibited. As an alternate technique, the researchers designed an EWSR1 inhibitory peptide (EIP-22) comprising 22 amino acids that prevent the interaction between circCUX1 and EWSR. Using EIP-22, the researchers discovered that EWSR1 could prevent circCUX1-EWSR1 connections from reducing the development and migration of neuroblastoma SH-SY5Y cells. In animal experiments, mouse survival was improved by EIP-22 by reducing lung metastasis of SH-SY5Y cells.

According to Zhang and colleagues, circCUX1 was associated with NB cell proliferation, migration, invasion, and glycolysis (14). miR-16-5p is the direct target of circCUX1. Studies have demonstrated that miR-16-5p targets MYCN mRNA and inhibits tumor progression in NB (15). miR-16-5p expression was inhibited by high circCUX1 expression. Further research revealed that, in NB cells, DMRT2 was the target of miR-16-5p; the DMRT2 effects on the tumor cells proliferation, migration, invasion, and glycolysis can be reversed by miR-16-5p overexpression. Therefore, circCUX1 can promote NB cell proliferation, migration, invasion, and glycolysis by miR-16-5p/DMRT2 axis. In a similar mechanism of action, Fang et al. found that circCUX1 works through the miR432-5p/NOL4L axis (16), and Wang found that circCUX1 works through the miR-338-3p/PHF20 axis (17).

Unlike the first two mechanisms, Yang discovered the mechanism of circCUX1 in NB metabolism reprogramming (18). They found a protein sub-type consisting of 113 amino acids encoded by the CUX1 gene (p113). Additional validation tests showed that nuclear p113 encoded by circCUX1 increased NB cell proliferation, invasion, metastasis, lipid metabolism reprogramming, and mitochondrial activity. The transcriptional regulatory complex formed by P113 Zuotin-related factor 1 (ZRF1), and bromodomain protein 4 (BRD4) upregulated aldehyde dehydrogenase 3 family member A1 (ALDH3A1), NADH: ubiquinone oxidoreductase subunit A1 (NDUFA1) and NADH: ubiquinone oxidoreductase complex assembly factor 5 (NDUFAF5), by transactivation of ZRF1/BRD4. Therefore, these genes enhanced lipid metabolism (the production and oxidation of fatty acids) and mitochondrial activity. By inhibiting the interaction of p113-ZRF1, inhibitory peptides can impede cancer cell growth and invasion. High expression of p113, ZRF1, or BRD4 was associated with a reduced survival rate among NB patients. Based on these findings, it was hypothesized that circCUX1 subtypes encoded by p113 subtypes increase tumor growth by transactivating ZRF1/BRD4.

CircKIF2A (circ_0129276)

CircKIF2A was first discovered by Ebrahim Mahmoudi's team (19), and then the expression level and function of circKIF2A in NB tissues and cell lines were investigated by Yang et al. It was discovered that circKIF2A contributed to the proliferation and invasion of malignant cells. CircKIF2A may facilitate a more efficient glycolysis rate and energy metabolism in tumor cells, hence promoting their growth and function. According to further research, circKIF2A was activated through the miR129-5p/PLK4 axis (20). Moreover, Jin's group discovered that circKIF2A was associated with elevated NB tissue levels and that circKIF2A mediated its activity by miR-377-3p/PRPS1 (21).

CircDGKB (circ_0133622)

Yang observed that circDGKB was upregulated in NB tissue relative to normal ganglia and that there was a negative correlation between circDGKB expression levels and survival rates of NB patients. CircDGKB overexpression caused NB cells to proliferate, migrate, invade, and tumorigenesis while reducing their apoptosis. According to the luciferase reporter gene study, this enhancement of NB cells was accomplished by reducing miR-873 expression and increasing GLI1 (glioma-associated oncogene 1) gene expression. GLI1 is an important transcription factor of the Hedgehog signaling pathway, which is involved in the tumor progression of various tumors (22), including NB. circDGKB appears to be a promising possibility for new therapies and diagnostic markers of NB, according to this study (23).

CircAGO2(Circ_0135889)

Argonaute 2 (AGO2) is the core component of microRNA-induced silencing complex. It plays a crucial function in microRNA-mediated gene silencing and significantly affects tumor development and progression. CircAGO2 comes from the AGO2 coding gene. circAGO2 is upregulated in numerous tumor tissues and cell lines, including gastric cancer, prostate cancer, colorectal cancer, and NB (24). There was a correlation between cancer prognosis and circAGO2 expression levels (24). Researchers have found that circAGO2 physically interacts with the human antigen R protein (HuR), activating and enriching it in the 3'-untranslated region of the target gene. Therefore, AGO2 binding is reduced, and microRNA-mediated gene silencing associated with cancer progression is inhibited. Using shRNA targeting circAGO2 could block downstream target gene activity and prevent the occurrence and growth of transplanted tumors in nude mice. Additionally, blocking circAGO2 and HuR connections with cell penetration inhibitory peptides will stop cancer cells from spreading and becoming invasive. These results indicated that circAGO2 facilitated tumor progression by blocking the inhibitory function of the key molecule HuR of the AGO2/microRNA complex.

CircACAP2

CircACAP2 was discovered for the first time in breast cancer research; it can increase tumor growth and metastasis (25). Subsequently, Zhu and colleagues found that circACAP2 and hexokinase 2 (HK2) abundance in NB tissues and cell lines increased significantly (26). By suppressing circACAP2, migration, invasion, and glycolysis of NB cells were reduced, and apoptosis was induced. According to bioinformatics analysis, a luciferase reporter assay, and an RNA pull-down experiment, circACAP2 was identified as a target of

miR-143-3p. In addition, the glycolytic enzyme HK2 was a direct target of miR-143-3p in NB cells. Thus, circACAP2 promotes tumor formation through the miR-143-3p/HK2 signal cascade. Moreover, the glycolytic enzyme HK2 was a direct target of miR-143-3p in NB cells. Thus, circACAP2 promotes tumor formation by the miR-143-3p/HK2 signal cascade.

CircDLGAP4

CircDLGAP4 was first implicated with nervous system diseases, including ischemic stroke (27) and Parkinson's disease (28). With the deepening of research, researchers gradually discovered its role in tumors (29) and nerve injury (30). Tan et al. investigated the role of exosome-delivered circDLGAP4 in the chemoresistance of NB cells (29). It was observed that doxorubicin-resistant cells showed HK2 higher expression and enhanced glycolysis. CircDLGAP4 delivered by the exocrine body promoted glycolysis, proliferation, and invasion of sensitive NB cells by regulating miR-143 and HK2 and established a new relationship between drug resistance and circDLGAP4/miR-143/HK2 axis in drug-resistant NB.

Circ_0013401

Zhu's team investigated the role of circ_0013401 in NB (31). They found that circ_0013401 expression increased in NB tissues. Circ_0013401 can accelerate tumor growth and metastasis in NB and inhibit tumor apoptosis and autophagy. This is accomplished by competitively binding miR-195, thus reducing its silencing inhibition on the target gene p21-activated kinase 2. (PAK2). The PAK2 increased expression contributes to the malignant biological behavior of NB tumor cells.

CircPDE5A (circ_0002474)

Chen et al. reported the molecular role of circPDE5A in the NB malignant progression (32). In their investigation, circPDE5A expression was higher in NB tissues and cells. When circPDE5A is silenced, NB cells *in vitro* are inhibited from proliferating, migrating, invading, and metabolizing glycogen, and tumors *in vivo* are reduced in size. Additionally, by binding to miR-362-5p, circPDE5A regulates miR-362-5p's effects on the malignant growth of NB *in vitro*, resulting in nucleolar protein 4-like (NOL4L) overexpression.

NOL4L has been reported to be an oncogene in multiple cancers, including NB (33). By altering the miR-362-5p/NOL4L pathway, the knockdown of circPDE5A at least partially inhibits the malignant evolution of NB, suggesting circPDE5A as a potential therapeutic target for NB and offering some evidence for its usage.

Circ0125803

Tang et al. reported the molecular role of circ0125803 in NB proliferation and metastasis (34). They used high-throughput chip analysis technology to analyze the circular RNA expression in NB tissue. It was found that circ0125803 was a highly upregulated circRNA in NB samples. circ0125803 inhibition significantly reduced the proliferation and invasion rate of NB. Circ0125803 promotes the NB progression by blocking miR-197-5p and increasing E2F1 expression.

CircHIPK3

CircHIPK3 has been confirmed to increase expression in various malignant tumors and promote tumor progression (35). However, there are few studies in NB. Wei Jiabin's team studied the expression of circHIPK3 in NB cells and its role in NB progression (36). The effects of circHIPK3 on the proliferation, migration, and invasion of NB cells were detected by qRT-PCR, CCK-8, plate cloning test, scratch test, and transwell invasion test. It was confirmed that circHIPK3 was highly expressed in NB cells, and silencing circHIPK3 could inhibit the proliferation, migration, and invasion of NB cells. This study did not investigate how circHIPK3 promotes tumor cell proliferation, migration, and invasion; however, it gave some evidence for circHIPK3's participation in NB.

Circ0075829

Ren Dong and his colleagues first studied the Circ0075829 expression in NB and its role in cell proliferation and migration (37). The circ0075829 expression was increased in NB tumor tissues and cell lines. After the circ0075829 deletion, the proliferation and migration of NB cell lines were boosted, and ERK phosphorylation activity was triggered, but p38 and JNK phosphorylation activities were unaffected. The circ0075829 expression was negatively correlated with the INSS stage and risk stage and positively correlated with the total survival period of patients. The study found that circ0075829 can inhibit NB cell proliferation and migration. Its high expression is well correlated with clinical phenotype. It may play a role by stimulating the ERK/MAPK pathway and is a potential NB biomarker and treatment target.

CircNHSL1

Liu Jingdong and colleagues discussed the circNHSL1 expression in NB and the role of chemotherapy tolerance (38). They found that the circNHSL1 expression in NB was higher than in normal tissues. The circNHSL1 expression in chemotherapy-resistant children and drug-resistant cell lines was higher than in chemotherapy-sensitive children. In chemotherapy-resistant cells, after silencing circNHSL1, the cell proliferation activity decreased, while the apoptosis rate increased, TGF- β The secretion level and expression level and the downstream expression level of p-Smad2 and p-Smad3 decreased. Donor recombinant TGF- β After treatment of circNHSL1 silenced drug-resistant cells, the cell proliferation activity increased, while the apoptosis rate decreased, and the drug-resistant characteristics were restored. CircNHSL1

may trigger the TGF-β/Smad signaling pathway associated with chemotherapy tolerance. Nonetheless, this report lacks extensive research on the circNHSL1 mechanism.

Cancer suppressor circRNA

CircRNA-TBC1D4, circRNA-NALAD2c and circRNA-TGFBR3

The research on circRNAs in NB is mostly related to promoting tumor progression. Lin and team members have found several possible tumor suppressor circRNAs (39). Five pairs of NB and adjacent normal fetal adrenal medulla samples were collected for high-throughput sequencing. The putative circRNAs were discovered by real-time quantitative reverse transcriptase polymerase chain reaction after bioinformatic analysis of the differentially expressed circRNAs host gene. Furthermore, an analysis was conducted of the clinical characteristics of NB and the key circRNAs.

Additionally, these key circRNAs were overexpressed in NB cell lines to investigate their biological functions. Consequently, 4704 differentially expressed circRNAs were discovered, including 2462 upregulated and 2242 downregulated circRNAs. As miR-21 is vital in the progression of NB, they further experimented with the circRNAs associated with miR-21. Numerous circRNAs were identified based on target prediction, including circRNA-TBC1D4, circRNA-NAALAD2, and circRNA-TGFBR3. Further study revealed that circRNA-TBC1D4, circRNA-NAALAD2, and circRNA-TGFBR3 were associated with clinical features. The expression of the three circRNAs in NB tissue was significantly lower than in normal adrenal tissue. The circRNA-TBC1D4 expression was related to the number of MYCN and lactate dehydrogenase concentrations.

Similarly, circRNA-NAALAD2 expression correlated with LDH concentration, while circRNA-TGFBR3 expression correlated with histological classification. A positive effect of circRNA-TBC1D4 overexpression on NB cell migration was seen *in vitro*, but it did not promote NB cell proliferation or colony formation. In conclusion, this study offered some evidence for the protective function of circRNAs in NB, suggesting that circRNAs may become an additional therapy option for NB.

CircRNA functions and mechanism unclear

Zhang and colleagues (40) downloaded the RNA-seq data of 39 NB and 2 normal cell lines from the Sequence Read Archive (SRA) database. They described the comprehensive characterization of circRNAs in NB Cell Lines. They discovered 29 circRNAs with altered expression levels. After constructing ceRNA networks, hsa_circ_0005379, hsa_circ_0002343, and hsa_circ_0001361 were identified as critical regulators in the ceRNA networks, which might regulate PI3K/Akt/mTOR signaling pathway and epithelial-mesenchymal transition (EMT). However, no more mechanistic investigations have been conducted on how these circRNAs affect signaling pathways and EMT processes.

Discussion

Non-coding RNAs (ncRNAs) are crucial in the pathogenesis of neuroblastoma (NB). In recent years, circRNAs have emerged as an important ncRNA in NB research, with increasing studies demonstrating their involvement in tumor cell proliferation, invasion, and migration. One of the key discoveries of prior research is that circRNAs are differentially expressed in NB relative to normal tissue, suggesting that they may play a role in the pathogenesis of the disease. Table 1 summarizes the current research and the role of circRNAs in NB. Like lncRNAs and

TABLE 1 Role of circRNAs in NB.

CircRNAs	Expression	Functions in NB	Potential mechanism	Reference
CircCUX1 (Circ_0132813)	Upregulated	1. Promotes aerobic glycolysis and NB proliferation and invasion	1. CircCUX1 combines with EWSR1 to promote its interaction with MAZ protein, resulting in the trans-activation of MAZ and the transcription change of CUX1 and other tumor progression-related genes	(13)
		2. Promotes the proliferation and invasion of tumor cells, and induce glycolysis metabolism	2. Through miR-16-5p/DMRT2 axis, miR432-5p/NOL4L axis and miR-338-3p/PHF20 axis	(14, 16, 17)
		3. Promotes lipid metabolism reprogramming, mitochondrial activity, proliferation, invasion and metastasis of NB cells	3. p113 encoded by circCUX1 promotes tumor progression *via* trans-activation of ZRF1/BRD4	(18)
CircKIF2A (Circ_0129276)	Upregulated	Promotes the proliferation and invasion of tumor cells and improve the glycolysis level of tumor cells	Through miR129-5p/PLK4, miR-377-3p/PRPS1 axis	(20, 21)

(Continued)

TABLE 1 Continued

CircRNAs	Expression	Functions in NB	Potential mechanism	Reference
CircDGKB (Circ_0133622)	Upregulated	Promotes the proliferation, migration, invasion and tumorigenesis of NB cells, and reduce cell apoptosis	Via miR-873/GLI1 axis	(23)
CircAGO2 (Circ_0135889)	Upregulated	Promotes the growth and invasion of NB tumor cells	CircAGO2 interacts with HuR protein to regulate the function of AGO2/miRNA complex	(24)
CircACAP2	Upregulated	Promotes the migration and invasion of cancer cells and inhibit the apoptosis of cancer cells	CircACAP2 acts through the miR-143/HK2 axis	(26)
CircDLGAP4	Upregulated	Promotes the proliferation and invasion of cancer cells, induce glycolysis, and induce drug resistance	CircDLGAP4 works through the miR-143/HK2 axis	(29)
Circ_0013401	Upregulated	Induces tumor growth and metastasis, prevent tumor cell apoptosis and autophagy	Circ_0013401 works through the miR-195/PAK2 axis	(31)
CircPDE5A (Circ_0002474)	Upregulated	Promotes the proliferation and invasion of tumor cells, and induce glycolysis metabolism	CircPDE5A works through miR-362-5p/NOL4L axis	(32)
Circ0125803	Upregulated	Promotes tumor proliferation and invasion	Circ0125803 works through the miR-197-5p/E2F1 axis	(34)
CircHIPK3	Upregulated	Promotes tumor proliferation and invasion, promote NB cell proliferation, migration and invasion	Further mechanism study not performed.	(36)
Circ0075829	Upregulated	Enhances the proliferation and migration of NB cells	It may work by activating ERK/MAPK pathway	(37)
CircNHSL1	Upregulated	Promotes the proliferation of NB cells, inhibit the rate of apoptosis, and induce drug resistance	It is possible to activate TGF- β/Smad signal pathway participates in chemotherapy tolerance	(38)
CircRNA-TBC1D4,	Downregulated	Inhibits the proliferation and migration of cancer cells	It may weaken the silencing of target genes by miRNA-21 by competing with miRNA-21	(39)
CircRNA-NAALAD2	Downregulated	Inhibits the proliferation and migration of cancer cells	It may weaken the silencing of target genes by miRNA-21 by competing with miRNA-21	(39)
CircRNATGFBR3	Downregulated	Inhibits the proliferation and migration of cancer cells	It may weaken the silencing of target genes by miRNA-21 by competing with miRNA-21	(39)
Circ_0005379	Unknown	Unclear	As a critical regulator in the ceRNA networks formed by 13 genes	(40)
Circ_0002343	Unknown	Unclear	It may work by regulating PI3K/Akt/mTOR signaling *via* RAC1	(40)
Circ_0001361	Unknown	Unclear	Possibly involved in EMT	(40)

EWSR1, EWS RNA binding protein 1; MAZ, MYC-related zinc finger protein; DMRT2, Doublesex and mab-3 related transcription factor 2; NOL4L, Nucleolar protein 4 like; PHF20, PHD Finger Protein 20; ZRF1, Zuotin-related factor 1; BRD4, bromodomain protein 4; PLK4, Polo-like kinase 4; PRPS1, Phosphoribosyl pyrophosphate synthetase 1; GLI1, Glioma-associated oncogene 1; AGO2, Argonaute 2; HK2, hexokinase 2; PAK2, P21-activated kinase 2; HuR, Human antigen R; RAC1, Rac family small GTPase 1; EMT, epithelial mesenchymal transition.

miRNAs, circRNAs exhibit a dual function in promoting tumor progression and inhibiting tumor development. Down-regulating the expression of upregulated circRNAs inhibits tumor growth, highlighting their potential as therapeutic targets.

Conversely, some down-regulated circRNAs exhibit protective effects in NB and may serve as potential drug targets for treating the disease. Other studies have demonstrated the potential of circRNAs as diagnostic biomarkers for NB patients, particularly in blood samples. However, most circRNA research has centered on their sponge adsorption and competitive binding to miRNAs to counteract the miRNA-mediated silence of target genes. Relatively less is known about additional action methods, such as the peptide encoded by circRNAs. A more comprehensive investigation of circRNAs would enhance our understanding of their function in NB and provide broader research avenues for NB diagnosis and treatment.

In addition to their potential as biomarkers, circRNAs have been demonstrated to modulate several signaling pathways involved in NB development and progression. For example, a study by Liu et al. (38) found that the circNHSL1 promoted NB cell proliferation, inhibited the apoptosis rate, and induced drug resistance by activating the TGF- β/Smad pathway. Similarly, a study by Tang et al. (34) identified a circRNA, Circ0125803, that promoted NB cell proliferation and invasion by targeting the miR-197-5p/E2F1 axis.

Despite these findings, there are still gaps and contradictions in the research that require attention. For instance, the functional roles of several circRNAs in NB are poorly understood, as are their

mechanisms of action. Furthermore, the circRNAs expression patterns can vary widely between different studies, which may be due to differences in sample size, tissue source, and analysis methods. More comprehensive studies that use larger sample sizes and standardized methods for circRNA detection and analysis are needed to better understand the role of circRNAs in NB.

In summary, previous studies have identified several circRNAs differentially expressed in NB and have been shown to regulate various signaling pathways involved in the disease's development and progression. Additional research is required to completely comprehend the physiological roles of circRNAs in NB and their potential as diagnostic and therapeutic targets.

Author contributions

CY and JT conceived the scope of the manuscript. CY and KW wrote the manuscript. All authors discussed the manuscript and made comments on the manuscript. All authors contributed to the article and approved the submitted version.

Acknowledgments

The figure of the article was drawn by Figdraw (www.figdraw.com).

Conflict of interest

The authors declare that the research was conducted in the absence of any commercial or financial relationships that could be construed as a potential conflict of interest.

Publisher's note

References

1. Maris JM. Recent advances in neuroblastoma. *N Engl J Med* (2010) 362(23):2202–11. doi: 10.1056/NEJMra0804577

2. Swift CC, Eklund MJ, Kraveka JM, Alazraki AL. Updates in diagnosis, management, and treatment of neuroblastoma. *Radiographics* (2018) 38(2):566–80. doi: 10.1148/rg.2018170132

3. Rabinowicz R, Barchana M, Liphshiz I, Futerman B, Linn S, Weyl-Ben-Arush M. Cancer incidence and survival among children and adolescents in Israel during the years 1998 to 2007. *J Pediatr Hematol Oncol* (2012) 34(6):421–9. doi: 10.1097/MPH.0b013e31826157ce

4. Fetahu IS, Taschner-Mandl S. Neuroblastoma and the epigenome. *Cancer Metastasis Rev* (2021) 40(1):173–89. doi: 10.1007/s10555-020-09946-y

5. Li J, Sun D, Pu W, Wang J, Peng Y. Circular RNAs in cancer: Biogenesis, function, and clinical significance. *Trends Cancer* (2020) 6(4):319–36. doi: 10.1016/j.trecan.2020.01.012

6. Li Z, Huang C, Bao C, Chen L, Lin M, Wang X, et al. Exon-intron circular RNAs regulate transcription in the nucleus. *Nat Struct Mol Biol* (2015) 22(3):256–64. doi: 10.1038/nsmb.2959

7. Chen R, Lei S, Jiang T, Zeng J, Zhou S, She Y. Roles of lncRNAs and circRNAs in regulating skeletal muscle development. *Acta Physiol (Oxf)* (2020) 228(2):e13356. doi: 10.1111/apha.13356

8. van Rossum D, Verheijen BM, Pasterkamp RJ. Circular RNAs: Novel regulators of neuronal development. *Front Mol Neurosci* (2016) 9:74. doi: 10.3389/fnmol.2016.00074

9. Lu Y, Li Z, Lin C, Zhang J, Shen Z. Translation role of circRNAs in cancers. *J Clin Lab Anal* (2021) 35(7):e23866. doi: 10.1002/jcla.23866

10. Qian L, Yu S, Chen Z, Meng Z, Huang S, Wang P. The emerging role of circRNAs and their clinical significance in human cancers. *Biochim Biophys Acta Rev Cancer* (2018) 1870(2):247–60. doi: 10.1016/j.bbcan.2018.06.002

11. Verduci L, Tarcitano E, Strano S, Yarden Y, Blandino G. CircRNAs: Role in human diseases and potential use as biomarkers. *Cell Death Dis* (2021) 12(5):468. doi: 10.1038/s41419-021-03743-3

12. Zhou Q, Ju LL, Ji X, Cao YL, Shao JG, Chen L. Plasma circRNAs as biomarkers in cancer. *Cancer Manag Res* (2021) 13:7325–37. doi: 10.2147/CMAR.S330228

13. Li H, Yang F, Hu A, Wang X, Fang E, Chen Y, et al. Therapeutic targeting of circ-CUX1/EWSR1/MAZ axis inhibits glycolysis and neuroblastoma progression. *EMBO Mol Med* (2019) 11(12):e10835. doi: 10.15252/emmm.201910835

14. Zhang X, Zhang J, Liu Q, Zhao Y, Zhang W, Yang H. Circ-CUX1 accelerates the progression of neuroblastoma *via* miR-16-5p/DMRT2 axis. *Neurochem Res* (2020) 45(12):2840–55. doi: 10.1007/s11064-020-03132-w

15. Chava S, Reynolds CP, Pathania AS, Gorantla S, Poluektova LY, Coulter DW, et al. miR-15a-5p, miR-15b-5p, and miR-16-5p inhibit tumor progression by directly targeting MYCN in neuroblastoma. *Mol Oncol* (2020) 14(1):180–96. doi: 10.1002/1878-0261.12588

16. Fang Y, Yao Y, Mao K, Zhong Y, Xu Y. Circ_0132817 facilitates cell proliferation, migration, invasion and glycolysis by regulating the miR-432-5p/NOL4L axis in neuroblastoma. *Exp Brain Res* (2021) 239(6):1841–52. doi: 10.1007/s00221-021-06091-y

17. Wang Y, Niu Q, Dai J, Shi H, Zhang J. circCUX1 promotes neuroblastoma progression and glycolysis by regulating the miR-338-3p/PHF20 axis. *Gen Physiol Biophys* (2021) 40(1):17–29. doi: 10.4149/gpb_2020041

18. Yang F, Hu A, Guo Y, Wang J, Li D, Wang X, et al. p113 isoform encoded by CUX1 circular RNA drives tumor progression *via* facilitating ZRF1/BRD4 transactivation. *Mol Cancer* (2021) 20(1):123. doi: 10.1186/s12943-021-01421-8

19. Mahmoudi E, Kiltschewskij D, Fitzsimmons C, Cairns MJ. Depolarization-associated CircRNA regulate neural gene expression and in some cases may function as templates for translation. *Cells* (2019) 9(1):25. doi: 10.3390/cells9010025

20. Yang Y, Pan H, Chen J, Zhang Z, Liang M, Feng X. CircKIF2A contributes to cell proliferation, migration, invasion and glycolysis in human neuroblastoma by regulating miR-129-5p/PLK4 axis. *Mol Cell Biochem* (2021) 476(6):2513–25. doi: 10.1007/s11010-021-04096-3

21. Jin Q, Li J, Yang F, Feng L, Du X. Circular RNA circKIF2A contributes to the progression of neuroblastoma through regulating PRPS1 expression by sponging miR-377-3p. *Biochem Genet* (2022) 60(4):1380–401. doi: 10.1007/s10528-021-10174-4

22. Avery JT, Zhang R, Boohaker RJ. GLI1: A therapeutic target for cancer. *Front Oncol* (2021) 11:673154. doi: 10.3389/fonc.2021.673154

23. Yang J, Yu L, Yan J, Xiao Y, Li W, Xiao J, et al. Circular RNA DGKB promotes the progression of neuroblastoma by targeting miR-873/GLI1 axis. *Front Oncol* (2020) 10:1104. doi: 10.3389/fonc.2020.01104

24. Chen Y, Yang F, Fang E, Xiao W, Mei H, Li H, et al. Circular RNA circAGO2 drives cancer progression through facilitating HuR-repressed functions of AGO2-miRNA complexes. *Cell Death Differ* (2019) 26(7):1346–64. doi: 10.1038/s41418-018-0220-6

25. Zhao B, Song X, Guan H. CircACAP2 promotes breast cancer proliferation and metastasis by targeting miR-29a/b-3p-COL5A1 axis. *Life Sci* (2020) 244:117179. doi: 10.1016/j.lfs.2019.117179

26. Zhu J, Xiang XL, Cai P, Jiang YL, Zhu ZW, Hu FL, et al. CircRNA-ACAP2 contributes to the invasion, migration, and anti-apoptosis of neuroblastoma cells through targeting the miRNA-143-3p-hexokinase 2 axis. *Transl Pediatr* (2021) 10(12):3237–47. doi: 10.21037/tp-21-527

27. Bai Y, Zhang Y, Han B, Yang L, Chen X, Huang R, et al. Circular RNA DLGAP4 ameliorates ischemic stroke outcomes by targeting miR-143 to regulate endothelial-mesenchymal transition associated with blood-brain barrier integrity. *J Neurosci* (2018) 38(1):32–50. doi: 10.1523/JNEUROSCI.1348-17.2017

28. Feng Z, Zhang L, Wang S, Hong Q. Circular RNA circDLGAP4 exerts neuroprotective effects *via* modulating miR-134-5p/CREB pathway in parkinson's disease. *Biochem Biophys Res Commun* (2020) 522(2):388–94. doi: 10.1016/j.bbrc.2019.11.102

29. Tan WQ, Yuan L, Wu XY, He CG, Zhu SC, Ye M. Exosome-delivered circular RNA DLGAP4 induces chemoresistance *via* miR-143-HK2 axis in neuroblastoma. *Cancer biomark* (2022) 34(3):375–84. doi: 10.3233/CBM-210272

30. Qiu L, He J, Chen H, Xu X, Tao Y. CircDLGAP4 overexpression relieves oxygen-glucose deprivation-induced neuronal injury by elevating NEGR1 through sponging miR-503-3p. *J Mol Histol* (2022) 53(2):321–32. doi: 10.1007/s10735-021-10036-8

31. Zhu S, Tang X, Gao X, Zhang J, Cui Y, Li D, et al. hsa_circ_0013401 accelerates the growth and metastasis and prevents apoptosis and autophagy of neuroblastoma cells by sponging miR-195 to release PAK2. *Oxid Med Cell Longev* (2021) 2021:9936154. doi: 10.1155/2021/9936154

32. Chen Y, Lin L, Hu X, Li Q, Wu M. Silencing of circular RNA circPDE5A suppresses neuroblastoma progression by targeting the miR-362-5p/NOL4L axis. *Int J Neurosci* (2023) 133(2):141–51. doi: 10.1080/00207454.2021.1896505

33. Yu Z, Zhang J, Han J. Silencing CASC11 curbs neonatal neuroblastoma progression through modulating microRNA-676-3p/nucleolar protein 4 like (NOL4L) axis. *Pediatr Res* (2020) 87(4):662–8. doi: 10.1038/s41390-019-0625-z

34. Tang J, Liu F, Huang D, Zhao C, Liang J, Wang F, et al. circ0125803 facilitates tumor progression by sponging miR-197-5p and upregulating E2F1 in neuroblastoma. *Pathol Res Pract* (2022) 233:153857. doi: 10.1016/j.prp.2022.153857

35. Wei Z, Shi Y, Xue C, Li M, Wei J, Li G, et al. Understanding the dual roles of CircHIPK3 in tumorigenesis and tumor progression. *J Cancer* (2022) 13(15):3674–86. doi: 10.7150/jca.78090

36. Yu JB, Chen WM, Yang BY, Yang L, Li SM, Wang Y, et al. The role of circular RNA circHIPK 3in the progreesion of neuroblastoma. *Chin J Pediatr Surg* (2021) 42 (11):1015–9. doi: 10.3760/cma.j.cn421158-20210116-00027

37. Ren D, Liu QY, Lu J, Wang SC, Li YH, Yu YB, et al. Circ0075829 is expressed in neuroblastoma tissues and inhibits cell proliferation and migration. *J China Pediatr Blood Cancer* (2021) 26(5):261–9. doi: 10.3969/j.issn.1673-5323.2021.05.002

38. Liu JD, Wang JJ. Expression ofCircular RNA circNHSL1 in pediatric neuroblastoma and its role in chemotherapy resistance. *J Pediatr Pharm* (2022) 28 (9):1–5. doi: 10.13407/j.cnki.jpp.1672-108X.2022.09.001

39. Lin W, Wang Z, Wang J, Yan H, Han Q, Yao W, et al. circRNA-TBC1D4, circRNA-NAALAD2 and circRNA-TGFBR3: Selected key circRNAs in neuroblastoma and their associations with clinical features. *Cancer Manag Res* (2021) 13:4271–81. doi: 10.2147/CMAR.S297316

40. Zhang L, Zhou H, Li J, Wang X, Zhang X, Shi T, et al. Comprehensive characterization of circular RNAs in neuroblastoma cell lines. *Technol Cancer Res Treat* (2020) 19:1533033820957622. doi: 10.1177/1533033820957622

frontiers | Frontiers in Oncology

TYPE Case Report
PUBLISHED 19 May 2023
DOI 10.3389/fonc.2023.1132702

OPEN ACCESS

EDITED BY
Jing He,
Guangzhou Medical University, China

REVIEWED BY
Zeinab Afify,
The University of Utah, United States
Yi Ji,
Sichuan University, China

*CORRESPONDENCE
Kai Li
likai2727@163.com

RECEIVED 27 December 2022
ACCEPTED 27 April 2023
PUBLISHED 19 May 2023

CITATION
Wang Z, Yan H, Ma Y, Yao W, Zheng S and Li K (2023) Case Report: Kaposiform hemangioendothelioma with PIK3CA mutation successfully treated with sirolimus.
Front. Oncol. 13:1132702.
doi: 10.3389/fonc.2023.1132702

Case Report: Kaposiform hemangioendothelioma with PIK3CA mutation successfully treated with sirolimus

Zuopeng Wang[1], Hanlei Yan[1], Yangyang Ma[2], Wei Yao[1], Shan Zheng[1] and Kai Li[1]*

[1]Department of Pediatric Surgery, Children's Hospital of Fudan University, National Children's Medical Center, Shanghai, China, [2]Department of Pathology, Children's Hospital of Fudan University, National Children's Medical Center, Shanghai, China

Kaposiform hemangioendothelioma (KHE) is an extremely rare, locally aggressive vascular neoplasm. The etiopathogenesis of KHE is still poorly understood. In the present study, we found a new mutation in KHE (c.685delA, p.Thr229fs). The KHE patient with the PIK3CA mutation showed complete regression after sirolimus treatment. We propose that the presence of the PIK3CA mutation in KHE may correlate with good response to sirolimus.

KEYWORDS

PIK3CA, mutation, sirolimus, Kaposiform hemangioendothelioma, mTOR

Introduction

Kaposiform hemangioendothelioma (KHE) is an extremely rare, locally aggressive vascular neoplasm resulting from abnormal angiogenesis and lymphangiogenesis during infancy or early childhood. It is commonly complicated by the occurrence of the Kasabach-Merritt phenomenon, which is characterized by the association of a rapidly growing vascular tumor, thrombocytopenia and consumptive coagulopathy (1). Recently, Carli et al. reported a patient with KHE with a phosphatidylinositol-4,5-bisphosphate 3-kinase catalytic subunit alpha (PIK3CA) mutation (c.323G > A, p.Arg108His) and suggested that KHE may be a subtype of PIK3CA-related overgrowth spectrum (PROS) (2). PROS is defined as a phenotypic spectrum of developmental disorders caused by activating variants of the PIK3CA gene (3). In the present study, we found a different PIK3CA mutation in KHE (c.685delA, p.Thr229fs), which provides new evidence that KHE may belongs to PROS.

Case report

A 3-month-old boy was referred to Children's hospital of Fudan university with a middorsal tumor growing for more than one month, which was misdiagnosed as hemangioma and received no treatment by the local hospital. Physical examination revealed an erythematous, poorly demarcated lesion (6 cm × 5 cm) on the patient's back

with no signs of inflammation or pain (Figure 1A). The patient had no family history of vascular disorders.

Laboratory examination found no obvious abnormality in routine blood and coagulation tests. Complete blood count at presentation revealed a platelet count of 302 × 10^9/L (normal range:188-472× 10^9/L) and hemoglobin level of 13.8 g/dl(normal range:11.2-14.9 g/dl). Coagulation function was normal including fibrinogen 209 mg/dl (normal range: 200-400 mg/dl), prothrombin time 13.3 s(normal range:11-14.5s), partial thromboplastin time 34 s (normal range:28-45s)and D-dimer level 1.99 mg/L (normal range: 0-0.5 mg/L).

Magnetic resonance imaging showed ill-defined margins and diffusive hyperintense signals in fat-suppressed T2 weighted images (Figures 2A, B) and obvious heterogeneous enhancement in T1 weighted images.

The patient underwent biopsy that confirmed the pathological diagnosis of KHE. Hematoxylin and eosin staining showed typical glomeruloid areas with spindle shaped cells. Immunohistochemical staining was positive for D2–40, PROX-1, LYVE-1, CD31 and CD34 (Figure 3). We also detected the extracted DNA in tumor tissue samples from biopsy by next generation sequencing and bioinformatics analysis. We focused on hot-spot mutation regions of 42 genes (Table 1) related to tumorigenesis and vascular diseases and found that the patient harbored PIK3CA mosaic pathogenic variants (c.685delA and p.Thr229fs).

The patient received sirolimus therapy following diagnosis of KHE without the Kasabach-Merritt phenomenon. We administered the sirolimus regimen at an initial dose of 0.8 mg/m^2, twice a day and maintained a drug trough level of 10-15 ng/mL (4). Sulfamethoxazole was then applied for prophylaxis of pneumocystis carinii pneumonia. The lesion shrank dramatically after one year of sirolimus therapy (Figures 2C, D). The patient achieved complete response after two years of sirolimus treatment (Figures 1B, 2E, F). The lesion showed total regression, and no serious complications were observed.

Discussion

The etiopathogenesis of KHE is still poorly understood. Sporadic vascular tumors have been documented with potential genetic anomalies. Most mutations are detected in genes that play crucial roles in pathways involved in angiogenesis and lymphangiogenesis, vascular cell growth, apoptosis and proliferation (5). There are no treatment guidelines for KHE, although there are some expert consensus (6) and treatment recommendations (7). Sirolimus (8), vincristine (9) and glucocorticoids (6) are the common medication regimens for KHE.

A few mutations and genes had been found to be related to the development of KHE. Zhou et al. demonstrated a somatic translocation between chromosomes 13 and 16 at the bands of 13q14 and 16p13.3 in 10% of cells with KHE nodules; normal cells were also present in the karyotype (10). Lim et al. identified a single heterozygous somatic single nucleotide variation, c.614A>T (p.Gln205Leu), in GNA14 (G-protein subunit alpha 14) in one of three KHE patients (11). They subsequently confirmed that somatic activation of the GNA14 mutation caused changes in cellular morphology and rendered cells growth-factor independent by upregulating the mitogen-activated protein kinase (MAPK) pathway. A recent study also revealed that PIK3CA mutations correlated with mammalian target of rapamycin (mTOR) pathway expression (12), but not with clinical or pathological features, in patients with fibro-adipose vascular anomaly (13), indicating that sirolimus may still be effective in patients without PIK3CA mutations. Sirolimus inhibits the mTOR pathway, with subsequent effects on angiogenesis and lymphangiogenesis. Maruani et al. reported that inhibiting mTOR may help shrink lesions and improve clinical symptoms associated with lymphatic anomalies, even with no evidence of PIK3CA variants (14). We analyzed the expression of mTOR-related proteins in KHE and found that the absence of tuberous sclerosis complex 2 and phosphatase and tensin homolog caused abnormal activation of the mTOR signaling pathway and may account for the pathogenesis of KHE (15). In our study, the patient with a new PIK3CA mutation showed complete response to sirolimus therapy. The PIK3CA mutation may have abnormally activated the mTOR pathway, although the pathogenicity of this mutation has not been confirmed. In our next study, we will construct the mutant gene in zebrafish to observe the phenotype of the PIK3CA mutation.

The patient is still in maintenance treatment using a lower concentration of sirolimus. At present the standard for sirolimus withdrawal is still controversial, since the rebound of KHE after sirolimus treatment has been reported in approximately 17% of patients (16). Additionally, Venot et al. provided the first direct evidence supporting PIK3CA inhibition as a promising therapeutic strategy in patients with PROS (17) by inhibiting the constitutively

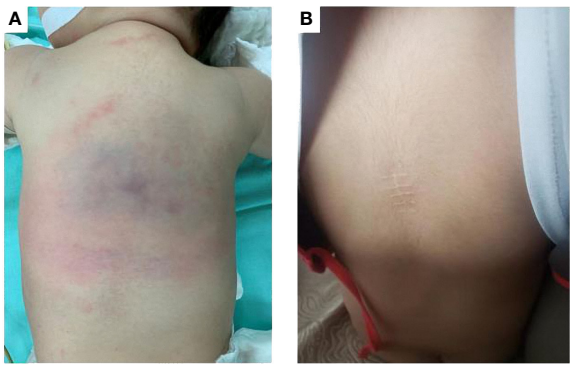

FIGURE 1
(A) Before treatment, an erythematous, poorly demarcated lesion (6 cm x 5 cm) on the back. **(B)** After two years of sirolimus treatment, the lesion regressed completely.

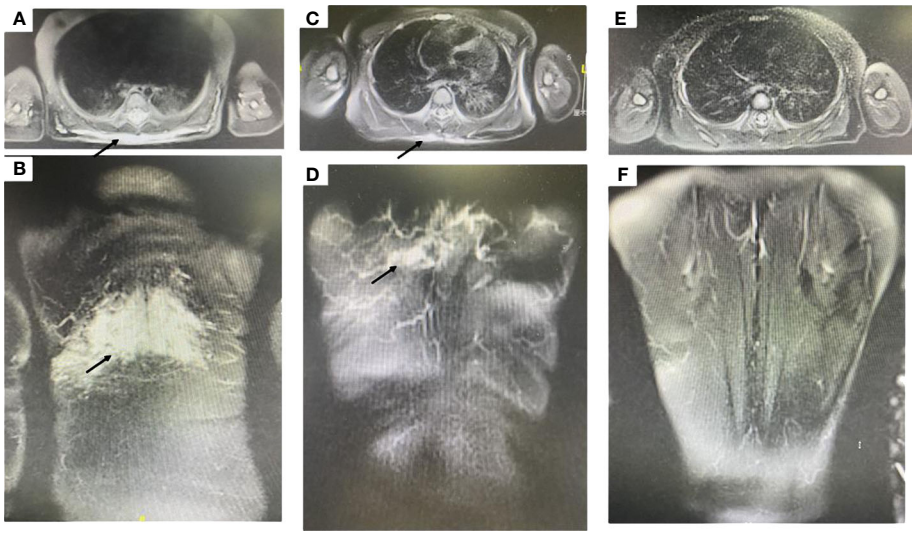

FIGURE 2
(A, B) Magnetic resonance imaging showed ill-defined margins, diffusive hyperintense signals on fat-suppressed T2 weighted images (black arrow designates the lesion). **(C, D)** After one year of sirolimus treatment, the lesion shrank dramatically (black arrow designates the lesion). **(E, F)** After two years of sirolimus treatment, the lesion regressed completely.

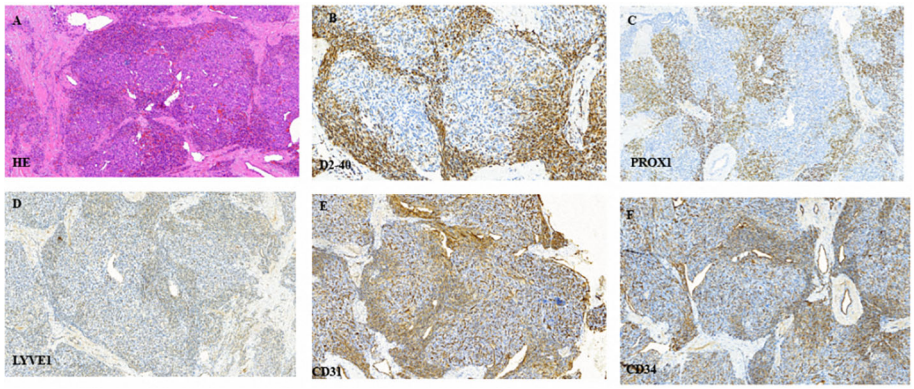

FIGURE 3
(A) Typical glomeruloid areas with spindle shaped cells following hematoxylin and eosin staining. **(B–F)** Immunohistochemical staining was positive for D2–40, PROX-1, LYVE-1, CD31 and CD34, respectively.

TABLE 1 Panel of 42 genes with mutations related to tumorigenesis and vascular diseases.

ABL1	ACVRL1	AKT1	ALK	BRAF	BRCA1	BRCA2
EGFR	ENG	EPHB4	ERBB2	FGFR2	FGFR3	FLT3
FLT4	GLMN	GNA11	GNA14	GNAQ	HRAS	IDH1
IDH2	KDR	KIT	KRAS	MAP2K1	MAP3K3	MAPK1
MAPK3	MET	mTOR	NRAS	PDGFRA	PDGFRB	PIK3CA
PTEN	RASA1	RET	SMAD4	STAMBP	TEK	TSC1

activated p110α subunit of PI3K using targeted molecules, such as BYL719 (Alpelisib) (18). They also proposed new ideas for the treatment of KHE, especially for KHE patients with PIK3CA mutations that show a poor response to existing treatment options.

In conclusion, we have presented a new PIK3CA mutation (c.685delA, p.Thr229fs) in KHE. KHE with this PIK3CA mutation may be correlated with a good response to sirolimus. However, more cases are required to validate our findings.

Data availability statement

The datasets presented in this study can be found in online repositories. The names of the repository/repositories and accession number(s) can be found in the article/Supplementary Material.

Ethics statement

Written informed consent was obtained from the patient's parents for the publication of any potentially identifiable images or data included in this article.

Author contributions

KL and ZW conceived and designed the study. ZW, HY, WY and SZ collected the clinical data and performed data analysis. SZ and YM offered the assist in data collection. ZW, HY and KL wrote the paper. KL, SZ and ZW reviewed and edited the manuscript. All authors read and approved the manuscript.

Funding

This study was sponsored by Shanghai Municipal Science and Technology Commission (21Y11912200 KL) and the Cyrus Tang Foundation, Hengjie Special Support Plan (2022 KL), Peak Climbing Program of Children's Hospital of Fudan University (EK112520180202 KL), Clinical Research Plan of SHDC (no. SHDC2020CR2009A), Shanghai Municipal Key Clinical Specialty (no. shslczdzk05703), and the Natural Science Foundation of Shanghai (22ZR1408400 ZW).

Conflict of interest

The authors declare that the research was conducted in the absence of any commercial or financial relationships that could be construed as a potential conflict of interest.

Publisher's note

All claims expressed in this article are solely those of the authors and do not necessarily represent those of their affiliated organizations, or those of the publisher, the editors and the reviewers. Any product that may be evaluated in this article, or claim that may be made by its manufacturer, is not guaranteed or endorsed by the publisher.

Supplementary material

The Supplementary Material for this article can be found online at: https://www.frontiersin.org/articles/10.3389/fonc.2023.1132702/full#supplementary-material

References

1. Ji Y, Chen S, Yang K, Xia C, Li L. Kaposiform hemangioendothelioma: current knowledge and future perspectives. *ORPHANET J RARE Dis* (2020) 15:39. doi: 10.1186/s13023-020-1320-1

2. Carli D, Kalantari S, Manicone R, Coppo P, Francia Di Celle P, La Selva R, et al. Kaposiform hemangioendothelioma further broadens the phenotype ofPIK3CA -related overgrowth spectrum. *Clin Genet* (2021) 100:624–7. doi: 10.1111/cge.14047

3. Douzgou S, Rawson M, Baselga E, Danielpour M, Faivre L, Kashanian A, et al. A standard of care for individuals withPIK3CA -related disorders: an international expert consensus statement. *Clin Genet* (2022) 101:32–47. doi: 10.1111/cge.14027

4. Wang Z, Yao W, Sun H, Dong K, Ma Y, Chen L, et al. Sirolimus therapy for kaposiform hemangioendothelioma with long-term follow-up. *J Dermatol* (2019) 46 (11):956-961. doi: 10.1111/1346-8138.15076

5. Queisser A, Seront E, Boon LM, Vikkula M. Genetic basis and therapies for vascular anomalies. *Circ Res* (2021) 129:155–73. doi: 10.1161/CIRCRESAHA.121.318145

6. Drolet BA, Trenor CR, Brandao LR, Chiu YE, Chun RH, Dasgupta R, et al. Consensus-derived practice standards plan for complicated kaposiform hemangioendothelioma. *J PEDIATR-US* (2013) 163:285–91. doi: 10.1016/j.jpeds.2013.03.080

7. Yao W, Li K, Qin Z, Li K, Zheng J, Fan X, et al. Standards of care for kasabach–Merritt phenomenon in China. *World J Pediatr* (2020) 17(2):123-130. doi: 10.1007/s12519-020-00379-9

8. Ji Y, Chen S, Zhou J, Yang K, Zhang X, Xiang B, et al. Sirolimus plus prednisolone vs sirolimus monotherapy for kaposiform hemangioendothelioma: a randomized clinical trial. *Blood* (2022) 139(11):1619-1630. doi: 10.1182/blood.2021014027

9. Yao W, Li K, Wang Z, Wang J, Ji Y, Zhou L, et al. Comparison of efficacy and safety of corticosteroid and vincristine in treating kaposiform hemangioendothelioma and tufted angioma: a multicenter prospective randomized controlled clinical trial. *J Dermatol* (2021) 48:576–84. doi: 10.1111/1346-8138.15767

10. Zhou S, Wang L, Panossian A, Anselmo DM, Wu SQ, Venkatramani R. Refractory kaposiform hemangioendothelioma associated with a chromosomal translocation t (13, 16) (q14; p13.3). *Pediatr DEVEL Pathol* (2015) 19(5):417-420. doi: 10.2350/15-09-1707-CR.1

11. Lim YH, Fraile C, Antaya RJ, Choate KA. Tufted angioma with associated kasabach-Merritt phenomenon caused by somatic mutation in GNA14. *Pediatr Dermatol* (2019) 36(6):963-964. doi: 10.1111/pde.13979

12. Hori Y, Hirose K, Aramaki-Hattori N, Suzuki S, Nakayama R, Inoue M, et al. Fibro-adipose vascular anomaly (FAVA): three case reports with an emphasis on the mammalian target of rapamycin (mTOR) pathway. *Diagn Pathol* (2020) 15:1–98. doi: 10.1186/s13000-020-01004-z

13. Hori Y, Hirose K, Ozeki M, Hata K, Motooka D, Tahara S, et al. PIK3CA mutation correlates with mTOR pathway expression but not clinical and pathological features in fibfibroipose vascular anomaly (FAVA). *Diagn Pathol* (2022) 17(1):19. doi: 10.1186/s13000-022-01199-3

14. Maruani A, Tavernier E, Boccara O, Mazereeuw-Hautier J, Leducq S, Bessis D, et al. Sirolimus (Rapamycin) for slow-flow malformations in children. *JAMA Dermatol* (2021) 157:1289. doi: 10.1001/jamadermatol.2021.3459

15. Wang Z, Zheng C, Sun H, Yao W, Li K, Ma Y, et al. Immunohistochemical analysis of mTOR pathway-related proteins in kaposiform hemangioendothelioma. *Dermatol (Basel Switzerland)* (2020) 236(3):262–70. doi: 10.1159/000503604

16. Zhou J, Li Y, Qiu T, Gong X, Yang K, Zhang X, et al. Long-term outcomes of sirolimus treatment for kaposiform hemangioendothelioma: continuing successes and ongoing challenges. *Int J Cancer* (2023). doi: 10.1002/ijc.34509

17. Venot Q, Blanc T, Rabia SH, Berteloot L, Ladraa S, Duong J, et al. Targeted therapy in patients with PIK3CA-related overgrowth syndrome. *Nature* (2018) 558:540–6. doi: 10.1038/s41586-018-0217-9

18. Pagliazzi A, Oranges T, Traficante G, Trapani C, Facchini F, Martin A, et al. PIK3CA-related overgrowth spectrum from diagnosis to targeted therapy: a case of CLOVES syndrome treated with alpelisib. *Front Pediatr* (2021) 9:732836. doi: 10.3389/fped.2021.732836

frontiers | Frontiers in Oncology

TYPE Original Research
PUBLISHED 30 October 2023
DOI 10.3389/fonc.2023.1144951

OPEN ACCESS

EDITED BY
Jing He,
Guangzhou Medical University, China

REVIEWED BY
Peiwei Chai,
Shanghai Jiao Tong University, China
Vanesa Olivares-Illana,
Autonomous University of San Luis Potosí, Mexico

*CORRESPONDENCE
Fabian D. Mairinger
Fabian.Mairinger@uk-essen.de

RECEIVED 15 January 2023
ACCEPTED 12 September 2023
PUBLISHED 30 October 2023

CITATION
Al-Ghazzawi K, Wessolly M, Dalbah S, Ketteler P, Kiefer T, Bechrakis N, Leyla J, Ting S, Biewald E and Mairinger FD (2023) PDGF, NGF, and EGF as main contributors to tumorigenesis in high-risk retinoblastoma. *Front. Oncol.* 13:1144951. doi: 10.3389/fonc.2023.1144951

PDGF, NGF, and EGF as main contributors to tumorigenesis in high-risk retinoblastoma

Karim Al-Ghazzawi[1], Michael Wessolly[2], Sami Dalbah[1], Petra Ketteler[3], Tobias Kiefer[1], Nikolaos Bechrakis[1], Jabbarli Leyla[1], Saskia Ting[4], Eva Biewald[1] and Fabian D. Mairinger[2*]

[1]Department of Ophthalmology, University Hospital Essen, Essen, Germany, [2]Department of Pathology, University Hospital Essen, University of Duisburg-Essen, Essen, Germany, [3]Department of Pediatric Hematology and Oncology, University Hospital Essen, University of Duisburg-Essen, Essen, Germany, [4]Institute of Pathology Nordhessen, Kassel, Germany

Retinoblastoma (RB) is the most common form of eye cancer experienced in childhood. Its aggressive malignancy is associated with excellent survival rates in high-income countries; however, the prognosis in third-world countries is less favorable. Early diagnosis can maximize the patient's visual outcomes and their survival rate. Therapy should be conducted in highly specialized treatment centers. Intravenous chemotherapy (IVC) in bilaterally affected children currently forms the majority of therapy. Local destructive procedures and local chemotherapies such as intra-arterial chemotherapy (IAC) or intravitreal chemotherapy can be taken into consideration depending on the extent and size of the tumor. Nonetheless, children and parents remain under constant stress, revisiting doctors for medical treatment and fearing vision loss and even enucleation of the eye. Adequate molecular patient stratification to improve targeted therapy is still lacking. This retrospective study analyzed formalin-fixed paraffin-embedded specimens from a cohort of 21 RB samples. A total of 11 of those samples showed undifferentiated retinoblastoma (URB) histopathological risk features, and the other 10 showed differentiated retinoblastoma (DRB) histopathological grading. RNA from all samples was isolated and analyzed via digital gene expression patterns. Conductors of cell survival and DNA repair were dominant in the DRB samples. In contrast, the agents responsible for cell–cycle progression and apoptosis were overexpressed in URB samples. Our work reveals the importance of molecular mechanisms within the immune system subjected to histologic subtypes of RB, providing more detailed background on their genetic behavior. This is of great interest for therapeutic strategies, such as targeted immune- and gene-based therapies, for retinoblastoma.

KEYWORDS

retinoblastoma - epigenetics, retinoblastoma, PDGF = platelet-derived growth factor, MAPK/ERK2 pathway 1, pediatric cancer and oncology, biomarkers, targeted therapy, growth factors (angiogenesis factors)

1 Introduction

Retinoblastoma (RB) is the most common primary intraocular malignancy in children. It has an incidence rate of 1 in 14,000–20,000 live births and has no gender predilections. From a genetic point of view, RB mainly presents in two distinct clinical forms: the non-heritable form (majority), in which the tumors are unifocal and unilateral, usually presenting at an older age, and the heritable form (minority), usually presenting as multifocal, bilateral lesions at an early age. Although a well-known RB therapy paradigm is survival over vision preservation, increasingly multimodal and interdisciplinary therapies have been developed that target the tumor in its local environment before drastic options such as enucleation of the diseased eye must be considered. For many children, especially those with an unilaterally progressing disease, enucleation is the only reasonable rescue treatment option. Patients are usually assessed in accordance with the International Classification of Retinoblastoma (ICRB), allowing consensus regarding therapy, optimally preserving diseased eyes, and maximizing visual acuity (1). Through early diagnosis, the survival rates of affected children remain high in first-world countries. Late diagnosis is likely to be tied to metastatic spread and therefore associated with high morbidity and mortality, and it is a major problem in developing countries (2). Advancing therapies such as immune checkpoint inhibitors and oncogene-targeted drugs improve the management of various cancers such as melanoma, lung adenocarcinoma, squamous cell carcinoma, colon cancer, bladder cancer, and gastric cancer (3). Effective targeted therapy would be a promising new therapy approach and potentially could preserve visual acuity in some RB cases. To date, there are neither effective nor recognized targeted therapies for the treatment of RB reported in the current literature. Comparing anaplastic differentially graded RBs on a molecular level, undifferentiated retinoblastoma's (URB's) pathophysiology contributing factors to tumorigenesis can be explained. Research in the field of molecular biology remains challenging but is still very much needed for future advances in targeted therapies and molecular biomarkers, especially in RB research.

2 Material and methods

2.1 Sample population

Our study cohort consisted out of 21 enucleated retinoblastoma patients, divided into two subgroups. The subgroup was selected upon histopathological grading of anaplasia in these samples. In addition, there were two controls (non-tumorous tissue).

2.2 RNA extraction

One to three paraffin sections with a thickness of 7 µm per sample were deparaffinized with xylene prior to RNA extraction using the RNeasy FFPE kit (Qiagen, Hilden, Germany) in accordance with the manufacturer's recommendations, albeit with slight adjustments. Total RNA concentrations were measured using a Nanodrop 1000 instrument (Thermo Fisher Scientific, Waltham, USA) (4).

2.3 nCounter CodeSet Design and Expression Analysis

Multiple genes involved in tumor- and inflammation-associated pathways were selected based on the current literature to screen for potential biological cues that could significantly differentiate RBs from the other lesions and also provide pathophysiological insights into these entities.

Gene expression patterns were screened for prognostic and predictive biomarkers using the NanoString's nCounter digital gene expression analysis platform with its PanCancer Profiling panel, consisting of 770 genes and 30 reference genes. Hybridizations were performed using the high-sensitivity protocol on the nCounter Prep Station. Post-hybridization processing was performed using the nCounter MAX/FLEX System (NanoString), and the cartridge was scanned on the Digital Analyzer (NanoString). The cartridge was read with maximum sensitivity (555 FOV). A 100-ng sample was used as the input for each reaction.

2.4 NanoString data processing

NanoString data processing was carried out using the R i386 statistical programming environment (v4.0.3). Considering the counts obtained for the positive control probe sets, the raw NanoString counts for each gene were subjected to a technical factorial normalization, carried out by subtracting the mean count plus two times the standard deviation from the CodeSet inherent negative controls. Subsequently, biological normalization using the included RNA reference genes was performed. In addition, all counts with $p>0.05$ after a one-sided t-test versus negative controls plus two times the standard deviation were interpreted as not sufficiently expressed to overcome basal noise (5).

2.5 Statistical evaluation

Statistical analyses were carried out using the R i386 statistical programming environment (v4.0.2). Prior to exploratory data analysis, the Shapiro–Wilk test was applied to test for the normal distribution of each data set for ordinal and metric variables. The resulting dichotomous variables underwent either the Wilcoxon Mann–Whitney rank sum test (non-parametric) or the two-sided Student's t-test (parametric). For the comparison of ordinal variables and factors with more than two groups, either the Kruskal–Wallis test (non-parametric) or an analysis of variance (ANOVA) (parametric) was used to detect group differences. Double dichotomous contingency tables were analyzed using Fisher's exact test. To test the dependency of ranked parameters with more than two groups, Pearson's chi-squared test was used. Correlations between metrics were tested by applying Spearman's rank correlation test and Pearson's product–moment correlation testing for linearity. A basic quality control of the

processed data was performed by mean versus variance plotting to find outliers in the target or sample levels. True differences were calculated by a correlation matrix analysis. To further specify the different candidate patterns, both unsupervised and supervised clustering, in addition to principal component analysis, were performed to overcome commonalities and differences. The sensitivity and specificity of markers were determined from receiver operating characteristic (ROC) curves, illustrating their ability to discriminate between the studied groups. The bootstrap procedure (1,000 iterations) was used for internal validation of the estimates in the ROC analyses. The best candidate genes were selected and binarized (0, 1; with 1 equaling a better chance of an event) by their respective cut-offs and finally summarized. The resulting scores were compared with respect to sensitivity and specificity. The probability for each entity was determined using the non-linear (weighted) least-squares estimates of the parameters of a non-linear fitted regression model (6, 7). Adaptations of profiles for diagnostic purposes were modeled with a supervised machine learning tool, conditional inference trees (CTrees), as implemented in the "party" library of R (8) using leave-one-out cross-validation. CTrees are a non-parametric class of regression trees leading to a non-parametric class of tree-structured regression models embedding a conditional inference procedure, applicable to all kinds of regression problems, such as nominal, ordinal, numeric, and censored, in addition to multivariate response variables and arbitrary measurement scales of the covariate (8). Owing to the multiple statistical tests, the p-values were adjusted by using the false discovery rate (FDR). The level of statistical significance was defined as $p \leq 0.05$ after adjustment.

3 Results

3.1 Study population

The mean age of the 21 patients was 1.7 years, and 10 patients (47.6%) were female. The median age at diagnosis was 14 months (range: 2–50 months). Additional clinical characteristics are included in Table 1 and Supplementary Data 1. We analyzed biopsy specimens from 21 RB patients, and these were divided into two subgroups: 11 URBs (Figure 1) and 10 differentiated retinoblastomas (DRBs) (Figure 2)

3.2 Anaplastic grade

The degree of differentiation in RB tumors was mostly defined by the development of fleurettes and rosettes. Samples were graded accordingly by a pathologist.

3.3 Expression analysis

Gene expression analysis was successful in all samples: 21RB samples and two control samples. After biological and technical normalization, 726 (94.3%) out of 770 genes were identified as transcripts with relevant gene expressions. We compared the transcriptomes of the two subtypes: 166 (22.9%) genes were found to be differentially expressed between subtypes (Figure 3), with an adjusted p-value of <0.05.

3.4 Gene set enrichment analysis

To identify biological mechanisms (pathways and biological functions) affected by the different expression patterns of immune genes in URB and DRB, a gene set enrichment analysis (GSEA) was performed.

3.5 Mitogen-activated protein kinase signaling pathway

The following main conductors for the classical mitogen-activated protein-kinase (MAP-K) pathway were elevated in the URB samples: nerve growth factor (NGF), neutrophin 3/4 (NT3/4) (9), epidermal growth factor (EGF), and platelet-derived growth factor (PDGF) and its downstream ligand platelet-derived growth factor receptor (PDGFR). Throughout the pathway, RAS, MEKK1 (10), FASL (11), and P53 were also elevated in these samples, all of which contribute to apoptosis.

3.6 The PI3K/AKT/mTOR signaling pathway

The main conductors to the activation of the Pi3K-Akt signaling pathway, GF, and extracellular matrix (ECM), were elevated in the DRB samples. Also, ECM's downstream ligands ITG-A and B, together with the common pathway PI3K, were elevated in these samples. Most ligands responsible for cell survival and DNA repair—Bcl-xL, Bcl-2, and MEK—were also elevated in the DRB samples, whereas ligands mostly responsible for cell cycle progression coming from the PI3K-Akt signaling pathway—CDK, Cyclin, and Myc—were elevated in the URB samples.

3.7 Cell-cycle progression and inhibition

URBs showed an upregulation of P300, P53, CyD, CDK4,6, and E2F1,2,3 when compared with DRBs, thereby contributing to cell-cycle progression in this configuration (Figure 4). Healthy cells experiencing oncogenic "stress" use the P53 pathway to exit the cell cycle and induce apoptosis; physiologically, it induces cell-cycle arrest to create time for DNA repair to restore genome stability. One hallmark of cancer is the evasion of apoptosis; achieving this continues proliferation, which can be achieved through P53 mutation and inactivation. DRBs showed upregulation in transforming growth factor-β (TGF-β) and SMADs2,3, together with their downstream ligands P15 and P19.

10.3389/fonc.2023.1144951

TABLE 1 Clinical characteristics of patients stratified by molecular subtype.

Characteristics	URBs	DRBs	*p*-value	Statistical test
Patients, *n* (%)	11 (52)	10 (48)		
Sex, *n* (%)				
Women	2(25)	6(75)	0.04	Chi-square
Men	9 (70)	4(30)		
Laterality, *n* (%)				
Unilateral	5(45)	6(55)	0.5051	Chi-square
Bilateral	6 (60)	4 (40)		
Age at diagnosis (months)				
Median (range)	14 (4–50)	10.5 (2–45)	0.436	Mann–Whitney test
<18, *n*	8	6	0.2	Kruskal–Wallis test
18–36, *n*	1	2		
>36, *n*	2	2		
Tumor stage:N*, *n*				
N0	3	4	0.06	Kruskal–Wallis test
N1	6	6		
N2	2	0		
C*, *n*				
C0	7	7	0.2	Kruskal–Wallis test
C1	2	2		
C2	2	1		
RB1 germline mutation, *n* (%)				
Yes	6 (75%)	2(25%)	0.1827	Fisher's exact test
No	5 (38.46%)	8 (61.54%)		

*The TNM classification for retinoblastoma, which is developed by the American Joint Committee on Cancer (AJCC).

4 Discussion

Current understandings of disease initiation in both hereditary and sporadic forms of RB tumors are linked to a loss of function in the RB gene (RB1) (12). Mutations leading to the aberrant function of the RB tumor suppressor protein (pRB) have been found not only in retinoblastoma cancer and cell lines but also in various other tumors, such as osteosarcoma, adenocarcinoma, small cell lung

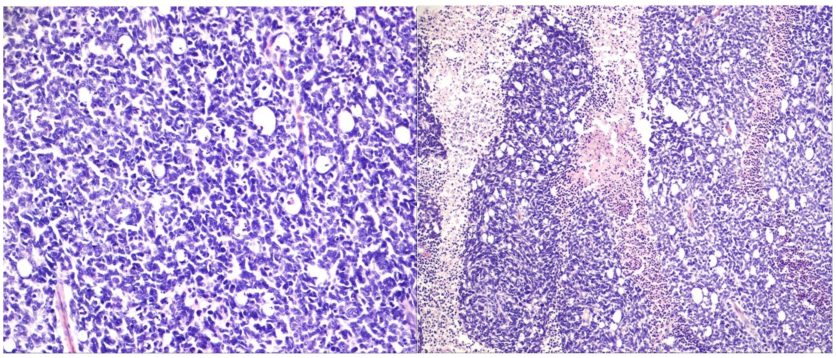

FIGURE 1
Undifferentiated retinoblastoma with proposed high-risk features. Left: histologic evaluation shows small tumor cells with scant cytoplasm and condensed chromatin; right: prominent necrosis. (Hematoxylin and eosin staining: left, 20×; right, 10×).

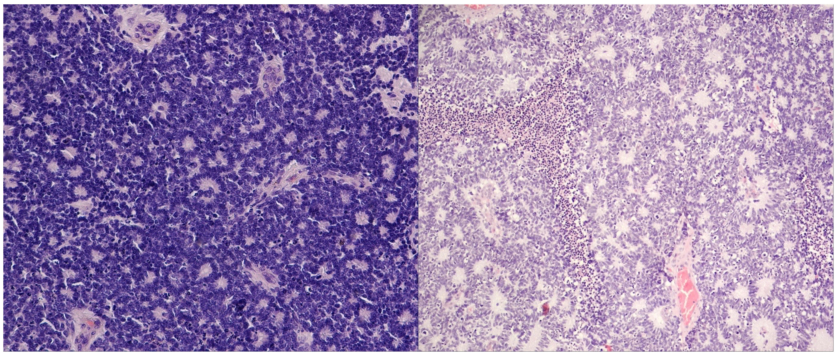

FIGURE 2
Differentiated retinoblastoma. Left: photoreceptor differentiation (Flexner–Wintersteiner and Homer Wright rosettes); right: enlargement of nuclei similar in size to moderate anaplasia, pleomorphism (angular, rhomboid, or fusiform), cell wrapping, numerous mitotic figures, and necrosis (hematoxylin and eosin staining: left, 40×; right, 10×).

cancer, breast cancer, and prostate cancer (13). In this study, we examined differentiated and undifferentiated RB samples. The degree of differentiation in RB is determined by the development of rosettes and fleurettes. Mendoza et al. examined clinical and pathologic findings in patients who underwent primary enucleation for RB. The study assessed the grade of anaplasia and differentiation regarding the presence or absence of high-risk features (14). What is debatable is whether or not prognosis in RB is concluded from differentiation, as studies have shown conflicting results (15, 16). Poorly differentiated tumors have been associated with high-risk features, especially massive choroidal invasion (17). As genetic profiling studies of RBs keep increasing (18–20), four studies based on gene expression profiling delivered partially conflicting results regarding RB subtypes (19, 21, 22). The aims of this study included differentiating RB on a molecular level by focusing on possible docking points for targeted therapies.

4.1 Pi3Akt and MAPK signaling pathways in retinoblastoma

This study examined different agents that regulate cell-cycle progression, inhibition, and apoptosis through pathways such as MAPK signaling (Figure 5), Pi3Akt signaling (Figure 6), and general cell-cycle control (Figure 7). On a molecular level, cell-cycle inhibition and progression are regulated by different pathways, such as MAPK signaling and Pi3Akt signaling. Both pathways are very complex, with interconnected signaling cascades, and are still not fully understood. Physiologically, both pathways are initiated by extracellular and intracellular stimuli in the form of proteins functioning as cytokines and binding other factors to form kinases, leading to regulated activation and inhibition. In a simplified scheme, the result of activating the MAPK pathway is increased cellular proliferation, whereas activating the PI3K

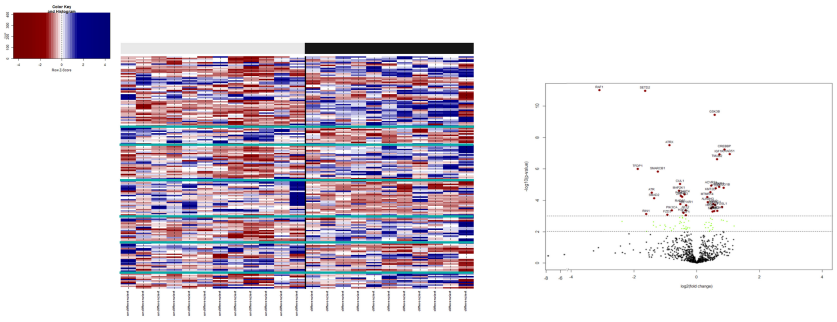

FIGURE 3
3.1: Heatmap: on the bottom x-axis, each investigated patient with its entity identifier is depicted. The upper x-axis shows the binary clusters of the entity groups with respect to their histopathological stratification. The virtual y-axis depicts 770 differentially expressed RNA targets. The color key on the left indicates the expression ratio, in which highly expressed genes are indicated in blue and poorly expressed genes in red. 3.2: Volcano plot illustrating the differential gene expression between URB and DRB. A total of 166 out of 770 differentially expressed genes with an adjusted *p*-value of < (0.05) are shown. In total, 38 genes (41.8%) show expression only or in a much stronger manner in DRB (left side), whereas 53 (58.2%) genes present with overexpression in URBs (right side). Red dots indicate a highly significant association and green dots indicate a significant association identified by explorative data analysis using either the Wilcoxon Mann–Whitney rank sum test (non-parametric) or the two-sided Student's *t*-test (parametric).

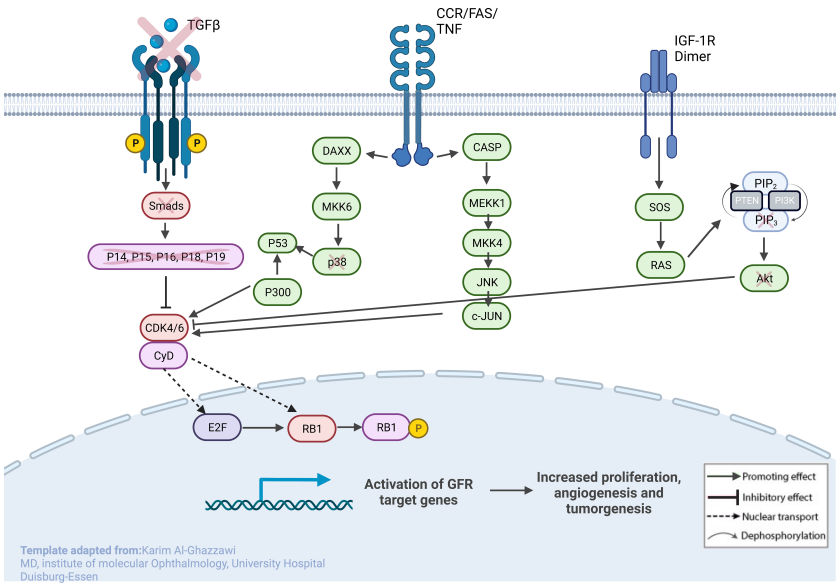

FIGURE 4
Sketch of the investigated genes that correlate with explicit molecules that contribute to tumorigenesis in RB, leading to predominant undifferentiated phenotypes. From left to right: (1) loss of TGF-β and SMADs in URB samples, leading to the missing inhibitory effects of p16, p15, p18, and p19 on CycD and CDK4,6; (2) CCR/FAS/tumor necrosis factor (TNF) receptor with main conductors CASP and DAXX being overexpressed in URBs; and (3) IGF-1R with downstream ligands SOS and RAS being overexpressed in URB samples. Together, this will ultimately lead to proliferative signals in the nucleus with invasiveness, prominent angiogenesis, and tumorigenesis.

pathway stimulates protein synthesis and inhibits apoptosis (23, 24). In a previously published study by Liu et al., a similar analysis of RB samples was performed; however, they chose to approach the problem distinctly (19). A high-risk retinal subtype was defined, converging with recurring genetic alliterations and less histopathologically identifiable differentiation. We therefore see a validation of our study results. We observed an increased signal for activators of the classical non-canonical MAP-Kinase pathway, NGF, NT3/4, EG, F, and PDGF, in the URB samples.

The Pi3K Akt signaling pathway (phosphatase and tensin homolog) subsequently dephosphorylates PIP3 to PIP2, an event that is a key element in regulating the pathway (24). Also, the URB samples showed activation for this enzyme. PIP2 is therefore more likely to be present in the cytoplasm, leading to the decreased catalytic activity of AKT, together with the effector ligands Bcl-xL and Bcl-2, causing cell progression instead of apoptosis (25, 26). Although GSK-3b and even p21 showed higher base expression levels in the URB group than in the DRB group, we considered this to be a feedback loop-like response, and this did not indicate the inhibition of the pathway. This undermined the stronger expression of CDK4/6 in addition to CDK2 overexpression and E2F activation; moreover, the loss of TGF-b and the SMAD-based induction of apoptosis and cell cycle stasis did not support this finding. One of the most altered pathways in cancer morphologies (27), the "RTK-RAS pathway", which cross-talks within the MAPK and the Pi3k-Akt signaling pathways (28, 29), showed significant differences when comparing both cohorts. URBs showed overexpression for SOS and RAS; in comparison, DRBs had elevated PI3K signals.

4.2 TGF-β

TGF-β signaling is one of the impaired pathways in RB. In the early stages of cancer, TGF-β inhibits cell-cycle progression and promotes apoptosis by exhibiting tumor-suppressive effects. However, in the late stages, TGF-β exerts tumor-promoting effects, increasing tumor invasiveness and metastasis. Physiologically, TGF-β acts as a tumor suppressor through the inactivation of TGF-β receptors and SMADs. The downregulation of receptors and increased expression of TGF-β signaling inhibitors have been reported in human cancers (30). URB samples showed significantly decreased levels of both TGF-β and its downstream ligands, SMAD 2, and 3, when compared with DRBs. Ultimately, the missing inhibitory effects of p16, p15, p18, and p19 on CycD and CDK4,6 in URBs will lead to proliferative signals in the nucleus (Figure 4). Several therapeutic tools such as TGF-β antibodies, have been tested for their anti-tumor effects. Antisense oligonucleotides and small inhibitor molecules of TGF-β receptor-1 (TGF-βR1) have shown potential inhibitory effects on TGF-β signaling (31).

4.3 E2F

In healthy cells, RB suppresses transcription by binding to the chromatin-remodeling proteins BRG and histone deacetylases (HDACs). Furthermore, it regulates the transition from the G1 to the S phase of the cell cycle by binding to the E2F family of transcription factors. In RB cells, dysfunction of the RB protein

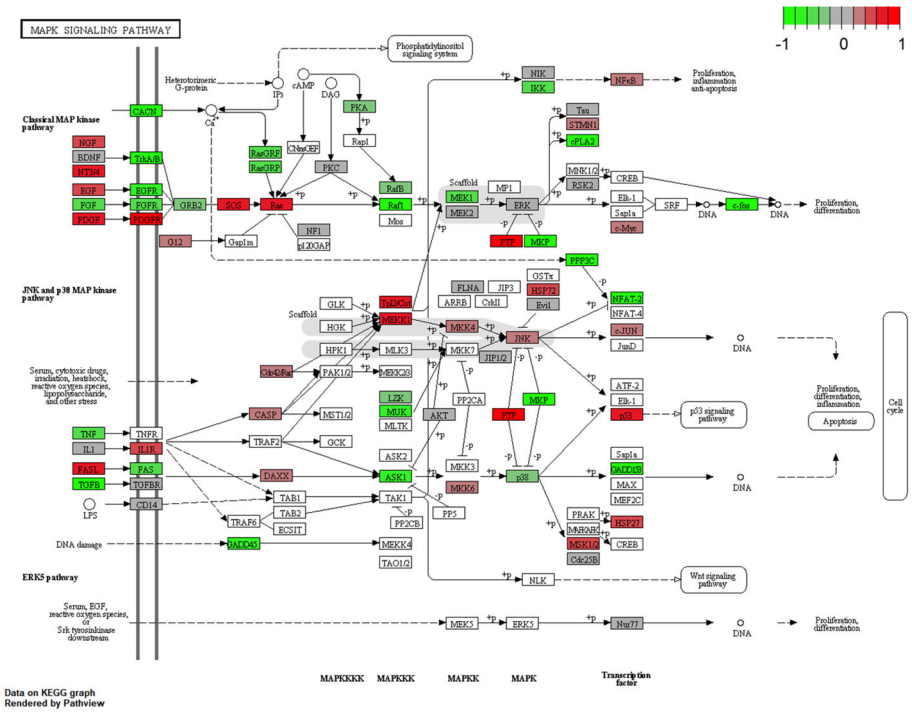

FIGURE 5
Expression of different pathways involved in the MAP-K signaling pathway. Pathways marked in red were overexpressed (1), and green pathways were downregulated (−1) when comparing URBs with DRBs. The main conductors for the classical MAP-K pathway, NGF, NT3/4, EGF, and PDGF, and its downstream ligand, PDGFR, were elevated in the URB samples.

leads to the constant activity of the E2F transcription domains. The cell cycle is therefore more likely to halt during the late G1/early S phase transition, leading to a continuous instigation of the cell cycle and tumor growth (32, 33). A recent study proposed that E2F is part of the E2F1/CKS2/PTEN signaling axis as a key regulator of malignant phenotypes in RB (34). We hypothesized that this tumor growth is accelerated and mediated by a constant loop-like transcription or translation regulation of effector genes of the growth factor family: NGF, NT3/4, EGF, and PDGF.

4.4 RB protein

RB* is a tumor-suppressor gene in Retinoblastoma and in many other cancers as well. Periodic phosphorylation of the RB protein makes cell division cycles possible. Studies have detected activated (hypophosphorylated) forms of the protein in G1, which inactivates (hyperphosphorylates) in late G1 and remains in this state throughout the S phase through mitosis. The RB protein acts as a tumor suppressor in the hypophosphorylated (active) state by restricting proliferation (35, 36). Cyclin-dependent kinases 4 and 6 (CDK4 and CDK6) play key roles in cell proliferation, in which they help to drive the progression of cells into the S phase of the cell cycle (37). In various cell models, it has already been shown that CDK4 and CDK6 are fundamental drivers of the cell cycle and are required for the initiation and progression of various malignancies (38).

The PTEN mutational status is known to be a crucial regulator and progressor in RB carcinogenesis. It induces various feedback loops, resulting in strong overexpression of the impaired catalytic protein activity. Moreover, clinically, the PTEN mutational status affects the response to combined therapy based on MEK and mTOR inhibitors in cancer (39); this should be taken into consideration when looking at individualized RB therapies in the future.

Circulating chemokines such as tumor necrosis factor (TNF) and interleukin (IL)-1 can influence the surrounding tumor tissue. For example, TNFs probably represent a danger signal in response to neoplastic tissue damage to rid the organism of premalignant tissue or to promote wound healing (40). A possible relationship between TNF-α overexpression and RB malignancy has been previously discussed by Pellestor et al. (41). The JNK signaling pathway, derived from MEKK/MKK signaling, is a possible target for these stimuli (42), forming appropriate cellular responses in the form of proliferation, differentiation, and apoptosis. The pathway has been described as being active for both apoptosis and differentiation, depending on the conditions (43). It has been described as being activated by environmental oxidative stress and inflammatory stimuli (44). JNK and its downstream cascade, c-JUN, were consistent in the URB samples. Transcriptional effectors of this cascade can modify nuclear DNA with proliferative signals in tumor cells (45). The molecular characterization of RB patient samples is currently being performed on tumor samples obtained from enucleation. The analysis of RB using liquid biopsy (46) could provide a more comprehensive picture of the

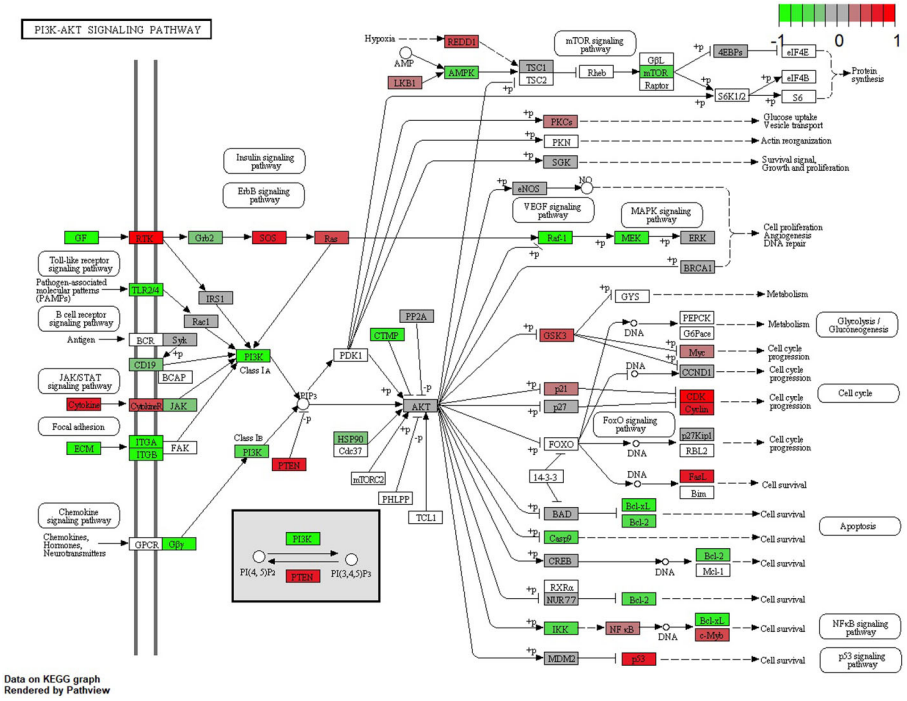

FIGURE 6
Expression of different pathways involved in the PI3K-AKT signaling pathway. Pathways marked in red were overexpressed (1) and green pathways were downregulated (–1) when comparing URBs with DRBs. The main conductors to the activation of the Pi3K-Akt signaling pathway, GF and ECM, were elevated in the DRB samples. In addition, ECM downstream ligands ITG-A and B, together with the common pathway PI3K, were elevated in these samples.

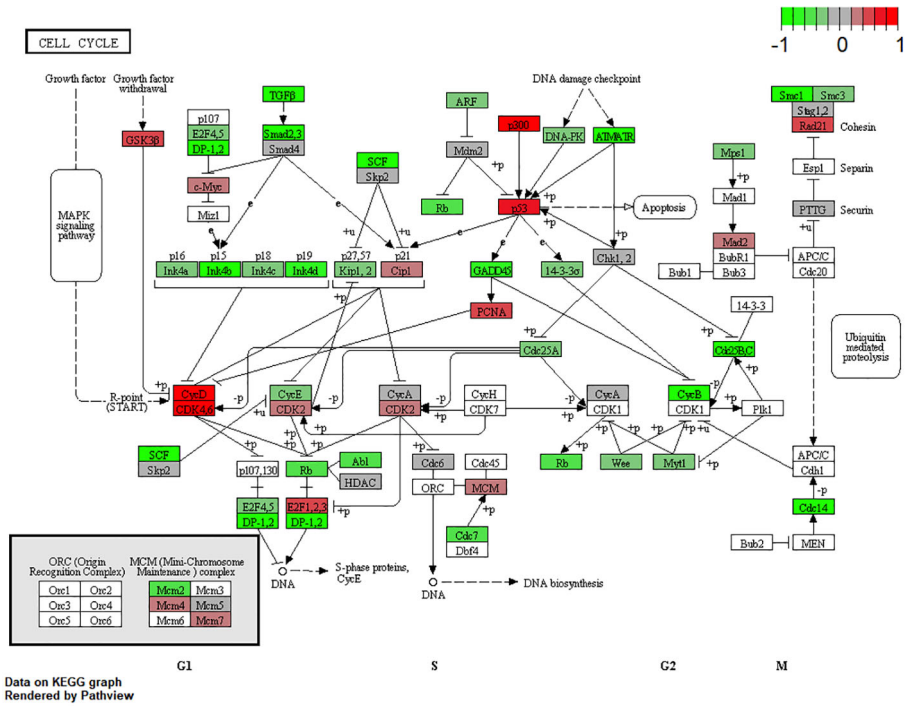

FIGURE 7
Expression of different pathways involved in the cell-cycle signaling pathway. Pathways marked in red were overexpressed (1), and green pathways were downregulated (–1) when comparing URBs with DRBs. URBs showed an upregulation of P300, P53, CyD, CDK4,6, and E2F1,2,3 when compared with DRBs. DRBs showed an upregulation of TGF-β and SMADs2,3, together with their downstream ligands P15 and P19.

disease. Cell-free DNA aliquots from blood samples could potentially be used to optimize RB treatment and prognosis.

The limitations of this study include the absence of non-tumoral retinal control samples. The harvesting of a non-tumoral healthy retina as a control is challenging, as there is no medical incentive to retrieve healthy retinal tissue from comparable patients. The use of detached retinal tissues from vitrectomies combined with retinectomies could be an option as a control; however, even this retinal tissue may show alterations due to the underlying disease and may not resemble a healthy retina. Another limitation is the unknown mutational status. To overcome this limitation, a thorough literature review was commenced. The gene panel used, with over 800 targets, is limited in size; however, the screened genes are part of the most important expression targets leading to carcinogenesis. A whole-transcriptome evaluation could investigate many more targets; however, it could also draw attention to faulty side players. With our current approach, we are therefore dealing with less background noise and taking only prominent trails into consideration. Based on regulatory feedback loops leading to increased expressions of affected tumor-suppression genes in our study, together with a detailed literature review, we have found supporting arguments for our hypothesis. In this study, we observed possible molecular targets through an expression analysis. Discriminative markers should also be examined in a traditional format to identify underlying relevant proteins, as changes may be transient, post-translational, and/or in non-target organs. Contributing genes to pathogenesis could be examined in a knock-down study to distinguish the cause and effect of specific genes. Despite obvious limitations such as low case numbers and limited transcriptomic cutouts, we are highly convinced of our general results and hypothesis, as the overall observed results support our hypothesis regardless of the complexity of further pathways and molecular mechanisms. Through the observed clinical behavior regarding outcome (metastasis and survival) and the biological risk features that resulted in the phenotypical expression of malignant transformation, we clearly see evidence for our proposed hypothesis.

5 Conclusion

From a biological point of view, there is a remarkable difference between both entities examined: the examined tissues showed various differences regarding key cancer regulatory pathways. The presence of growth factors through activators of the classical non-canonical MAP-Kinase pathway, NGF, NT3/4, EGF, and PDGF, was significant in URB samples when compared with DRBs. In contrast, DRBs were consistent with activators of the Pi3k-AKT signaling pathway altogether with DNA-repair mechanisms contributing to the cell cycle progression instead of the apoptotic conductors in URB samples. We are not sure where the loop-like induction of these pathways begins, but we are certain that it has regulatory effects on cancer formation and progression. The identification of molecular markers pointing to high-risk features should redefine further studies of this cancer, to include the identification of more specific treatments and improvements in diagnosis and prognosis.

Data availability statement

The original contributions presented in the study are included in the article/Supplementary Materials. Further inquiries can be directed to the corresponding author/s.

Ethics statement

The studies involving humans were approved by the Ethics Commission of the University of Essen. The studies were conducted in accordance with the local legislation and institutional requirements. The participants provided their written informed consent to participate in this study.

Author contributions

Conceptualization, FM, ST; methodology, MW, KA-G, and FM; software, FM, MW; validation, KA-G, and FM; formal analysis, EB, KA-G, and FM; investigation, KA-G, PK, JL, EB, and FM; resources, KA-G, SD, TK, JL, ST, EB, MW, NB and FM; data curation, FM, and KA-G; writing—original draft preparation, FM, KA; writing—review and editing, EB, KA-G, NB, FM, TK, JL,SD, ST, PK, and MW; visualization, FM, ST, KA-G; supervision, FM, PK, ST, project administration, MW, TK, SD, KA-G FM;NB funding acquisition, FM. All authors have read and agreed to the published version of the manuscript.

Conflict of interest

The authors declare that the research was conducted in the absence of any commercial or financial relationships that could be construed as a potential conflict of interest.

Publisher's note

Supplementary material

The Supplementary Material for this article can be found online at: https://www.frontiersin.org/articles/10.3389/fonc.2023.1144951/full#supplementary-material

References

1. Bornfeld N, Lohmann D, Bechrakis NE, Biewald E. [Retinoblastoma]. *Ophthalmologe* (2020) 117(4):389–402. doi: 10.1007/s00347-020-01081-x

2. G Global Retinoblastoma Study, Fabian ID, Abdallah E, Abdullahi SU, Abdulqader RA, Boubacar Adamou S, et al. Global retinoblastoma presentation and analysis by national income level. *JAMA Oncol* (2020) 6(5):685–95. doi: 10.1001/jamaoncol.2019.6716

3. Colli LM, Machiela MJ, Zhang H, Myers T.A, Jessop L, Delattre O, et al. Landscape of combination immunotherapy and targeted therapy to improve cancer management. *Cancer Res* (2017) 77(13):3666–71. doi: 10.1158/0008-5472.CAN-16-3338

4. Walter RFH, Werner R, Vollbrecht C, Hager T, Flom E, Christoph DC, et al. ACTB, CDKN1B, GAPDH, GRB2, RHOA and SDCBP Were Identified as Reference Genes in Neuroendocrine Lung Cancer via the nCounter Technology. *PloS One* (2016) 11(11). doi: 10.1371/journal.pone.0165181

5. Mairinger F, Bankfalvi A, Schmid KW, Mairinger E, Mach P, Walter RF, et al. Digital immune-related gene expression signatures in high-grade serous ovarian carcinoma: developing prediction models for platinum response. *Cancer Manag Res* (2019) 11:9571–83. doi: 10.2147/CMAR.S219872

6. Bates D, Watts DG. *Nonlinear Regression Analysis and Its Applications*. (1988). doi: 10.1002/9780470316757

7. Nonlinear Models and Regression. In: *Pharmacokinetic-Pharmacodynamic Modeling and Simulation*. Boston, MA: Springer US. p. 93–124.

8. Hothorn T, Hornik K, Zeileis A. Unbiased recursive partitioning: A conditional inference framework. *J Comput Graphical Stat* (2006) 15(3):651–74. doi: 10.1198/106186006X133933

9. Reichardt LF. Neurotrophin-regulated signalling pathways. *Philos Trans R Soc Lond B Biol Sci* (2006) 361(1473):1545–64. doi: 10.1098/rstb.2006.1894

10. Boldt S, Weidle UH, Kolch W. The kinase domain of MEKK1 induces apoptosis by dysregulation of MAP kinase pathways. *Exp Cell Res* (2003) 283(1):80–90. doi: 10.1016/S0014-4827(02)00018-6

11. Ju ST, Matsui K, Ozdemirli M. Molecular and cellular mechanisms regulating T and B cell apoptosis through Fas/FasL interaction. *Int Rev Immunol* (1999) 18(5-6):485–513. doi: 10.3109/08830189909088495

12. Guzman F, Fazeli Y, Khuu M, Salcido K, Singh S, Benavente CA. Retinoblastoma tumor suppressor protein roles in epigenetic regulation. *Cancers (Basel)* (2020) 12(10). doi: 10.3390/cancers12102807

13. Harbour JW, Dean DC. The Rb/E2F pathway: expanding roles and emerging paradigms. *Genes Dev* (2000) 14(19):2393–409. doi: 10.1101/gad.813200

14. Mendoza PR, Specht CS, Hubbard G.B, Wells JR, Lynn MJ, Zhang Q, et al. Histopathologic grading of anaplasia in retinoblastoma. *Am J Ophthalmol* (2015) 159(4):764–76. doi: 10.1016/j.ajo.2014.12.014

15. Ts'O MOM, Zimmerman LE, Fine BS. The nature of retinoblastoma. I. Photoreceptor differentiation: A clinical and histopathologic study. *Am J Ophthalmol* (1970) 69(3):339–49. doi: 10.1016/0002-9394(70)92263-4

16. Bogenmann E, Mark C. Routine growth and differentiation of primary retinoblastoma cells in culture. *J Natl Cancer Inst* (1983) 70(1):95–104.

17. Kashyap S, Meel R, Pushker N, Sen S, Bakhshi S, Sreenivas V, et al. Clinical predictors of high risk histopathology in retinoblastoma. *Pediatr Blood Cancer* (2012) 58(3):356–61. doi: 10.1002/pbc.23239

18. Sarver AL, Xie C, Riddle MJ, Forster CL, Wang X, Lu H, et al. Retinoblastoma tumor cell proliferation is negatively associated with an immune gene expression signature and increased immune cells. *Lab Invest* (2021) 101(6):701–18. doi: 10.1038/s41374-021-00573-x

19. Liu J, Ottaviani D, Sefta M, Desbrousses C, Chapeaublanc E, Aschero R, et al. A high-risk retinoblastoma subtype with stemness features, dedifferentiated cone states and neuronal/ganglion cell gene expression. *Nat Commun* (2021) 12(1):5578. doi: 10.1038/s41467-021-25792-0

20. Gudiseva HV, Berry JL, Polski A, Tummina SJ, O'Brien JM. Next-generation technologies and strategies for the management of retinoblastoma. *Genes (Basel)* (2019) 10(12). doi: 10.3390/genes10121032

21. Kooi IE, Mol BM, Moll AC, van der Valk P, de Jong MC, de Graaf P, et al. Loss of photoreceptorness and gain of genomic alterations in retinoblastoma reveal tumor progression. *EBioMedicine* (2015) 2(7):660–70. doi: 10.1016/j.ebiom.2015.06.022

22. McEvoy J, Flores-Otero J, Zhang J, Nemeth K, Brennan R, Bradley C, et al. Coexpression of normally incompatible developmental pathways in retinoblastoma genesis. *Cancer Cell* (2011) 20(2):260–75. doi: 10.1016/j.ccr.2011.07.005

23. Cargnello M, Roux PP. Activation and function of the MAPKs and their substrates, the MAPK-activated protein kinases. *Microbiol Mol Biol Rev* (2011) 75(1):50–83. doi: 10.1128/MMBR.00031-10

24. Braicu C, Buse M, Busuioc C, Drula R, Gulei D, Raduly L, et al. A comprehensive review on MAPK: A promising therapeutic target in cancer. *Cancers (Basel)* (2019) 11(10). doi: 10.3390/cancers11101618

25. Leslie NR. PTEN: an intercellular peacekeeper? *Sci Signal* (2012) 5(250):pe50. doi: 10.1126/scisignal.2003685

26. Bousova K, Jirku M, Bumba L, Bednarova L, Sulc M, Franek M, et al. PIP2 and PIP3 interact with N-terminus region of TRPM4 channel. *Biophys Chem* (2015) 205:24–32. doi: 10.1016/j.bpc.2015.06.004

27. Sanchez-Vega F, Mina M, Armenia J, Chatila WK, Luna A, La KC, et al. Oncogenic signaling pathways in the cancer genome atlas. *Cell* (2018) 173(2):321–337 e10. doi: 10.1016/j.cell.2018.03.035

28. Mendoza MC, Er EE, Blenis J. The Ras-ERK and PI3K-mTOR pathways: cross-talk and compensation. *Trends Biochem Sci* (2011) 36(6):320–8. doi: 10.1016/j.tibs.2011.03.006

29. Unni AM, Lockwood WW, Zejnullahu K, Lee-Lin SQ, Varmus H. Evidence that synthetic lethality underlies the mutual exclusivity of oncogenic KRAS and EGFR mutations in lung adenocarcinoma. *Elife* (2015) 4:e06907. doi: 10.7554/eLife.06907.015

30. Nagaraj NS, Datta PK. Targeting the transforming growth factor-beta signaling pathway in human cancer. *Expert Opin Investig Drugs* (2010) 19(1):77–91. doi: 10.1517/13543780903382609

31. Principe DR, Doll JA, Bauer J, Jung B, Munshi HG, Bartholin L, et al. TGF-beta: duality of function between tumor prevention and carcinogenesis. *J Natl Cancer Inst* (2014) 106(2):djt369. doi: 10.1093/jnci/djt369

32. Lee JO, Russo AA, Pavletich NP. Structure of the retinoblastoma tumour-suppressor pocket domain bound to a peptide from HPV E7. *Nature* (1998) 391(6670):859–65. doi: 10.1038/36038

33. Mendoza PR, Grossniklaus HE. The biology of retinoblastoma. *Prog Mol Biol Transl Sci* (2015) 134:503–16. doi: 10.1016/bs.pmbts.2015.06.012

34. Chen M, Zhao Z, Wu L, Huang J, Yu P, Qian J, et al. E2F1/CKS2/PTEN signaling axis regulates Malignant phenotypes in pediatric retinoblastoma. *Cell Death Dis* (2022) 13(9):784. doi: 10.1038/s41419-022-05222-9

35. Ludlow JW, DeCaprio JA, Huang CM, Lee WH, Paucha E, Livingston DM. SV40 large T antigen binds preferentially to an underphosphorylated member of the retinoblastoma susceptibility gene product family. *Cell* (1989) 56(1):57–65. doi: 10.1016/0092-8674(89)90983-5

36. Weinberg RA. The retinoblastoma protein and cell cycle control. *Cell* (1995) 81(3):323–30. doi: 10.1016/0092-8674(95)90385-2

37. Sherr CJ, Beach D, Shapiro GI. Targeting CDK4 and CDK6: from discovery to therapy. *Cancer Discovery* (2016) 6(4):353–67. doi: 10.1158/2159-8290.CD-15-0894

38. Goel S, DeCristo MJ, Watt AC, BrinJones H, Sceneay J, Li BB, et al. CDK4/6 inhibition triggers anti-tumour immunity. *Nature* (2017) 548(7668):471–5. doi: 10.1038/nature23465

39. Milella M, Falcone I, Conciatori F, Matteoni S, Sacconi A, De Luca T, et al. PTEN status is a crucial determinant of the functional outcome of combined MEK and mTOR inhibition in cancer. *Sci Rep* (2017) 7:43013. doi: 10.1038/srep43013

40. Andersen DS, Colombani J, Palmerini V, Chakrabandhu K, Boone E, Rothlisberger M, et al. The Drosophila TNF receptor Grindelwald couples loss of cell polarity and neoplastic growth. *Nature* (2015) 522(7557):482–6. doi: 10.1038/nature14298

41. Imbert I, Coignet LJA, Pellestor F. 6p abnormalities and TNF-α over-expression in retinoblastoma cell line. *Cancer Genet Cytogen* (2001) 128(2):141–7. doi: 10.1016/S0165-4608(01)00402-2

42. Eder J. Tumour necrosis factor α and interleukin 1 signalling: do MAPKK kinases connect it all? *Trends Pharmacol Sci* (1997) 18(9):319–22. doi: 10.1016/S0165-6147(97)01097-3

43. Clavier A, Rincheval-Arnold A, Baillet A, Mignotte B, Guenal I. Two different specific JNK activators are required to trigger apoptosis or compensatory proliferation in response to Rbf1 in Drosophila. *Cell Cycle* (2016) 15(2):283–94. doi: 10.1080/15384101.2015.1100776

44. Kyriakis JM, Avruch J. Mammalian mitogen-activated protein kinase signal transduction pathways activated by stress and inflammation. *Physiol Rev* (2001) 81(2):807–69. doi: 10.1152/physrev.2001.81.2.807

45. Wagner EF, Nebreda AR. Signal integration by JNK and p38 MAPK pathways in cancer development. *Nat Rev Cancer* (2009) 9(8):537–49. doi: 10.1038/nrc2694

46. Busch MA, Haase A, Miroschnikov N, Doege A, Biewald E, Bechrakis NE, et al. TFF1 in aqueous humor-A potential new biomarker for retinoblastoma. *Cancers (Basel)* (2022) 14(3). doi: 10.3390/cancers14030677

Frontiers in Oncology

Advances knowledge of carcinogenesis and tumor progression for better treatment and management

The third most-cited oncology journal, which highlights research in carcinogenesis and tumor progression, bridging the gap between basic research and applications to imrpove diagnosis, therapeutics and management strategies.

Discover the latest Research Topics

See more →

Frontiers

Avenue du Tribunal-Fédéral 34
1005 Lausanne, Switzerland
frontiersin.org

Contact us

+41 (0)21 510 17 00
frontiersin.org/about/contact